Wake - Separation Bubble Interactions in Low Reynolds Number Turbomachinery

A Dissertation Submitted for the Degree of Doctor of Philosophy

by

Robert Jeremiah Howell

Gonville and Caius College

Whittle Laboratory

Cambridge University Engineering Department

January 1999

Wake - Separation Bubble Interactions in Low Reynolds Number Turbomachinery

by Robert J. Howell

Summary

There is a continual demand for a reduction in the cost and weight of aero-engines. Suppliers of engines always need to reduce manufacturing costs and airlines want to carry more passengers or cargo. This thesis will show that reducing the number of blades in the low pressure turbine is a potent way of achieving both of these goals. Through a program of experimental and numerical work, it is shown how it is possible to reduce the number of blades in the turbine by approximately 15% relative to the first generation of high lift blading employed in the BMW Rolls-Royce BR715 low pressure turbine.

A series of measurements from surface mounted hot films are shown from two full scale BMW Rolls-Royce LP turbines. These measurements define the current state of the art for LP turbine blade design. It is demonstrated that the suction side boundary layer flow is entirely dominated by the passage of wakes from upstream blade rows.

Low speed measurements were carried out on a linear cascade of highly loaded low pressure turbine blades (designated TL10) similar in style to those used for the BMW Rolls-Royce tests. The rig used for these tests incorporated a moving bar wake generator to simulate the presence of a single upstream blade row. Reductions in loss were measured when wakes were present compared to the case with steady inflow at low Reynolds numbers. A novel technique was used to increase the blade loading to above the levels of the TL10 profile. The loss production of a number of suction side pressure distributions were then investigated for cases with and without incoming wakes. Loss reductions were again observed when wakes where present and this reduction in loss increased as the lift of the profiles increased. Hot film measurements indicated that moving the position of boundary layer separation aft will decreased the losses generated. Further measurements proved that aft loaded profiles performed better than forward loaded profiles with unsteady inflow. The key to the loss reductions was the interaction of the wakes (and the turbulent spots that they form) with the separation bubble.

To further understand the interaction of the separation bubble with wakes and turbulent spots, a further series of experiments were carried out in a large scale flat plate rig with an imposed low pressure turbine pressure distribution. Artificial turbulent spots were generated upstream of the separation bubble. The detailed interaction of these spots with the separation bubble was investigate using hot films and hot wires. A numerical scheme is presented that predicts the development of turbulent spots in the separated boundary layers seen on high lift turbine blades. The predictions are shown to reproduce the effects seen in the experiments.

As a proof of this research, a very highly loaded, low pressure turbine profile was designed and then tested in cascade. The profile was not designed or tested by this author. The new profile produced losses only marginally higher than those for the datum profile with unsteady inflow. However, the profile resulted in a 15% reduction in blade numbers. Overall there is a net benefit as there is a substantial reduction in the number of blades required in the low pressure turbine.

Preface

This dissertation is the result of my own work and includes nothing which is the outcome of work done in collaboration, except where stated otherwise. This work has not been submitted for any other degree or any other qualification at any University.

The Schiff Foundation of the University of Cambridge is gratefully acknowledged for providing continual financial support for the first three years of this project. I would also like to thank BMW Rolls-Royce gmbh. for granting permission to publish and funding the measurements presented in Chapter 4. Rolls-Royce plc. is acknowledged for the funding my work in Chapters 6 and 7.

Gillian encouraged me to start and then complete this thesis during difficult times, as did her parents. Thanks to all of you. Thanks are also due to Gillian for proof reading parts of this thesis. Not much fun for a biologist!

I owe a great debt to those at the Whittle Lab. Fred's efforts in placing the hot film sensor arrays onto the contorted surfaces of the BRR LP turbines is gratefully acknowledged. John Saunders kept the first moving bar rig in one piece, despite my best efforts to reduce it to is constituent elements. Trevor somehow managed to create a working rig from the single (and very poor) sketch I presented him with. He also never tired of making those 'minor' adjustments to parts of the rig that incorrectly!

Thanks for keeping me (relatively) sane during the preparation of this thesis and during my time in the Lab are due to Rajesh, Brian, Carmen, Jonathan, Shane, John, Graham, Mike, and others especially for the Frisbee 'action' during the long summer evenings spent at the Lab.

Thanks are also due to my supervisor, Howard. When life started to get extremely difficult, in the last months of my mothers illness, I could not have asked for anyone to be more understanding or helpful. I would also like to thank him for his constructive advise during the course of this research.

Finally, I would like to thank my mother who taught me that I should always finish what I start.

Length of thesis

This thesis contains approximately 45,000 words and 112 figures.

Robert. J. Howell

This thesis is dedicated to the memory of my mother

Shelia Noonan

Table of Contents

Nomenclature

Symbols

A	constant
B	constant
C	chord
C_d	dissipation coefficient
C_f	skin friction
C_p	pressure coefficient
D	drag
d	bar diameter
f	frequency (of wake passing)
$\bar{f} = f\ C/V_{te}$	reduced frequency
E	anemometer output voltage
E_0	anemometer output voltage with no flow
g	spot production rate (per unit span per unit time)
h	enthalpy
H	shape factor
l	length
Ma	Mach number
N	number of ensembles
p	pressure
Q	rate of heat transfer
R	resistance
RMS	root mean square
S	entropy, pitch
s	streamwise length (of blade or plate)
T	temperature
t	time
Tu	turbulence intensity
V	freestream velocity
U	freestream velocity
W	length
x	streamwise co-ordinate
Y	total pressure loss coefficient
y	streamwise normal co-ordinate
α	flow angle, propagation parameter
β	flow angle, propagation parameter
γ	intermittency factor
σ	spot area factor
δ	displacement thickness
$l_q = \frac{q^2}{u}\frac{dV}{ds}$	pressure gradient parameter
u	kinematic viscosity

m	molecular viscosity
r	density or electrical resistivity
t_w	wall shear stress
q	momentum thickness

Subscripts

bar	relates to bar in wake generator
l	laminar
ps	pressure surface
ss	suction surface
0	stagnation quantity
1	inlet
2	exit
∞	freestream
te	values measured at 96%s

Superscripts

-	time mean
~	ensemble averaged

1. Introduction

1.1 Introduction

Turbomachinery technology has been under development for many centuries. From water wheels and windmills to Parsons' first steam turbines at the turn of this century they have been used to develop mechanical as well as electrical power. Today, 80% of the worlds electrical power comes from steam turbines. The first gas turbines used for aeroplane propulsion were developed independently by von Ohain and Whittle during the second world war. The first jet powered aeroplane that took to the air was a Heinkel He178 which flew in 1939, while Whittle's first engine (the W-1) flew in a Gloster E28/39 during 1941.

Today, the gas turbine is used to power all but the smallest and slowest aeroplanes. The first jet engines developed only a few hundred pounds of thrust, while the latest generation of engines now in service are rated around 100,000 pounds. Modern gas turbines have high reliability, efficiency and power-to-weight ratios. Gas turbines are also increasingly being used for continuous electrical power generation and no longer just for standby supplies.

Figure 1.1 shows a picture of a modern gas turbine used in the Boeing 777 and similar to that for the airbus A330 and A340 families of aircraft. The air flow enters the fan after which it is split into two and some of the flow bypasses the core of the engine and is ejected as a low speed, high volume flow jet. The remainder of the flow goes through the core of the engine where it passes through the compressors, combustion chambers and turbines and is ejected as a high speed low volume jet. The so called bypass flow of such an engine produces around 80% of the of thrust and is powered by the low pressure

turbine. The LP turbine is shown magnified. The core flow therefore only contributes about 20% to the engines total thrust. Since most of the thrust is generated by the fan, it requires 6 low pressure turbine stages to drive it, whereas a single stage HP turbine drives a six stage HP compressor.

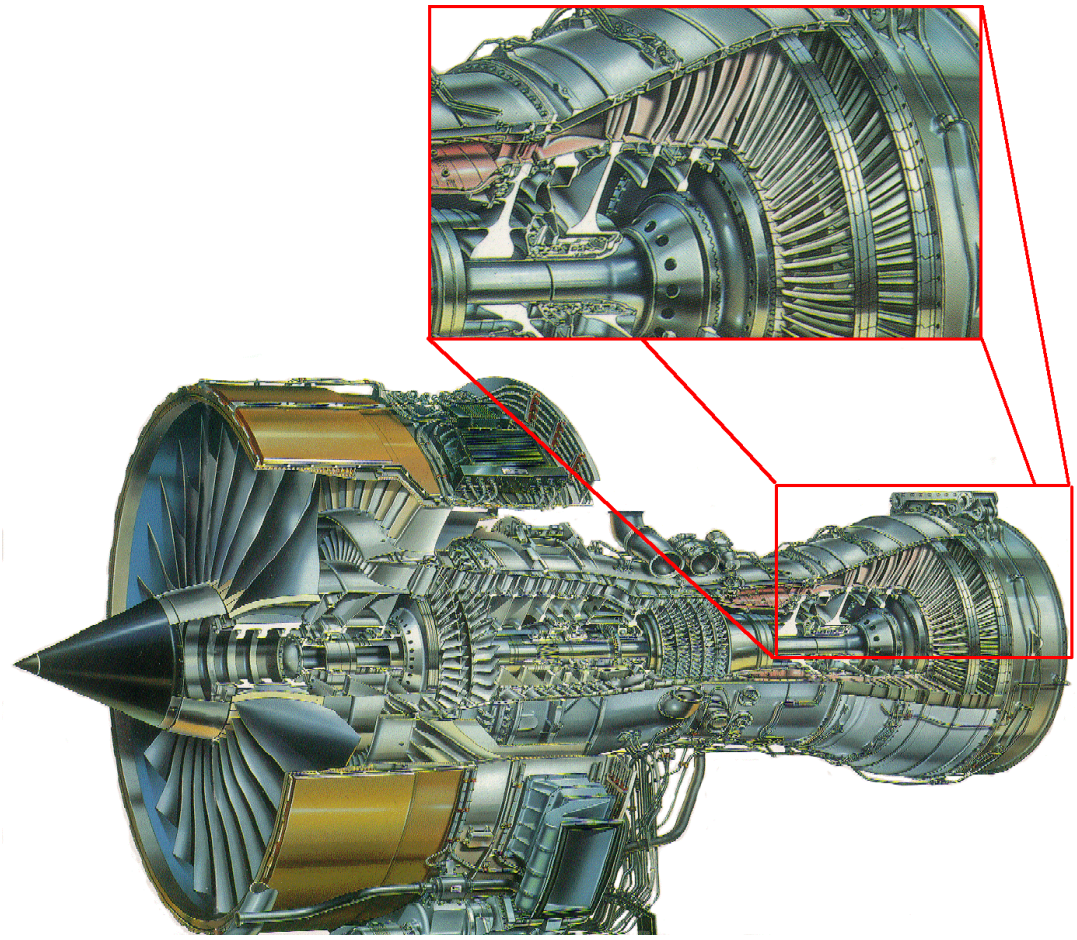

Figure 1.1.1 The Trent 800 Turbo-Fan Jet Engine.

The efficiency of the low pressure turbine has a large effect on the overall specific fuel consumption. Typically, a 1% increase in LP turbine efficiency gives rise to 0.7% increase in engine overall efficiency (Halstead, 1998). The first turbines developed obtained efficiencies of just under 80% whereas modern LP turbines reach above 93% efficiency. In over 50 years of extensive research the efficiency of the LP turbine has just

risen by around 13 percentage points. The development of the gas turbine as a whole and the LP turbine in particular has reached a stage where rises in efficiency are therefore increasingly hard to obtain. Manufacturers are therefore looking for other ways to make their products more competitive. At this point it should be mentioned that most of the reductions in the fuel consumption have come from increases in engine efficiency, not from reductions in airframe drag. Over the last 20 years engine specific fuel consumption has decreased by 30%, while drag reductions on the airframe account for only 8%.

A reduction in the production costs of an engine is of most benefit to the engine manufacturer, whereas a reduction in engine weight is of benefit to the airline. The initial cost of the engine, it's weight, it's fuel consumption, maintenance and servicing costs all contribute to the total cost of ownership. However, an engine's weight has a bearing on the manufacturing costs and fuel consumption. If one can reduce the number of components in an engine, then any aeroplane that it powers will be able to carry increased cargo for the same fuel load. In seeking to reduce the weight of an engine, every component must be scrutinised. However the heaviest single component is the LP turbine and in some engines it can comprise one third of the total engine weight. The LP turbine is then a prime component for reducing total engine weight and this could be achieved through a reduction in the number of blades.

Reducing the number of components (in this case blades) may also increase reliability, since there are fewer components to fail. However, if the number of blades is reduced then the remaining blades are required to carry a greater aerodynamic load. If they support a shroud there are also fewer to do this. These effects put greater strains on the remaining blades and therefore a increase in reliability may not necessarily be achieved.

1.2 Characteristics of the low pressure turbine.

Due to its large diameter the fan is constrained to rotate at low speed and since the LP turbine drives it, this must also rotate at the same low speed, unless a gearbox is used. Some engine manufacturers currently feel that the fan speed is already too high and would like to reduce it further, but this would put extra loads on the turbine as discussed below.

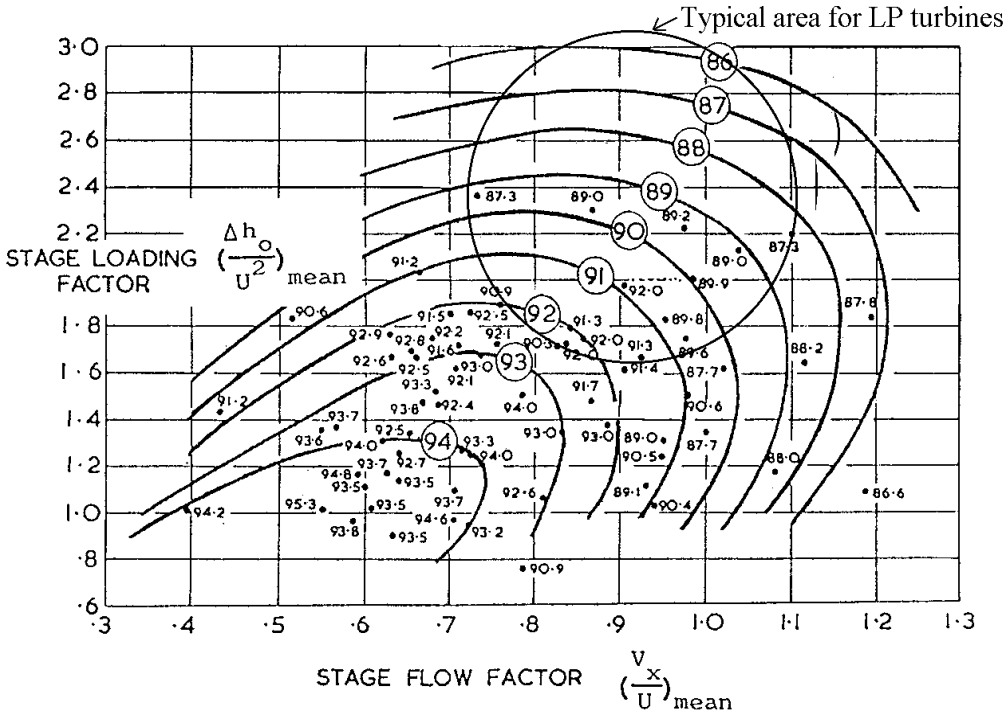

Figure 1.2.1 A smith chart illustrating increased efficiency at relatively low stage loading coefficients

For the turbine to develop the required power for the fan with as few stages as possible, each stage must be highly loaded. The stage loading coefficient is given by

$$\varphi = \Delta h_o/U^2 = 1 - (\tan \beta_2 / \tan \beta_1) \qquad \text{Equation 1.2.1}$$

where β are the relative inlet angles and exit flow angles respectively. The blade speed, U is fixed by the fan speed, which means that Δh_o must be high to obtain a high stage loading coefficient, indicating that the blade angles must be as large as possible. However, the

Smith chart shown in Figure 1.2.1 shows stage loading coefficient variation and indicates that the highest efficiencies are obtained at relatively low stage loading coefficients. In the case of the LP turbine, a reduction in weight that arises through a reduction in stage numbers wins over a slight reduction in efficiency. This indicates that high efficiency is not always the primary goal of an engine component design.

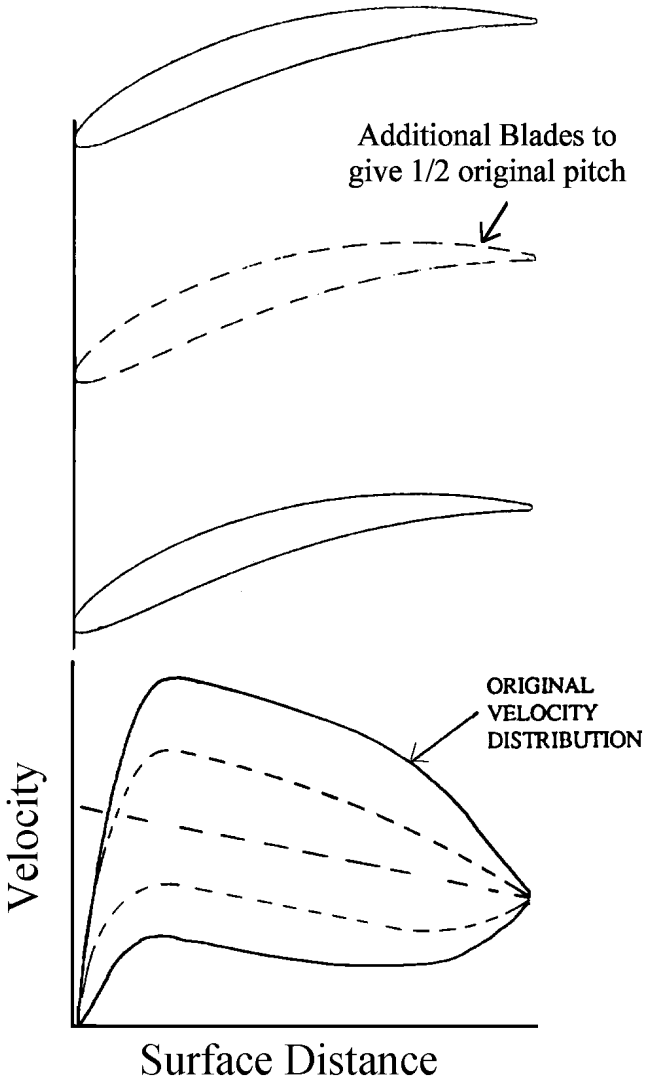

Figure 1.2.2 Changes in pitch chord ratio for compressor blades showing the resulting change in velocity distribution.

For each stage to be as light as possible few blades should be used, requiring each blade to be highly loaded. Increased blade loading requires that the difference in static

pressures between the suction side and pressure side of the blades are increased. Figure 1.2.2 shows the effect of changing the pitch chord ratio of a blade row on the resulting pressure distribution of a compressor cascade. If the pitch chord ratio is increased (i.e. fewer blades for a fixed chord) each blade (compressor or turbine) has to turn a proportionally greater mass flow and requires a greater pressure difference between suction and pressure side of the blades to do so. The loading of the blade therefore goes up.

1.3 Secondary flows and boundary layers

Having established the main mechanical constraints on the LP turbine and some of its basic aerodynamics, it is now appropriate to consider other flow conditions which characterise it. The flow over an LP turbine blade is complex. Part of the flow is essentially two dimensional, but there are regions (at the tip and hub) where the boundary layers on these end walls cause secondary flows. The flow over the surface of a blade can be visualised by painting a coloured viscous liquid onto the surface under investigation. The air flow causes the liquid to move in the direction of the local skin friction vector. Figure 1.3.1 shows such visualisation carried out on a modern LP turbine blade from the BMW Rolls-Royce 710 LP turbine. Red horizontal streaks indicate that the flow has a negligible radial component of velocity and can be classed as two dimensional flow. A characteristic of LP turbine blades is that only a relatively small amount of blade surface is covered by secondary flow because of the high aspect ratio, which in this case is approximately 6. The majority of the flow as seen in Figure 1.3.1 is two dimensional.

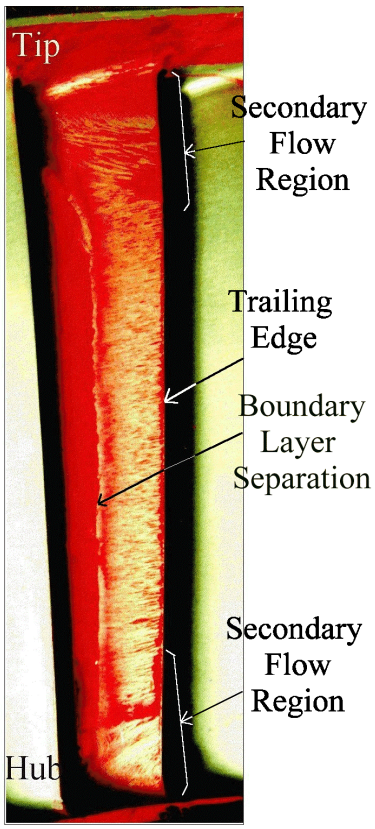

Figure 1.3.1 Flow visualisation on an BR710 LP turbine blade. Reynolds number 60,000, Mach number ≈ 0.1.

The loss breakdown for a typical turbine blade at mid span is 60% for the suction surface, 20% for the pressure surface, and 10% for the trailing edge region, Curtis *et al* (1997). It is therefore the suction side of the blade that is investigated in this thesis.

The primary mechanism for altering the (2D) profile loss of a turbine blade is the state of the boundary layer on the suction side. Figure 1.3.2 shows that the pressure distribution for highly loaded low pressure turbine blades. It is characterised by a high acceleration over the leading edge region after which there is a steady but more gradual increase in velocity. This acceleration keeps the boundary layers thin and attached to the surface.

The acceleration continues up to peak suction after which the flow diffuses rapidly, leading to flow separation, transition and turbulent reattachment of the flow before the

trailing edge. The pressure side is characterised by a small deceleration over the forward portion of the blade and then an increasing acceleration towards the trailing edge.

The state (laminar, turbulent or separated) of the boundary layers determines the profile loss produced by the blade. Denton (1995) gives the entropy production per unit surface area as

$$S = C_d \rho V^3 / T \qquad \text{Equation 1.3.1}$$

for a boundary layer, where C_d is the dissipation integral. This illustrates that it better to promote laminar flows rather than turbulent as the value of C_d is much lower in laminar boundary layers, than turbulent ones. It also shows that the entropy production is proportional to the local velocity cubed. This shows why the losses generated by the suction side are higher than those on the pressure side even without the additional losses generated by the separation.

Laminar flow will separate when it undergoes diffusion of around 5% (in velocity) over the rear of a blade, Hodson (1996). The flow rapidly undergoes transition after separation to turbulent flow.

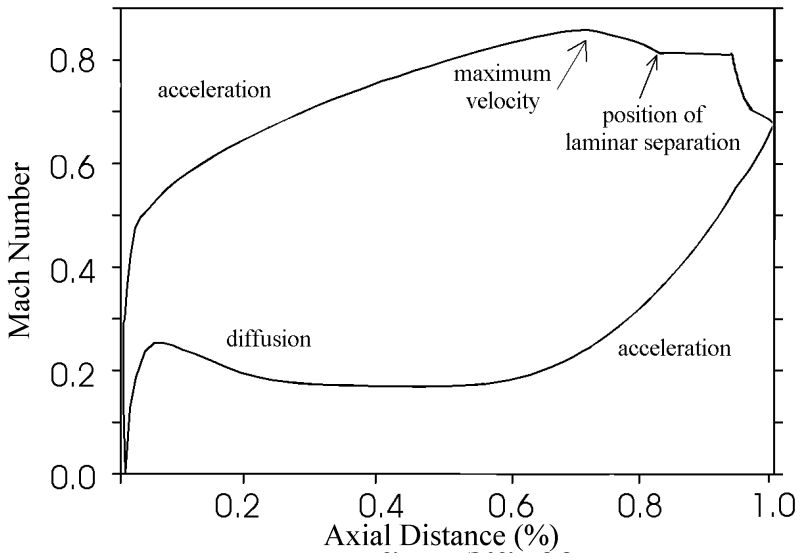

Figure 1.3.2 Pressure distribution of a modern LP turbine

The fluctuations and eddies in the separated flow region entrain high momentum fluid from the free stream which forces the boundary layer to reattach to the blade surface as a transitional or turbulent boundary layer. The loss generated by a reattaching separation can be considerable and will be discussed later in the thesis.

1.4 Unsteady Flow Considerations

Most, if not all, current turbine design methods assume that the flow into a blade row is steady. However, the only blade row that sees truly steady inflow is the fan and possibly the first stage stator of the HP turbine. All other blade rows see a number of upstream blades rows and are subjected to their effects. Upstream blades effect downstream blades primarily due to the wakes they shed. This is seen as a periodic disturbance of high turbulence fluid and a velocity defect by the downstream blade, see Figure 1.4.1. Downstream blades have an effect on upstream blades via their potential (pressure) field. The potential field also causes periodic disturbances to the flow in downstream blades, but the primary effect on boundary layer transition is that caused by wakes and not the potential field.

An important parameter in describing the effects of wakes from an upstream blade row on a downstream blade row is known as the reduced frequency. This can be defined in a number of ways, but is generally the ratio of the convection times of a particle in the freestream through the passage to the time between wakes passing the inlet to a blade row. The higher the reduced frequency the greater the number of wake segments in a blade passage at any one time and therefore the more ‘unsteady’ the flow in the passage.

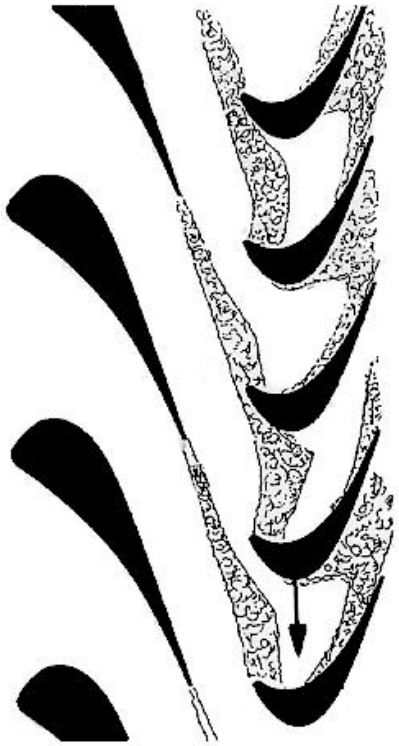

Figure 1.4.1 NGVs shedding wakes into the path of a downstream rotor.

1.5 Chapter summary and thesis outline

The introduction has shown that there is a need for manufactures to reduce the weight and cost of their engines while not loosing much efficiency. A potent way of reducing weight would be to reduce the number of blades in the LP turbine, so the research conducted in this thesis is therefore directed towards that goal. This was done by carrying out a series of experiments and some numerical modelling designed to understand the flow physics of LP turbine aerodynamics. The result of this was a new design of LP turbine profile with 15% higher lift and only a slight loss penalty.

Chapter 2 presents a review of pertinent literature concerning the effects of unsteady inflow and boundary layer transition on blade row performance. Chapter 3 presents the experiential methods and apparatus used in this study. Chapter 4 presents measurements taken in a high speed cold flow test facility at the University of Stuttgart,

using two BMW Rolls-Royce LP turbines. This data taken from these state of the art blades sets the scene and datum for the rest of the thesis. Chapter 5 presents experimental results from cascade tests and illustrates how the losses generated by a blade row are affected by upstream wakes. The results from Chapter 5 show how the understanding of wake separation bubble interaction leads to controlled diffusion blading being disregarded in favour of new design rules that allow higher blade loading, without any loss penalty. Chapter 6 presents detailed experimental measurements used to highlight the basic physics of what was seen in the previous chapters regarding spot-separation bubble interaction. Chapter 7 presents CFD simulations of flows that occur in the previous chapters and develops models to take account of those new developments. Chapter 8 shows further experimental measurements an the new ‘ultra high lift’ blade design based on the data in Chapter 5 and offers a proof of concept of the arguments presented earlier in the thesis. The blade design was carried out by Rolls-Royce plc. and the measurements were not taken by this author, but are presented for completeness. Chapter 9 presents the overall conclusions of this work and suggests avenues of further research that are likely to result in further understanding of the physics of LP turbine boundary layers and wake interaction.

2. Literature Review

2.1 Introduction

The purpose of this chapter is to place the research presented in this thesis into context with an examination of the relevant literature. Wake and boundary layer interaction is a large area of research and a complete review of the available literature beyond the scope of this thesis. This review is directed towards the transition mechanisms that are present when wakes interact with boundary layers and how those interactions causes blade losses to change. The research presented in this thesis has an impact on the economics of turbomachinery manufacture, efficiency and the engine weight and this aspect is also briefly examined.

2.2 Steady flow transition

Schlichting (1979) gives a comprehensive account of the mechanisms that lead to boundary layer transition. These are briefly described in the following section.

Natural transition occurs when a boundary layer becomes susceptible to small disturbances at a critical momentum thickness Reynolds number. These disturbances develop into two dimensional Tollmien-Schlichting waves, which are then amplified within the boundary layer until they become three dimensional and eventually role up into loop vortices, see Figure 2.2.1. The final stages of this process occurs when these vortices breakdown into turbulent spots. The details of this breakdown are not well understood. The newly formed spots travel downstream, grow and coalesce to form a fully turbulent boundary layer.

Bypass transition occurs when the first stages of natural transition are bypassed (due to a high freestream turbulence level) and turbulent spots form directly within the

boundary layer. This is the most common situation in a turbomachinery environment where the environment is highly disturbed due to the passage of wakes and the potential effects of blade rows. Many working models have been developed for the description of how turbulent spots develop and propagate and these are discussed later in this chapter.

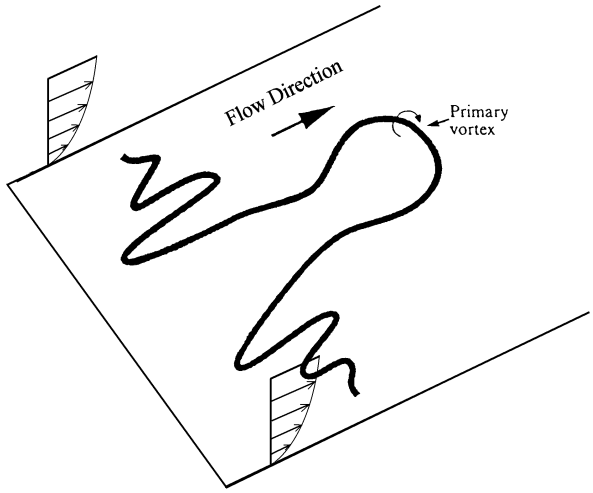

Figure 2.2.1 A loop vortex forming in a boundary layer.

The other method by which a blade surface flow changes state from laminar to turbulent, is if the flow forms a separated shear layer. Separated flows are common in turbomachinery wherever there are adverse pressure gradients. There is no significant pressure gradient normal to a blade surface in an attached boundary layer so fluid at all heights within the boundary layer experiences the same static pressure. The boundary layer flow nearest the surface has a lower momentum than that of the free stream and eventually stagnates under the streamwise adverse pressure gradient. The rest of the flow is then forced to separate from the blade surface because of this blockage and forms a separated shear layer. Shear layers are highly unstable, rapidly breakdown and undergo transition. The shear layer becomes turbulent and entrains higher momentum (energy) fluid from the freestream. The turbulent mixing of the freestream fluid with the shear layer transports

momentum from the outer layer to the inner parts of the layer. The increased momentum of the shear layer allows it to reattach to the blade surface as a transitional boundary layer. The result is a separation bubble.

Some researchers have detected Tollmien Schlichting type instabilities in separated shear layers indicating that some of the stages in natural transition may be present. Other workers have modelled separated flow transition with the use of attached flow models of turbulent spot formation and growth. Which of these two approaches is more physically correct is not known at present.

Abu-Ghannam and Shaw (1980) measured the effect of turbulence, pressure gradient and flow history on natural transition in a steady flow environment. Their correlations have been widely used in the turbomachinery industry. They claimed that there is almost no effect of pressure gradient on the start of transition after the free stream turbulence intensity becomes greater than 3%. However, there was very little data available for favourable pressure gradients. Transition onset and end correlations were developed but were forced to not allow transition before $Re_\theta = 163$. The value of 163 is the stability limit for zero pressure gradient flow with very low free stream turbulence intensities below which natural transition will not occur. In turbomachinery flows the higher turbulence intensities means that bypass transition is more likely to occur than natural transition and these correlations must therefore be used with care.

Walker and Gostelow (1989) showed hot wire traces which indicated that in adverse pressure gradients instability waves were seen continuously at a particular streamwise location. At the same location for zero gradient flows the instability waves occur in sets (packets) with relatively calm periods between where no waves are seen. The frequency spectra of the instabilities show that more harmonics of the fundamental

Tollmien-Schlichting appear as the level of adverse pressure gradient increases. An order of magnitude reduction in transition length was observed when comparing transition lengths in zero pressure gradient flows to those in the most severe adverse pressure gradients i.e. up to when separation is likely to occur. Most transition length correlations have been derived from data taken in zero or favourable pressure gradients. However, on the aft part of the suction surface of a turbine there is (an often large) averse pressure gradient. Transition in adverse pressure gradients occurs much faster than in favourable and zero gradients. The result is that transition lengths on turbine suction surfaces are therefore often overestimated.

For a comprehensive review of the then current state of the art in transition in turbomachinery environments, see Mayle 1991.

2.3 Turbulent spots

Emmons (1951) first discovered turbulent spots and produced a probability theory describing the development of the last stages of transition. Schubauer and Klebanoff (1955) generated artificial turbulent spots and showed their leading and trailing edge velocities to be 88 and 50% of the local free stream. The spots was found to be triangular in plan form with a half angle of approximately 15°, see Figure 2.3.1. They were also the first to note the existence of a calmed region which trail behind the turbulent part of the spots and also noted that the calmed flow was unreceptive to disturbances. Chen and Thyson (1971) produced approximations to the spot's geometry which are also shown in Figure 2.3.1.

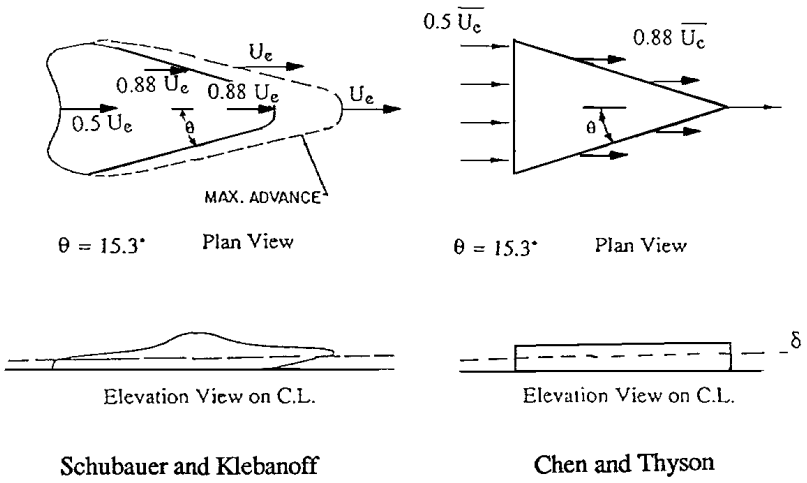

Figure 2.3.1 Measured turbulent spot and the simplifications made by Chen and Thyson.

Chin and LaGraff (1996) measured spot convection rates at different Reynolds numbers and concluded that artificially generated turbulent spots convected in the same way as naturally occurring spots. Gostelow *et al* (1996) investigated the behavior of artificially generated turbulent spots triggered with jets of compressed air. In particular they looked at the behaviour of the spot and calmed region in adverse pressure gradients. Initially the disturbance (a wave packet) was strongly amplified and then developed harmonic components above the fundamental frequencies of the initial wave packet. Eventually these breaks down to form a turbulent spot. The region of calmed flow which travels behind the turbulent part of the spot was shown to reduce the amplitude of fluctuations to about half their original level. Within the turbulent spot, the shape factor attains a value of approximately 1.6, which is the near value usually obtained for a fully developed turbulent boundary layer. This value relaxes back to the value of the undisturbed boundary layer shape factor, but takes considerable time in doing so. If the turbulent part of a spot takes a unit time to move past a streamwise location, then the calmed region was shown to take approximately 3 units to pass the same location.

Seifert (1998) presented data on how turbulent spots convect through a transitional laminar-turbulent boundary layer. For the laminar region of the boundary layer, the turbulent part of the spot caused a drop in shape factor from 2.8 to 1.6, while Re_θ and Re_δ increased which agrees with the measurements of Gostelow *et al* (1996). The effect of the calmed region was seem primarily in the variation of shape factor and Re_θ.

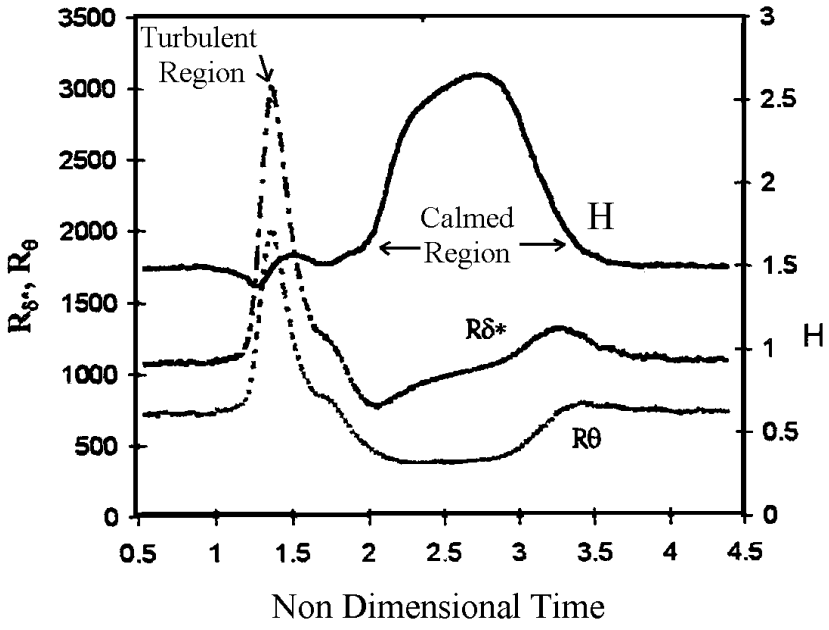

Figure 2.3.2 Variation in integral parameters as a turbulent spot and calmed region pass through a turbulent boundary layer.

The effect of a turbulent spot travelling through a fully turbulent boundary layer caused Re_δ and Re_θ to increase because the turbulent part of the spot formed further upstream than the turbulent boundary layer in which it finds itself. The calmed region caused an increase in shape factor from the turbulent value of 1.6 to a laminar like value of 2.6. and caused a drop in both momentum thickness (Re_θ) and Re_δ. It was also shown in the paper that by using an optimum reduced frequency for spot production, a maximum drag reduction of 3% was seen as the spot travelled through the turbulent part of the

boundary layer. In the laminar flow region on the plate an increase in drag was observed as the turbulent spot passes.

Intermittency $\gamma(x,z,t)$ is defined as the probability that a position (in time and space) is turbulent or not. Emmons speculated that spots could form at any location along a surface (continuous breakdown), but the resulting intermittency distribution did not agree well with measurements. Narasimha (1957) put forward the hypothesis that spots form at a preferred location along a surface, so called concentrated breakdown. A Dirac delta function and narrow Gaussian functions were used for the spot production rates, but the resulting intermittency distributions were very similar and so the added complexity of the Gaussian distributions were deemed unnecessary. Using the concentrated breakdown hypothesis the resulting intermittency takes the form

$$g(x) = 1 - \exp\left[-\frac{g(x_{tr})s}{U}(x - x_{tr})\right] \qquad \text{Equation 2.3.1}$$

Where $g(x_{tr})$ is the spot production rate at the breakdown location, σ is the spot geometry factor, U is the free stream velocity transition, and x is the streamwise co-ordinate. The problem of predicting the transitional activity of a boundary layer is then reduced to obtaining the transition onset location and the spot production rate at that location. The onset location can be calculated from correlations (Abu-Ghannam and Shaw (1980)), but often these are not very reliable for turbomachinery applications where pressure gradients and turbulence effects complicate matters.

Spot production rates are also available from correlations. Narasimha (1985) introduced the non dimensional group

$$N = \frac{g s q_{tr}^3}{n} \qquad \text{Equation 2.3.2}$$

where θ_{tr} is the momentum thickness at transition and g is the spot production rate. Narasimha gave N a value of 0.7×10^{-3} for freestream turbulence intensities greater than 0.5%. Others (Gostelow and Dey (1990)) have included the effects of pressure gradient.

In a review of the then state of the art for transition modelling in turbomachinery Mayle (1991) shows a number of transition correlations for spot production rates, transition onset location.

2.4 Separation bubbles and separated flow transition

Separation bubbles exist on most turbomachinery blade profiles, but this kind of flow is not very well understood and very few methods exist for predicting the development of separation bubbles. Figure 2.4.1 shows a schematic of a separation bubble and the effect is has on a pressure distribution of a compressor blade. The inviscid pressure distribution is also shown.

A comprehensive investigation into separation bubble behaviour was carried out by Gaster (1967). Measurements were carried out on a number of pressure gradients imposed on a flat plate. The transition from a short bubble into a long bubble was correlated with the momentum thickness Reynolds number at separation and Thwaites pressure gradient parameter. A short bubble is designated as one that has only a local effect on the pressure distribution (as in Figure 2.4.1), whereas a long bubble has an effect over the entire blade surface resulting in a large reduction in lift and turning.

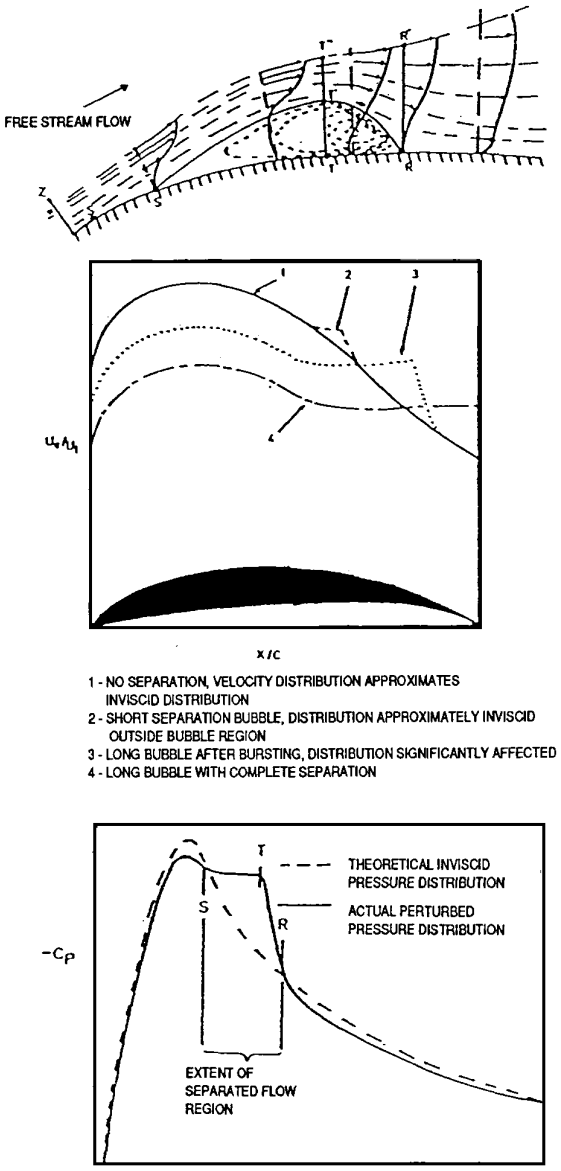

Figure 2.4.1 Schematic of a separation bubble and their effects on the pressure distribution, after Roberts, 1980.

Horton (1969) presented a method for calculating the growth of separation bubbles as well determining under what conditions they would burst, confirming the work of Gaster. Unfortunately for turbomachinery flows Horton's model does not account for turbulence effects. The effects of turbulence were to some extent included into Horton's model by Roberts (1975 and 1980) where a turbulence factor is included. The turbulence

factor includes a requirement for a specification of a length scale of the inlet turbulence as indicated by the work of Evans (1971).

Separated flow transition is probably the least well understood of all the transition mechanisms. A number of different approaches to modelling the process have been undertaken some of which are described below.

Malkiel and Mayle (1995) modelled the breakdown of a separated shear layer due to turbulence by using attached flow turbulent spot theory. As a separated shear layer develops and moves further away from the surface Malkiel and Mayle observed Kelvin Helmholtz type waves. These waves were amplified in the shear layer, as there is no mechanism to dissipate them because the streamwise velocity gradients are small. When the amplification of these waves reached a certain strength the waves started to interact with their neighbours causing sub harmonics of the primary frequency. The position where turbulent spots form was found to be the centre line of the shear layer and occurred when the sub harmonic frequency appeared. It should be noted however that no individual turbulent spots have actually been observed in the data of Malkiel and Mayle, their existence has only been inferred.

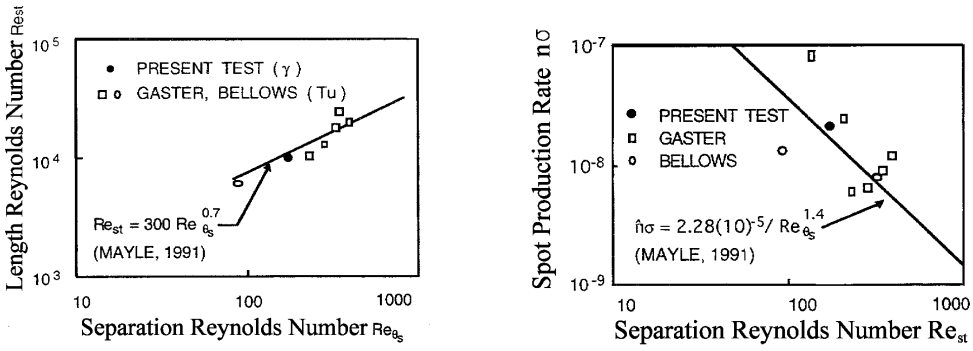

Figure 2.4.2 Correlations for separation Reynolds number based in momentum thickness vs. bubble length and spots production rates, after Mayle (1991).

Mayle (1991) showed that the momentum thickness Reynolds number at transition in a separation bubble correlated well with momentum thickness at separation. This indicated that separated flow transition can be modelled with attached flow transition ideas, albeit with spot production rates an order of magnitude higher than those for zero pressure gradients. The spot production rates in separated flows gave approximately the same values for adverse pressure gradient attached flows.

Walraevens and Cumpsty (1993) studied separation bubbles on the leading edge of compressor blades and noted a reduction in length of the bubble with an increased level of free stream turbulence.

2.5 Wake blade - row and boundary layer interactions.

Speidel (1957) was one of the first to look at the effects of wakes on the performance of an aerofoil. He was able to correlate the profile loss of an aerofoil with the frequency of wake passing using a reduced frequency parameter, but without knowledge of the state of the boundary layers. The reduced frequency parameter was defined such that it was a measure of the number of wake segments in a blade passage an any one time. This work was however not pursued to any great extent because attention switched to the influence of steady freestream turbulence level and its effect on the boundary layer.

Meyer (1958) showed the way in which a downstream rotor responds (in terms of drag and lift) to the unsteady pressure field created as wakes convect through the blade passage. The unsteady pressure field is caused by the velocity defect in the upstream wake as it convects through a downstream blade row. The velocity defect in the wake was modelled as a negative jet. In the case of a turbine, this effect removes fluid from the pressure surface and transports it to the suction surface, see Figure 2.5.1.

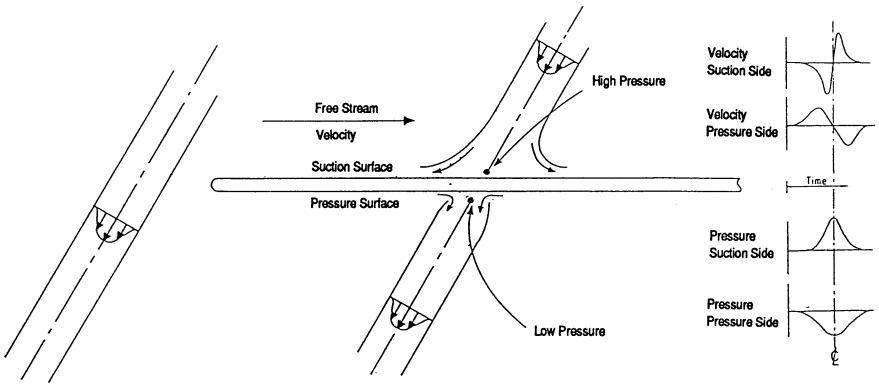

Figure 2.5.1 Schematic of the negative jet showing the velocity defect at inlet to a flat plate and the resulting velocity and pressure variations, after Hodson (1996).

Hodson (1985) predicted and Schulte (1995) measured the way in which rotor wakes were chopped at entry to a blade row and then formed two counter rotating vortices which convected through the passage.

In reality, for most modern turbine blade rows, no fluid from the pressure side boundary layer actually reaches the suction side. Wakes will normally have convected completely through the blade passage before the pressure side fluid has had time to travel very far. In fact fluid from the freestream just above the suction side boundary layer is transported through the boundary layer. For a fixed position above on the surface of a turbine it first sees an acceleration then a deceleration of fluid. Meyer's analytical model is valid for thin, lightly loaded compressor blades with little camber. However the highly loaded turbine blades discussed in this thesis distort the wake considerably which in turn effects the negative jet, see Figure 2.5.3.

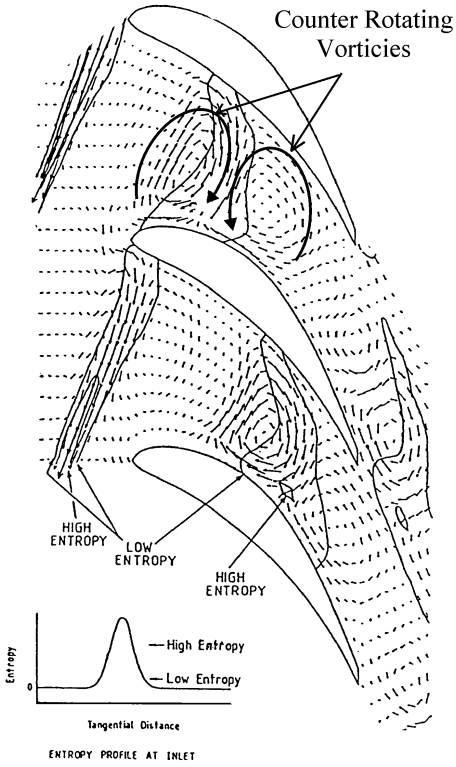

Figure 2.5.2 Simulation by Hodson (1985) showing the counter rotating vortices set up by the wake being cut at inlet to the blade row.

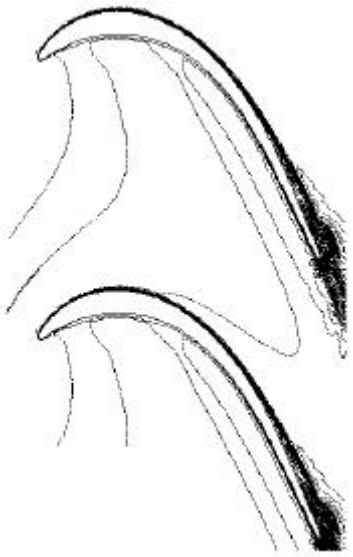

Figure 2.5.3 Distortion of a wake due to the different velocities on the suction and pressure sides of the blade.

Obremski and Fejer (1967) investigated the transition mechanisms that occur when a boundary layer is subjected to a sinusoidally oscillating free stream. This can be considered similar to the variation in velocity that a turbomachine blade surface sees as a wake passes through a blade passage, i.e. the negative jet as described above. The manner in which transition occurred was found to depend on an unsteady Reynolds number ($\mathrm{Re}_{ns} = L\Delta U/2pn$, where $L = 2pU_0/w$).

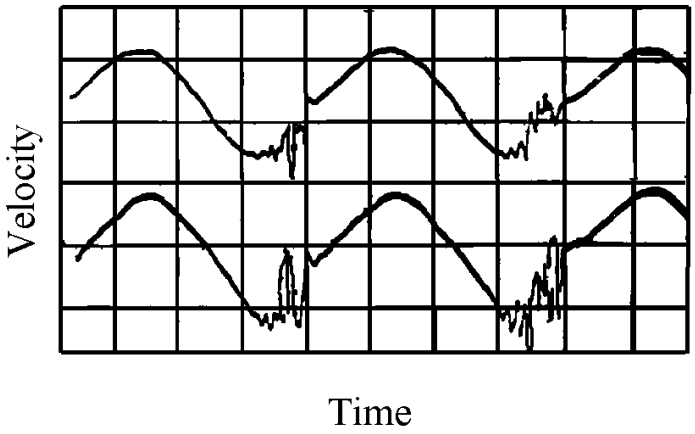

Figure 2.5.4 Velocity measurements due to Obremeski and Fejer (1967) showing instabilities in a boundary layer caused by oscillations in the freestream.

They found that it was the amplitude of the disturbance (i.e. ΔU) and not its frequency that determined the transition Reynolds number at onset. The transition process observed was similar to that observed in steady uniform flow boundary layers. Tollmien-Schlichting type waves were amplified until their amplitude reached a level where additional high frequencies were observed, see Figure 2.5.4. At this point turbulent spots were believed to have started to form. This is similar to the mechanisms described by Malkiel and Mayle (1995), but they observed Kelvin Helmholtz waves, not Tollmien Schlichting waves. When the non-steady Reynolds number reached a value of 26,000, turbulent spots appeared at the frequency of the freestream oscillations.

Walker (1974) attempted to predict the breakdown of the flows on a compressor by regarding the wakes as negative jets imposing a velocity fluctuation on the freestream. The effect of wake turbulence on the wakes on the boundary layer was not included. In

turbomachinery natural transition (i.e. of the Tollmien Schlichting type) does not occur because of the elevated levels of freestream turbulence. Breakdown occurs due to bypass transition. The relevance of velocity perturbations to onset modelling in these environment is therefore reduced. Schulte (1995) showed measurements of the variation of RMS intensity taken 6.5mm above the surface of an LP turbine blade. The blade chord was approximately 160mm. This is shown in Figure 2.5.5, which is an distance-time (ST) diagram of ensemble mean RMS intensity measured at the edge of the boundary layer. On an ST diagram, the y-axis shows the variation of time with the passage of wakes and the x-axis is the distance along the blade surface. Looking at the data along a horizontal line give the instantansous variation of flow along the surface. A vertical line would give the variation in time of a property for a given surface location. The line annotated U_{inf} is a trajectory of a particle travelling the freestream. The black regions contain low turbulence regions that occur between the wakes. The high turbulence regions are present only when the wake pass over the surface. The blade profile is the same one as used for measurements presented in Chapter 5 of this theses and it has a large separation bubble on the suction side. These measurements are important as they show the disturbance environment to which the boundary layer is subjected. The high levels of turbulence seen here indicate that bypass transition is the most likely to occur in this LP turbine environment and that it will occur at the frequency of the wake passing.

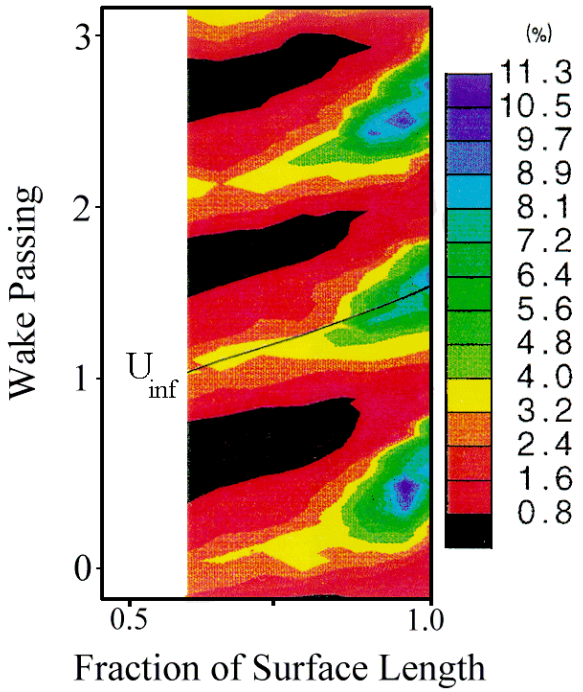

Figure 2.5.5 An ST diagram of ensemble averaged RMS intensity measured by a hot wire. Reynolds number = 130,000. $\bar{f} = 0.78$, $\Phi = 0.7$.

Walker *et al* (1993) presented wake and surface boundary layer measurements from a single stage research compressor. These showed that the appearance of turbulence in the boundary layer did not coincide with the wake passage in the freestream. In this case there seemed to be no direct effect of the wake turbulence on the transition process. However, wave packets were seen to appear in the boundary layer but they lagged well behind the wake. The passing wakes influenced transition indirectly through perturbations of the boundary layer velocity profile which created favourable conditions for wave packets to development. Also mentioned is that there was a time lag between the appearance of turbulent spots and an increase in skin friction. This delay must be considered when interpreting data from hot film sensors which indirectly measure skin friction.

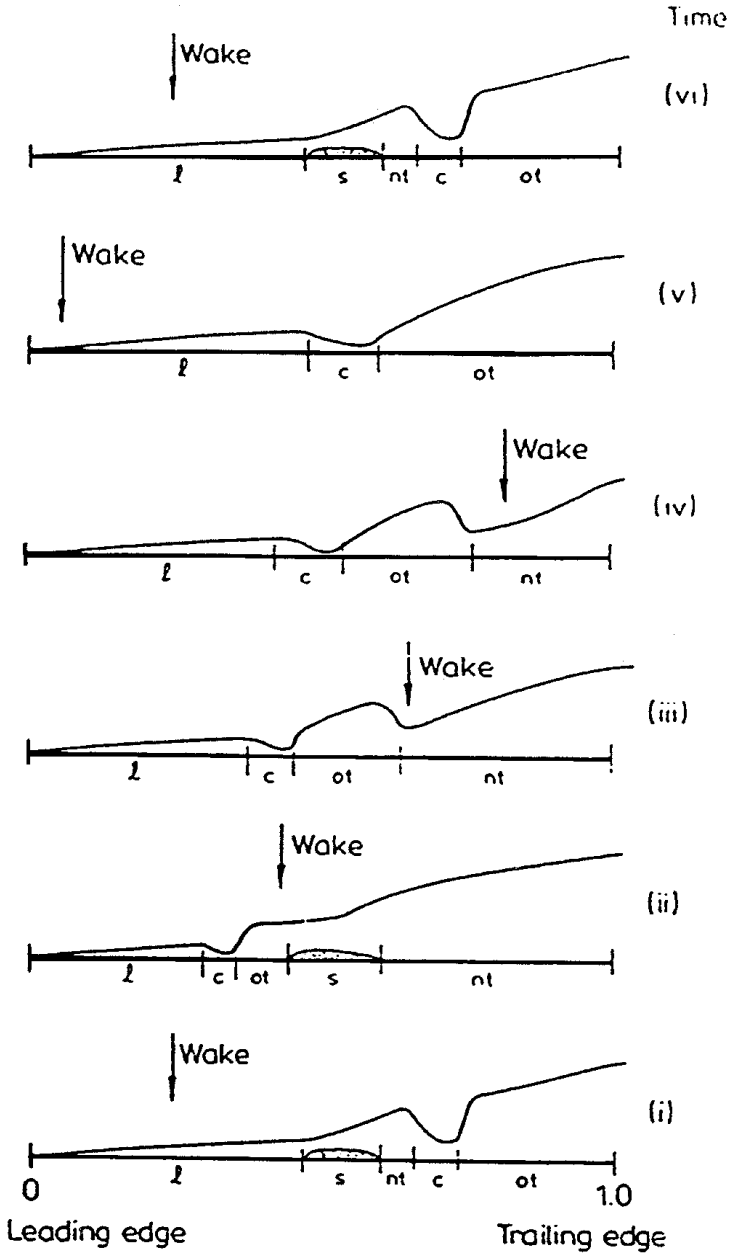

Figure 2.5.6 Boundary layer development on the suction side of a compressor blade, Cumpsty *et al* 1995.

Cumpsty *et al* (1995) showed the effect of a wake, turbulent spot and calmed region on the boundary layer development on compressor blades. Figure 2.5.6 shows the development of suction surface boundary layer height at five time instants during the passage of a spot. The first time instant is at the bottom of the figure. A separation bubble

exists at approximately mid chord, but periodically disappears as turbulent spots travel through it. The boundary layer height can be seen to vary a great deal with the passage of the wake. The velocity profile of the calmed region (shown in Figure 2.5.7) just after the turbulent part of the spot has passed was shown to be linear almost out the free stream. The skin friction was comparable to a turbulent boundary layer which indicated that the initial velocity profile of the calmed region resembles the viscous sub layer of a turbulent boundary layer, but extrapolated out to near the free stream. They also noted the ability for the calmed region to resist adverse pressure gradients that normally separate a laminar boundary layer.

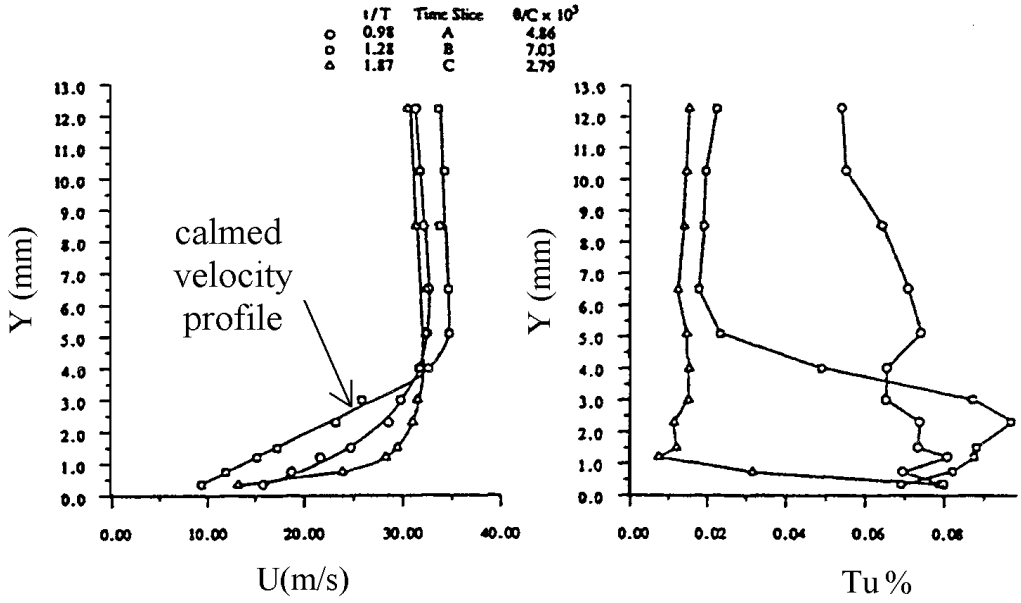

Figure 2.5.7 Velocity and turbulence profiles in a turbulent spot and calmed region

Funazaki and Koyabu (1998) investigated the effect of the changing wake direction on boundary layer development on a flat plate rig with a simulated turbine pressure distribution imposed. Distance time contour plots showed that when the wake direction was reversed, the streamwise spread of the wake over the surface was reduced, but the

peak RMS intensity was not. Unfortunately, information regarding the possible changing of transition onset location was not possible because in both wake direction cases transition seemed to occur very near the leading edge of the test section.

Ladwig and Fottner (1993) used stationary bars upstream of a high speed cascade to simulate the effect of multiple upstream blade rows. These measurements showed that by varying the pitchwise position of the upstream bars, a large variation in losses in the cascade occurred. Losses increased when the bars were placed in such a position where they caused transition far upstream of separation. An optimum pitchwise (circumferential) position was found where there losses were minimised when the effects of the wakes was to remove the separation, but not cause transition much upstream of the separation location. These kind of steady flow experiments cannot simulate the unsteady aspects of the flows in LP turbines properly as calmed regions can only exist in a truly unsteady environment. These calmed regions suppress separations long after the wake and turbulent spot has convected past. The losses with unsteady inflow under certain conditions are likely to be lower than those measured by steady flow experiments.

Halstead *et al* (1995) showed the effect of upstream blade row wakes on boundary layer development in an LP turbine and a compressor. Hot film gauges covered the blade surface from near the leading edge to the trailing edge. Measurements were taken at a variety of flow conditions including Reynolds number variations and a variation in loading on an embedded rotor. Beating effects were shown as the flow from upstream blade rows interacts with downstream blade row in a similar manner to measurements by Arndt (1991). With increased loading the position of the start of wake induced transition moved closer to the leading edge of the blade. Halstead *et al* also noted that the effect of the calmed region in stabilising the flow was much reduced at higher Reynolds numbers,

compared to the significant regions of calmed flow seen at the higher Reynolds numbers that are found at takeoff conditions.

Tiedemann (1998) investigated wake boundary layer and shock wave interaction in the rotor an HP turbine. Many of the transition mechanisms seen in LP turbines were found to be present in the HP turbine used in their investigation. Very few measurements are available from the rotors due to the difficulty with using instrumentation in the rotating frame. Little transitional activity was seen on the pressure side of the rotor due to the continual acceleration from leading to trailing edge. With steady inflow, i.e. without the upstream stator, separated flow transition occurred on the suction side. When the upstream stator was present more complicated multi-mode transition was observed. Between wakes passing bypass transition started, but was terminated by a separation bubble that was induced by a passage shock. The wake induced transition starts even earlier (at 31% surface length) on the blade surface in a region of flow acceleration. Although no reference is made to the flow conditions that the rotor sees, the stators do contain trailing edge blowing slots and hence have thick trailing edges. This will result in thicker and stronger wakes, which may be why transition occurs so far upstream. Few calmed regions were seen in the measurements but this could be due to the higher Reynolds numbers that occur in the HP turbine which are around 400,000.

2.6 Multistage wake blade row interactions.

There is little data available showing boundary layer development in multistage environments. This is often because such environments are found in high speed rigs where component performance (of the LP turbine for example) is required. Boundary layer measurements therefore do not usually assume a high priority. However some investigations have been published and are described below.

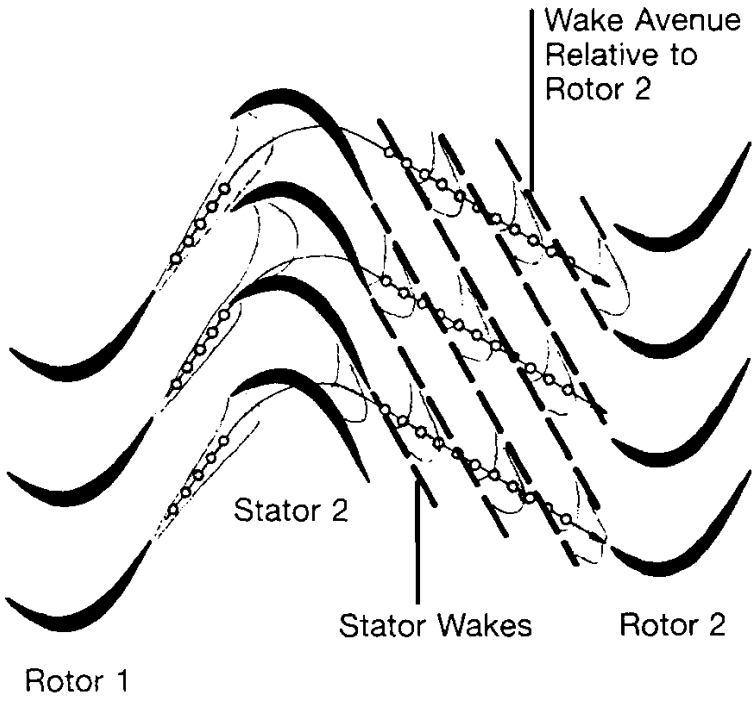

Figure 2.6.1 Part of a multistage turbine illustrating how rotor 2 sees wakes from both stator 2 and rotor1.

Arndt (1991) measured the effects that multiple blade rows have on each other by traversing a hot film probe downstream of the rotors of a 5 stage LP turbine. Measurements were carried out at two circumferential positions and at Reynolds numbers of 170,000 and 220,000. Figure 2.6.1 shows that despite the wakes from rotor 1 being chopped by stator 2, rotor 2 sees them at the same frequency as they were shed from rotor 1. Arndt noted that wake induced rotor-rotor interactions resulted in strong amplitude modulated periodic fluctuations before entrance to the third stator (NGV 3), see Figure 2.6.2. This figure shows the fluctuations in the velocity caused by the wake defect. The amplitude of the fluctuations has a low frequency component caused by the differing number of blades on rotor 1 and rotor 2. Ardnt noted that the number of nodes and anti-nodes in this data was equal to the difference in blade numbers of the rotors.

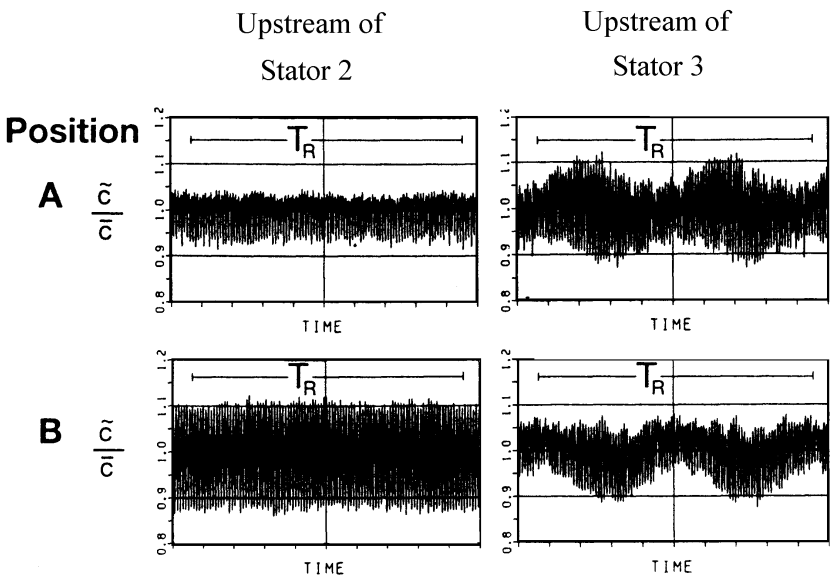

Figure 2.6.2 Ensemble averaged turbulent fluctuations at mid span, showing rotor-rotor interactions at two circumferential locations, Adrnt (1991).

Hodson *et al* (1993) investigated the boundary layer development on NGV3 of the four stage Rolls Royce Trent 700 LP turbine with surface mounted hot films sensors. Data was obtained at Reynolds numbers between 90,000 and 180,000. At these low Reynolds numbers, calmed regions can be seen in some data even at the sensor nearest the trailing edge. This shows that despite the harsh environment (in terms of high turbulence levels of an embedded stage) calmed regions still survived. The effect of multiple blade row beating effects was also investigated. As shown by Arndt (1991), the beating frequency occurs due to the difference in the number of rotor blades in each stage. The lack of any rotor-rotor interactions was due to the fact that the suction surface diffusion on the LP turbine blades is not very high and the Reynolds numbers are also relatively high, resulting in thin wakes. These wake do not therefore persist for any great distance downstream. The reason that Hodson saw no rotor-rotor interactions could also be due to the circumferential location of the hot film sensor.

Banieghbal *et al* (1995) investigated wake passing from the turbine used by Hodson *et al*, (1993) but in a cascade fitted with a moving bar wake generator and also in a steady flow transonic facility. They noted that wakes increased blade loss at Reynolds numbers above 1.0×10^5 and that wake induced transition was seen to occur upstream of the separation bubble. They attributed the loss increase to the increased turbulent wetted area found on the blade suction surfaces. For steady flow they concluded that the LP turbine blade velocity distribution used (with a 15% reduction in velocity from its peak to the that at the trailing edge) was about optimum in terms of loss generation with steady inflow in the low Reynolds number regime.

Schulte (1995) measured the boundary layer development on a more highly loaded LP turbine blade than Banieghbal *et al*, with a Zweifel coefficient of just above 1.0. This blade is the datum profile (named TL10) used for the first set of measurements presented in Chapter 5. He noted the importance of the calmed region and that it was this region that caused the slow re-establishment of the separation after a wake had passed. The calmed region and its ability to suppress separations was discovered to be the reason for loss reductions that occurred on this profile when wakes were present compared to the losses generated with steady inflow. Using a triple split hot film probe, the unsteady development of wake segments was also measured. He noted the re-circulating vortices that were set up when the wake segment was chopped at inlet to the blade passage.

2.7 Prediction wake boundary layer interaction

Many methods for the prediction and modelling of wake boundary layer interactions have been produced and a few examples are examined in this section.

Mayle and Dullenkopf (1989) produced a model to predict the time averaged intermittency due to wake interactions with attached boundary layers. The model assumed

that when a wake reached a particular streamwise location that it resulted in the formation of a fully turbulent strip under the wake. The model also included the effects of natural transition, if present. There are problems with this modelling approach. The first is that assuming that the effect of the wake is to produce fully turbulent strips assumes a minimum value on the spot production rate. Spot production rates are known to vary significantly with turbulence level, pressure gradient and Reynolds number etc. Another model presented by Mayle (1992) takes into account the time averaged effects of calming, but does not take account of wake width which has an effect on time averaged intermittency.

Addison and Hodson (1992) presented a model for determining the intermittency resulting from the transition caused by the passage of wakes. A boundary layer code by Cebeci and Carr (1978) was used to calculate the variation of θ_{tr} at transition for each instant in time. The time varying position of the start of transition needed to be specified. The non dimensional pressure gradient λ_θ is then calculated, from which the value of the non dimensional spot production rate parameter, N, can also be calculated. The unsteady intermittency was then calculated. A very important issue highlighted in this paper was that one must account for the changes in spot production rates in adverse pressure gradients. For example the transition length was over predicted when the effect of pressure gradient were neglected.

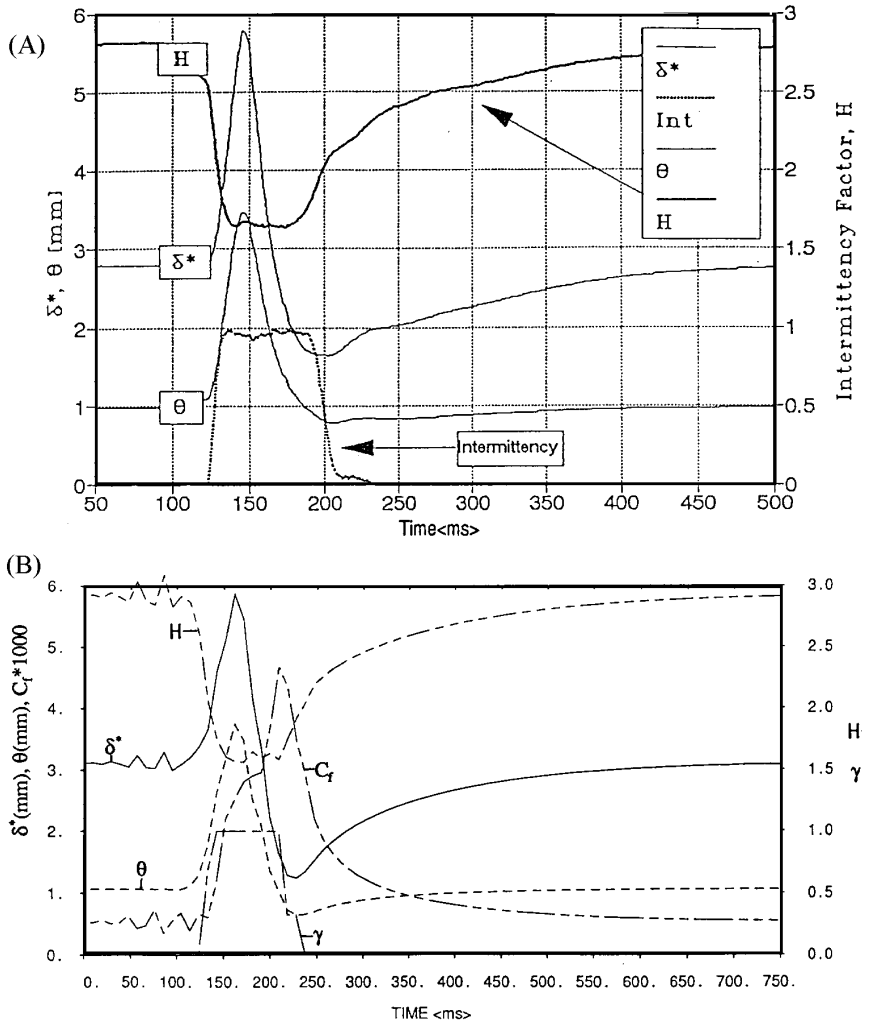

Figure 2.7.1 (a) measured and (b) predicted flow variables for the passage of a turbulent spot and calmed region in a laminar boundary layer.

Schulte (1995) continued the approach used by Addison and Hodson, using a modified version of the same Cebeci and Carr code and including the effects of calming. Using a previously calculated intermittency the passage of a turbulent spot and its calmed region was predicted, see Figure 2.7.1. The entropy production of the calmed region was also calculated and shown to be similar to that of a laminar boundary layer. It was argued that since the entropy production rates for the calmed region were lower than that

developed by the turbulent boundary layer following reattachment of the separation, it was the calmed region that caused the loss reductions measured when wakes were present.

2.8 Wake blade boundary layer interaction and loss generation

This section discusses the loss generation that occurs when the boundary layer flows are subjected steady inflow and also when they are subjected to the effects of wakes.

2.8.1 Steady Loss Generation in boundary layers

Denton (1992), provides a comprehensive summary of the loss production mechanisms in turbomachinery. In this summary, Denton derives an expression for the entropy creation in boundary layers as

$$\dot{S} = \int_0^d \frac{1}{T} t_{xy} dV_x \qquad \text{Equation 2.8.1}$$

where $\dot{S}$ is the rate of entropy production per unit surface area. Locally within the boundary layer, the entropy production rate per unit volume is given by

$$\dot{S}_v = \frac{1}{T} t \frac{dV}{dy} \qquad \text{Equation 2.8.2}$$

which can be interpreted as viscous shear work. This can be converted in to a dissipation coefficient defined by

$$C_d = \frac{T\dot{S}_a}{\rho V_d^3} \qquad \text{Equation 2.8.3}$$

The value of C_d is plotted for laminar and turbulent boundary layers in Figure 2.8.1 and indicates that at values of Re_θ greater than 100, laminar boundary layer produce less entropy that turbulent ones.

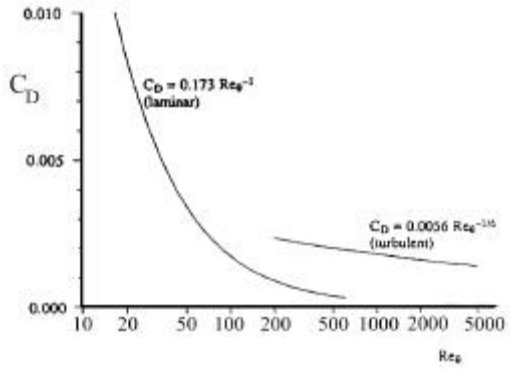

Figure 2.8.1 The variation of dissipation coefficient for laminar and turbulent boundary layers.

One can calculate the entropy production for the entire surface of a blade from

$$\dot{S} = \int_{LeadingEdge}^{TrailingEdge} \frac{r V_d^3 C_d}{T_d} dx \qquad \text{Equation 2.8.4}$$

This expression is difficult to use in practice when the boundary layer changes state along the blade surface. Highly loaded turbine and compressor blades will, in all likelihood, have separations of various sizes and severities. The chances of having accurate values of C_d for the laminar, turbulent, calmed and separated regions are unlikely. Attempting to predict unsteady flows compounds this difficulty.

Dawes (1990) describes the ability of two turbulence models to predict the flow in a compressor cascade and secondary flow in a LP turbine cascade. A mixing length turbulence model (Baldwin-Lomax) and is a one equation model for the transport of turbulent kinetic energy are used. The mixing length model produces a much smaller separation bubble than that produced by the transport model. Very little reverse flow was predicted with the mixing length whereas the transport model over predicts the size of the reverse flow region. Both models produce good predictions of the secondary flows in the LP turbine cascade. The position of the loss core is better predicted by the Baldwin-Lomax

model. The paper concludes that for separation bubble prediction the one equation bubble is preferable, not surprisingly as it can account for flow history. However, for loss prediction the better model was the mixing length. It therefore seems that for predictions of separation bubble flows the added complication of the transport turbulence models there does not produce significantly better results over the simple mixing length models. Adjustment of parameters in both turbulence models is required to fit experimental data. The secondary flow experiments and predictions of Moore and Gregory-Smith (1996) also showed that the low Reynolds number turbulence models did not produced much improvement in prediction over a mixing length model.

Dawes also showed that the loss generated at various heights through an attached boundary layer can be broken down as follows:

Region	Fraction of total loss produced
Sublayer	50%
Logarithmic	40%
Outer	10%

Table 2.8.1 Loss breakdown in a boundary layer

2.8.2 Loss generation with unsteady inflow

Hodson (1983) showed how the profile loss at midspan of a rotor of a turbine was 50% higher than the same blade profiles tested in a cascade with steady in flow. Hot film measurements were taken on the rotor and showed that the boundary layer was changing state in phase with the passage of the stator wake. The increase in loss was attributed to the extra surface covered in transitional boundary layer and was found to be largely independent of the rotor-stator axial gap.

Hodson (1989), introduced a new reduced frequency parameter which related the ratio of particle convection time to periodic time scales and specifically relating to the unsteady transition zone of the blade. The correlation takes the form

$$\frac{Y - Y_l}{Y_t - Y_l} = \begin{cases} 1 - \frac{1}{2}\frac{2p}{\bar{w}}; & \frac{\bar{w}}{2p} \geq 1 \\ \frac{1}{2}\frac{2p}{\bar{w}}; & \frac{\bar{w}}{2p} \leq 1 \end{cases}$$

Also included in Hodson's correlation is the effect of wake width and the effect of the spot leading edge propagation velocity on the variation of intermittency and reduced frequency, see Figure 2.8.2.

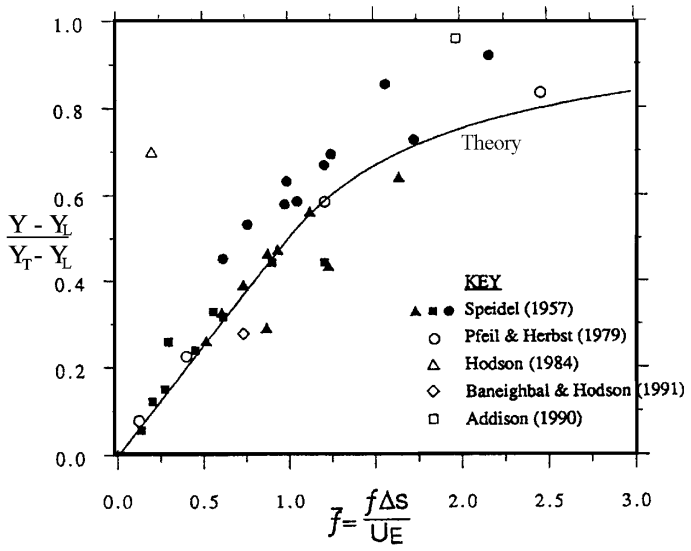

Figure 2.8.2 Loss verses reduced frequency correlation from Hodson (1985)

Schulte (1995) produced a loss model that accounted for the loss reductions that were measured in the highly loaded LP turbine that is used for the datum measurements in this thesis. The variation in momentum thickness for one wake passing cycle at the trailing edge of the blade is divided into a number of regions, namely the region due to the passage

of the turbulent part of the spot, the calmed region and the undisturbed region that would exists in steady flow. By varying the amount of time for which each regime exists, Schulte was able to predict the changes in loss that should occur as the reduced frequency of wake passing changes. An optimum frequency was also noted where the losses were minimised and compared favourably to measurements. This is illustrated as an ST diagram in Figure 2.8.3. The black wedge shaped region is turbulent flow caused by a turbulent spot. The differing leading and trailing edge velocities of the spot give rise to the wedge shape. The line marked AC is the trajectory of the rear edge of a calmed region, which is reported to travel at 30% of the local freestream velocity, Schubauer and Klebanoff (1955). For the case shown the end of the calmed region (ABCA) has reached the blade trailing edge, by the time the turbulent part of the next wake and spot has arrived at C. Schulte stated that this minimised the losses generated by minimising the amount of time that turbulent flow due to separated flow and reattachment existed.

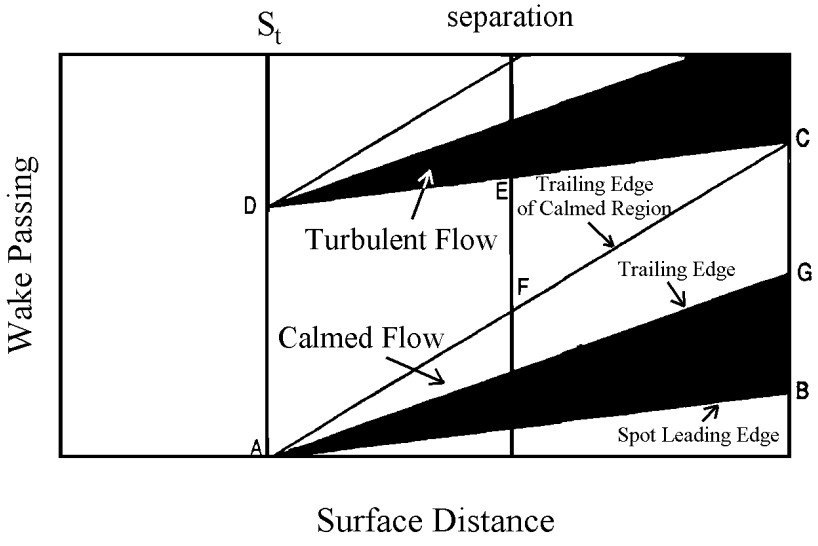

Figure 2.8.3 ST diagram illustrating Schulte's minimum loss hypothesis.

Wakes not only cause an increase in losses due to their effect on the boundary layer behaviour, but also in how they mix out. Deregel and Tan (1996) discuss how the effect of the mixing out of a rotor wake before or after a stator blade row effects the mixing loss and static pressure rise in a compressor. Smith (1970) showed that if the axial gap between rotor and stator was reduced from 37% chord to 7% chord a one percent increase in efficiency was recorded. In the 37% chord case the wakes were likely to be more mixed out than for the smaller rotor stator gap, decreasing the unsteady flow into the stator.

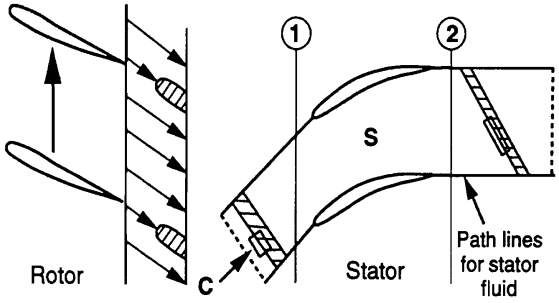

Figure 2.8.4 Wake stretching in a compressor.

Figure 2.8.4 shows an idealised wake interaction in a compressor stator. If one assumes an inviscid and incompressible flow, then the circulation around the contour ‘C’ is constant as the wake convects through the stator row. The wake increases in length as it convects through the stator row and the velocity difference between the wake and the freestream decreases. Since the velocity defect in the wake is now smaller when it mixes out the resultant loss will be reduced. In a turbine, the effect is reversed as the wake segment shrinks, increasing the difference in velocity between the free stream and the wake core. Deregel and Tan also noted an increase in static pressure rise when a wake is mixed out after the stator because of a reduction in the kinetic energy between the inlet and exit of the passage.

2.9 Secondary Flows and Transition

Transition investigations are usually concerned with the development of blade surface boundary layers, however Moore and Gregory-Smith (1996) investigated the transition effects on the end wall region of an HP turbine cascade. Figure 2.9.1 shows that the variation of measured intermittency on the end walls of the cascade indicating that the near fully turbulent inlet boundary layer re-laminarises near the trailing edge of the pressure side of the end wall. Excellent agreement between measurement and prediction of the three dimensional flow and loss core was obtained by using a simple mixing length turbulence model and the measured intermittency values.

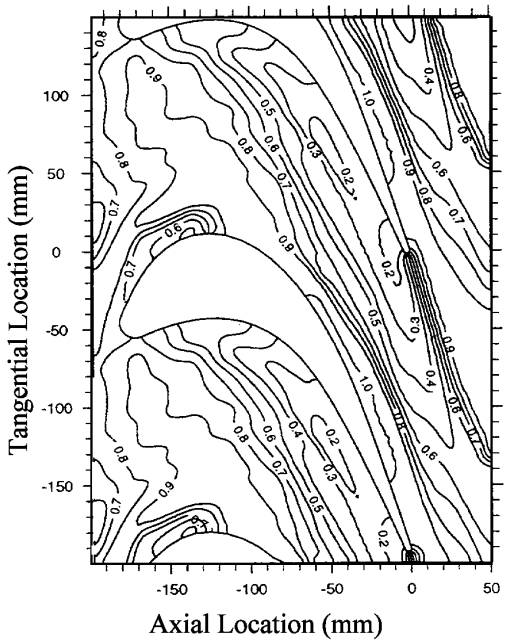

Figure 2.9.1 Intermittency measured on the end wall of a turbine cascade

Since this was a steady flow experiment wakes were not present. However, it would be of interest to find out whether or not wakes could suppress secondary flows and the losses they cause.

2.10 Engine economics

The economics of research into boundary layer transition in gas turbines was investigated by Wisler (1998). This shows that of all the components in an engine it is the LP turbine that has the biggest effect on specific fuel consumption. However, a 1% improvement in LP turbine efficiency would result in a saving of just $52,000 per year, per aircraft. A 1% decrease in direct operating costs would save over $200,000 per year. Direct operating costs include items such as fuel, airframe maintenance, landing fees, flight and cabin crew costs. Wisler concludes that improvements in transition modelling technology is unlikely to have a major impact on gas turbines. Reducing the number of components will however reduce both weight of an engine and have an impact on both production costs to the manufacturer and direct operating costs to the airline.

1% Change in Efficiency of:	Percentage change in Specific Fuel Consumption
Fan	0.62%
LP compressor	0.22%
HP compressor	0.66%
HP turbine	0.82%
LP turbine	0.96%

Figure 2.10.1 Component sensitivities for an engine at 35,000ft and M=0.8

2.11 Conclusions

This chapter has addressed some of the wide range of research that has been carried out in the field of wake separation bubble interaction particularly on the suction surfaces of LP turbines. It has demonstrated that the flow in LP turbine blade are highly unsteady and that the transition mechanisms are affected by the passage of wakes.

This review has also shown that little information exists on the interaction of separation bubbles turbulent spots and wakes. Since there is little information regarding

this interaction it is not surprising therefore that little progress has been made in the modelling of separated flow transition and wakes interaction as the process is extremely complicated. More information is required regarding the states of the boundary layer development (especially on high lift profiles) to advance the attempts at modelling the flows.

3. Experimental and Numerical Methods

3.1 Introduction

During the course of the research conducted for this thesis a number of experimental rigs and measurement techniques were used. These are detailed in this chapter. The measurements can be placed into two classes. Low speed measurement were carried out on rigs based at the Whittle Laboratory of the University of Cambridge. The high speed measurements were carried out in the ILA test facility at the Institut für Luftfahrtantriebe, Universität Stuttgart and in collaboration with BMW Rolls-Royce Gmbh.

3.2 Low Speed Experimental Facilities

3.2.1 Linear cascade and moving bar facility

The wind tunnel used for the cascade experiments had a total length of 11m and was driven by a centrifugal fan, see Figure 3.2.1.

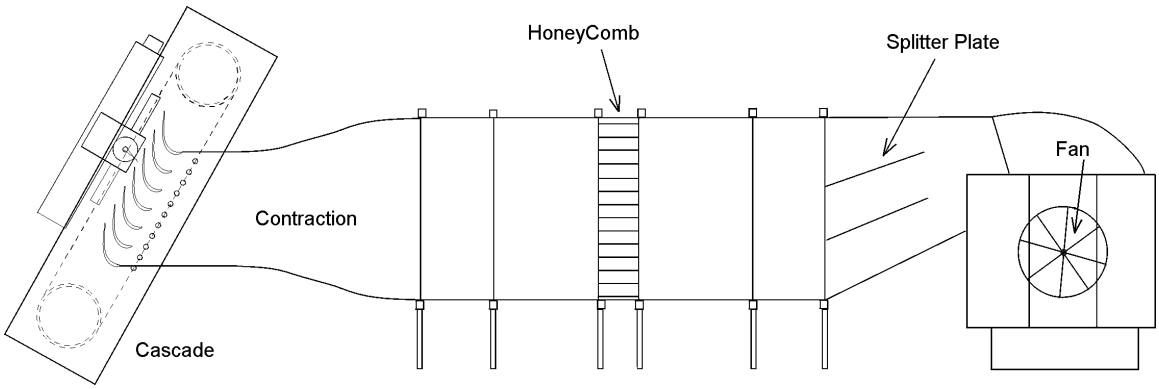

Figure 3.2.1 The wind tunnel used for the low speed experiments presented in this thesis

After the fan the flow is straightened by a honey comb mesh and made uniform by a number of gauzes. The total flow area reduces along the length of the tunnel, thinning the

boundary layers before the air arrives at the test section. With no turbulence grid in place the wind tunnel generated approximately 0.5% turbulence intensity.

The cascade of blades used for these measurements (designate TL10) are high lift designs and a summary of them is given in Table 3.1.

Number of Blades	7
Aspect Ratio	2.37
Chord	156mm
Axial Chord	134mm
Stagger	35.32° from axial
Inlet angle	-30.46°
Exit Angle	62.86°
Zweifel coefficient	1.05
Suction surface Length	195.7mm

Table 3.1 Characteristics of the datum profile TL10

Pfeil and Eifler (1976) showed that the structure of the far wake shed from a cylindrical bar has the same characteristics as that from an aerofoil. The passage of upstream blades row was therefore simulated by traversing bars upstream of the cascade leading edge. The bars moved in a plane 0.5 axial chord upstream of the cascade. The bars were carried on belts which were driven by a variable speed DC motor, see Figure 3.2.2

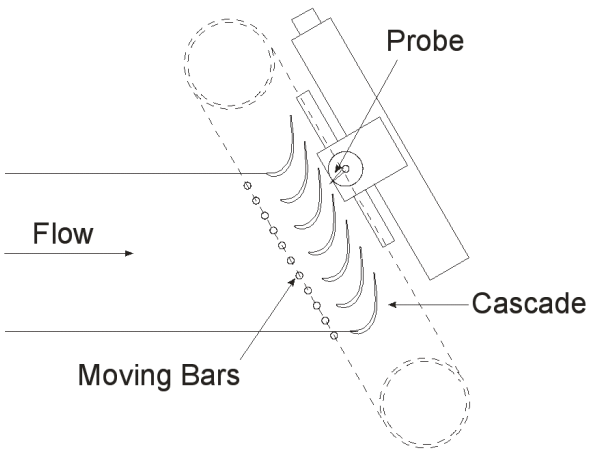

Figure 3.2.2 The moving bar cascade and traverse system, Curtis *et al* 1996.

The diameter of the bars were chosen so that the wakes they produced gave rise to the same loss as that generated by a typical LP turbine blade row. The bars used were 2.05mm in diameter, but for comparison purposes 4mm bars were occasionally used for some experiments. It can be shown that the total pressure loss coefficient for the bars is given by the following expression

$$Y_p = \frac{C_d D}{S_{bar} \cos b} \qquad \text{Equation 3.2.1}$$

where C_d is the drag coefficient of the bar at the bar Reynolds number and D is the bar diameter. The relative flow angle between the wake and the freestream is given by β. The value of β is determined by the reduced frequency and flow coefficient. The bar speed was set to produce a flow coefficient of 0.7 and the bar pitch set to give the same reduced frequency of 0.78, as found in the 1.5 stage model turbine environment of Banieghbal *et al* (1995). Both the flow coefficient and reduced frequency are defined in the nomenclature. The measured variation of turbulence intensity at the cascade inlet is shown in Figure 3.2.3. The peak value is 13%, while the minimum occurs between wake passings as is 0.5%.

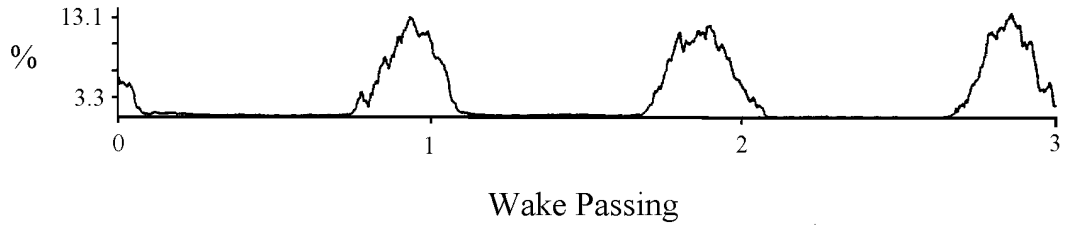

Figure 3.2.3 Measure turbulence intensity measure 0.1 axial chords upstream of the cascade leading edge. Generated by 2.05mm bars. Reynolds number=130,000, $\bar{f} = 0.78$, $\Phi = 0.7$.

The moving bars also accurately simulated the inlet turbulence intensity of an upstream blade row. Measurements showed that the bars produced a variation in inlet turbulence comparable to that at the inlet to a 1.5 stage large scale turbine with the same profiles, Banieghbal (1996).

More details of the simulation capabilities of the moving bar rig can be found in Schulte (1995). The inlet stagnation temperature was measured using a thermocouple placed within the inlet plenum. Although not specifically required for the measurements presented here, a Pitot probe placed downstream of the moving bars provided the reference cascade inlet stagnation pressure. There are however problems with measuring pressures downstream of the moving bars with a steady measurement system, Schulte (1995). In the current context, measurements of momentum thickness at the trailing edge of the profiles and not total pressure was used to gauge boundary layer losses, see section 3.6.1.

A three axis traverse system, driven by stepper motors, was used for moving probes around the blade passages. The stepper motors were controlled by a DIGIPLAN (type CD25) controller linked to a PC computer. Each stepper motor required 200 steps for one complete revolution and when attached to a 1mm thread, this gives a spatial resolution of 50μm per step.

3.2.2 Cascade and Flap Experiments

To explore a number of pressure distributions for their performance with steady and unsteady inflow, a flap was added to the blade below the one instrumented with static pressure tappings, see Figure 3.2.4. As the flap was rotated around the trailing edge of the blade to which it was attached it alters the effective exit area of the blade row above. Obviously, the cascade is no longer periodic, but since it is only the suction side

distribution that is of interest this does not matter. This technique allows production of pressure distributions with different lift coefficients. Details of how to treat the data obtained from this flap modified cascade can be found later in this chapter. In addition to the flap, a number of inserts were placed into the blade passage as shown in the same figure and these were used to alter the position of peak suction on the blade surface.

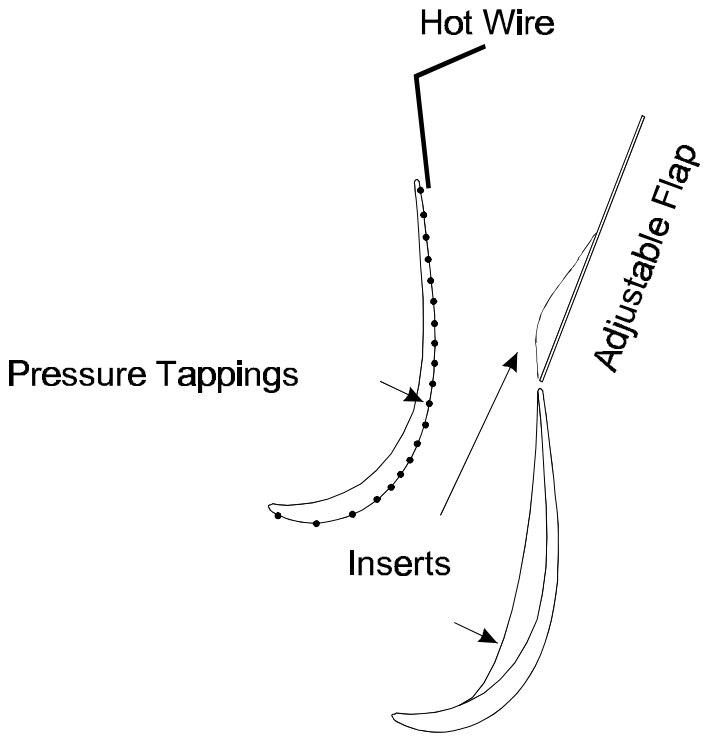

Figure 3.2.4 The flap and inserts used to alter the pressure distribution of the instrumented blade.

3.2.3 Flat Plate Rig with Turbulent Spot and Moving Bar Wake Generator

A flat plate rig was designed to allow a number of pressure distributions to be set up with ease for more detailed investigations of the most interesting profiles produced with the flap tests. This was achieved by using mechanisms designed by the author to allow the vertical position of a flexible wall above the flat plate to be varied. Figure 3.2.5 shows a schematic of this rig. A slot was made in the flexible wall to allow probe traverses of the

boundary layers along the plate surface. This rig has a traverse system with two degrees of freedom, allowing the boundary layers to be traversed at one spanwise location.

Chord	550mm
Thickness	30mm
Leading edge major minor axis ratio	3
Bar diameter	7mm

Table 3.2 The main characteristics of the flat plate rig.

A perforated sheet of metal was used for the top wall. Much of the perforated area was masked off with adhesive backed plastic sheet. Areas where the flow diffuses were not masked. This allowed suction to be applied to the top of the test section which drew off air from the boundary layer on the flexible wall stopping that boundary layer from separating. This allowed large diffusions to be applied to the lower surface.

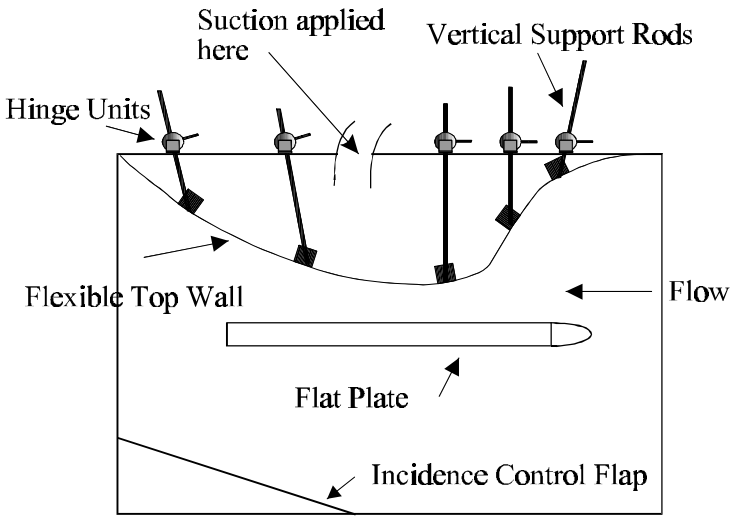

Figure 3.2.5 The flat plate rig with flexible upper wall and incidence control flap

The rig also included a flap to control the incidence of the flow on to the plate. The angle of the flap was set by using a smoke generator placed just upstream of the inlet to the test section. The control flap was adjusted until the smoke was observed to have a zero incidence with the flat plate. This was the only method of ‘measuring’ incidence as there

were no pressure tappings on the leading edge of the plate. This is not a very accurate method of setting the inlet flow incidence, but a few degrees of incidence does not have a large effect on the suction surface pressure distribution. In addition, only qualitative information was required from this rig so the method of incidence set up was thought adequate. Some numerical experiments showed that no separation would occur until the inlet flow was at up to ±5° incidence.

The flat plate (with a chord of 0.54m) was designed to give a large and easily accessible cavity into which instrumentation could be placed. The elliptical leading edge had a major to minor axis ratio of 3.0 which ensures little or no separation as the flow encounters the discontinuity in curvature moving from the curved leading edge region to the flat surface.

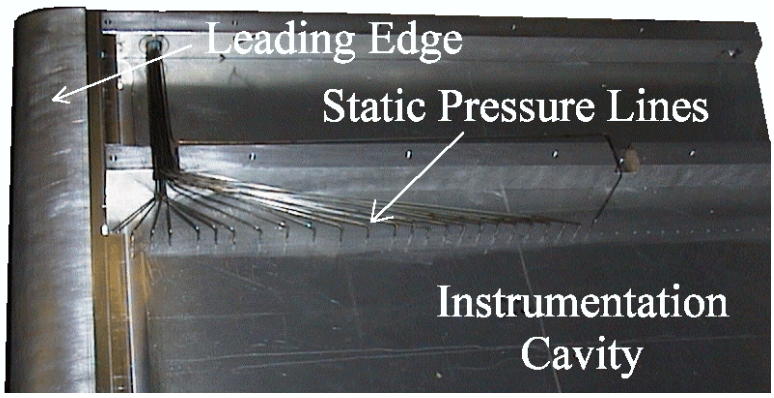

Figure 3.2.6 Instrumentation cavity of the flat plate.

A loudspeaker was placed into the cavity of the plate and was used to generate turbulent spots in the boundary layers, see Figure 3.2.6. The spots are generated by the diaphragm of the speaker moving towards the underside of the plate causing a small amount of air to issue from the hole in the plate surface and into the boundary layer above. It was found that spots could only be generated reliably by using a 12W loudspeaker.

Increasing the power of the loudspeakers increases the size of diaphragm and therefore mass ejected.

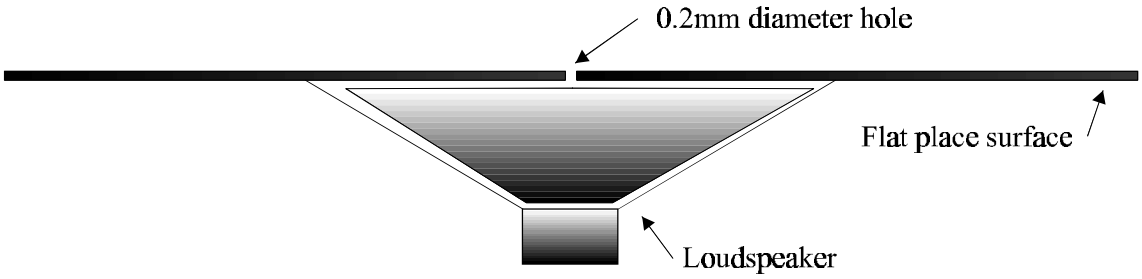

Figure 3.2.7 Loudspeaker below the flat plate

Exciting a boundary layer requires that the disturbance ideally contains a wide band of frequencies. Although boundary layers will amplify disturbances (i.e. will become unstable in the presence of) particular frequencies, those frequencies will probably not be known at the time of the experiment since the boundary layer velocity profile has not been measured. It is therefore easier to excite the boundary layer with a broad band of frequencies by using a short duration pulse. If the disturbance is not of sufficient strength then the disturbance will simply be dissipated (through viscous shear) within the boundary layer. Once the disturbance is sufficiently large it will be amplified and develop causing the boundary layer to undergo transition. To obtain the required amplitude of the disturbance the loudspeaker was driven by feeding the pulse generator signal to a power amplifier. The limit on the pulse duration was set by the frequency response of the loudspeaker. Most of the loudspeakers had a frequency response up to about 15kHz, which implies that the diaphragm can travel towards and away from the plate in a minimum time of approximately 0.12ms. In practice the boundary layer responded best (i.e. consistently formed turbulent spots) with a pulse duration of approximately 4ms.

The inlet stagnation temperature and pressure were measured in the same manner as for the cascade tests and flap tests.

3.3 High Speed Experimental Facilities

High speed measurements were carried out in a full scale cold flow rig based in a facility at the Institute for Aerodynamic Research at the University of Stuttgart in Germany. Measurements were carried out at five Reynolds numbers which simulated conditions from takeoff, to cruise and then to the maximum altitude at which the engine would be flown. Since a great deal of data was measured only the most interesting parts of that data are presented in Chapter 4 to save space. Hot film measurements were taken on two LP turbine designs, one set of measurements from the three stage LP turbine on the BRR 715 turbofan engine and the other from the LP turbine in a redesign of the BRR 710 engine. More of the details of these turbines is given in Chapter 4 where the results are also discussed.

3.4 Thermal anemometry

The anemometer bridges used with the hot films and hot wires were Dantec units, type 56C17. The main units were of type 56C01. The AC and DC coupled signals were logged separately, so that a maximum gain could be applied to the AC signal giving maximum signal resolution. The AC signals and time mean of the DC signal were then re-combined in software to produce the complete raw signal. The AC signals were band pass filtered with a Dantec signal conditioning unit (type 55N22). The low pass filter was set to 100kHz and the high pass filter set to 1Hz during the high speed measurements in Stuttgart and the data was acquired at a rate to 125kHz which is maximum logging rate of that data acquisition system. A DC signal was provided from the unconditioned raw output on the bridge. The Nyquist folding criteria for the data digitisation is taken care of due to

the role off of the frequency response of the hot film sensors which occurs at approximately 30kHz. This is very much less than half of the logging frequency.

The AC data for the low speed measurements were acquired at a rate of 20kHz and the low pass filter setting on the signal conditioning unit was set to 10kHz, while the high pass filter was set to 1Hz. The low pass filtering was set to one half of the logging frequency so ensure that the Nyquist data folding criteria was observed.

3.4.1 Measurements using Hot Wires

A Dantec single-wire boundary layer probe (type 55P15) was used for the boundary layer traverses. The hot wires were calibrated in a low turbulence calibration wind tunnel according to Kings Law

$$E^2 - A = BV^n \qquad \text{Equation 3.4.1}$$

where A, B, and n are calibration constants. The heat transfer from the hot wire to its surroundings is affected by the presence of walls and a correction (Hodson 1985) has been applied to the data taken from the cascade rig. Other corrections are available, but these make assumptions about the state of the boundary layer, for example using the Blassius profile to correct laminar boundary layers. For a given streamwise location, the boundary layers on the rear portions of LP turbines can be laminar, calmed, turbulent or separated at different time. Therefore the use of these sorts of corrections is not possible.

Due to the long run times, changes in ambient temperature were taken into account using the correction due to Bearman (1971). It should be noted that the hot wire probe was calibrated in a low turbulence *suction* wind tunnel, but the wire was used in a *positive* pressure tunnel. The work input to the air in the wind tunnel as it passes through the fan increases its temperature so the temperature where the probe is calibrated is different to

that at which the measurements are made. This is also taken in to account with the Bearman correction.

In the cascade, hot wires traverses were made near the blade trailing edge (typically at 96% surface length). Up to 30 positions through the boundary layer were measured, depending on the height of the boundary layer in the cascade rig. Because of the separation bubble, one cannot accurately predict the height of the boundary layer near the trailing edge on the pressure distributions created by the flap. It was therefore often necessary to oversize the height of the traverse to make sure that the whole of the boundary layer was covered out to the free stream. If the boundary layer was much thinner than the traverse height, the condition would be measured again with a more appropriate traverse height. This increased measurement times but ensured that maximum resolution was obtained in the measurements. Boundary layer surveys were also carried out on the flat plate rig at various streamwise positions.

When carrying out hot wire traverses, it is necessary to find the position at which the prongs of the hot wire probe touch the surface being traversed. This was carried out by manually stepping the probe towards a surface until an electrical contact was made. Once at the zero height position a magnifying glass was used to ensure that the hot wire was parallel to the surface. If the probe was not parallel to the surface the probe would be stepped away from it and manually rotated. The probe would again be stepped towards the surface and checked for parallelism again. This procedure would continue until the probe was parallel to the surface. If a hot wire is not parallel to a surface then different parts of the wire will experience different flow velocities according to the height they are within the boundary layer. The velocity profile in the layer is non linear (except in parts of the calmed region, Cumpsty *at al* (1995)) and therefore non-linear averaging of the profile will take

place. Problems caused by this averaging are more likely to be acute in thinner boundary layers on the cascade than on the flat place rig where the boundary layer heights were much larger.

3.4.2 Measurements using Hot Films.

The measurement of wall shear stress using hot film sensors was developed by Bellhouse and Schultz (1966) and is now a well established technique. The operation of hot film sensors relies on the similarity between the velocity boundary layer and the thermal boundary layer generated by a hot film sensor. The heat transfer (consisting of conduction into the substrate, radiation and convection) from the hot film gauge (Q) is related to the bridge output voltage (E) as shown below

$$Q \propto E^2 \propto \text{temperature difference between the air and sensor}$$

The relation between the wall shear stress and the heat transfer by convection to the fluid takes the form

$$t_w \propto (E^2 - A^2)^3 \qquad \text{Equation 3.4.2}$$

where t_w is the wall shear stress, E is the output voltage, and A is a constant.

It is possible to calibrate hot films, but this is a difficult and time consuming process, Hodson (1983). Also, errors of 20% or more can arise when hot films are calibrated in a laminar flow are used in a turbulent flow, Davies and Duffy (1998). The hot film sensors were used on the aft part of the suction surface were likely to see laminar, turbulent and separated flow at different positions of the upstream rotor, so the proper calibration would be extremely difficult and quite probably impossible. However, meaningful information can be obtained by assuming that the constant A, in the above

expression, is equal to the bridge output under zero flow conditions, denoted E_0. The above expression is re-cast in non-dimensional form as quasi shear stress

$$t_w \propto \left(\frac{E^2 - E_0^2}{E_0^2} \right)^3 \qquad \text{Equation 3.4.3}$$

The effects of variations in the gauge and surrounding air temperature is reduced by casting the shear stress in the form of equation 3.4.3. Since the gauges were operated at constant temperature rather than constant overheat, if the temperature of the air changes so did the value of the zero flow voltage. This is because E^2 and E^2_0 are proportional to the temperature difference between the surroundings and the hot film sensor temperature. Zero flow voltages must therefore be measured at the same air temperature as the flow voltage E.

Three hot film designs were used for the measurements presented here and were all manufactured by DANTEC. A standard hot film design (type 55R47) was used for the low speed measurements. The high speed measurements were carried out on full size LP turbine blades, with chords of the order of 20mm. One of the specifications for these measurements was that as many sensors as possible should be used on the blade suctions surfaces after peak suction to the trailing edge. New sensor arrays were designed by the author for this task and are shown in Figure 3.4.1.

The values of the zero flow voltages are dependent on the blade metal and local air temperatures. During the zero flow calibration of the NGVs at the Whittle Laboratory, every possible measure was taken to minimise these difference in the calibration oven. Inevitably though, there are likely to be some differences in these temperatures.

The hot film arrays were mounted on the blade suction surfaces using M-BOND610 adhesive, in such a way that the final sensors were as close to the trailing edge

of each blade as possible. They are shown mounted on their blades in Figure 3.4.2 and Figure 3.4.3.

When conducting measurements in an industrial environment it is necessary to simplify all possible aspects of the measurement system so that trouble shooting can be accomplished as easily as possible. All the instrumentation must function correctly and first time as the cost of running the rigs are so high that re-running different conditions is not possible. One of the most important sensors in these tests was the final sensor on the blade surface. If the acquisition channel for this sensor failed it would be necessary to reconnect it quickly to another channel which might be deemed to be less important. To do this it would be necessary for the two hot film sensor and lead resistances to be similar. The resistance of the leads also had to be as low as possible so that the maximum overheat could be applied to the sensor without reaching the limit of the anemometer system. The final and most important reason for the constant resistance of the leads is that if everything else is same then there are no variations to be concerned with regarding the lack of calibration of the sensors.

The array design used for NGV2s of both the 710 and the 715 LP turbines is shown in Figure 3.4.1. The angled part of the leads are not of constant length so that the hot film sensors could be placed just 1.5mm apart in the streamwise direction. This was required so that a streamwise split could be made in the film near the first sensor so as to allow the 2-dimensional film to be placed onto the 3-dimensional surface of the blade. This arrangement gives rise to variable lead width and angle so a method of calculating the lead resistances is required. It is possible to show that the total resistance of the angled part of a lead is given by

$$R_{total} \approx r \ln\left(\frac{W_2}{W_1}\right)\left(\frac{l}{\cos a\,(W_2 - W_1)}\right) \qquad \text{Equation 3.4.4}$$

where W_1 and W_2 are the widest and narrowest part of the lead respectively. The resistivity of the lead is denoted by r per unit area, a is the angle between the horizontal and the lead centre-line and l is the length of angled part of the lead.

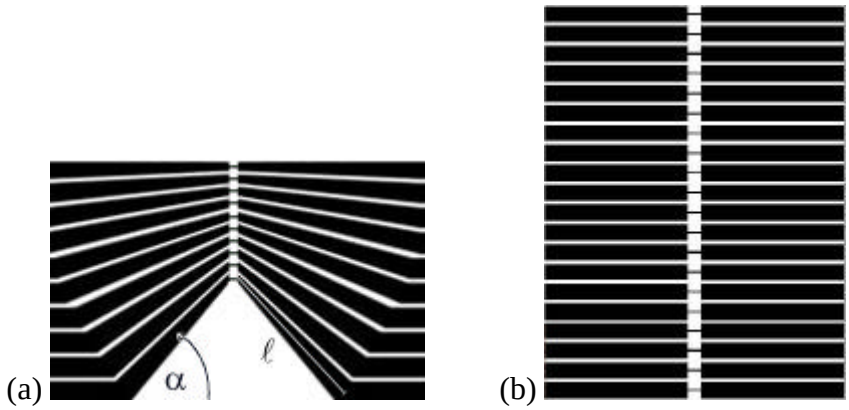

Figure 3.4.1 The hot film mask showing the sensor array used for instrumenting (a) the 710 NGV and NGV2 of the 715 LP turbine. Sensor (b) was used for NGV3 of the 715 LP turbine. The flow direction is from the bottom of the figure to the top.

The specifications for these measurements required that the sensors were to be spaced 1.5mm apart over the NGV suction surfaces from approximately 50% chord to the trailing edge and at 40% span for the 710 and 50% span for B715. Due to problems associated with adhering the film to the curved blade surface and curing the adhesive, 4 sensors failed on the BR710 NGV film. All the sensors on NGV3 of the BR715 were functional, but a number failed on NGV2 because of short circuits. Due to extreme time constraints during the preparations for the project it was not possible to correct the faults. However analysis of the data does not seem to be hampered to any great extent by these failures.

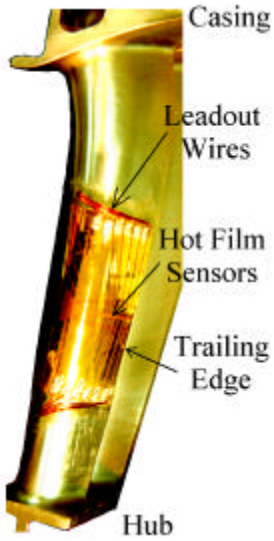

Figure 3.4.2 NGV2 segment of the 710 LP turbine with leadout wires.

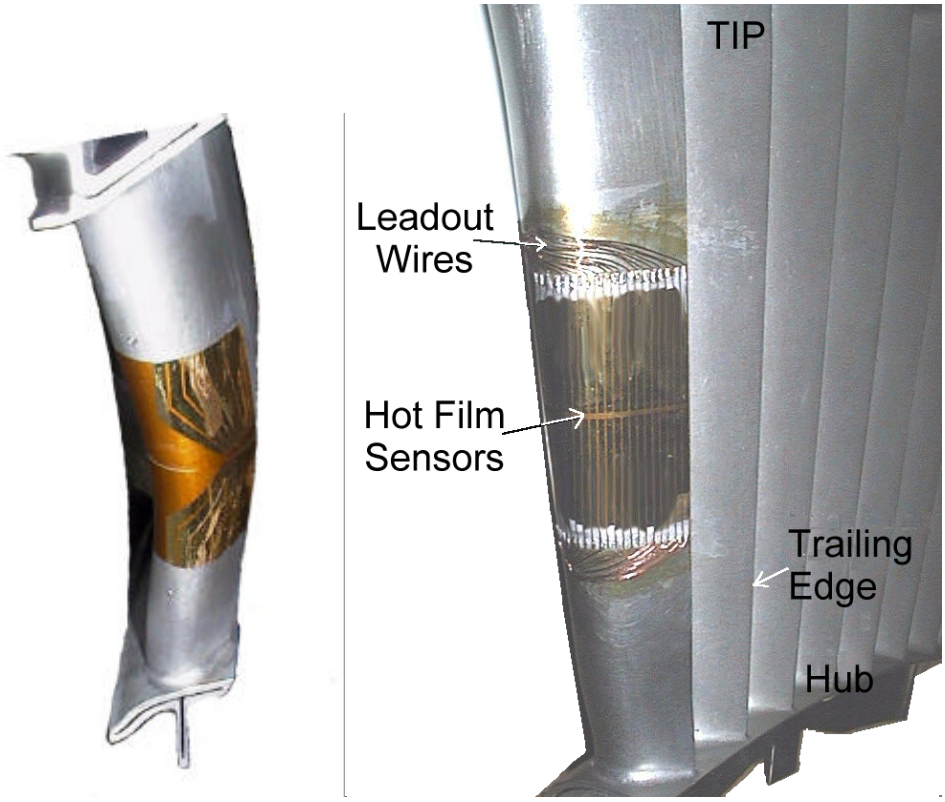

Figure 3.4.3 NGV2 (without leadout wires) and NGV3 (with leadout wires) from the B715 LP turbine.

3.4.3 Over heat ratios and frequency response

The overheat ratio is defined as

$$Over\ Heat\ Ratio = \frac{R_{hot}}{R_{cold}} \qquad \text{Equation 3.4.5}$$

where R_{hot} is the resistance of the sensor (wire or film) at the overheat temperature, and R_{cold} is the resistance of the sensor at the flow temperature. Using the highest possible overheat ratio ensures the highest frequency response from the system. The frequency response of the films and wires were further optimised with a square wave test signal that was available from the anemometer bridges. For hot wires, an over heat of 1.8 was used, while this value was 1.5 for the hot film sensors. The temperature of a sensor can be calculated with knowledge of its thermal coefficient of resistivity, α from the following formula

$$T_{hot} = T_{amb} + \left(\frac{R_{hot}}{R_{amb}} - 1\right)\frac{1}{a} \qquad \text{Equation 3.4.6}$$

Typical values (for a hot film sensor) for α are 0.001, while the values of R_{hot}, and R_{amb} are 16 and 12Ω respectively. T_{amb} is approximately 20°C, which results in a hot temperature for the sensor of approximately 300°C for a film. Higher temperatures still are obtained for hot wires (because of the higher overheat ratio used) means that wires are also prone to oxidisation which eventually invalidates their calibrations. This oxidation effectively puts a limit on the over heat ratio possible, but the other limit on overheat ratio is that the sensors could melt if they get too hot!

3.5 Pressure measurement

The pressure measurements were carried out using a DRUCK type PDCR-22 (35mbar) differential pressure transducer. This is a differential pressure transducer where the inlet total pressure to the low speed rigs was used as a reference. The pressure lines that ran from the pressure tappings on the rig to the pressure transducer were made from plastic with an inside diameter of 1mm. The pressure lines were linked to the transducer via a computer controlled SCANIVALVE switch. The signal from the pressure transducer was sent to the data acquisition system and then to a PC computer where it was converted into a pressure with a previously obtained calibration. An average of 500 samples taken over a period of two seconds was used to determine the average pressure reading for each pressure tapping.

With the trailing edge flap fitted to one of the blades, the cascade is not periodic and the downstream static pressure is no longer representative of the exit flow conditions. A more representative choice was the static pressure from the last pressure tapping on the suction side of the blade. Blade static pressures are presented in the form of the pressure coefficient shown below

$$C_p = \frac{P_{01} - P_{surface}}{P_{01} - P_X} \qquad \text{Equation 3.5.1}$$

where P_x is the blade static pressure tapping at 96% suction surface length for the cascade (flap) tests when the flap was being used or the cascade exit static pressure when no flap was present.

3.6 Data Presentation.

3.6.1 Loss and Momentum Thickness

The momentum thickness of the trailing edge boundary layer (obtained from the measured velocity profiles) was used to calculate the equivalent profile loss of the suction surface boundary layer. This profile loss was calculated using the relationship

$$\Delta P_{0\,profile} = \frac{2q}{S\cos a} \qquad \text{Equation 3.6.1}$$

Denton (1995). In the derivation of this expression Denton obtained additional terms for losses due to the pressure side boundary layer, base pressure losses and losses due to blockage. These extra terms have been dropped from the expression as we are only interested in the suction side profiles. It is possible to assume constant values for the other terms but this poses difficulties. The values are likely to change with changing suction side profiles but it is unknown exactly how they would change. Assuming that the values are constant with changing suction side profiles will simply dilute the effect of gains in performance that will be shown in Chapter 5 because the efficiency gains become a smaller part of the total losses. It was therefore decided to calculate the suction side losses only.

The trailing edge momentum thickness is defined in the usual way as

$$q = \int_{y=0}^{y=d} \frac{u}{U_d}\left(1 - \frac{u}{U_d}\right) \qquad \text{Equation 3.6.2}$$

and was obtained from the hot wire measurements made at 96%s.

3.6.2 Calculating Blade Loading - equivalent pitch

When the trailing edge flap is used to alter the original pressure distribution, the actual pitch of the cascade was no longer meaningful. To obtain the equivalent pitch of a

blade that would result in the modified pressure distribution produced by the flap, it was necessary to measure the suction surface pressure distribution. The pressure distribution (i.e. loading) was then converted into the pitch of an equivalent cascade. Since lift is proportional to the circulation, i.e.

$$Lift \propto \oint V ds \qquad \text{Equation 3.6.3}$$

where V is the measured blade surface velocity and ds is the distance between pressure adjacent tappings. Once the loading and pitch for the datum cascade are known, it is possible to calculate the pitch of an *equivalent* cascade from the following expression

$$\frac{Pitch}{DatumPitch} = \frac{\int_{Suction} \frac{V}{V_{te}} \frac{ds}{S_{\max}} - \left(\int_{\text{Pressure}} \frac{V}{V_{te}} \frac{ds}{S_{\max}} \right)_{Datum}}{\left(\int_{Suction} \frac{V}{V_{te}} \frac{ds}{S_{\max}} - \int_{\text{Pressure}} \frac{V}{V_{te}} \frac{ds}{S_{\max}} \right)_{Datum}} \qquad \text{Equation 3.6.4}$$

where S_{max} is the total surface length and the subscripts ‘ indicate that the integral is performed along the pressure side or suction side of the blade from leading edge to trailing edge.

3.6.3 *Ensemble mean data*

The ensemble mean (or phase locked average) of a quantity is found by taking an average of the signal at a fixed time past the trigger pulse and over a large number of periods. The phase (or time) is measured with reference to that trigger pulse. The ensemble mean of a quantity is defined as

$$\tilde{x}_w(t) = \frac{1}{N} \sum_{n=1}^{N} x_w(t)_n \qquad \text{Equation 3.6.5}$$

where t is the time from a once-per-revolution trigger signal and x could be velocity, shear stress etc. Once per revolution triggers were available from the moving bar rig by using a magnet placed into the belt which carry the wake producing bars. The passage of the magnet is picked up with a Hall effect sensor. The small voltage change from this sensor was fed to the comparator unit in the data acquisition system which fed a TTL signal to trigger the capture system. The high speed measurements used an optical device that supplied a TTL signal directly from the rotor shaft of the LP turbine. The number of ensembles required to average out the aperiodic fluctuations differed for each rig. It was not possible to carry out any test measurements to optimise the number of ensembles required for the high speed measurements, so 200 ensembles were taken. This was found to give good ensemble data, but perhaps it would have been possible to have less. The hot film measurements at low speed required 100 ensembles, whereas measurements with hot wires required about 150.

3.6.4 Ensemble RMS data

The ensemble root mean square (RMS) of a signal at a particular phase or time shows the amount of deviation (positive or negative) from the mean of that signal at that phase (or time past the trigger signal). The ensemble RMS represents the modulus of the deviation, so it does not distinguish between positive and negative deviation from the mean. When considering hot film data a high value of RMS is representative of a transitional boundary layer. In the transition region, the highest value of RMS is usually found where transition is approximately 50% complete, since the signal is swings equally between laminar and turbulent values of shear stress. This is because the change of level of τ_w associated with a change of boundary layer state is much larger than the changes of amplitude of the turbulent fluctuations in a signal.

The ensemble RMS is defined as

$$\tilde{x}(t) = \sqrt{\frac{1}{N}\sum_{n=1}^{N}(x(t)_n - \bar{x}(t))^2} \qquad \text{Equation 3.6.6}$$

where t is the time from a once-per-revolution trigger signal and $\tilde{x}(t)$ is the ensemble mean at that time.

3.6.5 Ensemble Skew data

The ensemble skew of a signal distinguishes the positive or negative deviation of the signal at a particular time from the mean of the signal at the same time. With hot film measurements, the skew of a signal is useful for detecting how far the boundary layer has progressed through transition (see Hodson, 1984). If a boundary layer is completely laminar then the skew of the signal will be near zero. If it is predominately laminar with the occasional turbulent component then the skew of a signal will be small, but positive. Where the RMS is maximum (at an intermittency of approximately 50%) then the skew would be approximately zero. As the signal becomes turbulent with a smaller laminar component the skew becomes negative. As the boundary layer becomes completely turbulent, the skew of a signal once again approaches zero. It is a characteristic of hot film gauge signals from transitional flows, that the positive skew, early in transition, is more obvious than the later negative skew.

Skew is defined as

$$s(t) = \frac{\frac{1}{N}\sum_{n=1}^{N}(x(t)_n - \bar{x}(t))^3}{\tilde{x}(t)^3} \qquad \text{Equation 3.6.7}$$

3.7 Data Acquisition Systems

Two data acquisition systems were used for the research presented in this thesis. The high speed hot film measurements in Chapter 4 and the cascade and cascade 'flap' measurements described in Chapter 5 used a MICROLINK transient capture system. This allows up to 24 channels to be logged simultaneously with high speed 12 bit analogue to digital converters (CH12B units). Each channel was capable of storing 4096 samples at a capture rate of up to 125kHz. The data stored in each channel was then downloaded to a PC compatible computer for processing. This system therefore allowed the simultaneous logging of the signals from up to 24 hot film gauges used in the high speed measurements. The MICROLINK system also contains other instrumentation cards, including a frequency counter and a multiplexed data acquisition card (the PGA16) allowing 16 channels of data to be logged on a single card. The PGA16 is used for logging pressures at a low sampling frequency. Since it is multiplexed logging all 16 channels occurs at a lower frequency than is possible with a CH12 unit.

A newer data acquisition system based on the National Instruments NiDaQ PC card was used for the flat plate rig experiments presented in Chapter 7. The NiDaQ system allows the simultaneous logging of up to 16 analogue channels, again with 12 bit accuracy. As stated above, a total of 25 hot film channels were required for the high speed measurements so the MICROLINK system was used in preference to the NiDaQ system. Because the NiDaQ system is multiplexed, its frequency response when logging all 16 channels is below that of the non-multiplexed MICROLINK system. The high speed measurements required the fastest possible logging frequencies for each channel, which also ruled out the NiDaQ system at that time.

The NiDaQ system, like the MICROLINK system provides for a number of programmable digital outputs lines and these were used to control other devices such as the Scanivalve used for the pressure measurements.

3.8 The UNSFLO code

The current approach to modelling transitional boundary layer flows uses the well tested inviscid-viscous 2D solver UNSFLO, Giles (1990). This code solves a structured 'C' mesh around the blade profile for the viscous boundary layer region and a structured or unstructured mesh in the inviscid region. An example of a typical mesh can be seen in Figure 3.8.1

A full description of the code's prediction abilities can be found in Giles (1990). The code can predict separation bubbles and has a number of turbulence models available, including a mixing length or eddy viscosity model.

The UNSFLO code has been modified to allow the eddy viscosity as calculated by the algebraic (Baldwin-Lomax) turbulence model to be weighted by an intermittency, Coupland (1998). Additional changes have been made by the author. This approach is similar to that used by Schulte (1995) and Schulte and Hodson (1997).

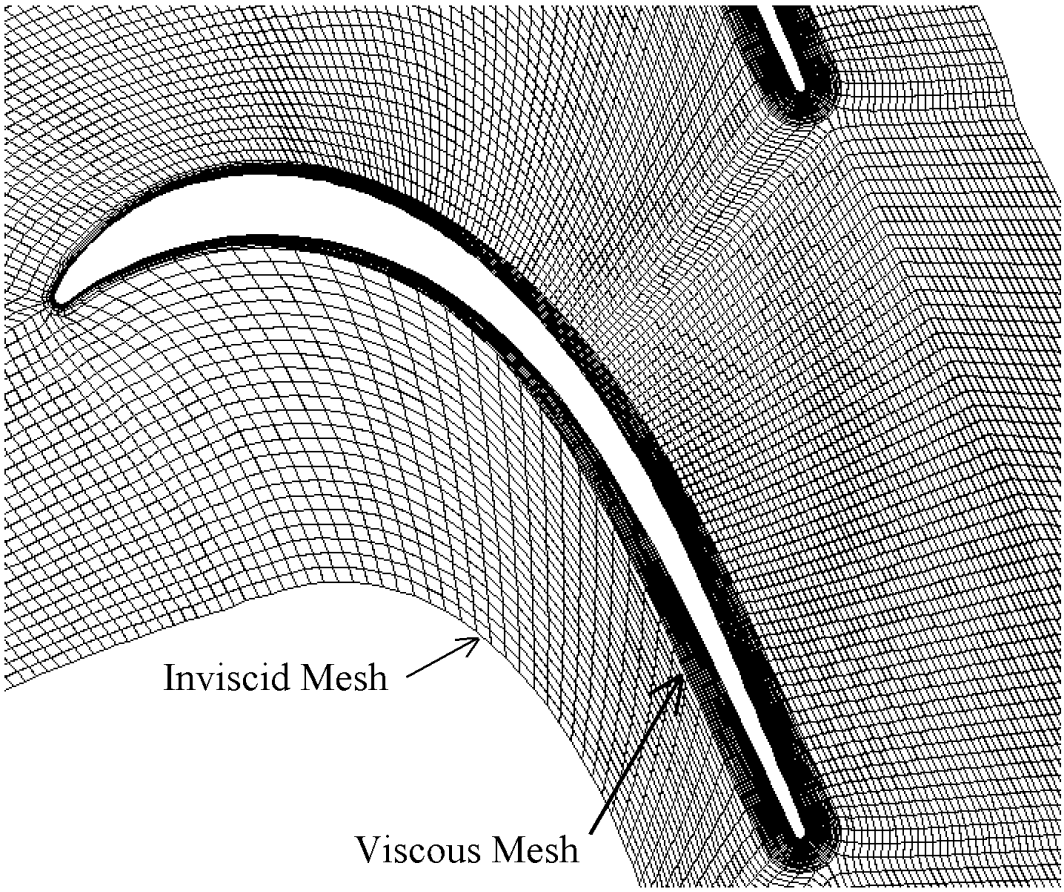

Figure 3.8.1 A typical UNSFLO inviscid and viscous mesh.

3.9 The Prescribed Unsteady Intermittency Calculation Method

Schulte and Hodson (1999) developed a fairly general routine for the calculation of the unsteady intermittency, naming it PUIM ('Prescribed Unsteady Intermittency Model'). This series of routines calculate an ST diagram of intermittency by integrating the dependence volumes described by Emmons, (1955). The effects of calming are also included, Schulte (1995). Spot production rates are calculated from correlations that include the effects of the variation in pressure gradient and freestream turbulence level, Mayle (1990), Abu-Ghanham and Shaw (1980). Transition onset correlations are also available and are used in the same manner as discussed in section 7.2.1. The variation of freestream turbulence intensity at inlet to the blade row is required as an input to the

intermittency code. The variation of freestream turbulence within the blade passage can be calculated by assuming frozen turbulence or frozen turbulent kinetic energy. The latter option has been employed for the work presented here, where the turbulence level is assumed to be inversely proportional to the local freestream velocity. The code requires knowledge of the steady flow pressure distribution of the blade profile under investigation as this provides the pressure gradient information. A question arises as to whether an inviscid or viscous solution should be used for this purpose. The viscous solution can contain the constant pressure plateau caused by the separation bubble. Whereas the inviscid (or a fully turbulent) solution will not have any separation. The absence or not of the pressure plateau will cause changes in the propagation velocities of the spots in that region. It will be shown in Chapter 6 that turbulent spots seem to travel through separation region almost as if it is not there. In other words, as far as the propagation velocities of the spot are concerned, the spot does not seem to see the pressure plateau and travels as if doing so according to the inviscid pressure distribution.

4. High Speed Hot Film Measurements.

4.1 Introduction

This chapter describes the results of surface mounted hot film measurements from NGV2 of the BMW Rolls-Royce 710-48 LP turbine and from both NGV2 and NGV3 of the BMW Rolls-Royce 715-58 LP turbine. The BR710 engine is a 15,000lbs thrust class engine with a two stage LP turbine. It has only recently entered service with the Gulfstream 5 business jet. The BR715 is a 22,000lbs thrust engine with a three stage LP turbine that will soon enter service on the new Boeing 717-200, (previously the MD-95). Table 5.1 shows some additional details regarding these engines.

The measurements were carried out during the tests in the ILA Test Bed at the Institut fur Luftfhartantriebe, Universitat Stuttgart, Germany.

Engine	BR710-48 Turbo Fan Engine	BR715-58 Turbo Fan Engine
Fan	48 inch wide chord fan	58-inch wide chord fan
Stages on the HPC	10	2-stage booster (on LP spool) 10-stage HPC
Stages on the LPT	2-stage LPT	3 stage LPT
Design conditions	Ma ~ 0.8 at 45000ft	Ma ~ 0.76 at 35000ft
Reynolds number at cruise	> 40,000	> 80,000
Comments	LP turbine profiles are relatively low lift as found in Trent 800.	LP turbine profiles are high lift TL10 style

Table 4.1.1 Some characteristics of the BRR 700 series of turbofan engines.

The opportunity to take boundary layer measurements in a real engine, albeit with cold inflow, is of use for several reasons. The first is that one gains an insight into the flow in real engine components with less of the abstraction found in low speed experimental rigs. It is also possible to validate the approach of low speed experimental investigations and check that they faithfully reproduce the flow physics for which they were designed.

The measurements were carried out on behalf of BMW-Rolls Royce so as to validate their design approach for high lift blading. These turbines represent the current state of the art as they incorporate some of the latest design methodologies. Information regarding the flows in multistage environments will also be described which gives rise to ways in which the unsteady effects of wakes may be used to further improve performance of the low pressure turbine which is the objective of Chapter 5. As well as presenting new data and analysis, the results presented in this chapter give a datum for the thesis.

4.2 Discussion of the Results

The industrial environment in which these tests were carried out allowed few detailed experimental measurements, indeed the only boundary layer data available is that from the hot films. Data on such characteristics of integral boundary layer properties or data from within blade passages is unavailable. The only way in which to interrogate the design is through the use of CFD and the little experimental data that is available. To allow investigation of the blade passages and boundary layers, the UNSFLO code was used. This code is described in Chapter 3.

4.2.1 Description of the predicted blade pressure distributions

Before a discussion of the hot film results is presented it is necessary to show the pressure distributions and numerical predictions for the NGVs. All the measurements presented in this chapter were obtained in a real cold flow engine and are therefore subjected to unsteady in flow. The predictions were obtained from a steady flow solutions of UNSFLO. It will be shown that all the wake induced transitional activity occurs around or after boundary layer separation. The predictions are expected to be reasonably accurate up to separation, but when run in a steady sense cannot predict boundary layer

development after separation. Predictions shown in Chapter 7 will illustrate a method that does allow for the prediction of unsteady wake effected flows.

Figure 4.2.1 shows the predicted pressure distribution for NGV2 of the 710 LP turbine. Peak suction here occurs at approximately 45%s, than the datum profile described in Chapter 5. Separation was detected by observing when the skin friction dropped to around zero which occurred at about 54%s. The length of the separation bubble was user defined such that reattachment of the flow occurred well before the trailing edge of the profile.

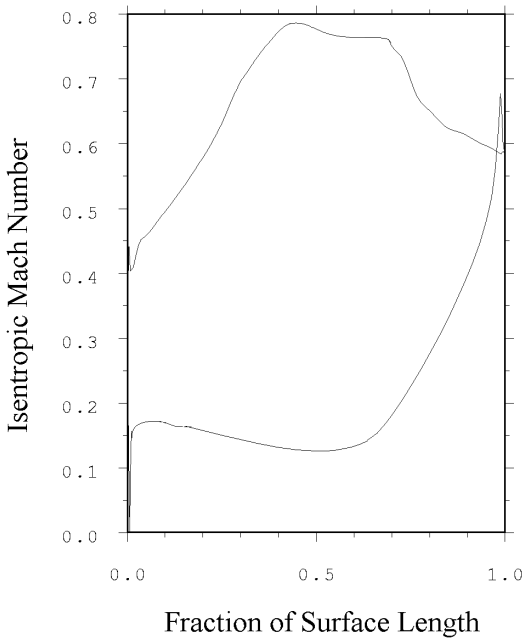

Figure 4.2.1 Mach number distribution of NGV2 of the 710 LP turbine. Exit Mach number = 0.6. Reynolds number = 60,000.

The pressure distribution for NGV2 of the 715 LP turbine is shown in Figure 4.2.2. There is a larger acceleration (and therefore loading) over the leading edge of the blade when compared to the 710 LP turbine. Then there is a continual but more gradual acceleration up to peak suction at 55%s. Separation occurs at 67%s, where the value of

Re_θ reaches 195. The pressure side is fairly unremarkable as the flow has a little deceleration over the leading region of the profile and then accelerates continually towards to trailing edge.

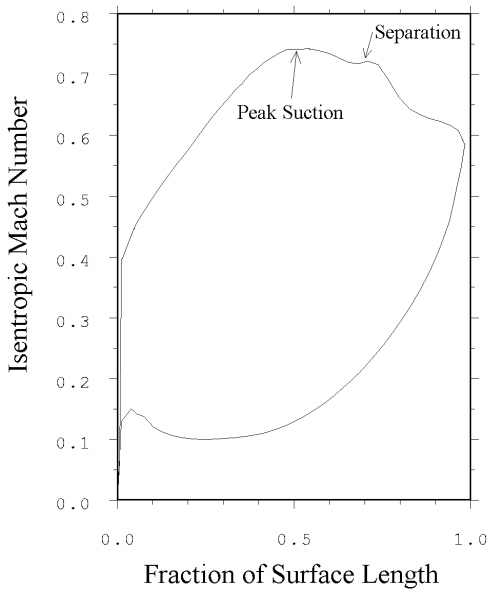

Figure 4.2.2 Pressure distribution for NGV2 of the BR715 LP turbine at a Reynolds number of 100,000.

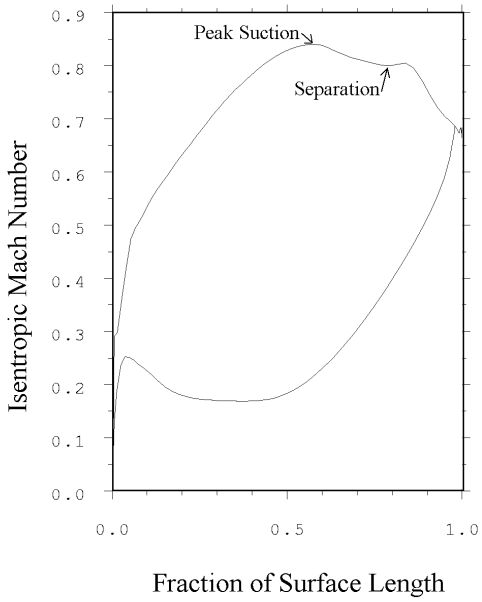

Figure 4.2.3 Pressure distribution for NGV3 of the BR715 LP turbine at a Reynolds number of 80,000.

Figure 4.2.3. shows the pressure distribution for NGV3 of the BR715 LP turbine. In a similar way to the pressure distribution NGV2 of the same turbine, there is a larger amount of leading edge loading than from the BR710 LP turbine. At design incidence there is only a small amount of diffusion on the pressure side ensuring no separation. Peak suction occurs at 57%s and laminar flow separation is predicted to occur at 66% where the value of skin friction drops to zero and the acceleration parameter reaches 0.082 and Re_θ is 184.

These profiles are developments from a profile known as TL10, which is described in Chapter 5 (see Figure 5.2.1) and also by Schulte (1995). This is a highly loaded profile designed to reduce blade numbers by 20% below those used in current LP turbines. The profile results in peak suction at around 55%s which is later than on the profiles already described. Also, the TL10 profile has large leading edge loading maximising the lift from the profile, but still allowing an acceptable margin for positive incidence tolerance.

4.3 NGV2 from the LP turbine of the BR710 engine

4.3.1 710 - Cruise Conditions - at 45,000ft.

The Reynolds number for this condition is approximately 60,000.

The upper plot in Figure 4.3.1 shows the variation of the time-mean shear stress $\bar{t}(s)$ (solid line), the maximum and minimum values of the ensemble mean shear stress (solid lines above and below the mean) and the maximum and minimum of the raw signal (dashed lines). The black circles at the top of the figure indicate the position of the functional sensors. For the exact surface positions of the sensors, see Appendix A. The true maxima and minima are unlikely to be detected in flows with rapidly varying conditions due to the relatively low frequency response of the hot film sensors. The

highest frequencies associated with turbulent fluctuations are thought to be of the order of 300kHz, where as the frequency response of the gauges is around 30-40kHz[*]. The centre plot shows ensemble RMS with the solid line and the lines above and below this giving the maxima and minima of the envelope. The centre line of the lower plot shows ensemble skew with the lines above and below giving the maxima and minima of the envelope of this data.

The level of shear stress is fairly constant over the first few sensors, but increases dramatically over the last two. Similar trends are seen in the RMS plot. There is also no indication that the RMS or shear have reached their maximum. The increasing shear at these locations indicates that more of these regions of blade surface are increasingly covered in a transitional boundary layer. There not much negative skew at this condition, indicating that transition is not complete. In fact this probably indicates that transition is probably less than 50% complete by the sensor nearest the trailing edge.

[*] The upper frequency was calculated assuming the time scales in the boundary layer are proportional to δ/ν

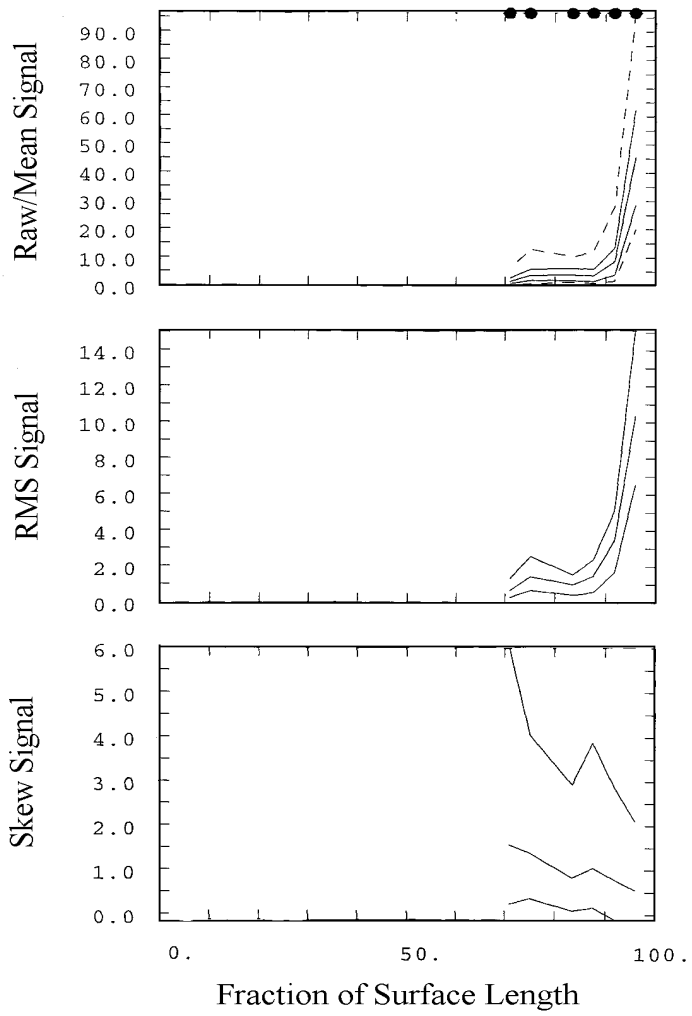

Figure 4.3.1 Envelope plots for the cruise flow condition for NGV2 of the BR710 LP turbine.

The raw signal plots (in Figure 4.3.2) show a number of sharp peaks in shear stress. These are turbulent spots and are marked ‘S’. Turbulent spots and their calmed regions can also be seen in the data and are marked C for the sensor at 87.6%s. The calmed regions are characterised by a relaxation in level of shear stress, and low RMS. No turbulent spots are initiated around wake passing 11 so a form of steady separated flow transition can be seen occurring further downstream. The region in Figure 4.3.2 within the ellipse shows increasing fluctuations in the boundary layer similar to those seen by Schulte (1995) in separated flow transition with steady inflow on a low speed cascade. The

frequency of the fluctuations doubles between the sensors at 87.6 and 91.8%s which is often observed in a separation bubbles. The amplitude of those fluctuations increases by a factor of nearly 4 by the sensor at 96%s, but has yet to break down to complete turbulence. It should be noted that despite the wake not having caused the birth of turbulent spots at this location, the wake turbulence is still present above the boundary layer. This will obviously modify the behaviour of the separation bubble transition and it cannot be considered to be a truly steady transition process.

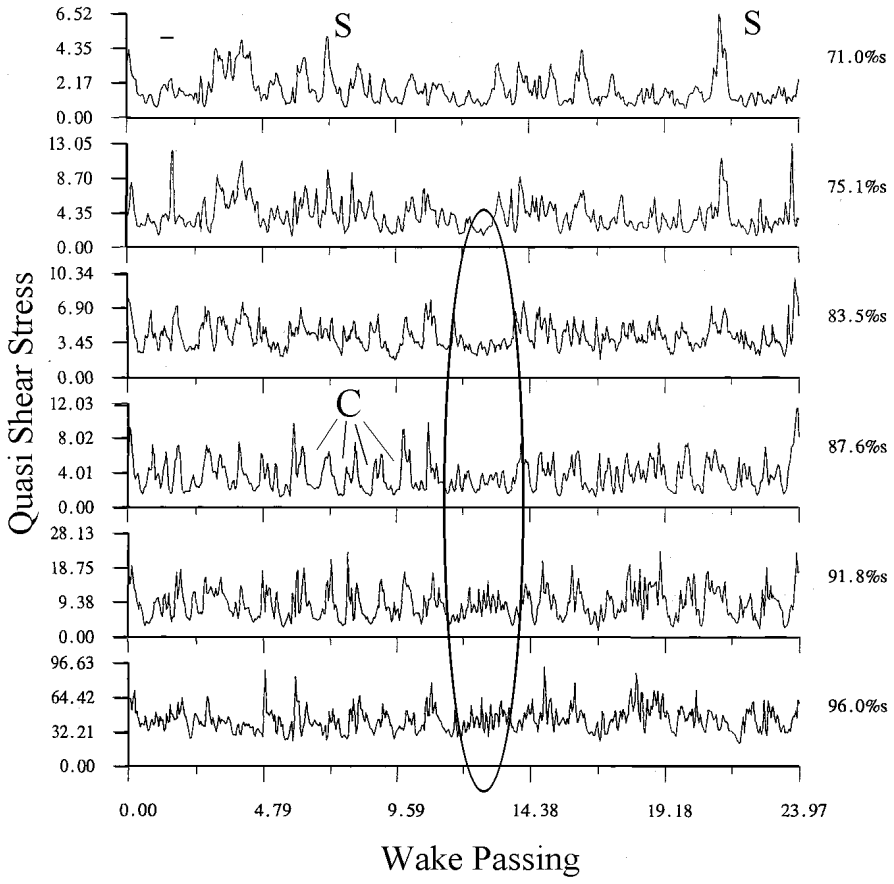

Figure 4.3.2 Raw hot film data for the cruise condition for NGV2 of the BR710 LP turbine.

The raw data showed that wake induced transition starts at around 71%s, which is after the predicted position of flow separation. The fact that wake induced transition onset occurs after laminar separation seems to be a common feature of transition mechanisms on

LP turbine blades and is discussed in more detail in later chapters. This is also shown in the ST diagrams of non-dimensional ensemble mean shear, ensemble RMS and ensemble skew, see Figure 4.3.3. The non-dimensional ensemble mean shear stress is defined as $\tilde{t}_w(s,t)/\tilde{t}_{w,\max}(s)$. The ensemble mean shear stress data presented in this figure is non-dimensionalised in such a way that the periodic fluctuations are enhanced at the sake of the overall levels of shear stress. In fact, the values of shear stress around the first sensor at 71%s are much less than those nearer the trailing edge. A wedge shaped region is caused by the formation and passage of turbulent spots due to the different celerities of the leading and trailing edges of the turbulent spots. A number of trajectories are also plotted on the ST diagrams. These were obtained from a prediction with fully turbulent boundary layers thus resulting in a pressure distribution with no separation bubble. Observations from work shown later in the thesis show that turbulent spots travel through a separation bubble almost as if it were not present. The trajectories are of the local free stream velocity, the spot leading edge, trailing edge and calmed region velocities and are labelled U_∞, U_{le}, U_{te} and U_{ca} respectively. In these plots the propagation values for the spots are taken to be 88%, 50% and 30% of the local free stream velocity. The calmed regions that follow a spot are known to suppress boundary layer separation (Schulte 1995), but separation (and separated flow transition) start to re-establish before the next wake arrives as there are occasionally regions of high RMS between wake passings, see region circled ‘S’. This may mean that the optimum reduced frequency for complete suppression of the bubble was not attained at this condition.

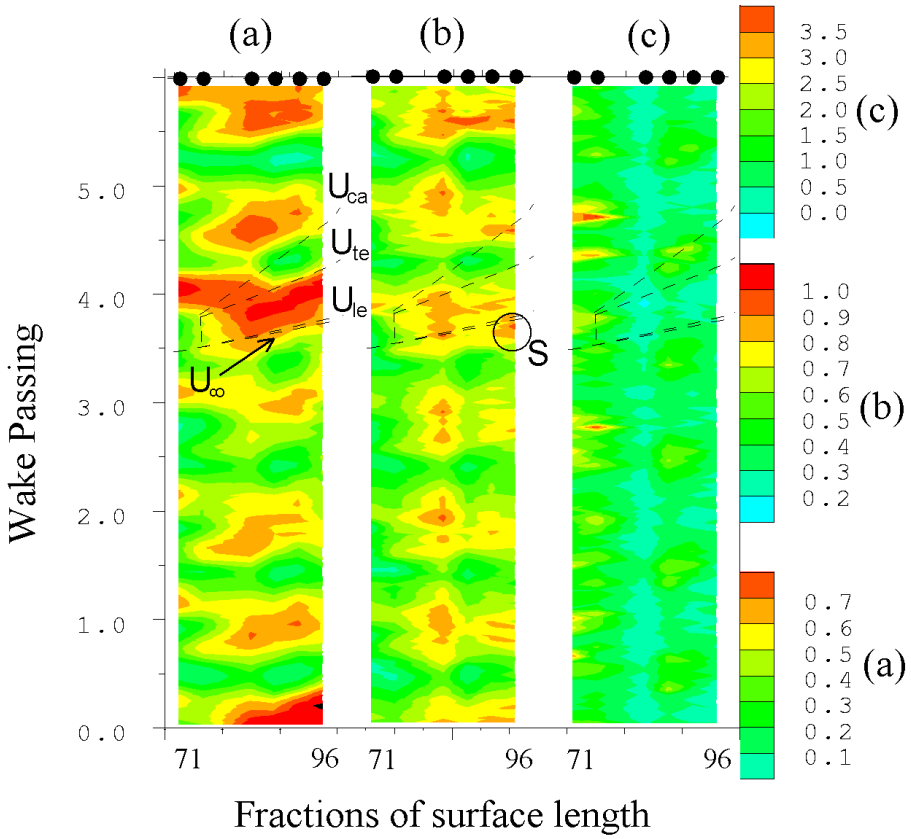

Figure 4.3.3 ST diagrams of (a) Non-dimensional Ensemble Mean Quasi Shear Stress, (b) RMS(s)/RMS(s)$_{max}$, (c) Skew for the cruise conditions for NGV2 of the BR710 LP turbine.

The PSD plots in Figure 4.3.4 for this condition show the wake passing frequency to be approximately 5800Hz. Small peaks in the PSD at double this frequency (11.59kHz) can also be seen. It is interesting to note that other peaks in the PSD occur at a frequency of approximately 7kHz, due to the potential effects of the downstream rotor, as this row is the blade row in the turbine that could produce such a frequency. This frequency is seen most clearly at the trailing edge sensor and strength reduces at more upstream sensors. This gives some indication of the strength of the potential interaction and the way in which it decays with distance in the upstream blade row, assuming that all hot film have the same sensitivity.

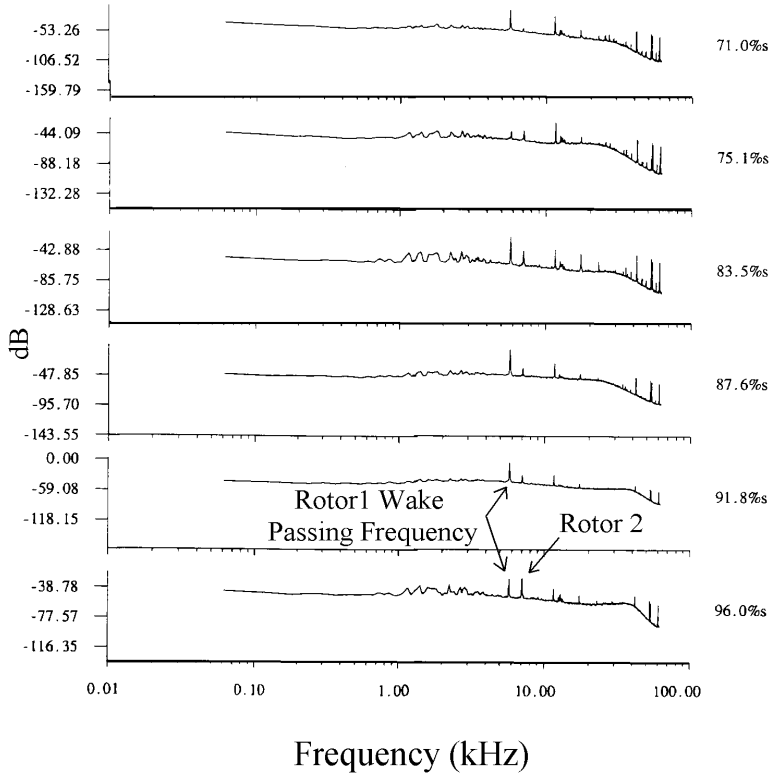

Figure 4.3.4 PSD plot for the cruise condition of NGV2 of the 710 LP turbine.

This section has shown that the suction side flow on this LP turbine blade is dominated by the transitional effects due to the passage of the wakes. Separation is predicted to occur at approximately 50%s, which is before the location of the first hot film sensor. Wake induced transition occurs after separation. The PSD plot indicated the presence of the *downstream* rotor, showing that the potential effects of the rotor extend upstream to the NGV. The fact that the strength of the peaks seen in the PSD data from the hot film at the frequencies of both rotor 1 and rotor 2 are very similar cannot be explained at present. However, it effectively means that the profile switching caused by the wakes is of a similar magnitude to the potential effect of rotor 2.

4.4 Variation in Reynolds number for NGV2 of the BR715 LP turbine

4.4.1 Takeoff conditions, Re = 1.43×10^5

The results obtained for this condition were the first in this series of measurements. PSD data (not shown) indicate that the frequency response of this data was not as well optimised when compared to the data from NGV3 shown later. Data from some of the hot film sensors are shown in Figure 4.2.1, which shows that the frequency response of these gauges is lower than that of the NGV from the BR 710 LP turbine in figure 4.3.2. Note that at 78%s very few wakes result in the formation of turbulent spots, but by 90%s every wake has formed a turbulent spot.

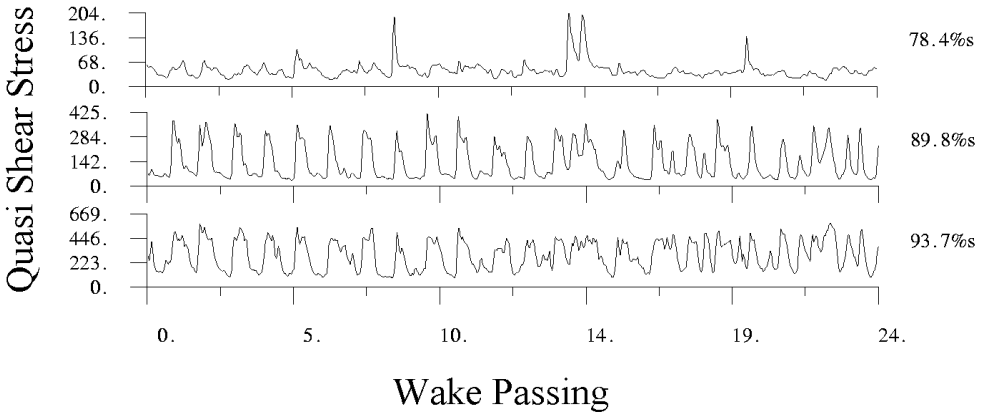

Figure 4.4.1 Raw data from the BR715 LP turbine at take off conditions.

It was impossible to improve the frequency response during the rig tests. Figure 4.4.2 presents the envelopes of the data obtained at this condition.

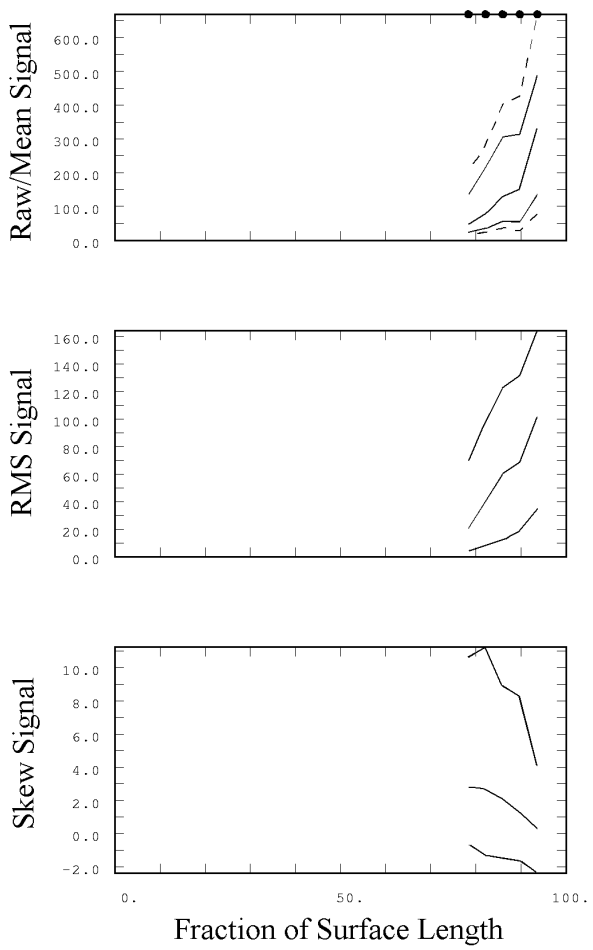

Figure 4.4.2 Envelope plots of the statistical data for NGV2 of the BR715 LP turbine at takeoff conditions.

The mean level of shear stress continuously increases from the first sensor to the last sensor on the blade surface, with the largest increase occurring over the final two sensors. The lowest shear stress is seen over the first few sensors and indicates that the boundary layer is separated for some positions of the upstream rotor at these surface positions. The increasing shear indicates that there are increasing amounts of attached turbulent flow on the surface further downstream. Separation was predicted to occur at around 65%s indicating that wake induced transition has again not occurred until the flow has separated.

The centre plot of Figure 4.4.2 shows the distribution of ensemble mean RMS. The lowest plot shows the equivalent values for the ensemble skew. Like the plot of mean

shear stress, the mean values of RMS increase from a minimum at the first sensor continually towards the trailing edge indicating more rapidly changing flow conditions over these sensors. The mean level of skew is always positive, but from the envelope of the skew, it can be seen that there are some rotor positions where the skew becomes negative. The large difference in maximum and minimum skew indicate that there are significant differences in the flow at differing positions of the upstream rotor. The presence of negative skew near the trailing edge indicates that at some rotor positions the flow has nearly completed transition.

Figure 4.4.3a shows the non-dimensional ensemble mean shear stress as an ST diagram. Wake induced transition can be seen occurring on average at 82%s indicated by a wedge shaped region of high shear (contours coloured red to black). A number of trajectories are drawn onto the figure and are again calculated from the predicted pressure distribution. The lines correspond to the same fractions of local freestream velocity as those for NGV2 of the BR710 LP turbine shown in Figure 4.3.3.

It is noted that near the leading edge the contour travels faster than the local free stream velocity. This is not because individual turbulent spots travel faster that the local freestream, but instead it is due to the process of ensemble averaging, Addison and Hodson (1990). The wake causes transition by causing the formation of turbulent spots under its path. The wake convects at the local freestream velocity, but the spot's leading edge travels at approximately $0.88U_{\infty}$. Therefore the wake overtakes the spots it has formed, allowing it to form further spots ahead of the original ones. The wake then finds itself further downstream and over a region of flow that is more receptive to disturbances. Spots may also form under regions of the wake where the turbulence level is lower, that

is, ahead of the wake centre line. In this way, the leading edge of the wake affected zone may seem to travel faster than the free stream.

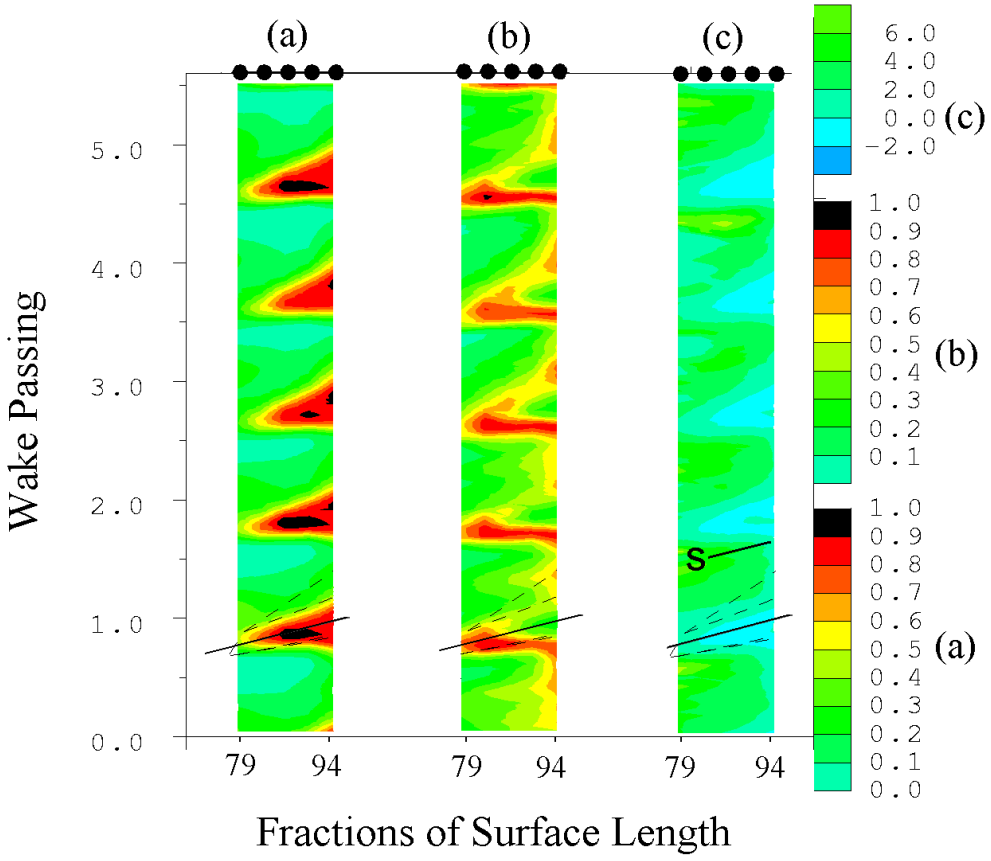

Figure 4.4.3 ST diagrams of (a) Non-dimensional Ensemble Mean Shear Stress, (b) RMS/RMSmax, and (c) Skew. Takeoff conditions for NGV2 of the BR715 LP turbine.

At the most downstream sensor there are levels of shear stress that are (relatively) much lower than those where the turbulent spots pass, this is consistent with the existence of calmed regions trailing the spots.

Figure 4.4.3b shows a peak in the non-dimensional RMS that moves between the first and last sensors. Since the signals for NGV2 only pick up the formation and passage of turbulent spots and not the turbulent fluctuations, the measured signals seems to be either turbulent (i.e. a turbulent spot and high shear) or laminar/separated flow (low

shear). As a wake passes over the sensors, on average it causes the formation of a turbulent spot at around 82%s. If one follows the solid line in the flow direction in Figure 4.4.3b, one first sees a region of high RMS then a sudden drop to low RMS. At the same position in time and space, in Figure 4.4.3c one sees a negative value of skew. The suddenness with which the RMS and Skew change along this trajectory would normally indicate that the boundary layer under the wake has suddenly become fully turbulent. However, because of the relatively low frequency response, the smaller fluctuations (at frequencies above the cut-off frequency of the sensors) are not picked up. The fact that the sensors seem to measure the flow as either being laminar or turbulent is likely to be a simplification of the true flow, as the real flow is likely to be more transitional in behaviour i.e. with a less clear difference between laminar and turbulent states. Care must therefore be exercised in the interpretation of the results from NGV2.

The regions marked ‘S’ in Figure 4.4.3 contains positive skew, but this decreases to near zero as the flow reaches the trailing edge. This may be the first indications of separated flow transition, however there is not much evidence of an increase in RMS in these regions, so the transition may be at a very early stage.

In summary, the results obtained at the takeoff (and therefore highest Reynolds number) condition indicate that boundary layer separation probably occurs before the first sensor (at 78.4%s). Passing wakes cause transition via the formation of turbulent spots at around 82%s, where the boundary layer is still partially separated. Separated flow transition may be starting to occur between wake passings, indicated by the positive, but decreasing skew before the next wake arrives.

4.4.2 45kft - CRUISE CONDITION

Figure 4.4.4 shows the envelope plots of the S-T diagrams for this condition. They show the same characteristics as the previous conditions, but the rise in mean shear stress is less rapid over the first three sensors. In fact the mean shear stress increases very little until the last two sensors, indicating that the transition process is less complete at this condition than the previous condition. The RMS increases in line with the level of shear, but the skew is almost universally positive, with few rotor positions resulting in much negative skew. The transition process is therefore probably less than 50% complete by the trailing edge.

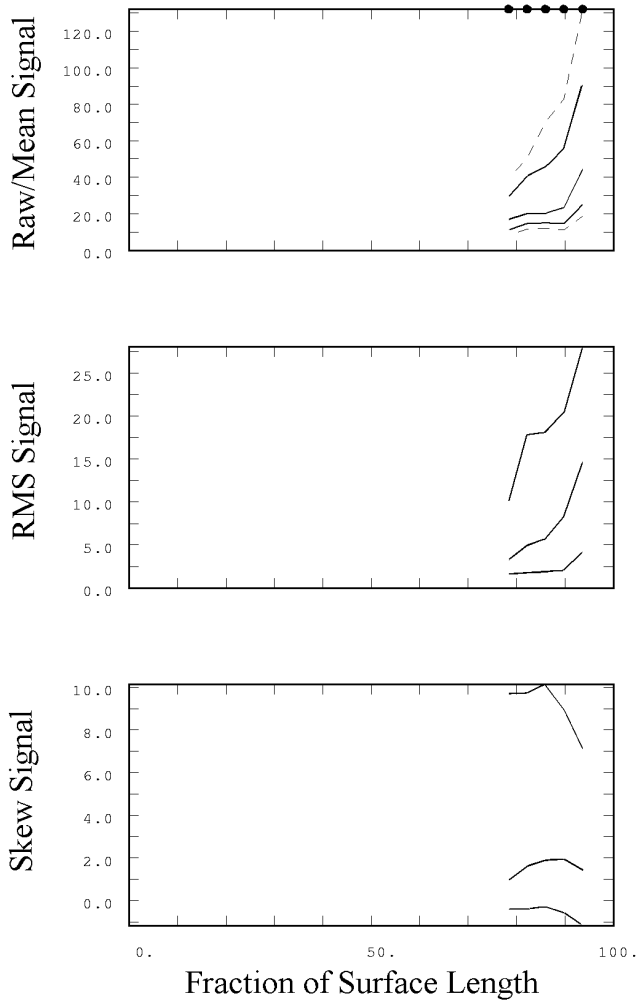

Figure 4.4.4 Envelope plots of the data from NGV2 of the 715 LP turbine at cruise conditions.

By this Reynolds number, wake induced transition is starting to occur near 89% surface length as can be seen from Figure 4.4.5. This is further along the blade surface than for the previous condition. The first sensor (at 78.4%s) indicates a laminar but disturbed boundary layer. Occasionally a wake will pass that causes the formation of a turbulent spot at 82%s, see the region marked P. By the time this spot reaches the final sensor, its calmed region seems to have disappeared, and other turbulent spots may be forming, see regions marked ‘S’. The oscillations marked ‘S’ may also be due to separated flow transition, but since the frequency response of this data is quite low, it makes this interpretation difficult.

The wedge shaped regions of high shear in Figure 4.4.6a start at approximately 89%s, occurring just after the rise in shear the RMS starts to rise, see Figure 4.4.6b. A rise in skew in Figure 4.4.6c also occurs, before the shear starts to rise. This streamwise location is therefore the mean location of wake induced transition onset. The reason that the RMS rises before the mean shear is because the front of the wake disturbs the boundary layer but may not necessarily cause transition. The wake causes a rise in RMS, but it is near the wake centre line where the disturbances are largest. For a given surface position, the boundary layer therefore sees a relatively low turbulence front which just disturbs the laminar boundary layer. The disturbances increase as the centre line of the wake passes that position and once those disturbances reach a critical level the boundary layer responds with the formation of turbulent spots: bypass transition. This is why the RMS rises as the front of the wake passes over a particular position, but spots are formed slightly later (in time) when the centre line of the wake passes that position. It is then that the high shear region is seen.

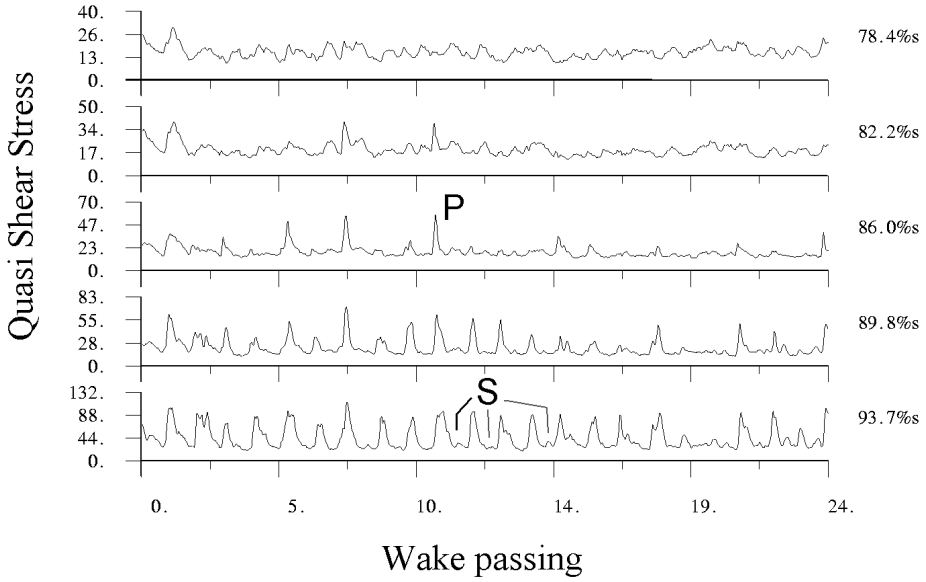

Figure 4.4.5 Raw shear stress signals for NGV2 of the 715 LP turbine and cruise conditions.

Slightly later in time after the wedge shaped region of high RMS passes there is a region of low RMS marked ‘L1’ in Figure 4.4.6. After this region, an even lower RMS is noted, marked ‘L2’. This probably indicates that it is a region of separated flow. Looking at the same time and space on the skew plot one can see that there is a small amount of positive skew. It is likely that the separated shear layer is starting to undergo transition, but it is in the very early stages of doing so, see region ‘S’. It is often easier to see multimode transition mechanisms in ST diagram form rather than is raw time history form. Despite this one cannot be *certain* that separated flow transition is actually taking place in these regions.

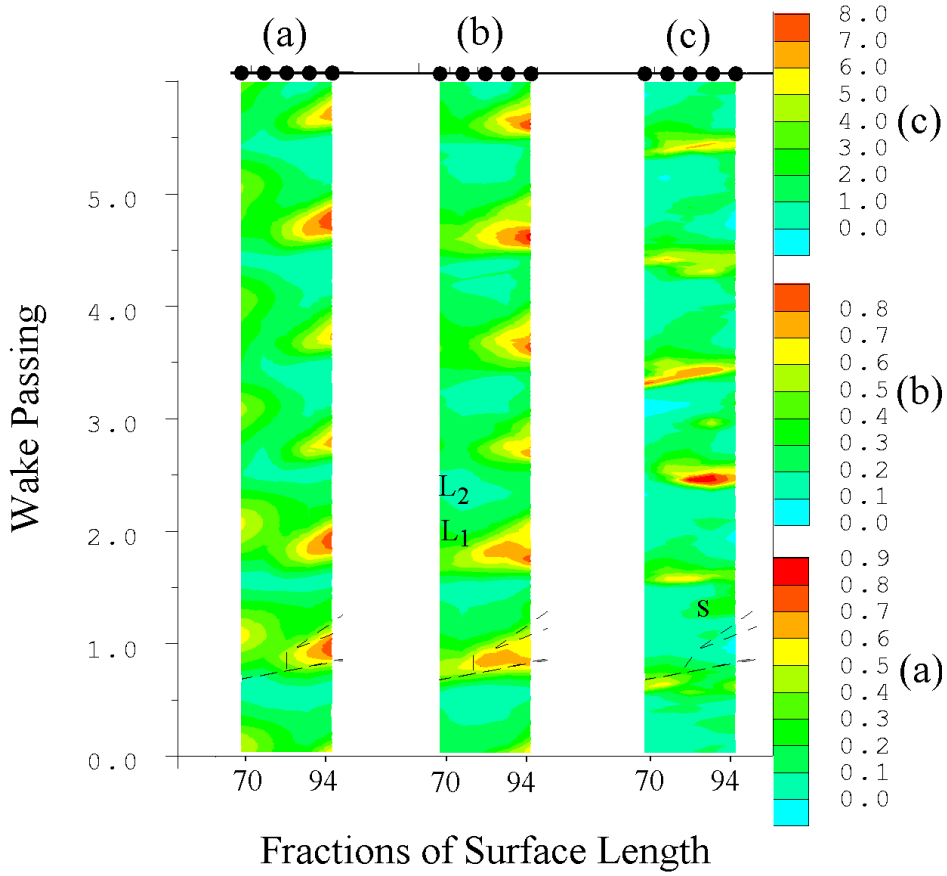

Figure 4.4.6 ST diagrams of (a) Non-dimensional Ensemble Mean Shear Stress, (b) RMS(s)/RMS(s)$_{max}$, and (c) Skew. Cruise conditions for NGV2 of the BR715 LP turbine.

In summary, at cruise wake induced transition occurs later than for the takeoff. There is some evidence that flow separation seems to establish itself between wake passings, but is only starting to undergo transition by the final sensor on the blade.

4.5 NGV3 of the BR715 LP turbine

4.5.1 45kft - Cruise Conditions

Figure 4.5.1 shows the envelope plots of the ST diagrams for NGV3 at cruise conditions. The minimum shear stress occurs at 75%s indicating the time-averaged position of flow separation after which it then rises to its highest value at the final sensor. The RMS stays constant over most of the surface up to about 79%s before it then starts to rise. After the position of time-mean flow separation, the positive values of skew start to reduce and by 90%s there are some positions of the upstream rotor where the skew is negative as can be seen from the envelope of skew. The mean shear and RMS have begun to fall by the trailing edge. This means that the flow is not fully turbulent at the sensor nearest the trailing edge.

The plots of the time history of the raw signal indicate that the boundary layer at 26.8%s is laminar and highly disturbed, see Figure 4.5.2. By 64.0%s, the boundary layer can be seen to clearly respond to the passage of wakes with relatively large fluctuations in shear stress. Some of these fluctuations result in the formation of turbulent spots. By 86.4%s turbulent spots are clearly seen in much of the data, being superposed onto a highly fluctuating boundary layer, see regions marked ‘B’. Regions of flow that appear to be calmed are also visible and are marked ‘C’. Many calmed regions can be seen at the penultimate sensor, but very few at the last one. One can also see a high frequency fluctuation (at 50kHz) on the last two gauges which will tend to mask the calmed regions. This high frequency is due to ringing of the anemometer signal processing system and it has nothing to do with the signal. Unfortunately, this ringing was not detected until after

the data had been acquired. The conclusion that the flow at the final sensor is not fully turbulent is confirmed by the raw data (at 98%s) as there are still large fluctuations in the shear stress levels. The fluctuations have an amplitude of up to approximately 50% of their time-mean values.

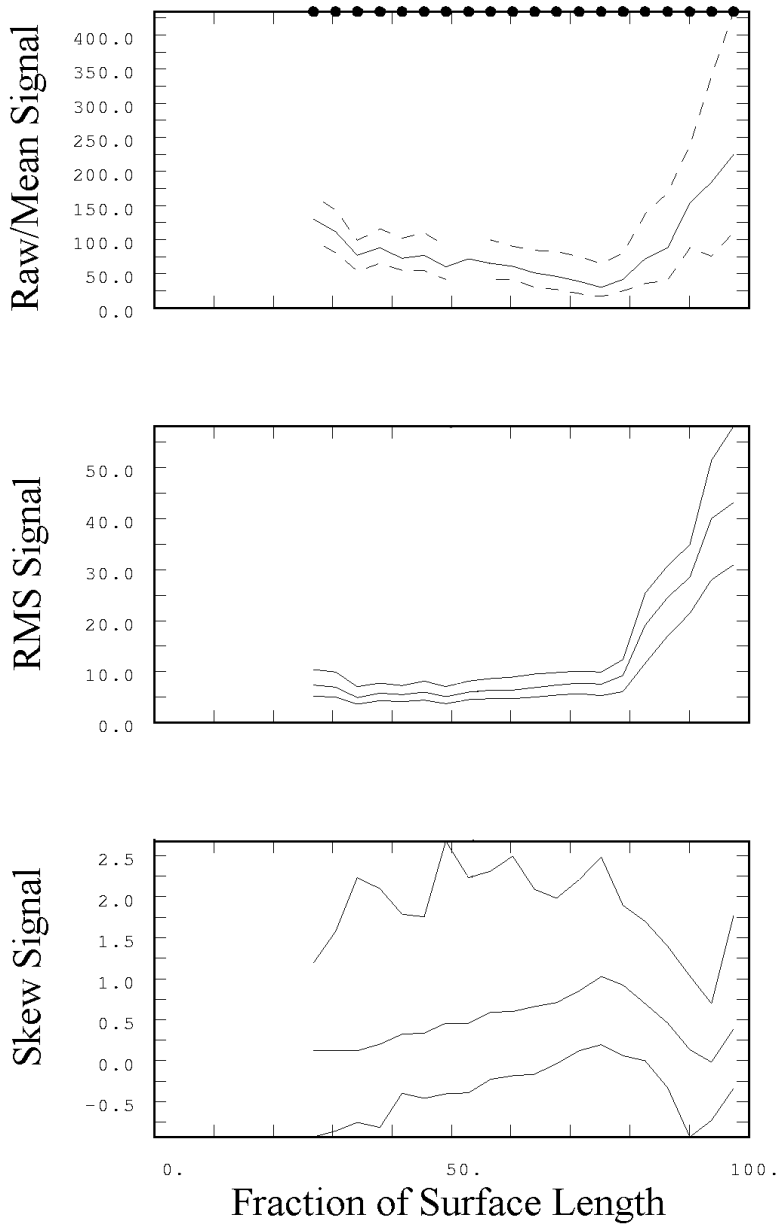

Figure 4.5.1 Envelope plots of data from NGV3 of the 715 LP turbine, cruise conditions.

Figure 4.5.3 shows the non-dimensional ensemble mean shear stress as an ST diagram. The fluctuations in the laminar boundary layer of the passing wakes can be seen as regions marked ‘L’. Transition caused by the wakes from Rotor 2 can be seen occurring (in the time-mean) at approximately 80%s and are marked as ‘H2’. Relatively high shear regions also occur between these rotor 2 transition regions, but these start at about 68%s. The take-off condition (i.e. at a higher Reynolds number) for this profile has not been shown, but at that condition, the formation of high shear regions ‘H1’ and ‘H2’ occurred further along the surface than for the present condition where they occur at 68 and 78%s respectively. By the time transitional regions ‘H1’ reach the trailing edge of the blade (marked ‘H3’) they have a value of shear that is five times lower than the regions caused by the wakes of rotor 2 (‘H2’). On average the amplitude of the regions marked ‘H3’ are only between 40 to 60% of the maximum shear that occurs in regions caused by rotor 2. This happens because this transitional boundary layer is older, i.e. started earlier along the surface, has become thicker and therefore its shear stress is lower compared to the newer transitional boundary layer that appear slightly later in time.

In Figure 4.5.3, regions of very low shear can be seen at some rotor positions at 86 and 90%, see region ‘L1’. This is likely to be the effect of the calmed regions that were illustrated in Figure 4.5.2. Calmed flow can very occasionally be seen at the trailing edge in the raw data.

Figure 4.5.4 shows the ST diagram of RMS/RMS_{max}. Its variation is less periodic than the ensemble mean shear stress data. However, regions of high RMS generally coincide (in time and space) with regions of high shear stress. There is still a large variation of RMS at the sensor trailing edge also indicating that the boundary layer is not

fully turbulent. Figure 4.5.5 shows only small amounts of negative skew at the sensor nearest the trailing edge.

An extremely interesting phenomena is illustrated by the two lines that are labelled 70% and 100% in Figure 4.5.3. These lines are trajectories at 70 and 100% of the local freestream velocity. The turbulence in a wake will convect with the freestream, i.e. along the 100% trajectory. However, it is noted that the perturbation to the boundary layer (seen as a rise in shear stress) travels at the slower rate of 70% of the local freestream velocity. Similar observations were made by Walker *et al* (1993) from hot film measurements take on compressor blades.

When the trajectory for the wake reaches the position of flow separation for the laminar boundary layer a sudden rise in shear stress occurs (see the region marked ‘x’). The wake convects over the surface disturbing the laminar boundary layer underneath. The disturbance due to the wake slowly diffuses through the layer such that it is seen by the hot film sensors only after the wake has passed by. The momentum thickness of the laminar boundary layer up to separation is too low to allow transition to occur. Predicted momentum thickness for this profile reaches 250 at around the separation position. Information presented in later chapters shows (for all the profiles tested) that wake initiated transition does not occur until flow separation, where the Reynolds number based on momentum thickness reaches approximately 250. The exact value obviously depends on the pressure distribution, but the mean value of Re_θ obtained from most of the profiles was around 250. This must mean that as soon as the wake reaches the position where the flow is probably most unstable it causes an almost immediate start to the flow undergoing transition.

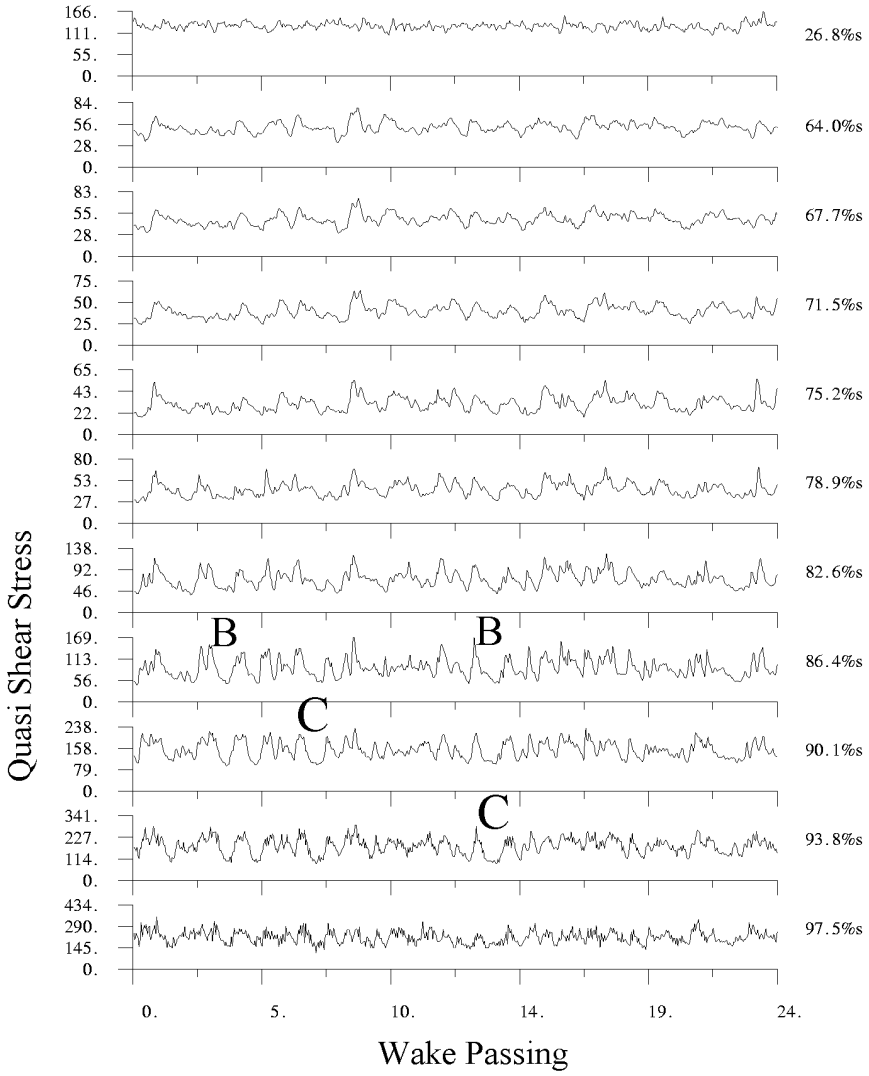

Figure 4.5.2 Raw shear stress signals for NGV3 of the LP turbine at cruise conditions.

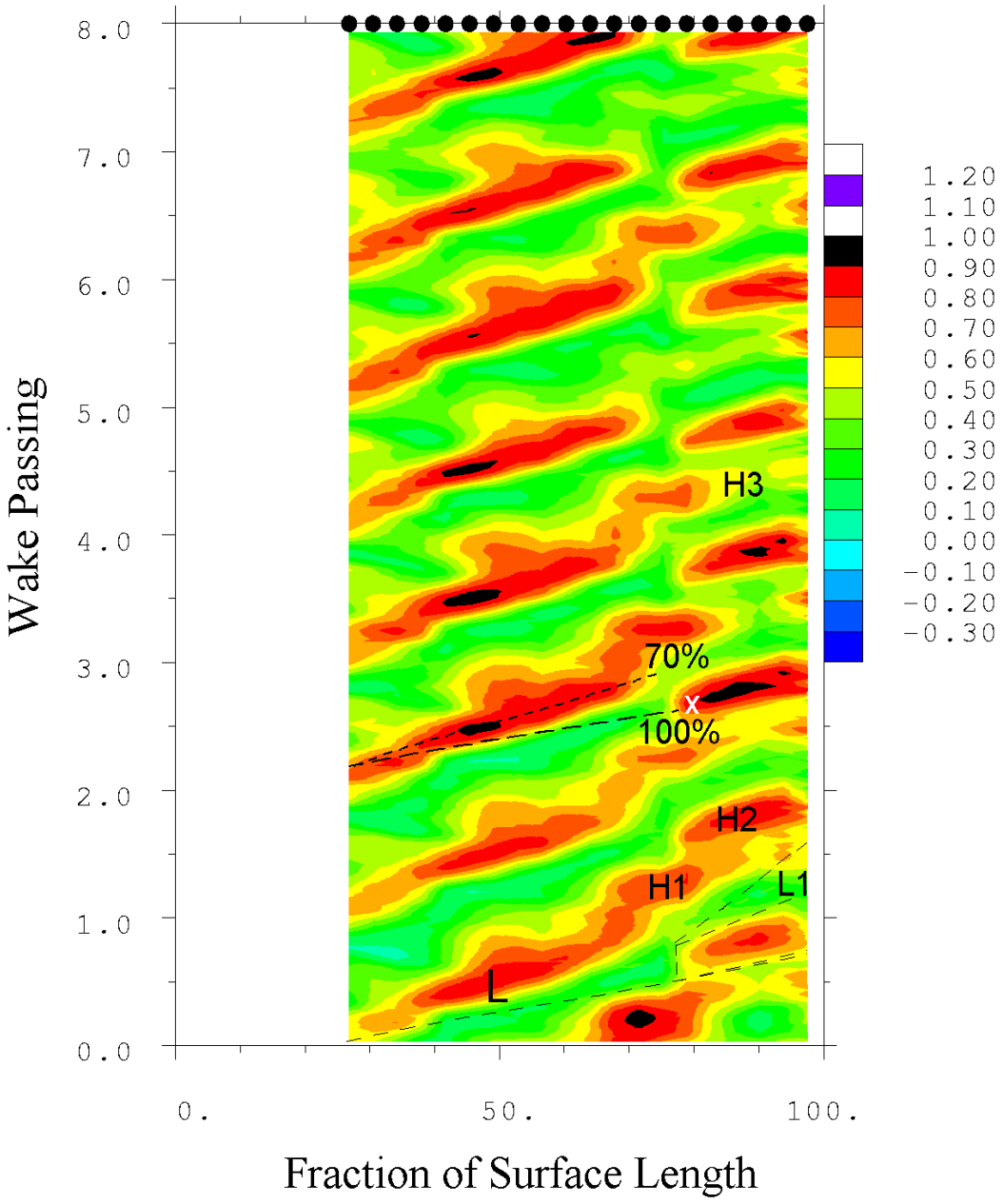

Figure 4.5.3 ST diagrams of Non-dimensional Ensemble Mean Shear Stress for the cruise conditions for NGV3 of the BR715 LP turbine.

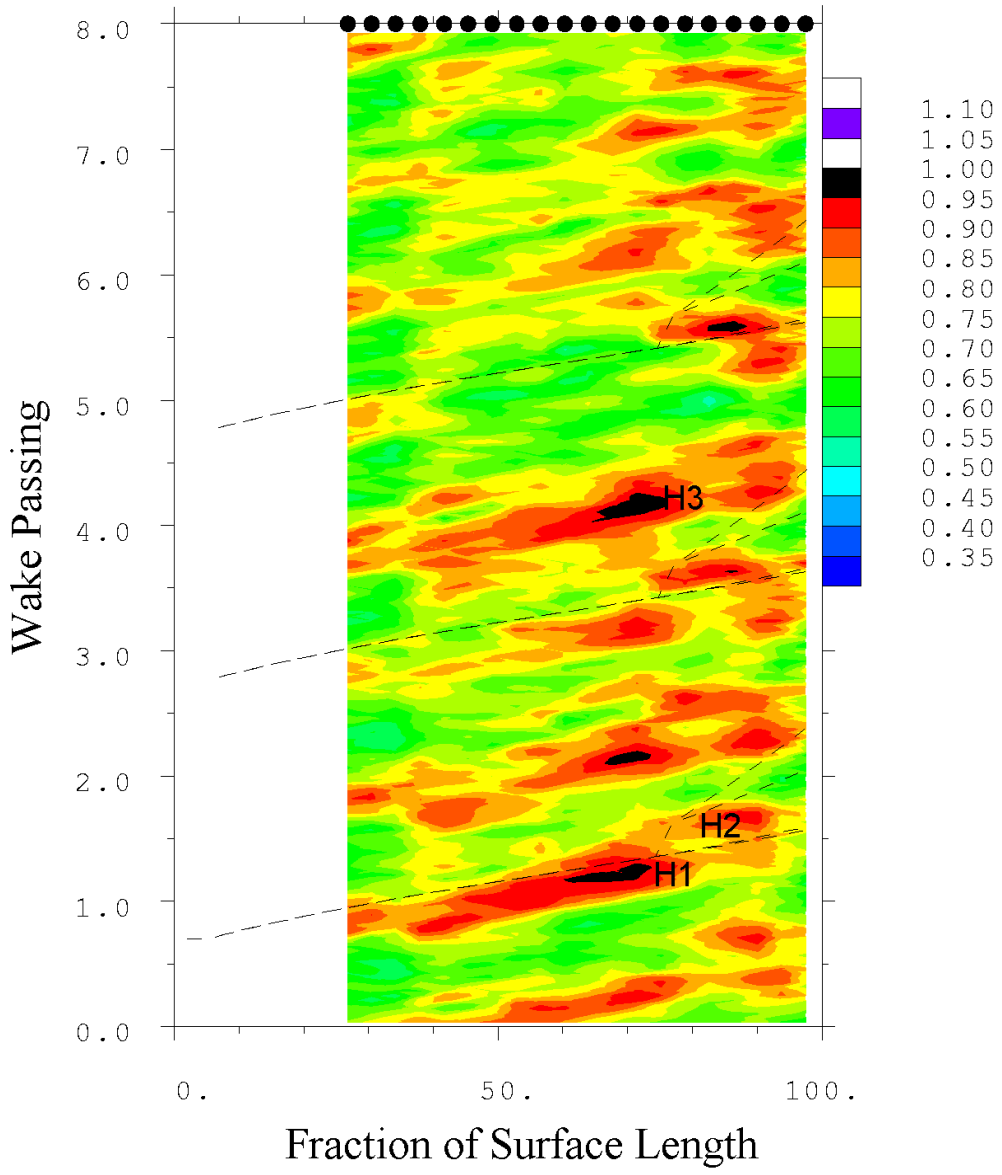

Figure 4.5.4 ST diagrams of Rms/Rms_{max}, for the cruise conditions for NGV3 of the BR715 LP turbine.

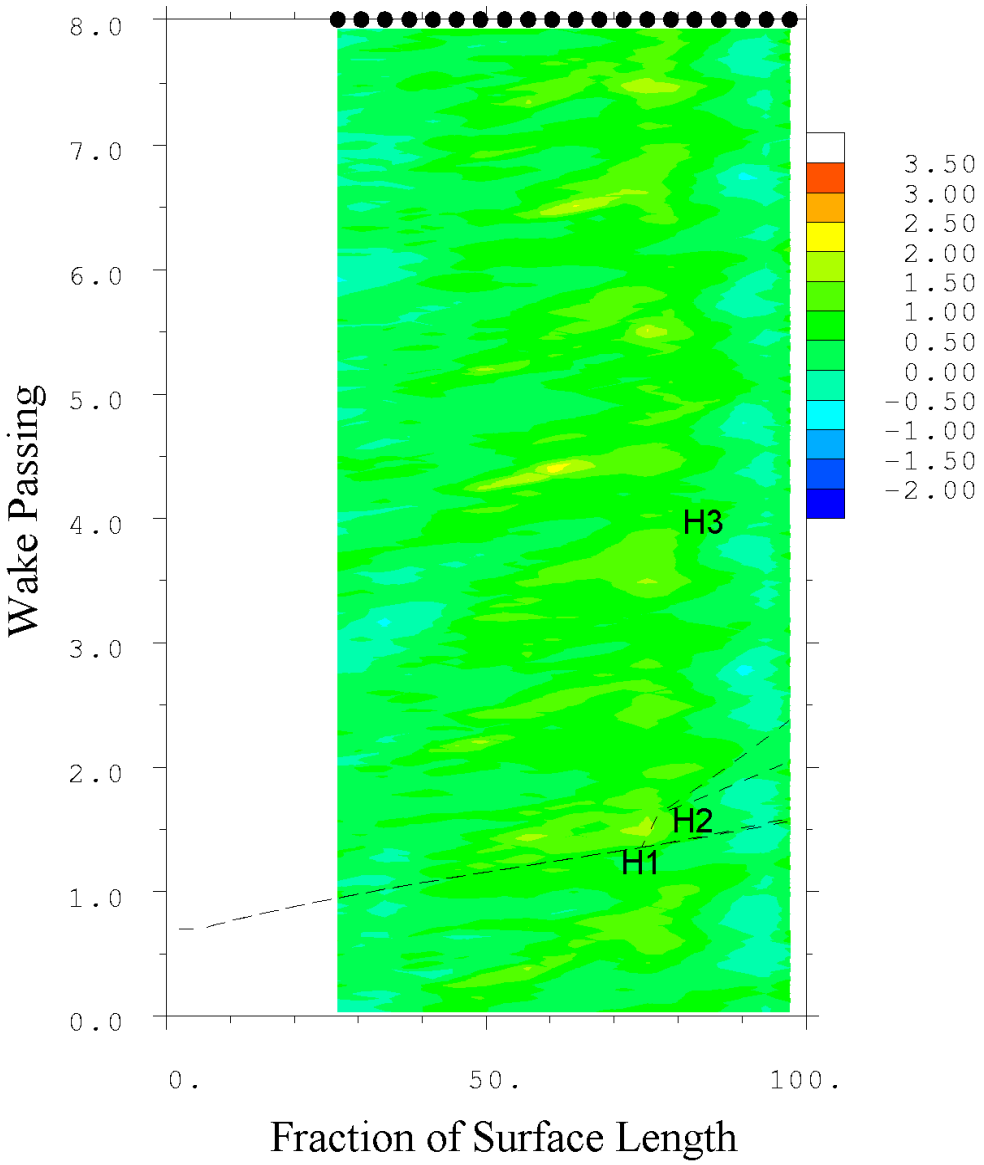

Figure 4.5.5 ST diagrams of skew for the cruise conditions for NGV3 of the BR715 LP turbine.

4.5.2 The multistage effects as seen by NGV3

It has been noted that multiple blade rows upstream of NGV3 effect the transitional behaviour of its boundary layers in a more complex manner than those upstream of NGV2. In this section the boundary layer behaviour of NGV3 due to the fact it is a relatively highly imbedded stage are explored in more detail.

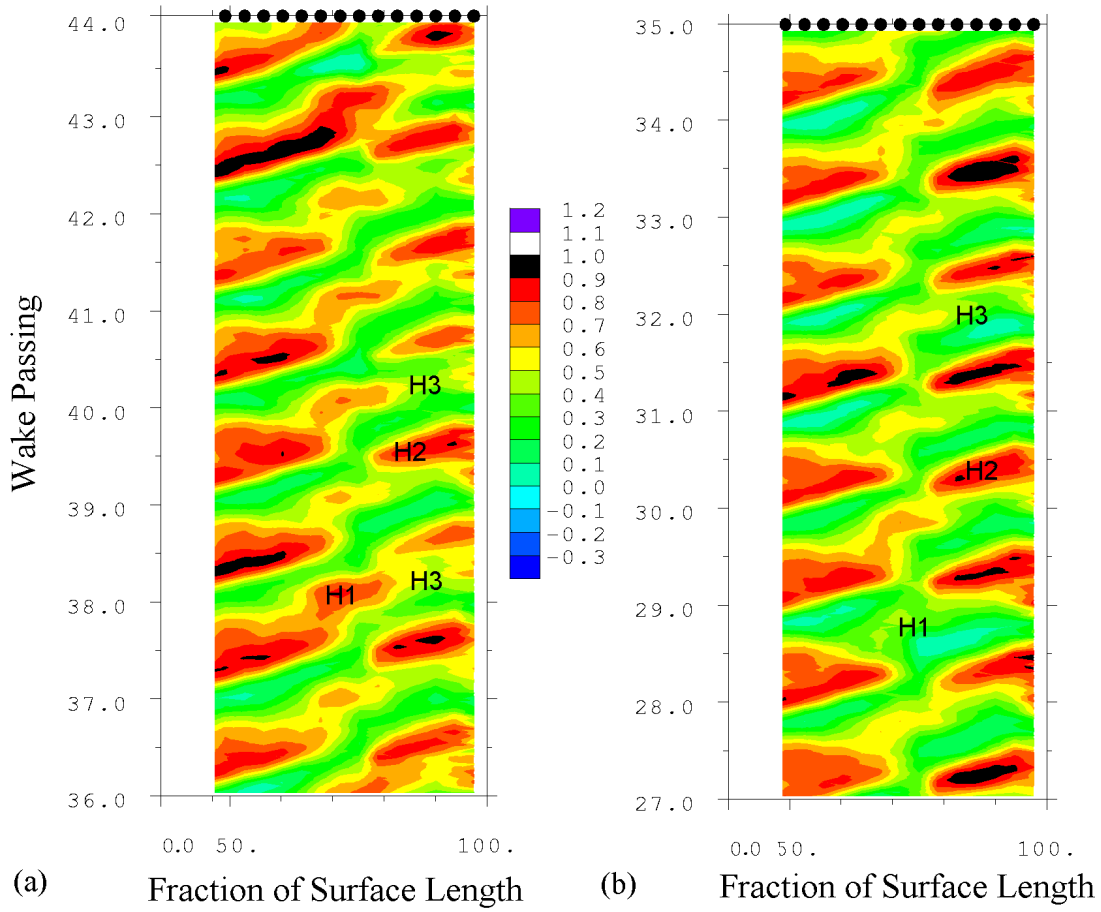

Figure 4.5.6 ST diagrams of non-dimensional ensemble mean shear stress for two different sets of positions of the upstream rotor.

Figure 4.5.6 shows the variation of non-dimensional ensemble mean shear stress at different wake passings to those seen in Figure 4.5.3. They correspond to the wake passings when rotor 2 is roughly half a circumference on from Figure 4.5.3. The high shear regions to compare are in the region around wake passings 41 from figure a and 31

from figure b. At rotor passing 31 the regions of shear stress are much lower than for wake passings around 41. The level of shear stress due to wake caused by rotor 2 are approximately the same between both figures. Arndt (1991) showed that in an LP turbine the interactions of the wakes due to rotor 1 and rotor 2 gave rise to an amplitude modulation of the wake strength that entered NGV3. Arndt's measurements were carried out with a hot film probe traversed upstream of the inlet to NGV3. The amplitude modulation of the turbulent fluctuations seen in those measurements is also responsible for the variation in transition 'strength' seen here. The first transition region seen in the ST diagrams (marked 'H2') is caused by Rotor 2 at 80%s. The other transition region is caused by wakes from NGV2 that pass through Rotor 2. NGV2 wakes whose strength is in turn modulated by Rotor 1. The difference in the number of blades for rotor 1 and rotor 2 leads to the low frequency beating (modulation), whereby at some rotor 2 positions the strength of the second transition region is diminished. The difference in blade count between rotor 1 and 2 is two blades and the beating frequency therefore is expected to occur at half the rotor rotational frequency. This is shown in Figure 4.5.7 where T_R is the time period for one revolution of the upstream rotor.

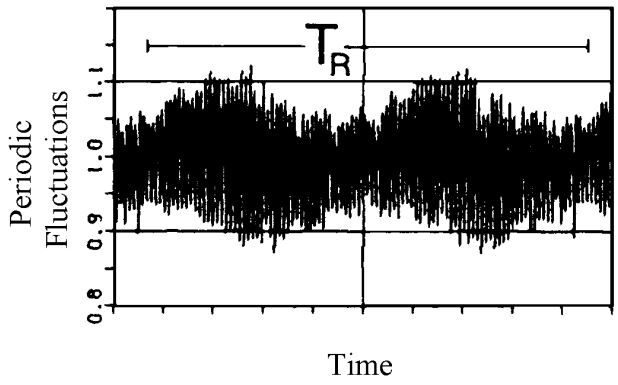

Figure 4.5.7 Ensemble averaged turbulent fluctuations at mid span downstream of rotor 2, Adrnt (1991).

Figure 4.5.8 shows the variation of shear stress for a hot film sensor located at 71.5%s on NGV3 for a complete revolution of rotor 2. Although the data is not as clear as that shown by Arndt it is still possible to see the variation in the strength (amplitude) of the shear stress in regions A and B. This variation in shear stress is a consequence of the variation in wake turbulence intensity. When the wake strength is highest (region B) this gives rise to more rapid transition which gives rise to higher shear stress.

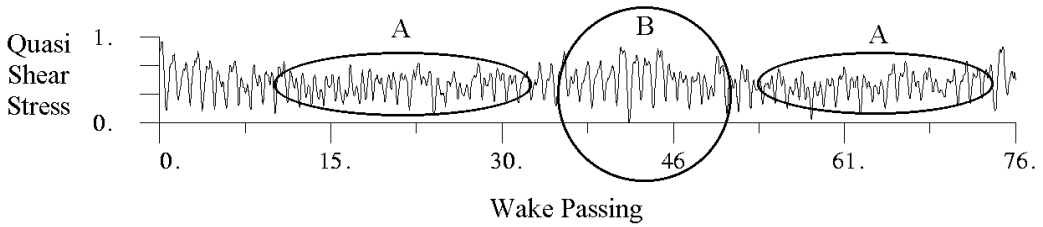

Figure 4.5.8 Shear stress measurements at 71.5%s on NGV3 for one complete revolution of rotor 2.

4.6 Conclusions

4.6.1 NGV2 of the 710 LP turbine Rig tests

Boundary layer separation is predicted to occur at approximately 60%s, but reattachment, as interpreted by the hot film sensor data, occurs (in the time-mean and at all Reynolds numbers) before the trailing edge. Wake induced transition seems to be starting by 71% surface length. No hot film sensors were upstream of this location so the predicted separation position could not be verified by measurement. As the Reynolds number is reduced wake induced transition seem to complete slightly later. Separation bubble reattachment occurs after the end of the wake induced transition region, but separated flow transition is not completed by the trailing edge at any Reynolds number. Calmed regions which trail behind a turbulent spot can be seen in many of the raw hot film signals.

4.6.2 NGV2 of the 715 LP turbine Rig tests

The results from NGV2 of the BR715 LP turbine show periodic wake induced transition starting at around 71%s. As the Reynolds number drops, the position of wake induced transition moves nearer the trailing edge of the blade. Flow separation occurs before the first sensor but is only likely to occur between wake induced transition regions. The separation bubble extends in length as the Reynolds number drops. Calmed regions, which trail behind turbulent spots can be seen in much of the data, even at the trailing edge sensor at all conditions. It is possible that there is an open separation at the trailing edge at some rotor positions at the lowest Reynolds numbers, but on average (in time) the trailing edge flow is attached.

4.6.3 NGV3 of the 715 LP turbine Rig tests

The results for NGV3 are far more complicated than those for NGV2. This blade row is subjected to a more disturbed flow as there is another stage upstream of it. It appears as if wake induced transition (caused by Rotor 2) occurs at around 80%s at the cruise Reynolds number. A second disturbed region occurs between those caused by rotor 2, and is must be caused by NGV2 and a combination of NGV1, and Rotor 1 causing a beating frequency with Rotor 2. RMS and skew data are consistent with this interpretation. The boundary layer at the trailing edge is attached in the time-mean at all Reynolds numbers.

While the wake turbulence convects at the freestream velocity, the perturbations seen by the hot film sensors travels at 70% of the local freestream velocity. The phase lag is due to the time that it takes the wake turbulence to diffuse through the laminar

boundary layer. However, when the wake reaches the position of flow separation it causes almost immediately start to transition, with no phase lag.

5. Linear Cascade and Flap Test Results

5.1. Introduction

The aim of this chapter is to illustrate how it is possible to increase the loading (i.e. lift) of certain LP turbine blades above the levels found in present day engines without any loss penalty. Pressure distributions, trailing edge boundary layer profiles and hot film measurements are used to illustrate how this can be achieved.

The chapter begins with a description of the flow on a datum profile, designated TL10. The measurements presented in the rest of the chapter are non-dimensionalised by a set of datum values taken from the TL10 profile at a Reynolds number of 130,000 and with unsteady inflow. The main details of the cascade are given in Chapter 3. The datum blade used in these tests is a very highly loaded profile that is of a type that is only now finding its way into current aircraft engines i.e. the BR715 turbo fan as described in Chapter 4. The rig used for these experiments is more fully described in Chapter 3.

The next set of measurements are presented from the cascade with an additional flap placed below the instrumented blade, (again see Chapter 3). This allows pressure distributions with increased lift to be investigated in terms of loss production and surface boundary layer characteristics. On the basis of these measurements a further set are presented with additional inserts placed into the rig. These measurements alter the pressure distributions still further by shifting the position of peak suction and boundary layer separation further aft, effectively aft loading the profiles.

The chapter concludes by showing that it is indeed possible to produce a suction surface profile that allows for an increased pitch chord ratio of 15% beyond that of the high lift datum profile with no loss penalty. This is achieved by understanding what

physical mechanisms allow these increases in loading to be achieved and understanding the surface boundary layer interaction with wakes shed from the upstream bars or blade rows.

5.2. Measurements from the datum blade TL10.

The trailing edge velocity profile and pressure distribution measurements for TL10 at a Reynolds number of 1.3×10^5 with steady inlet are shown in Figure 5.2.1. This pressure distribution shows the highly loaded character of TL10 to be mainly due to the high acceleration around the forward region of the blade.

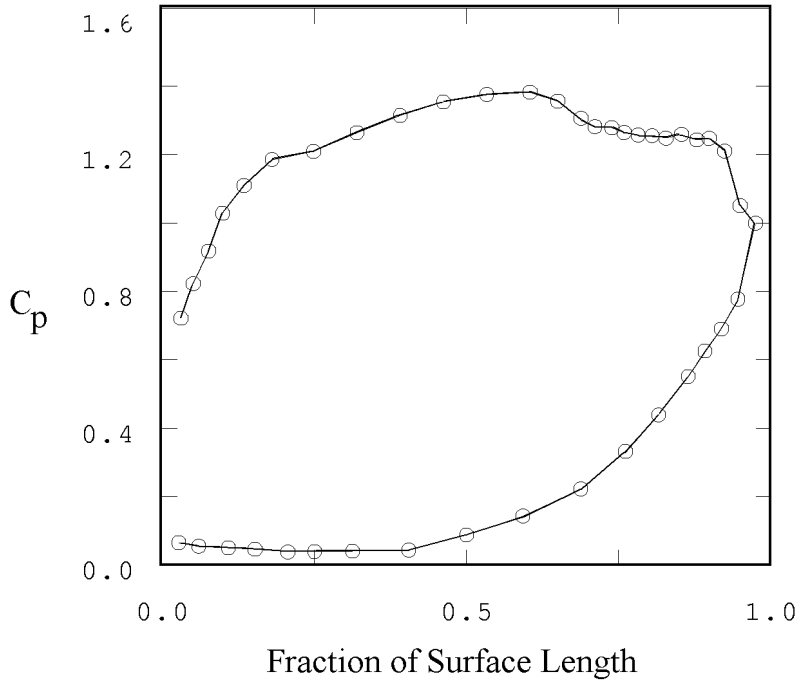

Figure 5.2.1 (a) TL10 datum pressure distribution with steady inlet flow at a Reynolds number of 1.3×10^5

The pressure distribution shows that the flow must also undergo a large rear surface diffusion which causes the boundary layer to separate at approximately 75%s. Reattachment occurs just before the trailing edge of the blade at approximately 95%s at this Reynolds number. The velocity profile for this pressure distribution (at 96%s) will be shown later in the chapter to be that of a transitional boundary layer.

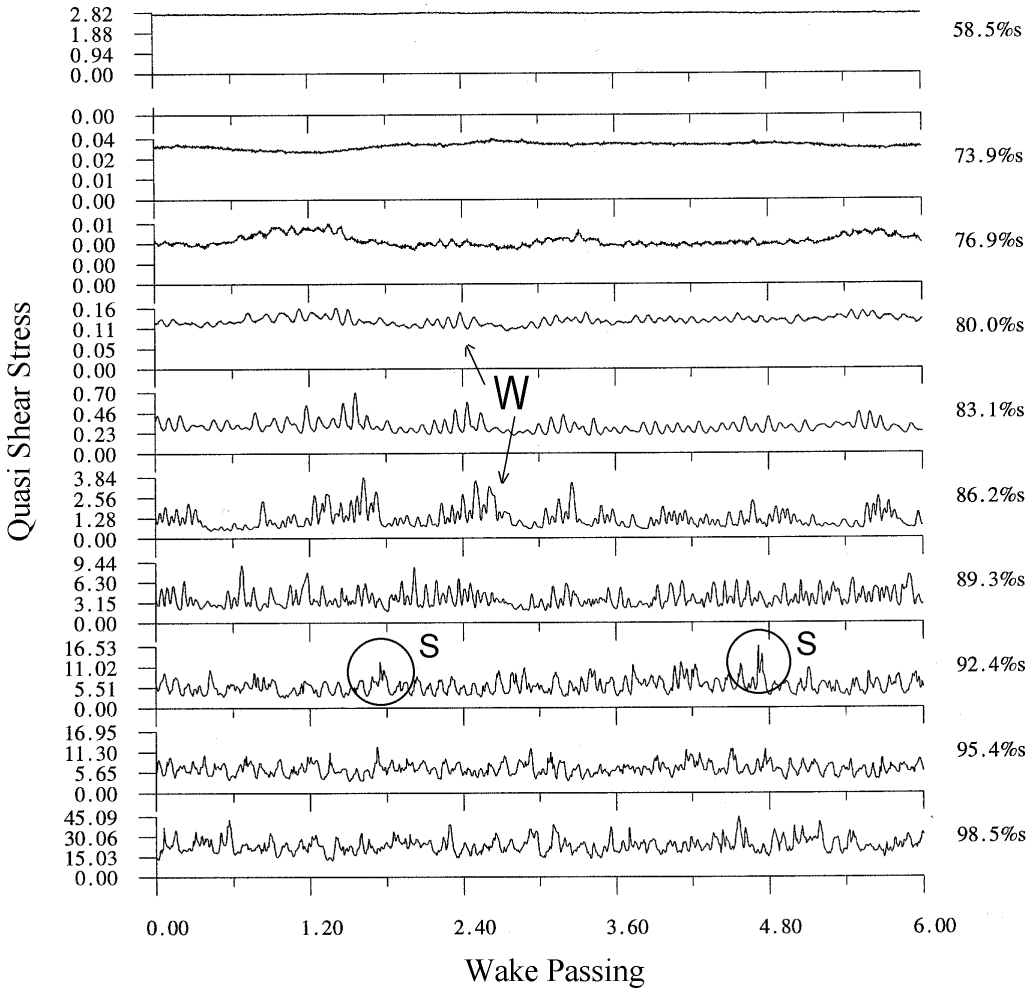

Figure 5.2.2 Hot film measurements from TL10 datum at a Reynolds number of 130,000 with steady inlet flow.

The raw signal hot film results in Figure 5.2.2 shows the time history of shear stress as measured at locations along the blade surface from 58.5%s to 98.5%s. The lowest value of shear occurs at 76.9%s although other low values occur at 73.9%s. It is therefore likely that the flow separates somewhere in the region of these sensors. The time history of the raw shear stress with no wakes present is plotted for the equivalent number of wake passings to the traces where wakes are present. This makes for easy comparison of measurements taken with and without wakes. At 76.9%s, the flow exhibits small fluctuations and develops wave packets (marked W) which grow rapidly as the flow travels downstream. The fluctuations become largest at 89.3%s, after which the flow starts

to break down. The mean level of the signals also rises rapidly towards the trailing edge of the blade where the final sensor shows the characteristics of a transitional, but attached boundary layer i.e. a high mean value of shear, with large fluctuations. The boundary layer at the final sensor is not fully turbulent despite the fact that transition occurred through a separated flow regime.

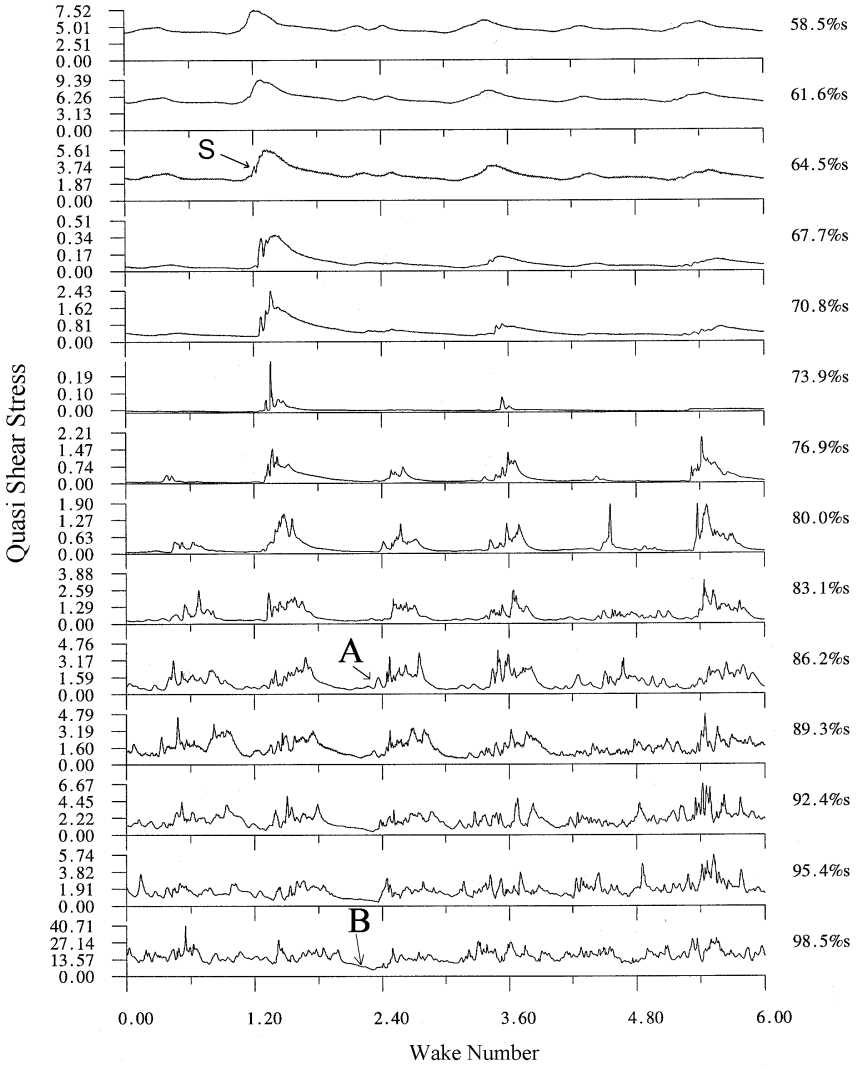

Figure 5.2.3 TL10 hot film measurements at a Reynolds number of 1.3×10^5 with wake passing. $\bar{f} = 0.78,\ \Phi = 0.7$.

The hot film traces contain some evidence that after some of the wave packet disturbances have been amplified sufficiently they form into turbulent spots, see regions marked ‘S’ at 92%s. This is probably open to other interpretations, but these regions do

contain a sudden burst of high frequencies with a small area that follows which could be considered the turbulent spot and calmed flow respectively.

Figure 5.2.3 shows hot film measurements for the case with unsteady (wake affected) inlet flow. Very low values of shear are visible between wake passings for the sensor at 73.9%s and 76.9%s, indicating that at some upstream wake positions the boundary layer is separated. The effect of calming is very evident in this figure. An important point to note from this data is that when a spot forms earlier than others, its calmed region seems to survive longer than those that are formed further downstream. Generally, wakes cause transition in the region of flow separation at 74%s, but if a wake causes transition before the flow separation then it is likely that its calmed region will survive longer, region ‘S’. Once the effect of the calmed region has passed, separated flow transition can be seen starting (see region marked B). This disturbance can be traced to the region marked ‘A’ further upstream. In a similar manner to the steady flow case, these small fluctuations of region ‘A’ are amplified until breakdown occurs.

Separated flow transition can be seen occurring more clearly between wake passings when this data is viewed on an ST diagram.

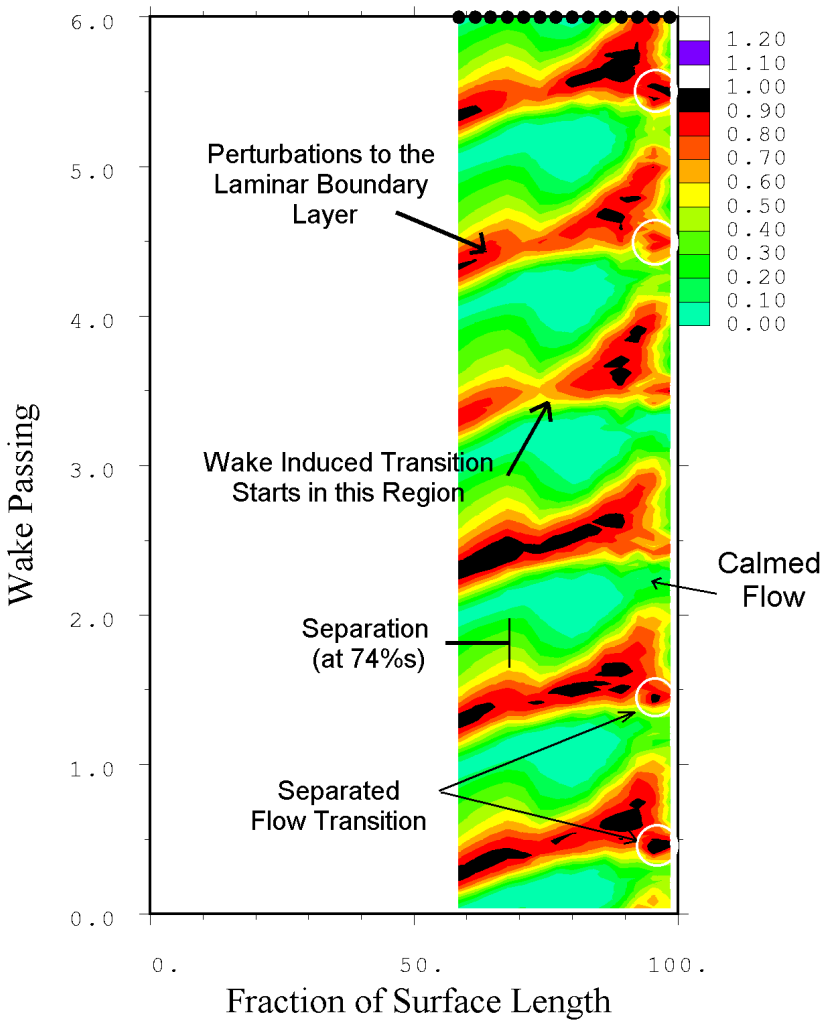

Figure 5.2.4 ST diagram of non-dimensional ensemble mean shear stress showing wake inducted transition (TL10, Re = 130,000, $\bar{f}$ = 0.78, $\Phi = 0.7$).

The ensemble mean shear stress data presented in Figure 5.2.4 is non-dimensionalised in such a way that the periodic fluctuations are enhanced at the expense of the overall levels of shear stress. In fact, the values of shear stress around the first sensor at 60%s are much less than those nearer the trailing edge. The flow transition shown here indicates more of the details of the wake transition process occurring around 74%s. The wedge shaped region of transitional flow then spreads out from this location formed by the difference in convection rates of turbulent spots. Their leading edges travel

at about 90%U_{inf} and the trailing edges travel at about 50%. The exact values of these convection rates are a function of pressure gradient, Solomon (1995)

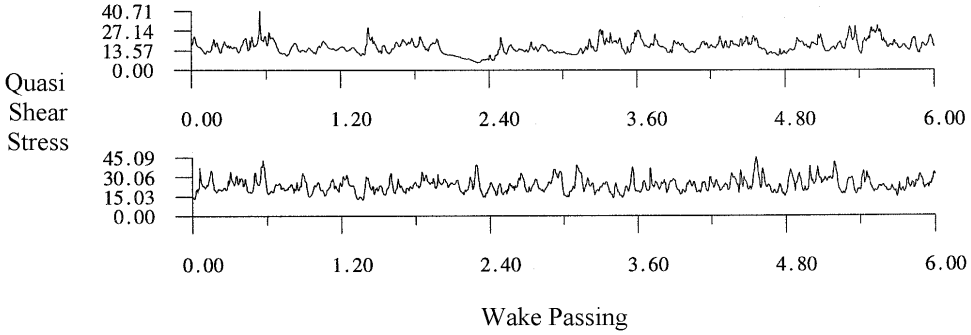

Figure 5.2.5 Comparison of hot film data steady and unsteady from TL10, surface location 96%s. Reynolds Number = 130,000 for both cases. For the unsteady case $\bar{f} = 0.78,\ \Phi = 0.7$.

Figure 5.2.5 shows the hot film measurements from the final sensor on the blade surface (located at 96%s) for flows with and without wakes (the upper and lower traces respectively). At the trailing edge the lowest shear is due to the presence of calmed regions. A comparison of the signals at the trailing edge sensors for the steady and unsteady inlet flow shows that far more laminar like flow exists for the case with wakes present. This is because calmed regions can only exist with unsteady flow, Schulte (1995).

5.3. Reynolds number variation for the Datum TL10 Profile

Figure 5.3.1 shows hot film measurements at a higher Reynolds number of 2.1×10^5 with steady inlet flow. Separation again occurs at 73.9%s and reattachment has started to occur at around 86.2%s. The size (streamwise length) of the separation bubble is approximately halved in length when compared to the lower Reynolds number. This is because breakdown to turbulent flow in the shear layer occurs very rapidly at this higher Reynolds number.

Since in this case the separation bubble is smaller, any possible loss reduction due to it being effected by wakes is also likely to be smaller. This is shown to be the case in Figure 5.3.2. Eventually a Reynolds number will be reached where the bubble and its loss becomes sufficiently small that the effect of wakes will only be to increase the loss generated as more of the blade surface is covered by turbulent boundary layer, (Hodson, 1985).

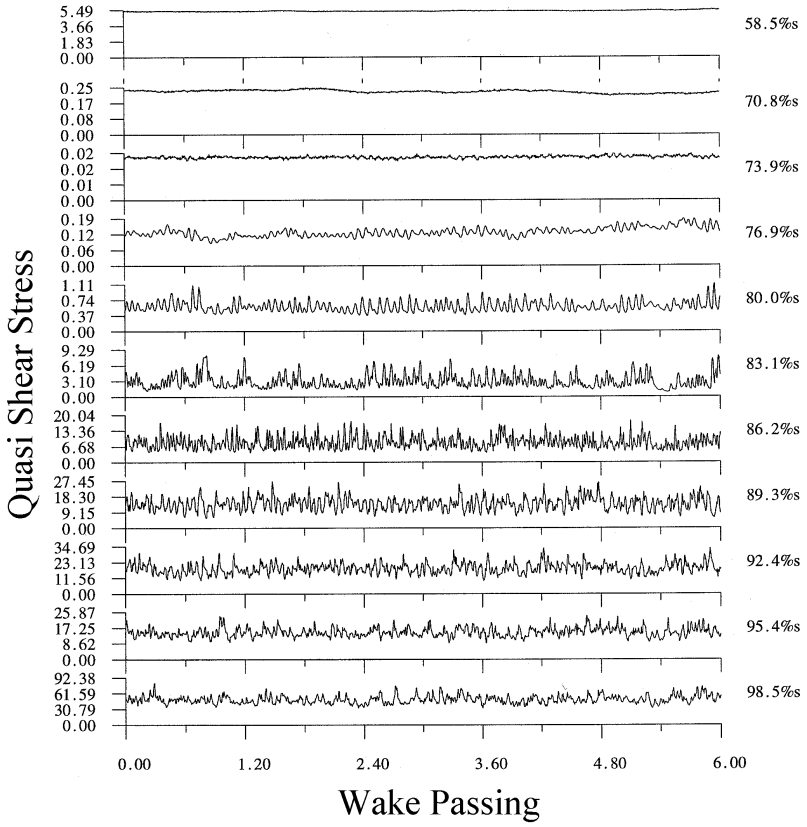

Figure 5.3.1 Hot film measurements from TL10 at the higher Reynolds number of $2.1x10^5$ with steady inlet flow, (no wakes).

As stated in chapter 3, when the flap is used to alter the pressure distribution one can no longer carry out wake traverses to measure loss. The boundary layer momentum thickness measured at 98%s is converted into a loss coefficient according to Denton (1990). In Figure 5.3.2 the trailing edge momentum thickness is non-dimensionalised by

the unsteady *high* Reynolds number momentum thickness. This serves to show how the loss increases with the size of the separation bubble which in turn increases due to the drop in Reynolds number. As already stated all other plots are non-dimensioned by the low Reynolds numbers values i.e. Re=130,000.

There is a large loss reduction at low Reynolds numbers due to the effects of the wakes, but as the Reynolds number is increased, the loss reduction diminishes. At a Reynolds number of 2.1×10^5 there is almost no reduction in loss when wakes are present.

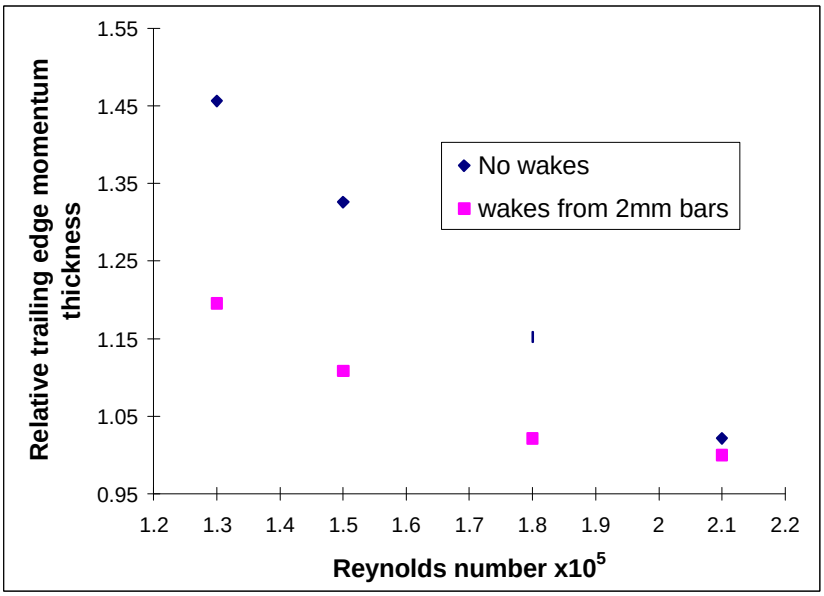

Figure 5.3.2 Relative trailing edge momentum thickness vs. Reynolds Number for the TL10 profile.

The low Reynolds number condition (1.3×10^5) was selected for the majority of the tests since this is where the greatest loss reduction occurred. This Reynolds number is that found in the last stages of the largest turbofan engines (such as the Trent 800) and it is also that found in the first few stages of smaller engines (such as the BR700 series). The blade loading shown in Figure 5.2.1 and the measured trailing edge momentum thickness are

taken as the datum values for non-dimensioning the rest of the results this chapter, see Table 5.3.1.

Datum value of momentum thickness	0.67mm
Datum suction surface circulation $\int \frac{V}{V_{te}} \frac{ds}{S_{\max}}$	1.079
Datum pressure surface circulation	0.379
Optimum Reduced Frequency	0.78
Assumed base pressure coefficient	0.1

Table 5.3.1 Loss and lift values for the TL10 profile at a Reynolds number of 130,000 and with wakes $\bar{f} = 0.78$.

5.4. Increased Loading

Since it is possible to decrease the losses generated by a blade row with the use of incoming wakes, the next logical question posed is can this be exploited in the pursuit of reducing the blade count? If it can this will reduce the cost and weight of the LP turbine. To answer this question, measurements were taken from pressure distributions with increased lift. To increase the lift the a flap was attached to the trailing edge of one of the blades (as described in Chapter 3).

5.4.1. Increased loading and losses

To increase the loading on a blade, i.e. to reduce the static pressure at the throat, the flap was rotated away from the suction surface of the instrumented blade. The pressure ratio driving the flow through the passage is that from the inlet to the cascade, to the exit created between the instrumented blade suction surface and flap. When the outlet area increases so does the mass flow through the passage, since the exit velocity is approximately constant. Since the throat area is constant, the velocity there must increase resulting in a larger diffusion over the back surface.

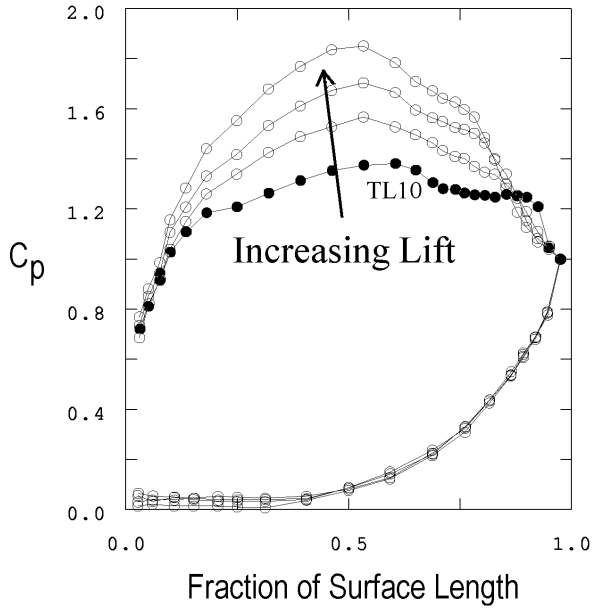

Figure 5.4.1 Increased loading: 9%, 15% and 21% lift above the datum TL10, with steady inlet flow at a Reynolds number 130,000 and $\bar{f}$ = 0.78.

Figure 5.4.1 shows the effect of increasing the flap angle and the resulting pressure distributions. TL10 is shown with solid symbols.

The geometric position of the throat and therefore peak suction was kept constant in these measurements. Figure 5.4.1 shows that the reattachment location of the separation bubble moves away from the trailing edge of the blade with increased loading. It is interesting to note that despite the increase diffusion that the flow must undergo the separation position remains at a constant surface location.

Hot film measurements were taken for the pressure distributions shown above, but with wakes present. Some of these are shown in Figure 5.4.2. For the case of a 9% increase in loading above TL10 (Figure 5.4.2a) flow separation occurs still occurs at around 74%s. It was found that there was no change in the location of flow separation for pressure distributions with the same location of peak suction when wakes were present or

absent. The no-wake pressure distributions were therefore shown in the previous figures as they more clearly highlight the separation bubble compared to the cases when wakes are present. Wake induced transition caused by every wake passing occurs just before 83%s and separated flow transition probably starts to occur between wake passings at around 89%s. The equivalent positions for the start of wake induced transition on the datum profile, TL10, and separated flow transition between the wakes are at approximately 80%s and 86%s respectively. The datum profile generally starts to show the initiation of turbulent spots downstream of the 9% increase in loading case. By the trailing edge, a number of becalmed regions can be seen for this condition which are similar to those seen in the measurements for TL10.

When the lift is increased to 21% above the datum profile (see Figure 5.4.2b), separation again occurs in the region of 74%s but a low shear stress is measured at 68%s. Wake induced and separated flow transition both occur at around 77%s. Some becalmed regions can still be seen, but the flow is far more turbulent at the trailing edge than for the previous conditions. Calmed regions therefore find it more difficult to survive if the flow has to undergo a increased diffusion.

Flow separation for all profiles for which the pressure distributions are shown in Figure 5.4.1 occurs at around 74%s and does not change much with increased loading, however the length of the separation bubble reduces. The increase in diffusion causes the boundary layer to become more receptive to any disturbances and it starts to undergo transition and reattachment earlier. The increased loading therefore leads to a reduction of the laminar length of the separation bubble. The position of the start of wake induced transition does move forward, but to a much lesser extent than the position of separated flow transition.

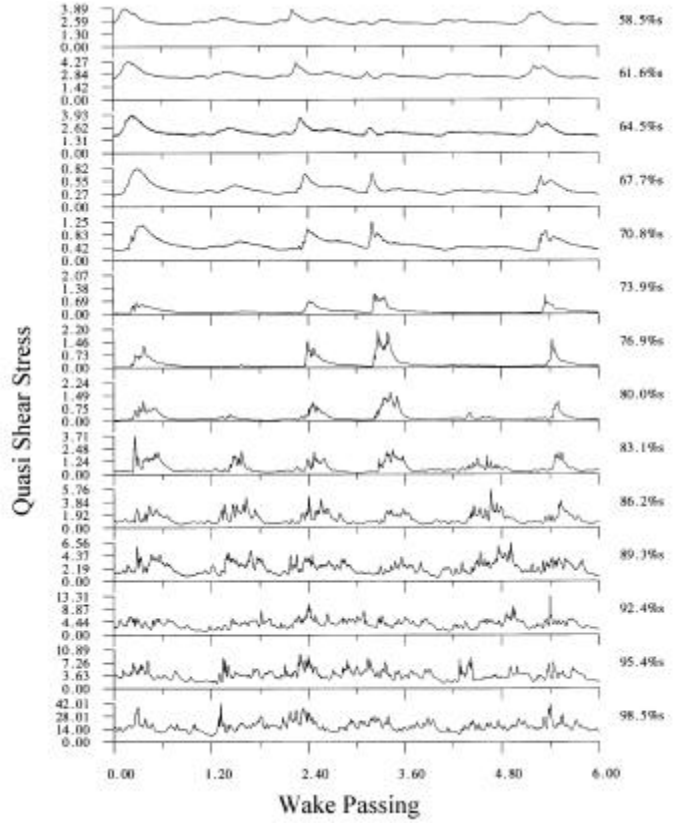

(a)

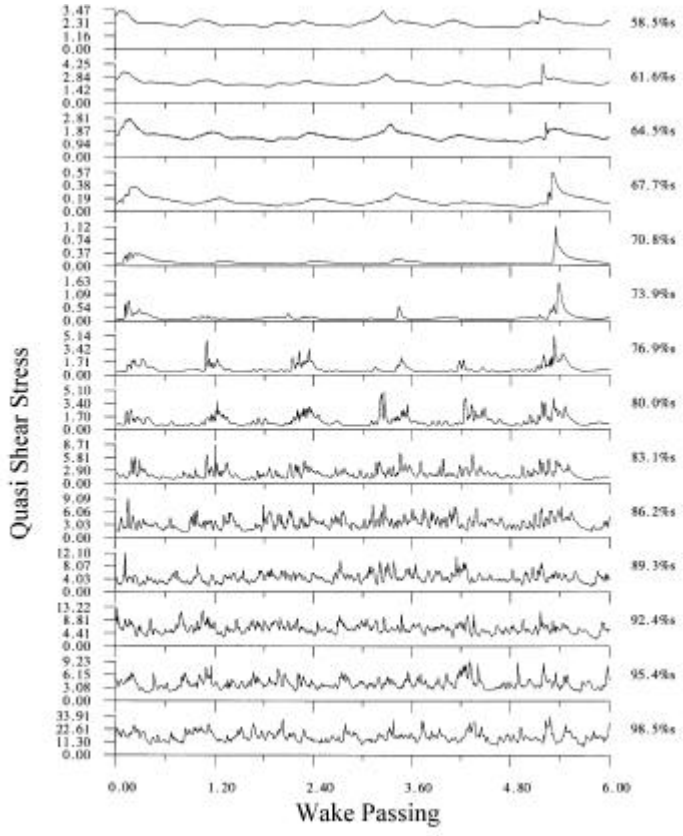

(b)

Figure 5.4.2 Hot film measurements for relative lifts of 9% and 21% above the datum blade. Unsteady inlet flow. Reynolds number = 130,000 $\bar{f} = 0.78$, $\Phi = 0.7$.

With increased loading comes increased diffusion, so the reattachment process occurs under more extreme conditions which is partly why the losses generated by these profiles are likely to increase. As the loading is increased, the hot film measurements show that an increasingly large amount of blade surface is covered by turbulent boundary layer. This is the other reason why the losses generated by these profiles are likely to increase above that of the datum profile.

Figure 5.4.3 shows the suction side boundary layer loss ratio against lift ratio relative to the datum profile. As expected, when the lift is increased above that of the datum profile, the suction surface loss increases. This loss increase is due to the increased length of turbulent boundary layer that is allowed to form as the laminar bubble length is reduced. The laminar region of the separation bubble produces little loss as it is a region of low shear and low velocity flow. Since this region is reduced in length in favour of more surface length covered in turbulent flow it is understandable that the losses increase.

Figure 5.4.3 also shows that the potential for obtaining a loss reduction with the use of wakes increases as the loading increases. The difference in the gradients of increases in loss with increases in loading, with and without wakes, shows that it may be possible to keep the losses well below the steady flow loss at lift levels higher than were possible with the current experimental rig. It is not unreasonable to assume however, that there will come a loading level where the ability of becalmed regions to suppress separation bubbles may be lost. The figure also shows that only when the loading level reaches around 20% above TL10 do the losses generated with wakes then become higher than the level of loss produced by TL10 with steady inflow.

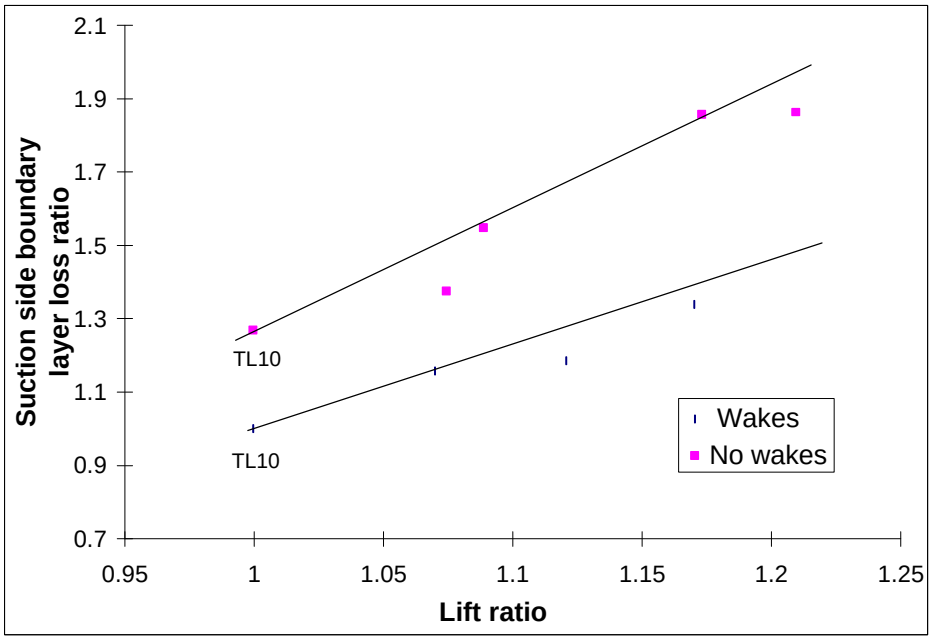

Figure 5.4.3 Suction side boundary layer loss ratio vs. lift ratio for a number of pressure distribution, with and without wakes. Re = 130,000, $\bar{f} = 0.78$, $\Phi = 0.7$.

Figure 5.3.2 showed that at a higher Reynolds number of 2.1×10^5 the loss reduction between the steady and unsteady cases for the datum profile was minimal. Since the data with and without wakes have different gradients in Figure 5.4.3, is it possible that when higher lifts are generated at higher Reynolds numbers, a greater loss reduction would occur than at the datum lift at the same high Reynolds number.

Current steady flow designs avoid large separation bubbles near the trailing edge because it is believed that there is always a danger of the flow not reattaching. If this happens the result would be an *open* separation and as a consequence a large loss would be generated. Since the laminar length of the separation bubble decreased with increasing lift open separations do not form with the rig in this configuration. It will be shown later that when aft loaded pressure distributions were produced, sometimes these did result in open separations.

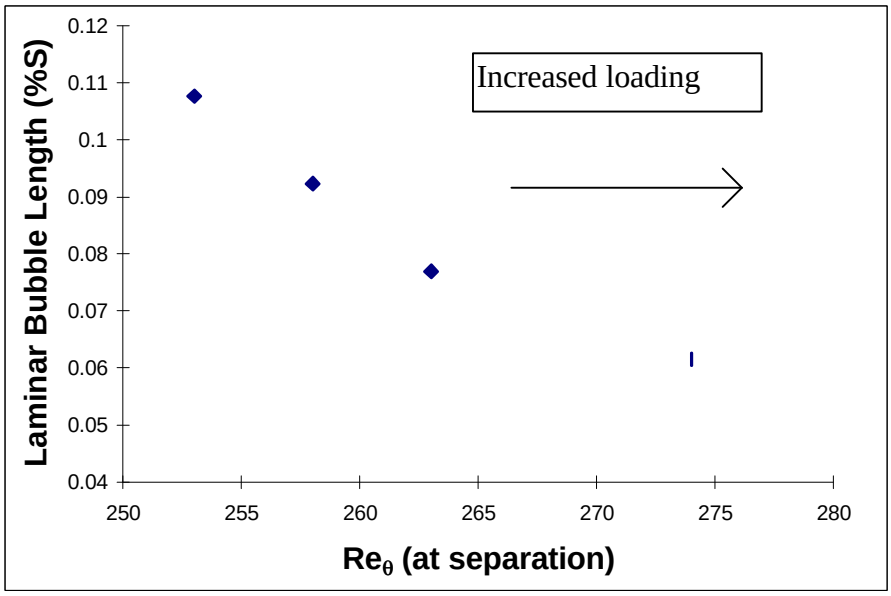

Figure 5.4.4 The length of the laminar region of a separation bubble with increased lift. All measurements taken at a Reynolds Number 130,000.

Figure 5.4.4 shows how the lift of the profiles increases to 121% of TL10 the laminar bubble length is reduced by half. In effect the length of the separation has reduced with increasing lift (and therefore diffusion). This effect is discussed later in this chapter.

5.5. Aft Loading

The effect of upstream wakes on the profile loss of a downstream suction surface boundary layer has been shown to be beneficial especially at high loadings and low Reynolds numbers. The hot film measurements shown in the previous section (Figure 5.4.2) indicated that there was a large amount of surface covered in transitional and turbulent flow after boundary layer reattachment. This was shown to increase with higher loadings as the laminar length of the separation bubble reduced. In terms of loss production, it is better to promote laminar flow and reduce the amount of blade surface covered by turbulent boundary layer. If the extent of the turbulent boundary layer could be reduced, then so could the profile loss produced by it. To this end, the position of peak

suction was moved aft along the instrumented blade surface, so that separation and reattachment occurred later so reducing the amount of turbulent wetted area.

The TL10 profile produced a pressure distribution with peak suction at about 53%s. In the following investigations, the position of peak suction was moved to 60, 65 and 68%s. Under steady flow conditions, it was found that sometimes the separation bubble did not reattach before the trailing edge of the blade, resulting in an open separation and a large loss. However, when the blade was subjected to incoming wakes, it was found that the boundary layer was *always* attached, no matter what the loading, or position of peak suction.

To move the position of peak suction, the blade below the one fitted with instrumentation was fitted with additional shapes (see chapter 3, Figure 3.2.2). When the flap was at large angles from the vertical, suction was also applied to the flap surface facing the blade under investigation. This was designed to keep the flap's boundary layer attached to the flap, thus maximising the possible loading available.

Due to the construction of the experimental rig, it was not possible to conduct a well ordered parametric investigation, as little detailed or accurate control over the pressure distributions was possible. An ideal pressure distribution would look like the one for the datum blade but with a higher loading and/or a position of peak suction nearer the trailing edge. Some pressure distributions produced large diffusions, but little leading edge loading or loading over the forward part of the blade. These sorts of pressure distributions resulted in only a small or no increase in lift over the datum profile. Therefore, a wide spread of measurements for various pressure distributions were obtained, some of which turned out not to be optimum.

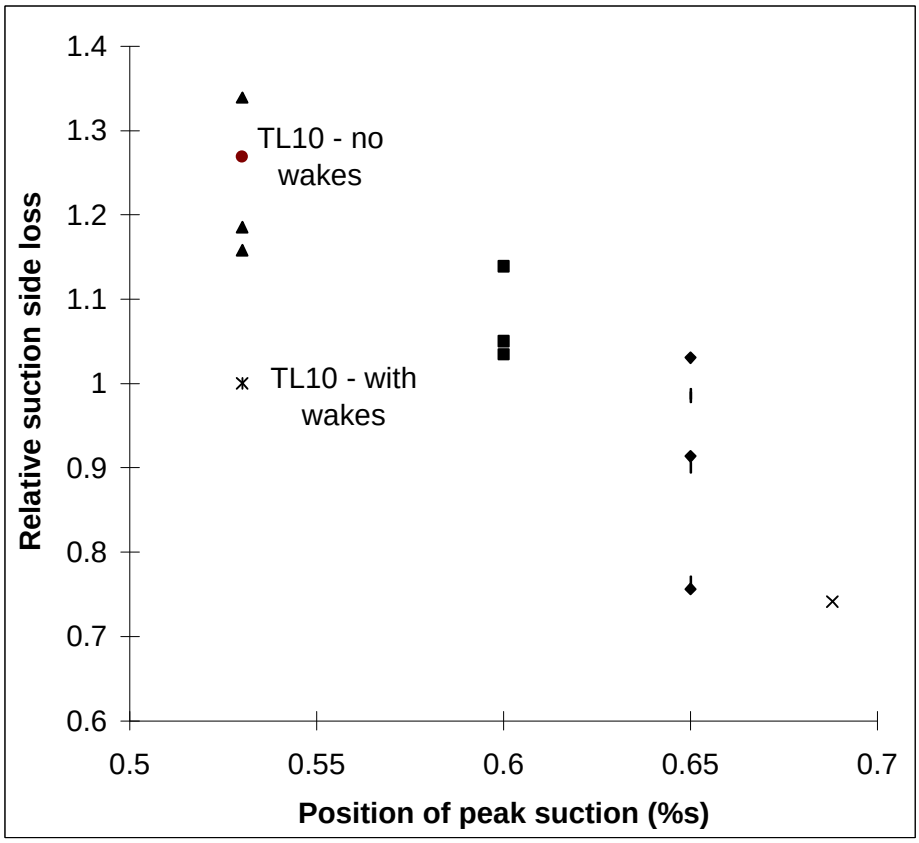

Figure 5.5.1 Relative suction side loss vs. position of peak suction. All measurements taken at a Reynolds Number 130,000, $\bar{f} = 0.78$ (i.e. with wakes).

Figure 5.5.1 shows the variation in relative suction side loss vs. the position of peak suction. These measurements are non-dimensionalised by the values taken from TL10 with wake affected inflow. There is a trend for the losses produced by a blade surface to reduce when the position of peak suction is moved aft. Unless otherwise stated, all the measurements in this figure were measured with wakes. The reduction in loss can be attributed to a reduction in turbulent boundary layer after separation bubble reattachment and the reduction in the size of the separation bubble due to the action of the turbulent spots and their calmed regions. As described by Schulte (1995) the entropy produced by the calmed region is approximately the same as that produced by a laminar boundary layer. In the context of separation bubbles and the losses they produce the entropy produced by a

calmed region is mush less than that produced by a the reattachment of a separation bubble. The details of the losses generated by a separation bubble are discussed in Chapter 6.

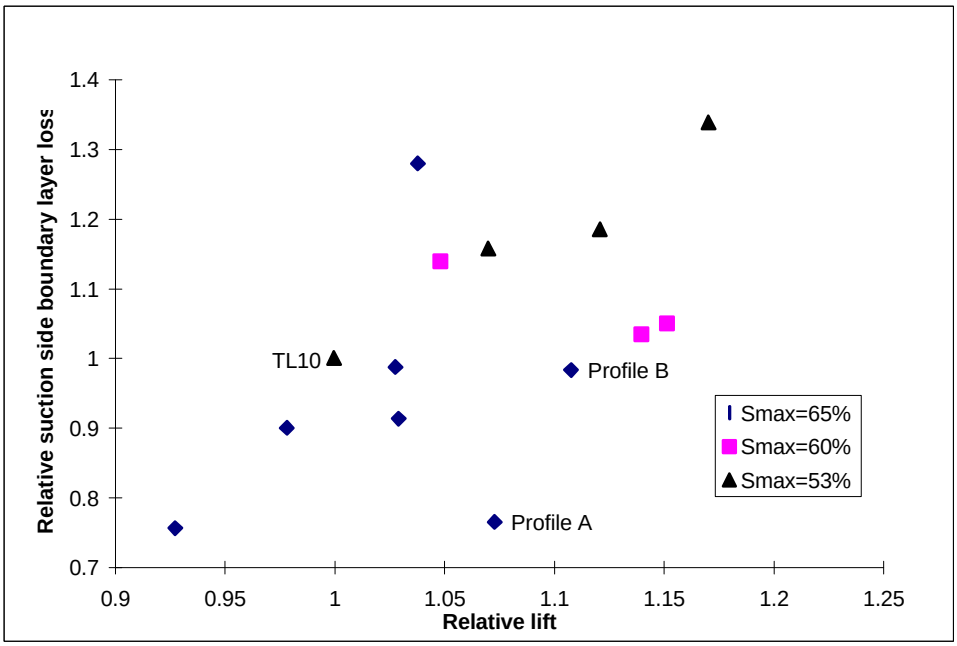

Figure 5.5.2 Suction side boundary layer loss vs. relative lift for different positions of peak suction. Reynolds Number 130,000. $\bar{f} = 0.78$, $\Phi = 0.7$.

Figure 5.5.2 shows the relative suction side boundary layer loss vs. relative lift for different positions of peak suction. Pressure distributions with peak suction at 65%s generally produced the lowest loss and were capable of achieving the highest relative lifts. Some profiles with peak suction at 60%s indicate an increased lift, but also an increase in loss above the datum. For the present study any losses above the datum ruled those profiles out of further investigation as the objective was to achieve increased lift without a loss penalty.

This pressure distribution in Figure 5.5.3a shows the high leading edge loading for a profile with a peak suction that occurs at 65%s. There is only a small increase in velocity in the region from 25% to 45%s after which the flow accelerates towards peak suction at

65%s. The flow then diffuses rapidly to the trailing edge. The diffusion factor is 0.26 based on velocity. It is likely that a further increase in lift could be achieved with this profile, if there was a more rapid increase in velocity in the region between 25 and 45%s. It should be possible to increase the loading without any increase in loss boundary layer losses as the boundary layer is unlikely to undergo transition in this region of flow acceleration. It should be noted that there may be reduction in incidence tolerance if the loading as increased too much around leading edge of the profile. Therefore at high incidences, this profile might produce greater losses than TL10.

In Figure 5.5.3b, trailing edge boundary layer profiles, take at 96%s, are shown at one quarter intervals of one wake passing period for the pressure distribution designated profile A. It can be seen that the free stream velocity changes by nearly 10% as the wakes pass, but there is little change in the shape of the inner part of the velocity profile. The inner region (out to 1.0mm) is almost linear. There is then a region between 1mm and 3mm where the flow merges into that of the freestream. The changes in the free stream can be attributed to the velocity defect of the wakes and the consequent negative jet effects. The fact that the boundary layer does not separate at any time during a wake passing event is due to the reduced frequency. If the reduced frequency was lower, then the boundary layer would be more likely to separate after the effect of the wake turbulent spot and calmed region had passed. Were the reduced frequency to be lower one would expect to see the boundary layer separate at some fraction of the wake passing cycle and this might increase the losses.

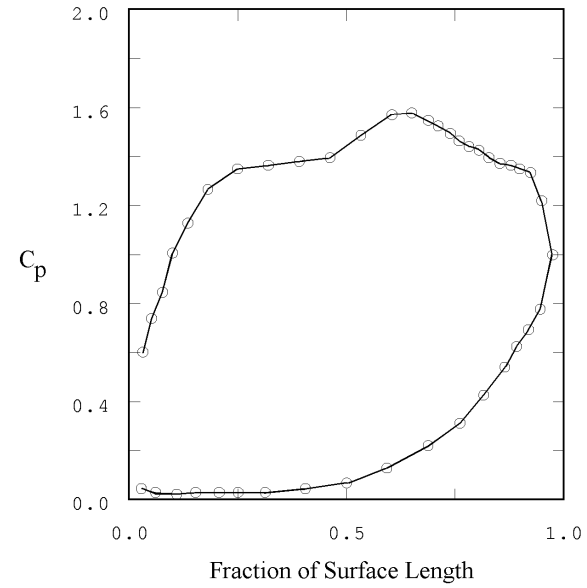

(a)

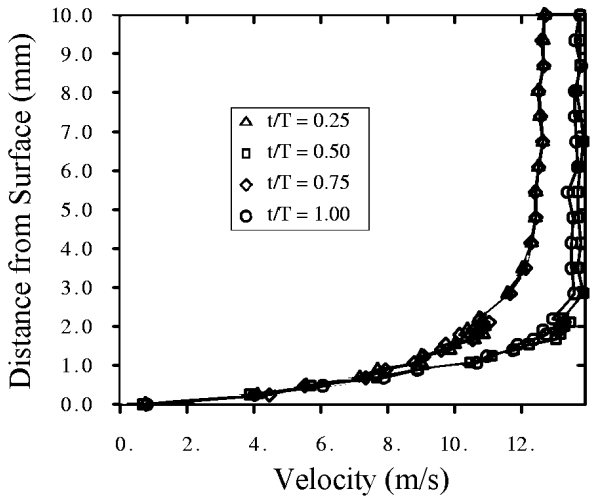

(b)

Figure 5.5.3 Pressure distribution for profile A and four velocity profiles taken during the passage of a single wake, S_{peak} = 65%s. Reynolds Number 130,000. $\bar{f} = 0.78$, $\Phi = 0.7$.

Figure 5.5.4c shows the hot film measurements for profile A. Separation seems to occur at around 80.0%s, but there are low values of shear upstream and downstream of this sensor position. The passage of wakes produces perturbations in the laminar boundary layers from 58.5%s to 73.9%s. After this position, some of the perturbations develop into

turbulent spots. A spike in the shear stress signal occurs at wake passing number two, for the sensor at 67.7%s. As this spot develops, a becalmed region forms behind it. However, as the spot travels downstream another spot either forms or spreads in a spanwise direction to destroy the calmed region of the first spot at 86.2%s, labelled S. However, the calmed region of the ‘new’ spot can clearly be seen at the trailing edge sensor. Despite the high mean value of shear stress near the trailing edge, there are large amplitude fluctuations and many low shear ‘troughs’ in the signal. The reductions in shear down to the levels of the troughs is due to the This boundary layer contains regions of calmed flow and is therefore not fully turbulent.

The hot film measurements show that the boundary layer at 58.5%s is laminar where the first hot film sensor is located, with a periodic perturbation imposed by the passage of wakes. It should be noted that wake induced transition does not occur in the constant velocity region from 25 to 45%s.

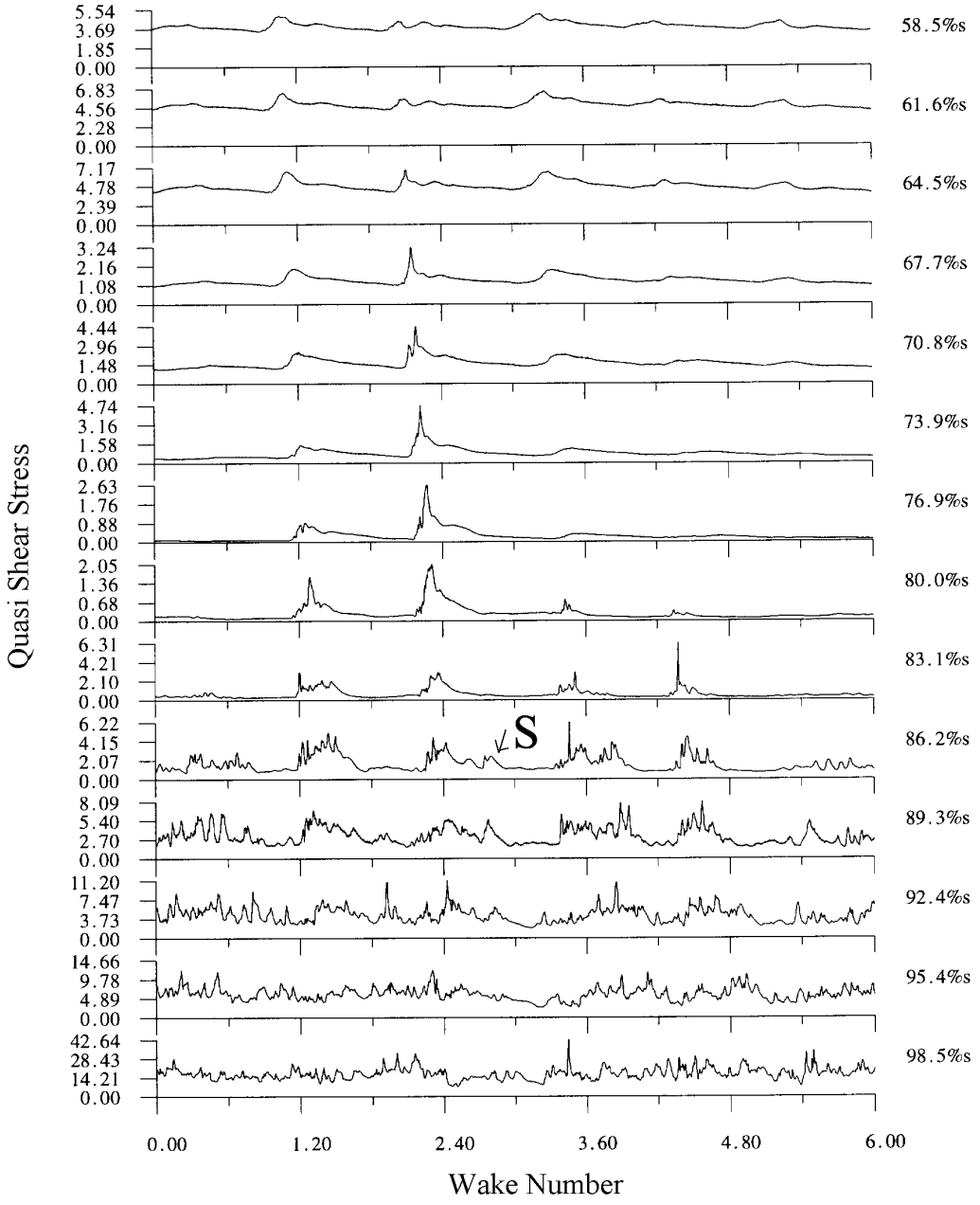

Figure 5.5.4 Hot film measurements for profile A, (S_{peak} = 65%s). Reynolds Number 130,000. $\bar{f} = 0.78$, $\Phi = 0.7$.

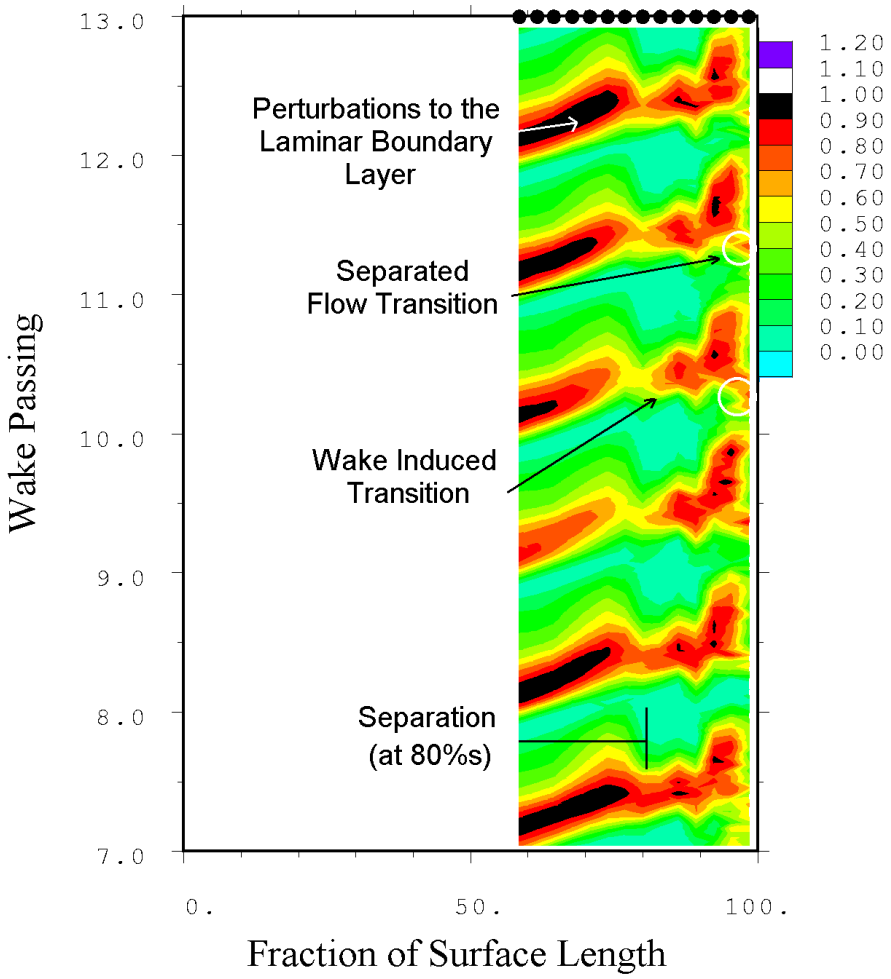

Figure 5.5.5 ST diagram of non-dimensional ensemble mean shear stress for the aft loaded profile A. Reynolds Number 130,000. $\bar{f} = 0.78$, $\Phi = 0.7$.

The ST diagram of non-dimensional ensemble mean shear stress is shown in Figure 5.5.5. This contains similar characteristics to that of the datum profile TL10. Wake inducted transition can again be seen occurring around the separation position at 80%s. The classical wedges seen in Figure 5.2.4 have been slightly modified in the region at around 89%s. The exact cause of this is unknown at this time, but this could be due to the effects that these highly loaded profiles have in distorting the wake and negative jet.

Another good pressure distribution is that for profile B, see Figure 5.5.6. This has similar characteristics to TL10, in that there is a large amount of leading edge loading, then an easing off of the acceleration after 20%s and a steady acceleration up to peak suction. However like profile A, this profile has peak suction at 65%s and a loading 11% greater than TL10, but only 95% of the loss. There is some evidence of a separation bubble, but as this pressure distribution was measured with wakes present, the effect of the bubble is small. The hot film measurements (Figure 5.5.6) show that separation occurs at around 80%s which is the same as for profile A. This is unsurprising as peak suction is at the same streamwise position in both cases. However the diffusion level for profile B is slightly higher (0.41 vs. 0.37 based on pressure), which may be why profile B has a larger loss than profile A.

It is interesting to note that despite the increased diffusion for profile B, the boundary layer separates at the same surface location as profile A. This would lead one to the conclusion that it is indeed the diffusion level not the rate of diffusion with the surface length that is most important.

When comparing the hot film measurements from Figure 5.5.4 and Figure 5.5.6 it is interesting to note that the wake induced turbulent spots formed in profile B earlier than those formed for profile A. As noted above the diffusion for profile B is slightly higher than for profile A. This means that an increased level of diffusion makes the boundary layer more receptive to disturbances, so that wake induced turbulent spots can form earlier. Despite the earlier formation of turbulent spots, their calm regions do not seem to survive any more than for profile A and again this could be due to the increased diffusion level for profile B.

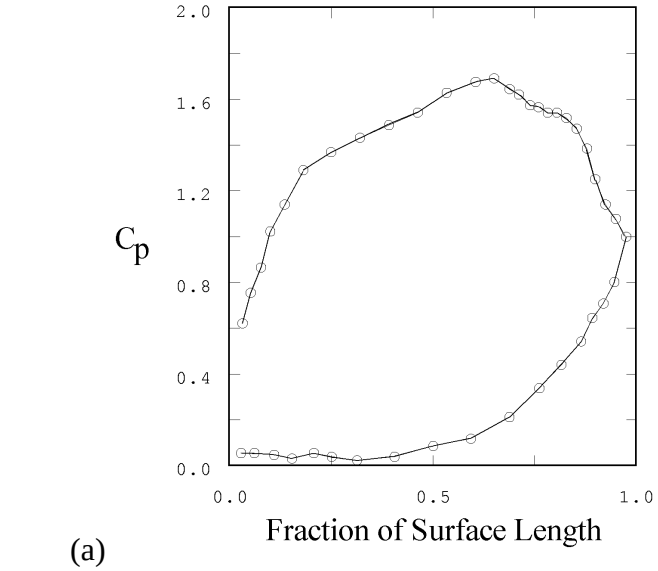

(a)

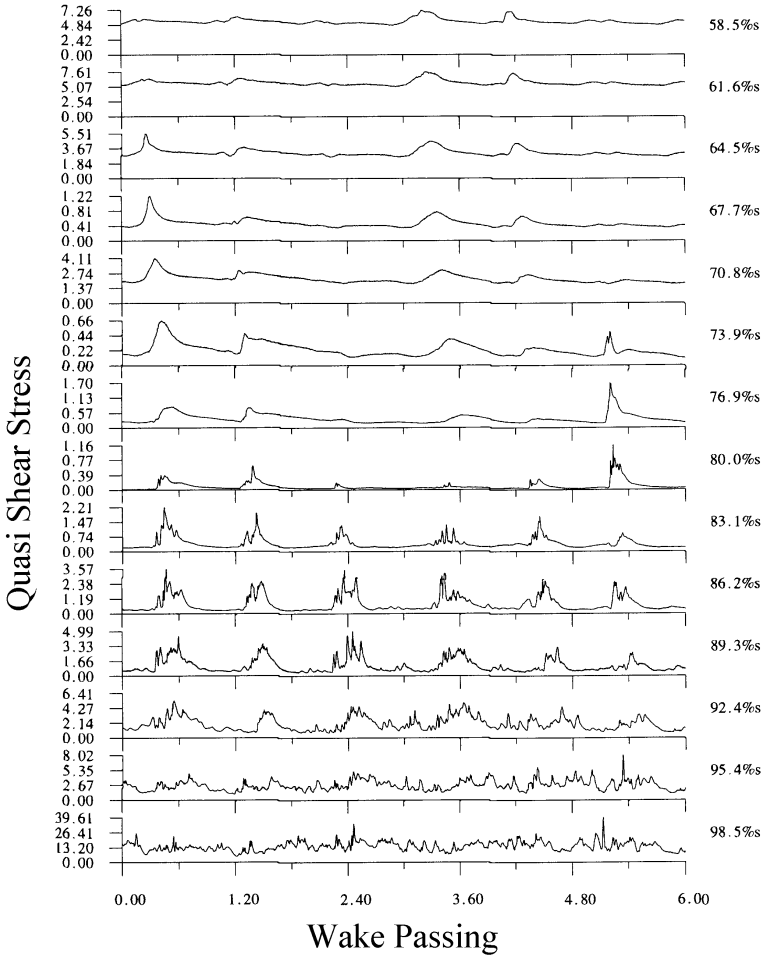

(b)

Figure 5.5.6 Pressure distribution (a) for profile B with 11% greater lift than datum blade and hot film measurements (b). Unsteady inlet flow. Reynolds number 130,000. $\bar{f} = 0.78$, $\Phi = 0.7$.

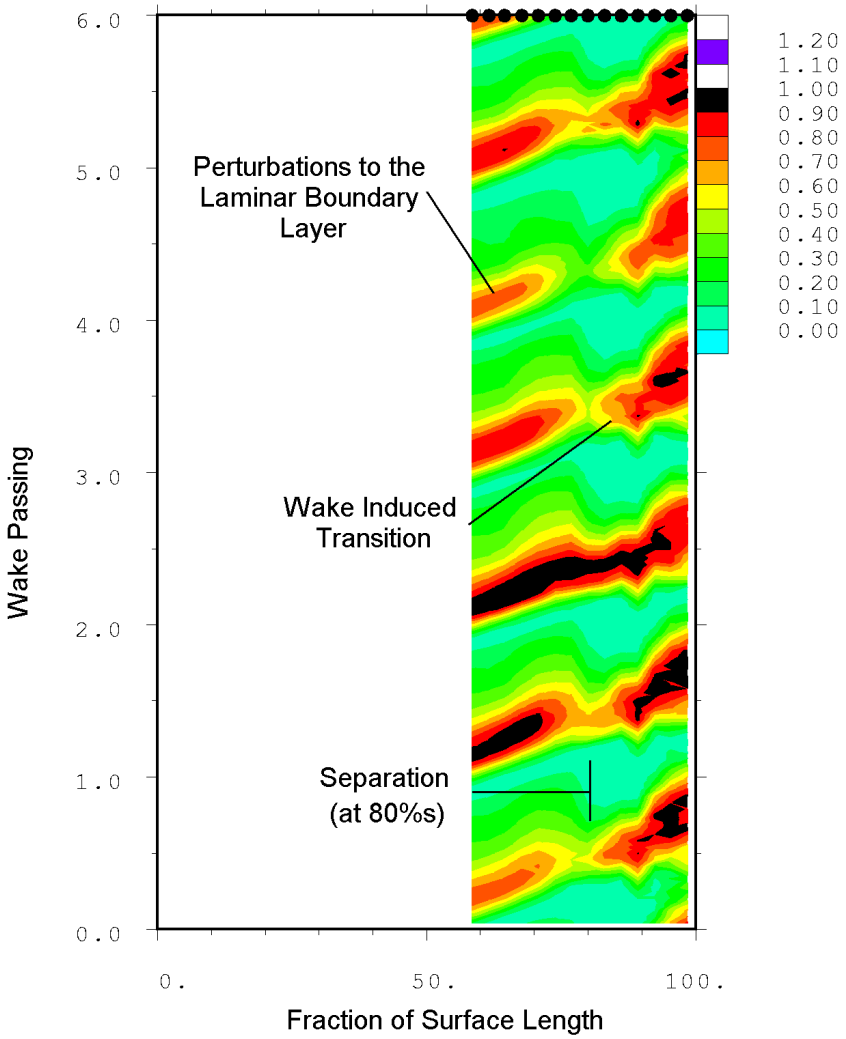

Figure 5.5.7 ST diagram of non-dimensional ensemble mean quasi shear stress for profile B. Reynolds number 130,000. $\bar{f} = 0.78$, $\Phi = 0.7$.

Figure 5.5.2 showed how the suction side boundary layer loss varied with position of peak suction. The profile loss for a blade row includes contributions from the trailing edge, pressure side boundary layer and losses associated with boundary layer blockage. In the following analysis, these terms are included and assumed to be constant, despite the changes in loading etc. The values for each loss component are taken from the TL10 datum profile at a Reynolds number of 1.3×10^5 and are taken from Curtis (1996). Figure 5.5.8 shows the loss breakdown.

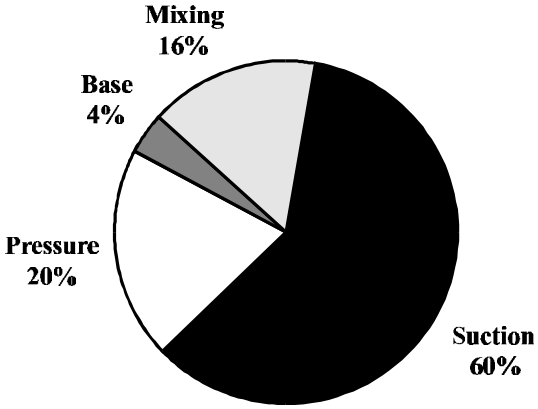

Figure 5.5.8 Loss breakdown for a typical high lift low pressure turbine blade, Curtis, 1996.

The extra terms now included in the analysis will result in a dilution of the effects of the suction surface loss reduction. Figure 5.5.9 shows the same data as Figure 5.5.2 but with the extra contributions terms included.

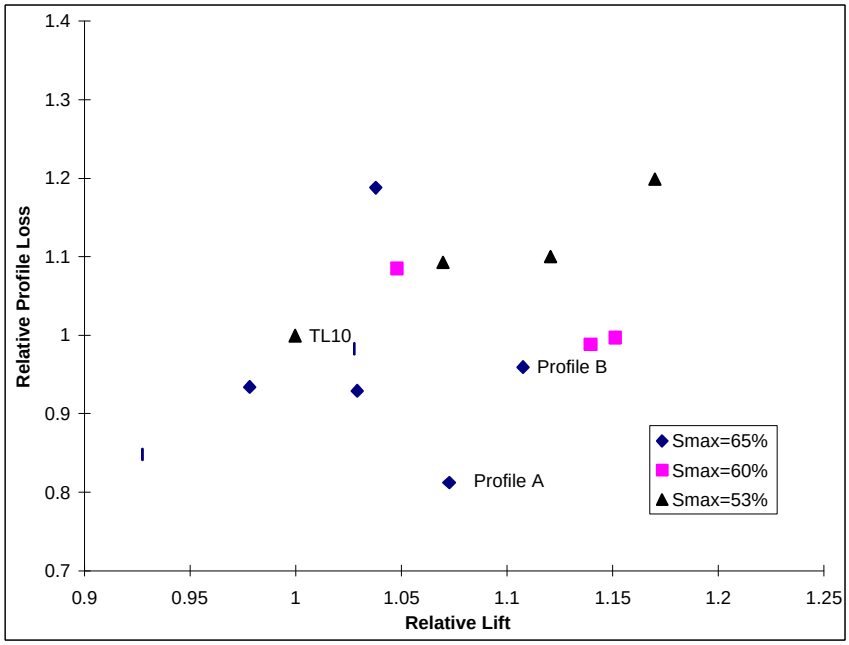

Figure 5.5.9 Relative calculated total pressure loss vs. Relative lift for peak suction at 53%, 60% and 65% surface length.

Including the contributions of the pressure side boundary layer, trailing edge and blockage losses, the 'best' pressure distribution discussed above (profile A) now shows a reduction in loss to 81% of the datum up from 78% without the other contributions.

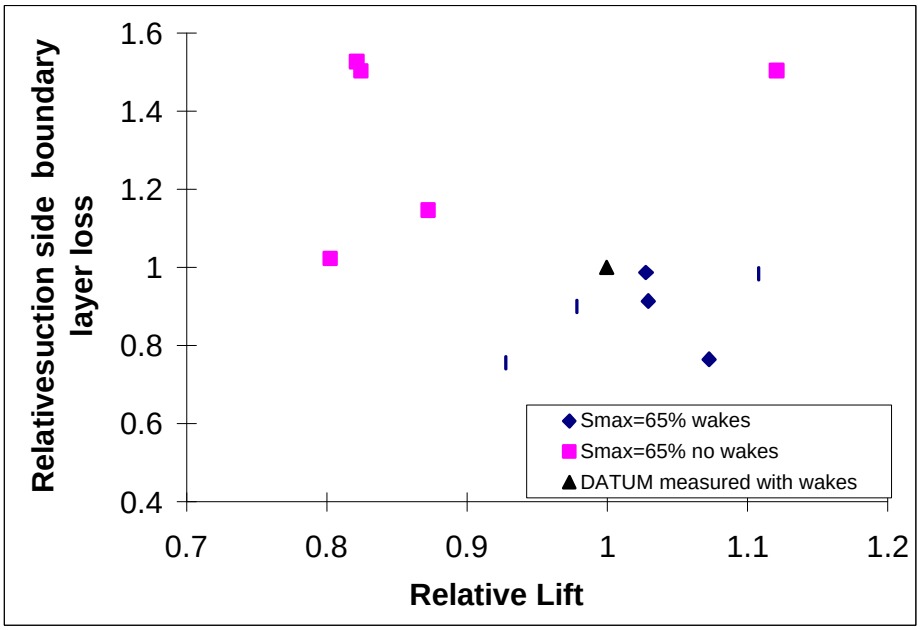

Figure 5.5.10 Relative suction surface boundary layer loss vs. relative lift for distributions at 65%s with and without wakes.

Figure 5.5.10 shows relative suction surface boundary layer loss against relative lift for distributions at 65%s with and without wakes. Unfortunately, there are not many pressure distributions available with steady inflow in the region of a relative lift of 1.0. However this figure does show that aft loading turbine blades is only possible when wakes are present to control the losses generated by the separated flow region as the measured losses are much high when wakes are not present. Therefore, if a blade is to be aft loaded and one is to avoid large separation bubble and losses, wakes must be present.

5.6. Conclusions

In low Reynolds number flows (typically 130,000), the presence of wakes on the suction side boundary layer on a highly loaded low pressure turbine blade has a profound effect on the losses generated. Losses generated by the separation bubble can be reduced with the effects that incident wakes have on the boundary layer. The greater the lift, the greater the benefit of the wakes. It was shown that up to a 20% increase in lift could be achieved with wakes present before the suction side boundary layer losses reached the values of the datum profile measured without wakes.

With a 20% increase in lift above the datum blade, the laminar length of the separation bubble reduced by nearly 50% and the suction surface losses increased by approximately 30%. For a fixed position of peak suction with increased loading, reattachment of the separation therefore moved further from the trailing edge and resulted in a large amount of blade surface covered in turbulent boundary layer. Aft loading the pressure distributions decreased the amount of turbulent boundary layer that was present which reduced losses generated from the suction surface. Most aft loaded profiles were only viable when they are used with incoming wakes because without wakes the separation bubble would not always reattach by the trailing edge of the blade.

Hot film measurements showed that separated flow transition occurred at the same streamwise position in steady flow and also between wake passing if the wake reduced frequency was low enough.

6. Turbulent Spot and Separation Bubble Interaction

6.1 Introduction

Previous chapters have shown that a loss reduction occurs on highly loaded LP turbine blades through the interaction of the separation bubble, wakes and turbulent spots. This chapter shows measurements using the flat plate rig described in Chapter 3 that illustrate this interaction in more detail. These experiments were carried out to gain a greater understanding of the physics of turbulent spot and wake interaction with separation bubbles. They were also carried out to help validate the numerical predictions which are presented in Chapter 7, that is, to check that those predictions correctly capture the physics of the interactions.

In addition to the artificial turbulent spot interaction with separation bubbles, moving bars have also been used to simulate wakes for the same conditions as the artificially generated spots. With these two types of experiment one can attempt to subtract the effect of the spots and observe the effect of wake turbulence alone on the separation. This is important because the work of Schulte (1995) and Cumpsty *et al* (1995) indicated the importance of the calmed region on the separation bubbles and separating the effects of the wakes will give a clearer picture of how this interaction occurs.

6.2 The Flow for the Datum Profile

It is first necessary to show that the flat plate rig is capable of reproducing the flow physics seen in experimental rigs used in the previous chapters. In this section some of the

basic flow features are shown and they illustrate that this rig does adequately reproduce the correct flow conditions and features.

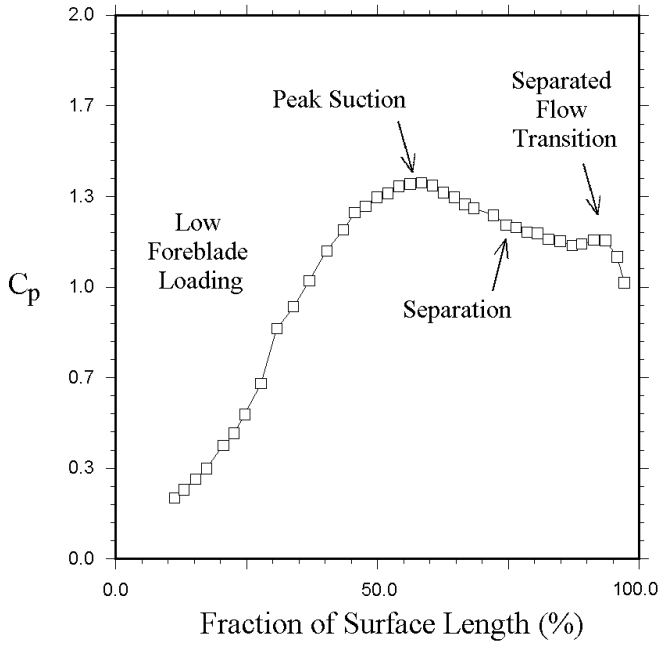

Figure 6.2.1 Pressure distribution representing the TL10 datum profile from the flat plate. Reynolds number 130,000. Steady inflow.

The first set of experiments was carried out on the rig to obtain measurements from a TL10-style pressure distribution and to validate the rig operation under steady flow conditions. The effects of the spots and wakes on the separation bubble were then investigated. Table 6.2.1 shows some time mean boundary layer characteristics at the trailing edge of the flat plate and the TL10 profile in cascade. These indicates that the time averaged boundary layer states are similar for both at the trailing edge. Although the leading edge loading of the pressure distributions on the flat plate were different to those on the TL10 profile, see Figure 5.2.1, the diffusion on the flat plate and TL10 were matched, see Figure 6.2.1. From an engineering point of view, the separation bubbles produced by the flat plate pressure distribution are similar in character to those generated by TL10. It was found to be impossible to obtain similar forward loading to the TL10

profile with this arrangement of the flat plate rig. The Reynolds number (based on momentum thickness) at separation are approximately the same. It was felt that the interactions of the wakes and spots (from a qualitative point of view) were most important, so the pressure distribution was deemed acceptable.

Blade	TL10 - cascade	Flat Plate Rig
θ / Chord	5.45	5.21
Shape factor	1.6	1.6
Re_θ at separation	253	265

Table 6.2.1 Boundary layer characteristics from the TL10 profile and the flat plate rig at a Reynolds number of 130,000.

In summary, the time averaged properties of the boundary layer match very closely to those seen in the moving bar rig of Chapter 3. The next section will show that the transient details of the flow also match very well.

6.3 Spot separation bubble interaction - TL10 style profile

6.3.1 Unsteady Quasi Shear Stress Measurement for a TL10 style profile

Figure 6.3.1 shows hot film measurements for a Reynolds number of 130,000, with spots generated using the loudspeaker pulsing at a frequency such that the reduced frequency of this experiment matches that of the experiments in Chapter 5. Three spot passings are shown. As is often seen in other rigs, not all wakes (or as here, pulses from the loudspeaker) result in the formation of turbulent spots. The second turbulent spot does not start to form until much later along the surface. Although not shown in the figure, artificial spots start to form at approximately the same location as those produced by wakes, i.e. at around 80-84%s. Hodson and Gostelow (1998) showed that artificially

generated turbulent spots have the same characteristics as those generated by wakes, for example they have the same turbulent and calmed region velocity profiles.

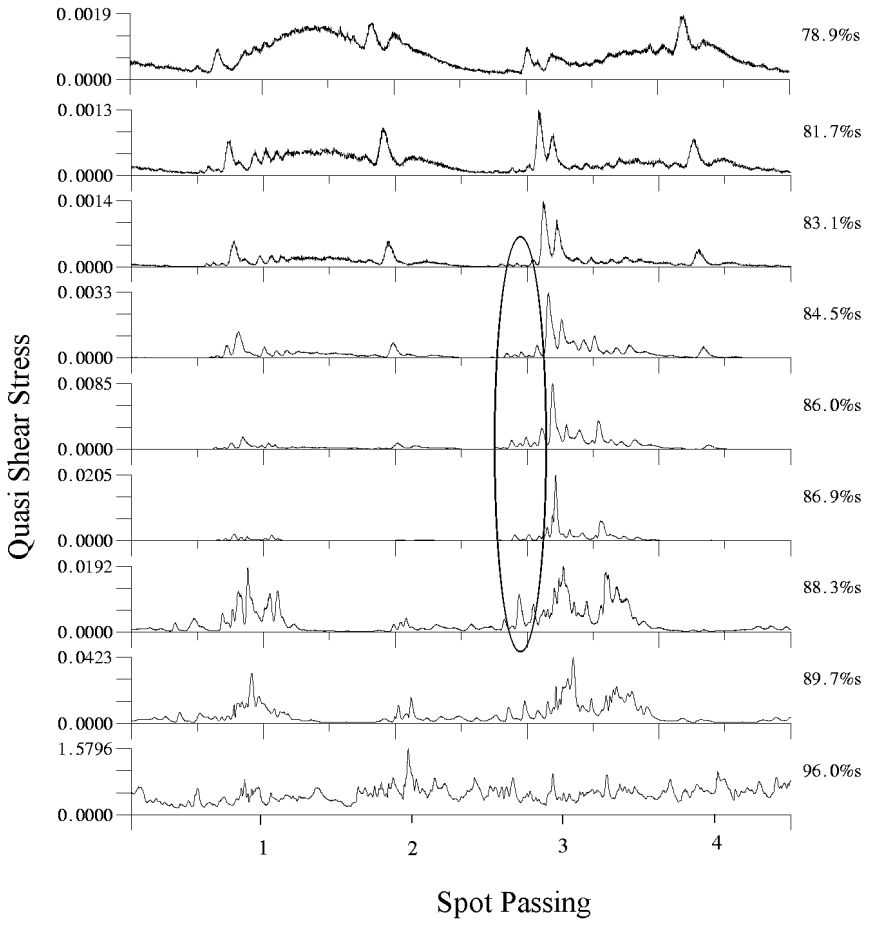

Figure 6.3.1 Hot film measurements of raw quasi shear stress from the flat plate rig showing turbulent spots forming due to impulses from the loudspeaker. Reynolds number = 130,000. $\bar{f}$ = 0.78.

The region within the ellipse in Figure 6.3.1 shows that separated flow transition starts to occur between spots at approximately 88%s. Frequency doubling of the oscillations occurs between 89.7 and 91.1%s (within the circled region) in the separation bubble as observed for TL10 in Chapter 5. Breakdown of the flow occurs before the trailing edge of the plate and as with TL10 in cascade at this Reynolds number, the flow is not fully turbulent.

In this section the details of the interaction of a turbulent spot with a separation bubble are discussed. Some workers have investigated the development of turbulent spots in laminar and transitional or turbulent boundary layers e.g. Seifert and Hodson (1999), but this investigation is thought to be the first where an individual spot has been introduced into a separation bubble.

The pressure distribution used in this section is the same as for TL10, as described in section 6.2, (Figure 6.2.1).

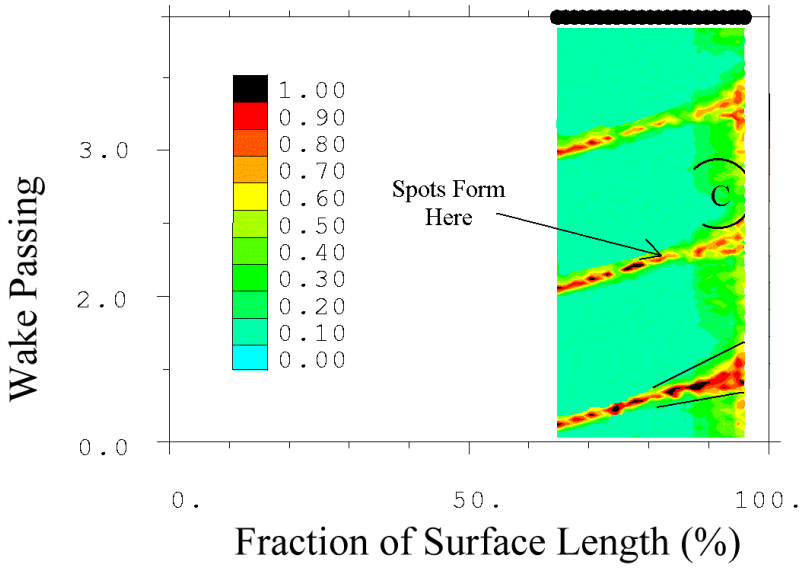

Figure 6.3.2 ST diagram of non-dimensional ensemble mean quasi shear stress resulting from artificially generated turbulent spots travelling through a TL10 style pressure distribution. Reynolds number of 130,000. $\bar{f}$ = 0.78.

Figure 6.3.2 shows an ST diagram of non-dimensional ensemble mean shear stress for a Reynolds number of 130,000 for three artificial spots. The reduced frequency was set to 0.78. The disturbance from the loudspeakers occurs just after peak suction at 58%s and the first hot film sensor was at 64.8%s. The initial disturbance is convected with the flow at the freestream velocity and is amplified in the first part of the separation, see oscillations from the sensors at 79%s to 83%s. However from 84%s the oscillations are amplified to a

far greater extent that before and it is in this region that the oscillations actually form into turbulent spots. This is better seen in the raw data, but this position is indicated on the figure. This is slightly later along the surface than occurred with the moving bar rig used in Chapter 5. The effect of calming can be seen in the data of Figure 6.3.2. A region of low shear can be seen extending into the separated flow and is marked as region 'C' in Figure 6.3.2. This region suppresses transitional activity in the separation bubble, but it does not seem to do so for as much of the spot passing period as measurements with wakes suggest. Since the turbulent spots are formed relatively late along the surface, they are not well established and their calmed regions are probably not fully formed. This may reduce their ability to resist disturbances and may be the reason why the calming effect does not last for much of the wake passing period.

6.3.2 Variation of Boundary Layer Integral Parameters

The data presented in this section is shown as the time variation of integral parameters and velocity profiles for the passage of one turbulent spot and its calmed region through the separation bubble. The data was taken with a single hot wire and the data for each height in the boundary layer has been ensemble averaged over 200 spot passings. All the data presented in this section was taken from the TL10 style pressure distribution shown in Figure 6.2.1.

The vertical black lines in Figure 6.3.3 annotated with a number represent a time instant for which a velocity profile is plotted. The velocity profiles in Figure 6.3.4 are normalised by the local freestream velocity i.e. $u(y)/u_{\infty}$. Because plotting more than about 4 or 5 velocity profiles on a single figure makes the figure very difficult to interpret,

the figures are divided into two. The first for each streamwise location shows the passage of the turbulent part of the spot, and the second shows the passage of the calmed region.

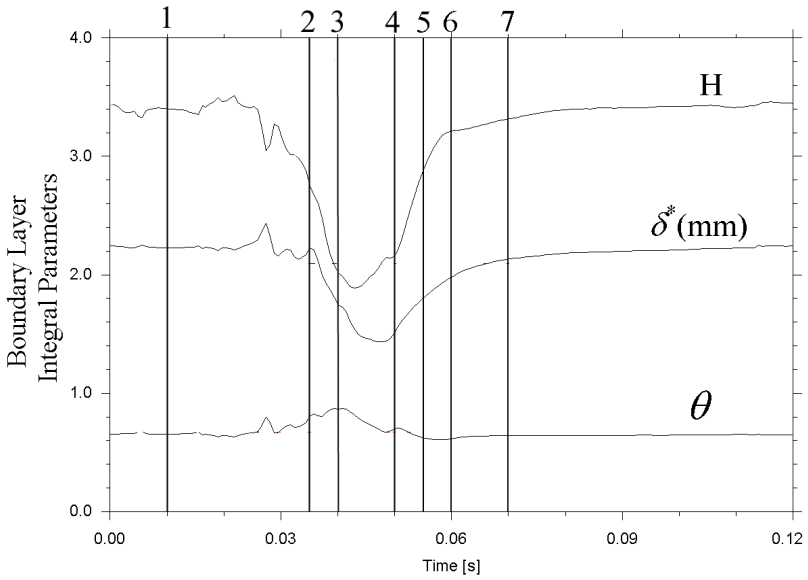

Figure 6.3.3 Boundary layer integral parameter variation for a spot interacting with a separation bubble at 78%s. Reynolds number 130,000, $\bar{f}$ =0.78. TL10 style pressure distribution.

The spots do not fully formed until they are in the separation bubble. Until then the hot film data seems to indicate that the disturbance is just a perturbation in the flow. It could perhaps be argued that they are turbulent spots, but spots in the very early stages of formation. As stated earlier, not much is known about how these perturbations breakdown to turbulent spots and this is why at present the oscillations are termed perturbations rather than spots.

Figure 6.3.3 shows the time variation in the integral parameters as the perturbation travels through the separation bubble at a streamwise position of 78%s from the plate leading edge. Before the perturbation arrives (at approximately time t = 0.03), the momentum thickness is approximately 0.62mm, the displacement thickness is 2.22mm and the shape factor is approximately 3.4, indicating a separated boundary layer. Figure 6.3.4a

shows the velocity profile for time index 1 and confirms that the boundary layer is indeed separated, with a low, constant velocity region extending to 0.5mm above the surface. At time index 2, the momentum thickness has started to rise and the shape factor and displacement thickness have started to drop. There is however little change in the velocity profile for this time index. At the peak in momentum thickness (time index 3) the inner region of the velocity profile has changed dramatically and is now attached. The shape factor is now near its minimum of 1.9. The outer region at this time index however has not been effected by the perturbation. By time index 4, as the momentum thickness has dropped from its peak, the boundary layer is now fully attached as can be seen by the velocity profile 4 (triangles).

As already mentioned, the raw hot film data could indicate that, at this streamwise position, the disturbance is just a perturbation to the boundary layer. However, the shape factor reaches a minimum value of 1.8. This is well below the accepted value for a laminar boundary layer and very close to that of a turbulent boundary layer. Although the PSD for the hot film data is not shown, it is obvious from raw quasi shear stress data that there is very little high frequency information in the signals from the sensors at 78%s when compared to the data from sensors further downstream. The raw data presented is representative of the flow as it has been compared to many more data traces from other experiments. However, the variation of integral parameters does show that the minimum in shape factor is near the value for a turbulent boundary layer.

Figure 6.3.4b shows the same variation in parameters as the previous figure but for time indexes as the rear of the perturbation travels through the separation. The first time increment in this figure is the same as the last one in Figure 6.3.4a. Time index 6 is taken slightly later then the previous one but already the velocity profile has regained most of its

pre-perturbation characteristics as the rapid increase in shape factor shows. The boundary layer is almost fully separated again. This surface location is closest to the birth of the perturbation so the spot will be small and so the time for which it affects the separation will also be small.

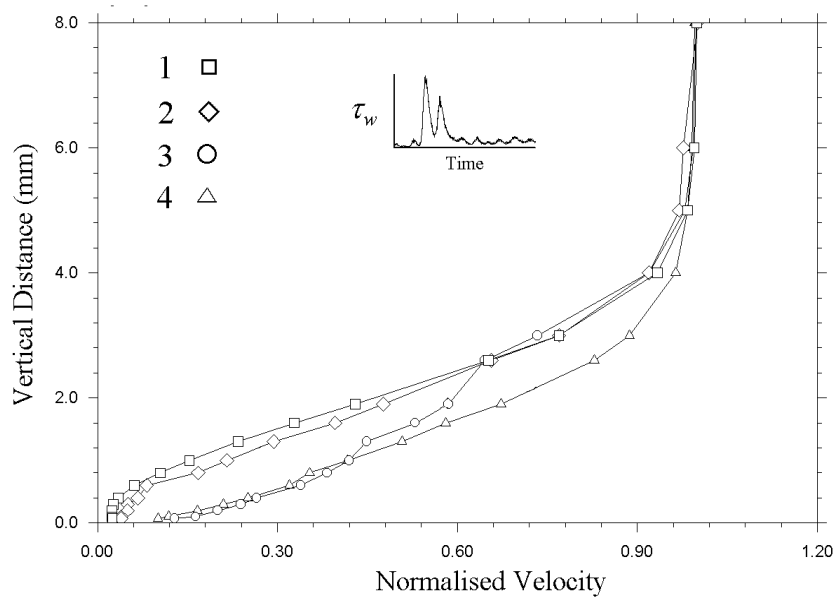

(a)

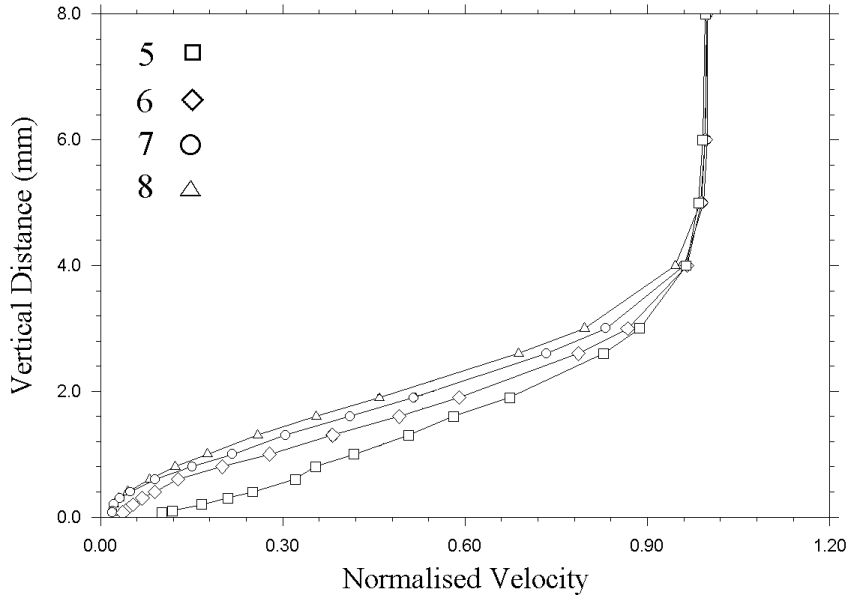

(b)

Figure 6.3.4 Variation of velocity profiles through a separated boundary layer as a turbulent spot (or perturbation) travels through it at 78%s. Reynolds number 130,000, $\bar{f}$ =0.78. TL10 style pressure distribution.

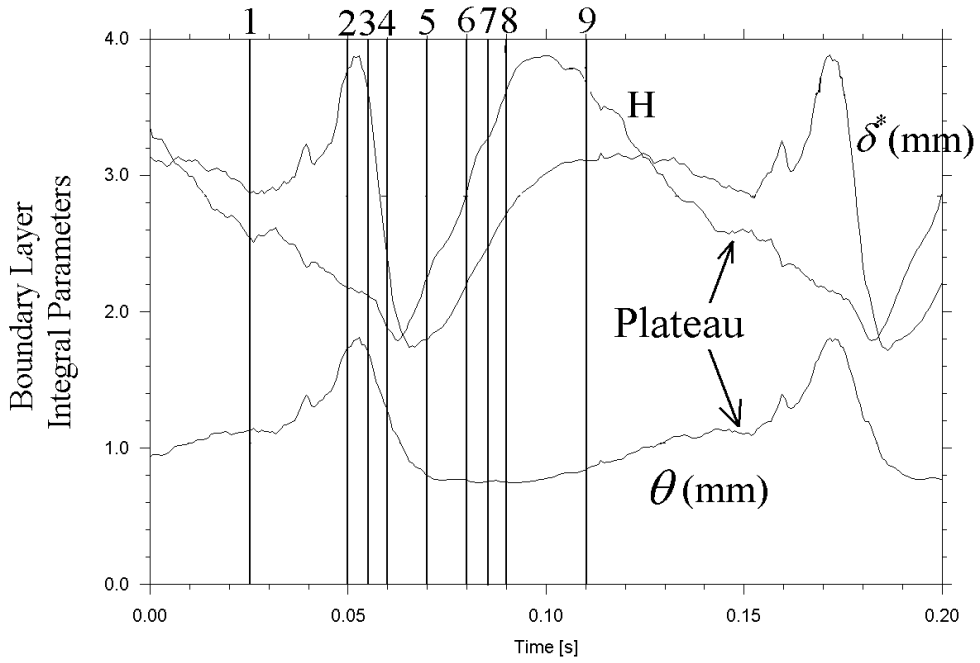

Figure 6.3.5 Variation in integral parameters as a turbulent passes by, at 89%s. Reynolds number 130,000, $\bar{f}$ =0.78. TL10 style pressure distribution.

Figure 6.3.5 shows the variation of integral parameters at a streamwise location of 88%s. At this location the perturbation has formed a turbulent spot, see the inset picture of quasi shear stress measured by a hot film sensor in Figure 6.3.6a. There are 5 increments in time during the passage of the turbulent part of a turbulent spot. Before the rise in momentum thickness the boundary layer is separated as shown by the square symbols. Time indexes 2 and 3 (around the peak in momentum thickness) indicate that the boundary layer has become slightly thicker. By time index 4, the momentum thickness is reducing and there is a minimum in shape factor. The boundary layer becomes much thinner and continues to reduce in thickness until time index 5 when a minimum in shape factor occurs. Figure 6.3.6b shows the changes that occur to the velocity profiles as the calmed region

passes that measurement location. Time index 5 shows the same velocity profile as time index 5 on the Figure 6.3.6a. The turbulent spot is now older as it has travelled a greater surface distance that it had at the previous measurement location. As can be seen from the figure, it takes much more time for the separation bubble to re-establish i.e. for the velocity profiles to start to separate again. By time index 8 the boundary layer is almost fully separated. The shape factor of a calmed region in the separated boundary layer behaves very strangely. In a laminar boundary layer the shape factor would drop to approximately 1.6 and then rise slowly to the value for a laminar boundary layer once the calmed region has passed, Seifert (1996). However, in this separation bubble the changes in shape factor are very different. Once the minimum in shape factor is reached and the momentum thickness starts to rise slowly (i.e. in the calmed region) the shape factor increases linearly (and dramatically) from 1.8 to near 4 in half the length of the calmed region. There is then a linear drop in shape factor to a plateau (as shown). It is believed that this marks the end of the effect of the calmed region on the separation and the separation has now almost fully formed again. It only survives for a short time before the arrival of the next turbulent spot. This behaviour underlines the complex interaction of the calmed region and a separation bubble.

Figure 6.3.7 shows boundary layer properties at a measurement location at 96%s from the leading edge. The separation has started to reattach as can be seen from the pressure distribution in Figure 6.2.1. There are no times at which the boundary layer is separated, but the profiles do fluctuate over a large range during the passage of the turbulent spot. The variation in shape factor is much reduced as the flow is nearly always near turbulent. Even in the region that would be considered calmed, the shape factor is still approximately 1.8. Seifert (1997) measured the turbulent part of a turbulent spot in a

slightly diffusing laminar boundary layer and found that the shape factor drops to 1.6. The difference in the value of shape factor within the turbulent part of the spot of these two experiments is probably due to the more severe adverse pressure gradient that causes the separation in these experiments.

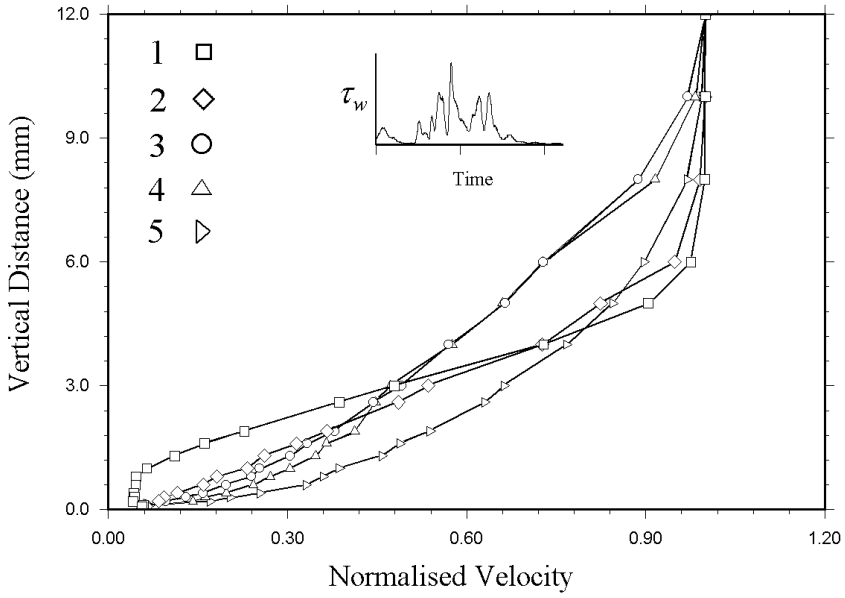

(a)

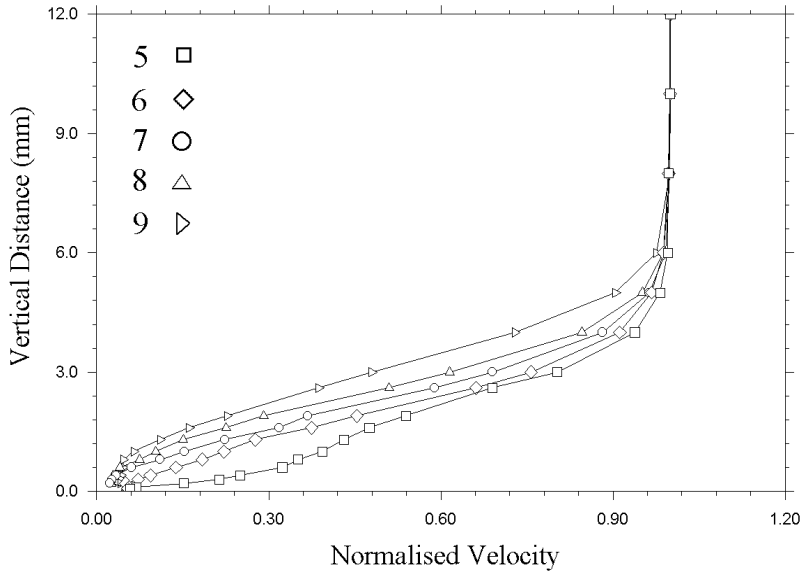

(b)

Figure 6.3.6 Variation of velocity profiles through a separated boundary layer as a turbulent spot travels through it at 78%s. Reynolds number 130,000, $\bar{f}$ =0.78. TL10 style pressure distribution.

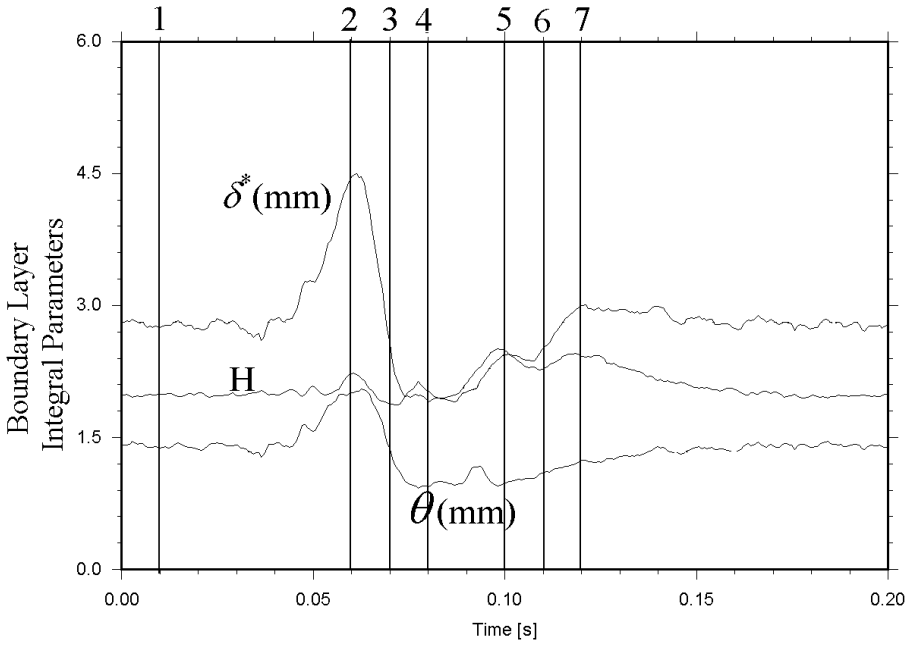

Figure 6.3.7 Variation of integral parameters through a separated boundary layer as a turbulent spot travels past at 96%s. Reynolds number 130,000, $\bar{f}$ =0.78. TL10 style pressure distribution.

Figure 6.3.8b shows the variation of properties as the calmed region passed. In contrast to the previous figure, there is much less variation in the velocity profiles, however the calmed region profile is thinner than the turbulent boundary layer, see time index 5, compared to time index 1. Dong and Cumpsty (1990) measured the velocity profile of the calmed region in a laminar boundary layer and showed it to be linear out to near the freestream. This is almost the case in a separation bubble, as shown by time index 4. As the calmed region relaxes its velocity profile remains approximately linear out to the freestream, but the gradient of velocity profile increases as the boundary layer thickens. Once the calmed region has passed by completely, the velocity profile resumes its pre-turbulent spot shape.

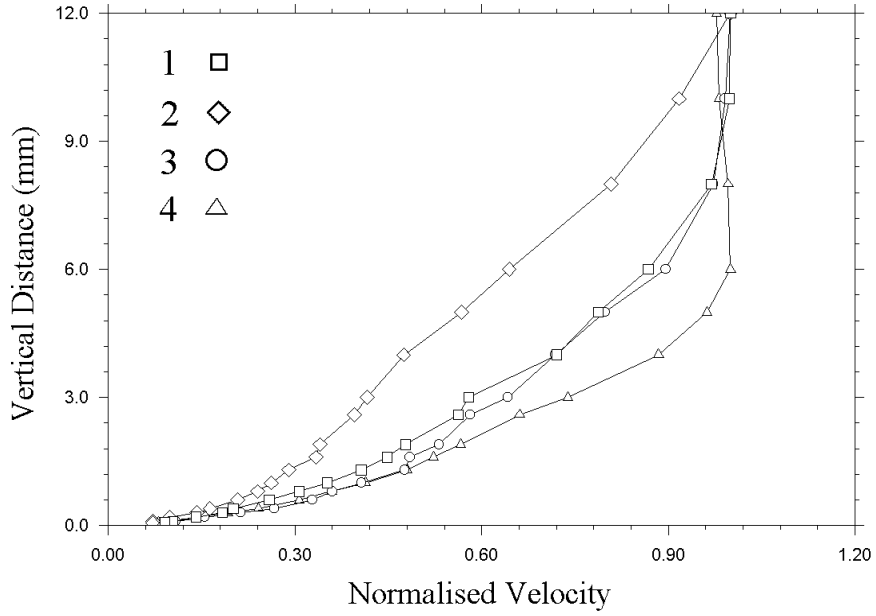

(a)

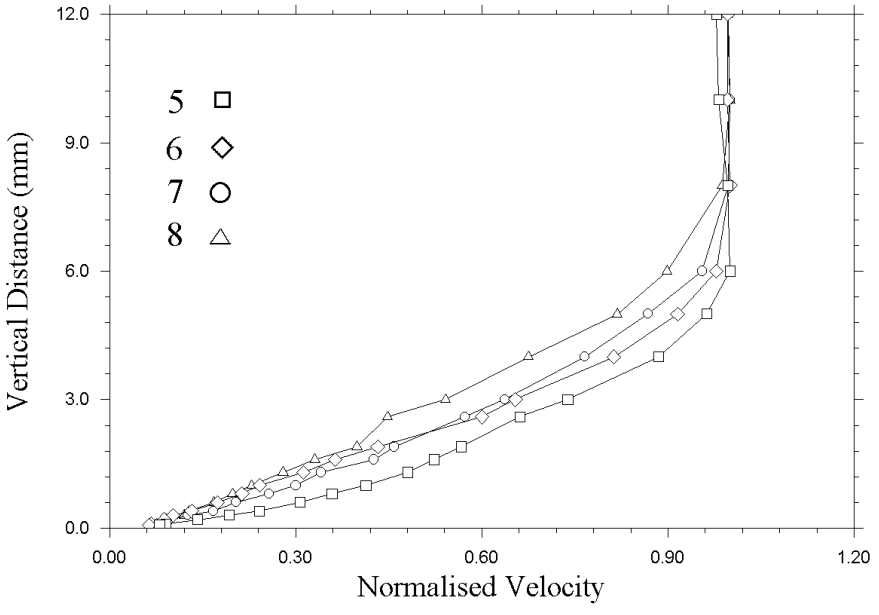

(b)

Figure 6.3.8 Variation in velocity profiles as a turbulent spot travels through a separated boundary layer, at 96%s. Reynolds number 130,000, $\bar{f}$ =0.78. TL10 style pressure distribution.

6.3.3 Summary of spot separation bubble interaction

The following section is a summary of the effects of the single turbulent interacting with a separation bubble.

The turbulent spot may not be fully formed in the early part of the laminar region of the separation bubble, none-the-less the spot/perturbation still has a large effect on the velocity profiles. Initially, the inner part of the separated profile becomes attached while the outer half of the boundary layer remains unaffected by the spot/perturbation. Rapidly, the whole profile becomes an attached boundary layer and attains a shape factor of 1.8, indicating a flow somewhere between laminar or turbulent. The rear of the spot/perturbation (measured after the minimum in shape factor to where it reaches its value as if in an undisturbed boundary layer) passes by in just 13% of the spot passing period. In this short time the attached profile has once again resumed a separated profile. There are only very small changes in the overall height of the boundary layer as the perturbation passes through the separation.

By 89%s the hot film measurements that the spot is fully formed. The turbulent spot is now greater in height than the separation. There are greater changes in the velocity profiles as the spot passes than at the previous position in the separation bubble. Once again it is the inner region of the separation that is affected first, with little effect in the outer half of the boundary layer. As the main body of the spot passes this position the total boundary layer height does not change a great deal, but the velocity in the mid region of the boundary layer decreases. This profile is almost linear out to the free stream. The profile then becomes fuller as the calmed region passes this location and the flow eventually relaxes back to a separated profile. However, as the spot is now fully formed, it takes 45% of a spot passing period for the effect of the calmed region to disappear.

When viewed from hot film data the spot at the last measurement station (at 96%s) is difficult to distinguish from the background turbulence due to separated flow transition. Despite this, there are once again large changes in the velocity profiles as the turbulent part of the spot passes through the separation, but there is not much change in shape factor. Even as the spot and calmed region pass through the reattaching boundary layer. At previous locations the shape factor of the calmed region in the laminar part of the separation reached a value of 4, here it reaches a value of just above 2. The calmed region persists (as seen from momentum thickness data) for 45% of the total spot passing period.

6.3.4 Spanwise variation of flow with wake affected inflow

The spanwise development of the onset of turbulent spots was also investigated. Mayle and Dullenkopf (1990) and others have developed transition models that assume a spanwise strips of turbulent flow forms under wakes. This puts a minimum value on the possible spot production rates. Measurements shown here will show that this is not necessarily the case, as transition is a three dimensional unsteady process. A number of measurements were carried out with a hot film array measuring the spanwise variation of the flow at two streamwise locations. The hot film array used for these measurements was the same as that used for all others presented in this chapter. The array was first located where the turbulent spots start to form in the boundary layer, i.e. just after separation. The other location was where the separation bubble started to transition between the passage of wakes. The length of the sensor array was such that it allowed the measurement of the middle 64% span of the flat plate, with a spanwise resolution of under 2% of span.

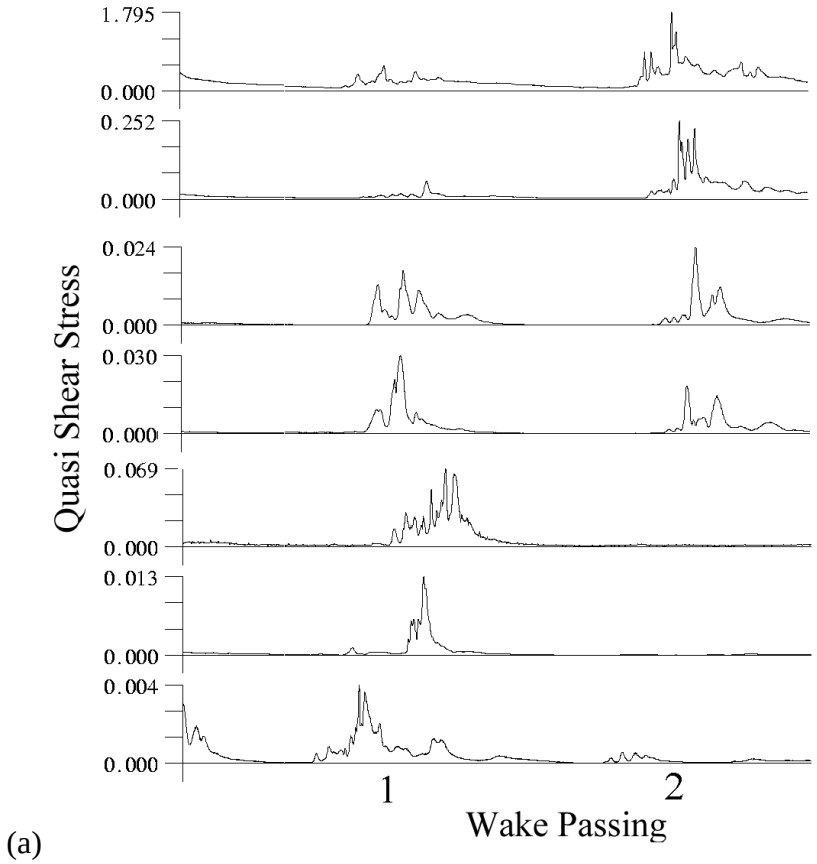

(a)

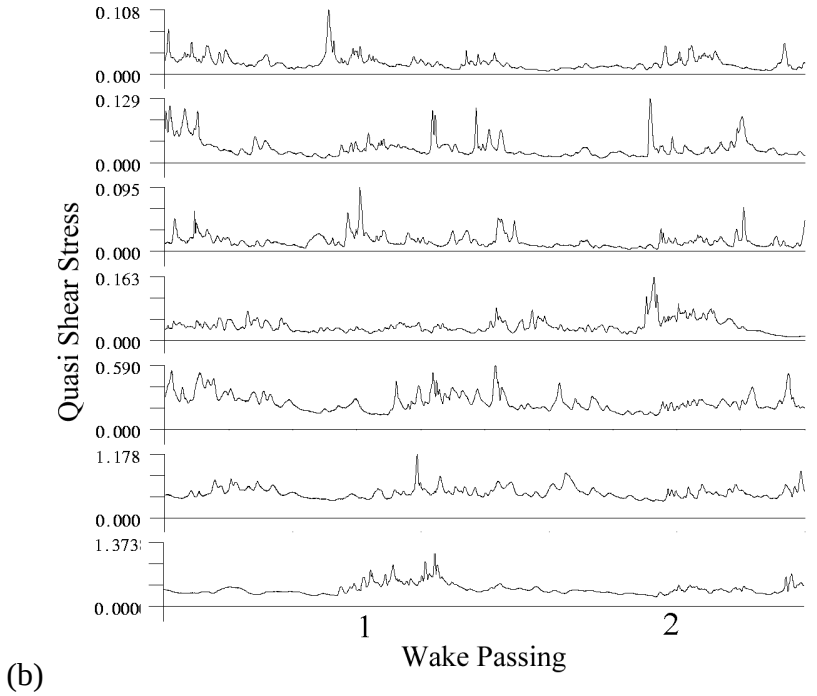

(b)

Figure 6.3.9 Spanwise variation of flow at (a) 84%s just after flow separation and (b) where separated flow transition starts to occur, at 90%s. $\bar{f}$ =0.78. TL10 style pressure distribution.

Figure 6.3.9a shows the spanwise variation of quasi shear stress where turbulent spots have started to form in the separation. It can be seen that the flow is not in any way spanwise uniform. Some regions have large fully formed turbulent spots, some have none and this situation changes with each wake passing. Measurements taken on the TL10 cascade showed similar non-uniformity. Zhong (1998) showed similar non-uniformity in the onset location of turbulent spots. Ideally, a two dimensional array of hot film sensors covering a region of surface would provide more information regarding the formation and development of spots. From this data it can be seen that for a given location around the position where turbulent spots on average, it can be seen that there is probably less that a single spot produced per wake passing, per unit span. As one progresses in a streamwise direction the probability that a spot forms increases, as can be seem from the spanwise data take in the location where separated flow transition occurs where more spots have formed.

The development of the separation bubble as turbulent spots travel through it presented in previous sections can therefore only be considered to take place as shown at one spanwise location. Other positions along the span are likely to be in a very different state. The process of wake and separation bubble interaction can therefore be considered a highly complex process that occurs in three dimension and it is also highly unsteady. All of the differences and non-uniformities between wake passings further complicates the modelling necessary to predict these flows.

6.4 Loss Generation in Separation Bubbles

6.4.1 Steady Inflow

This section investigates the effect of the spots and wakes on the losses generated in the separation bubble on the flat plate. A number of pressure distributions with increasing lift and diffusion are used to show how and where the losses occur in a separation bubble.

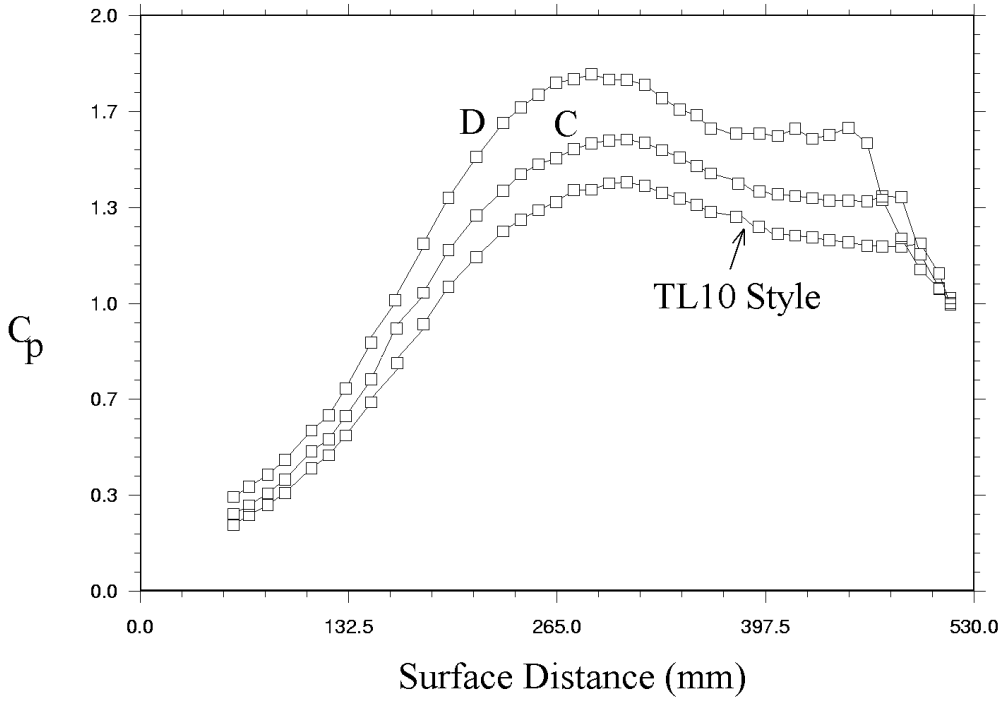

Figure 6.4.1 Pressure distributions with increased diffusion for determination of losses through a separation bubble.

To assess the loss generation in the boundary layer, the momentum thickness was calculated at the trailing edge of the plate. The ability of wakes and artificially generated turbulent spots to suppress the separation and losses was investigated for a number of conditions. Flow separation occurred at 74%s.

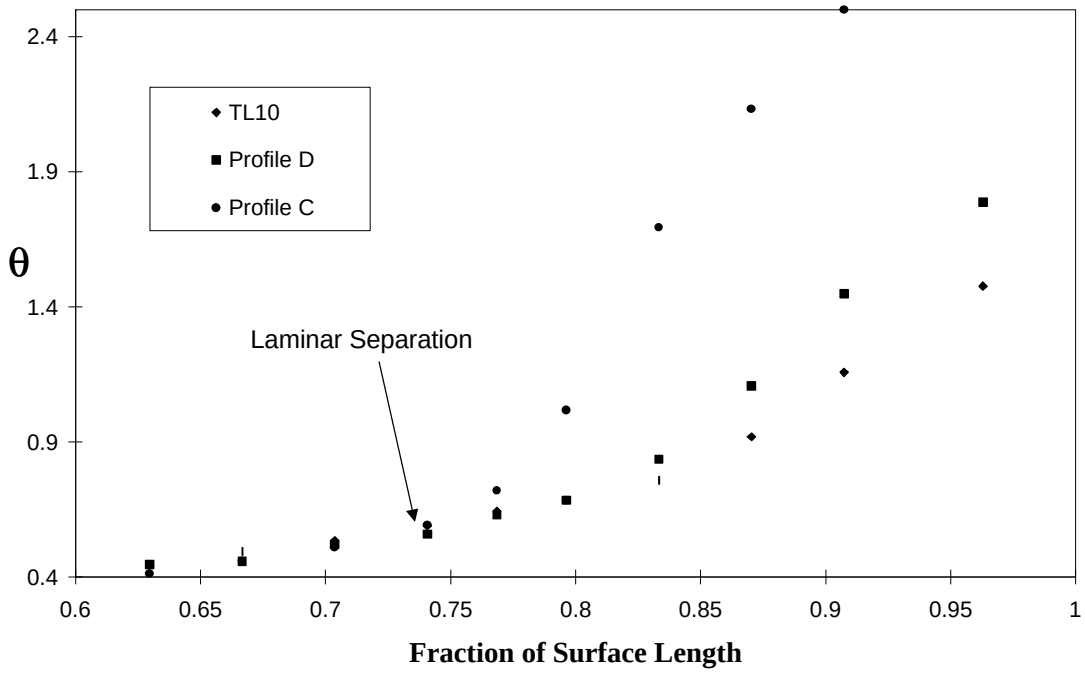

Figure 6.4.2 Variation of momentum thickness through the separation bubble for profile A and TL10 and also a higher diffusion profile. Reynolds number 130,000. Steady inflow.

Figure 6.4.2 shows the pressure distributions used for these investigations. The first is that of the datum profile, TL10. Increased lift profiles are also shown. The variation of momentum thickness for these are shown in

Figure 6.4.2. Regardless of the level of diffusion, the very first part of the boundary layers up to separation grow at similar rates. From approximately 75%s, the boundary layer momentum thickness grows more rapidly for the higher diffusion profiles. The position where the rapid increase starts to occur also moves nearer the leading edge of the plate as the diffusion is increased. Figure 6.4.3 shows contour plots of non-dimensional velocity and RMS through the bubble for two of the three profiles used for

Figure 6.4.2. Figure 6.4.3a shows the variation in velocity through the bubble for a TL10 level of diffusion. The dark blue region is the dead air region where the velocities are

very low, whereas the red is higher freestream velocity. It can be seen that as the diffusion increases from TL10 to profile C and profile D the surface length covered by dark blue reduces. This reduction in length of the bubble agrees with the behaviour of the bubble in the cascade tests presented in Chapter 5. The height of the same separated region increases with increased diffusion. Figure 6.4.3b, d and f, shows of RMS contour plots. The regions of highest RMS (coloured red) occupy an increasing amount of surface as the diffusion increases. More importantly, regions of high RMS occupy much greater height normal to the surface, indicating that the boundary layer is thicker and generating more loss.

The regions of flow where the RMS rises above the low levels (coloured blue) can be interpreted as the position where the shear layer undergoes transition and the flow breaks down to turbulence. The positions marked '**x**' on the RMS plots and indicates the probable position in the shear layer where transition begins. These are the first positions where the RMS starts to rise.

If transition occurs in a higher diffusion flow, turbulent entrainment seems to be more severe, meaning that entrainment normal to the surface is increased dramatically. Entrainment introduces more high momentum freestream fluid into the boundary layer allowing it to overcome the adverse pressure gradient, so the laminar bubble length is reduced.

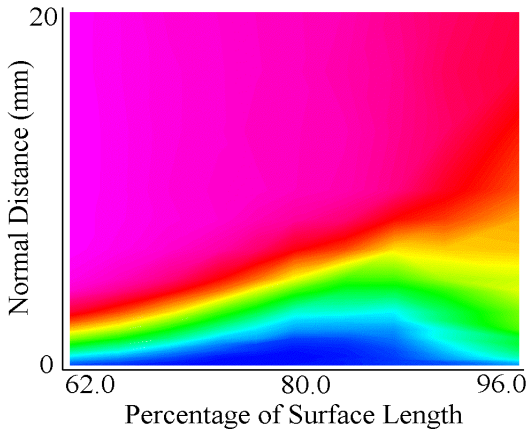

(a) TL10 - velocity contours

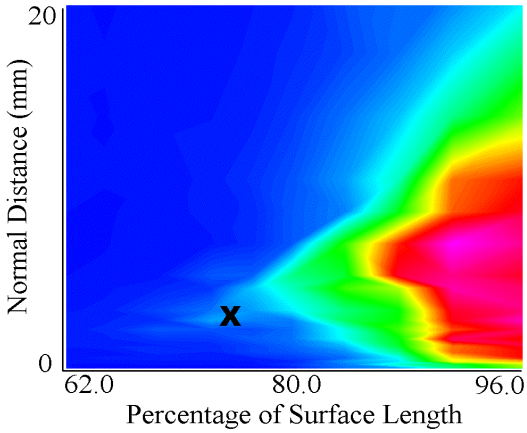

(b) TL10 - RMS contours

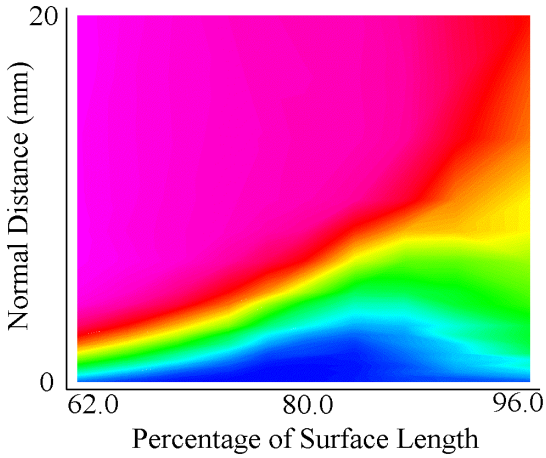

(c) Profile C - velocity contours

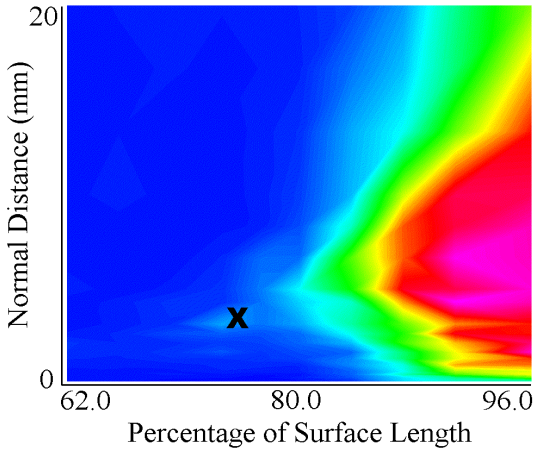

(d) Profile C - RMS contours

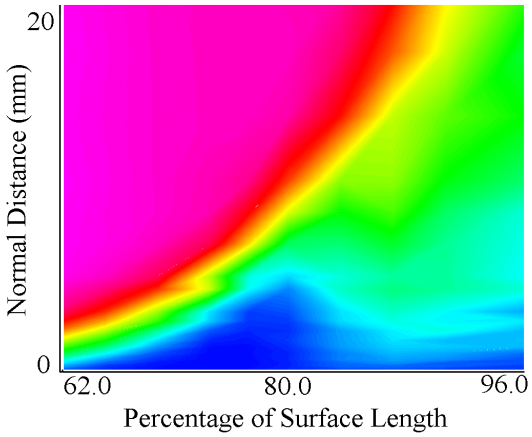

(e) Profile D - velocity contours

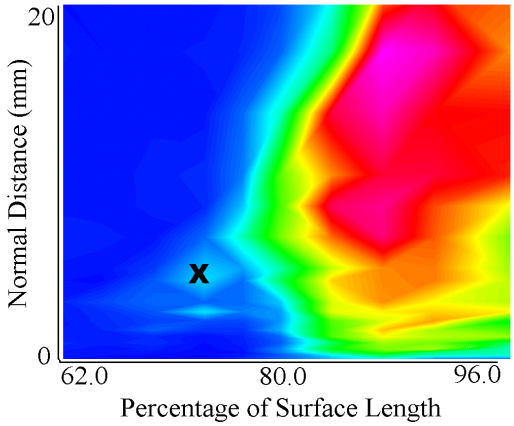

(f) Profile D - RMS contours

Figure 6.4.3 Time mean properties through separation bubbles of increasing diffusion for TL10 and profiles C and D.

6.4.2 The effect of wakes and artificial turbulent spots

Having described the development of a separation bubble with steady inflow for a number of pressure distributions (essentially different diffusion levels), it is now appropriate to show what happens to the boundary layers if they are affected by wakes or just turbulent spots.

Table 6.4.2 shows the time mean momentum thickness measurements for the profiles discussed above. As can be seen, when artificial spots are introduced a reduction in loss (θ) is measured for both profiles. However, when wakes are present there is a greater reduction in loss than that due to spots alone.

Profile	θ - Steady	θ - Spots Only	θ - Wakes
TL10	1.75	1.35	1.30
Profile C	1.79	1.66	1.57
Profile D	3.704	3.615	Not tested

Table 6.4.2 Loss (momentum thickness) measurements (at 96%s) for profiles with steady and unsteady inflow. Reynolds number 130,000. Wake or spot reduced frequency = 0.78.

If one compares the effects of wakes on the boundary layer at the trailing edge, in Figure 6.4.4 similar trends are observed in the variation of integral parameters to those seen in data for the passage of individual turbulent spots.

Probably the most important difference in the data is the length of time for which the ‘calmed’ region persists when wakes are present. For the same streamwise position as the spot case, the calmed region persists for 60% of a wake (or spot) passing period at 96%s. The reason for this difference in persistence of the calmed region could be due to the number of spots (and therefore calmed regions) that are formed per unit span or streamwise distance. The artificial spots were produced such that only one was generated

at a time and the effect of this single spot on the separation bubble was investigated. When a wake produces spots it can do so at a number of spanwise positions and these spots can coalesce. Conglomerations of spots may well produced calmed regions that are stronger than those which are part of a single spot.

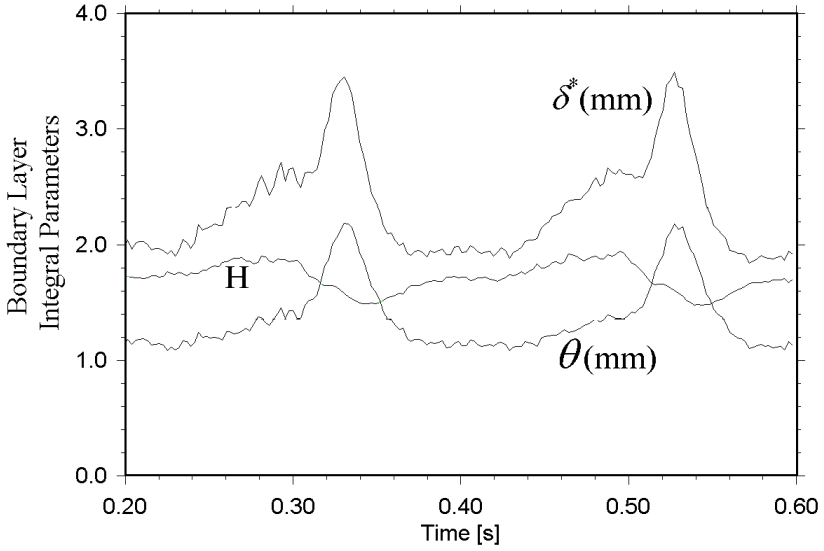

Figure 6.4.4 Integral boundary layer parameters for two wake passing at 96%s. Reynolds number 130,000, f = 0.78, $\Phi = 0.7$. TL10 style pressure distribution.

An alternative reason for the greater loss reduction that occurs could be due to the wake turbulence. When wakes are present the turbulence travels ahead of any spots it creates, Addison (1990). This is because the leading edges of spots travel at approximately 90% of the local freestream whereas the wake is convected *with* the freestream. Elevated levels of freestream turbulence are known to reduce the extent of separation bubbles and therefore the losses they generate, Ladwig and Fottner (1993). The wake turbulence arrives slightly ahead of the turbulent spots and reduces the size and losses of the bubble. Then the spots arrives and continue to suppress the separation for a longer period of time. Given that spots form so late along the surface, there could be wake turbulence behind the

last turbulent spots because of the width of the wakes. This means that once the spots have passed, there is still some wake turbulence left that is probably not strong enough to form spots and simply keeps the size of the separation small. At this stage it is not possible to be conclusive as more experimentation would be necessary.

6.4.3 Variation of reduced frequency of spot production on profile losses

Schulte (1995) showed that the losses generated by a turbine blade varied with the variation of reduced frequency of the passing the upstream wake passings. This process was investigated here by varying the frequency of artificial turbulent spot generation. A similar variation of profile loss was measured with reduced frequency. Once again, the momentum thickness of the boundary layer (measured at 96%s) was used as a measure of the loss generated by the boundary layer. Figure 6.4.5 shows the variation of trailing edge momentum thickness.

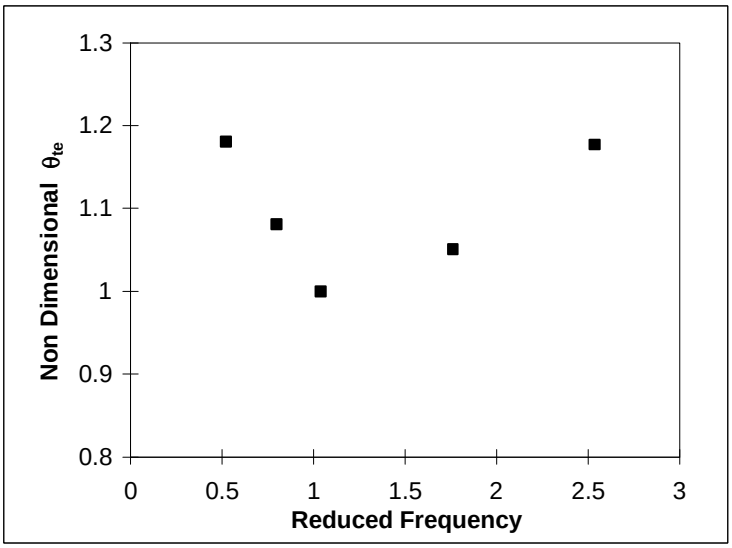

Figure 6.4.5 Losses generated by the datum profile on the flat plate with artificial turbulent spots, Reynolds number 130,000. TL10 style pressure distribution.

This result is a further validation of the work of Schulte (1995) who showed that it is the turbulent spots that are partly responsible for the loss reductions observed with unsteady inflow.

6.5 Conclusions

An investigation of the interactions of artificially generated turbulent spots and wakes with separation bubbles has been carried out on a large scale flat plate. The interactions have been shown to be highly unsteady and three dimensional.

Separated velocity profiles are attached by turbulent spots as they pass through the separation. For one streamwise position, it is the inner part of the bubble that is deformed first rather than the whole boundary layer uniformly. As the main body of the turbulent spot travels through the separation, the shape factor reaches its minimum (of about 1.8) near the rear of the turbulent spot. Calmed regions are difficult to discern from raw data traces, but are noticeable in ensemble mean plots of the variation with time of momentum thickness at (for example) the trailing edge of the blade. The calmed regions take considerable time to relax back to the type of flow that is seen before the spot arrives. As it does so, the velocity profiles in the calmed region stay roughly linear, but their gradient increases and eventually become non-linear once pre-spot boundary layer has reformed.

When wakes are present the boundary layer losses generated are reduced further than when just artificially generated turbulent spots are present. This could be due to either the wake turbulence reducing the size and losses of the separation for a longer time than the spots alone. Alternatively, it could be that more than a single spot is formed by a wake and these interact to produce more persistent calmed regions. More experimentation is necessary to clarify this position.

7. Boundary Layer Flow Predictions

7.1 Introduction

Having presented the measurements of unsteady, suction side boundary layer flows and their interpretation in previous chapters, this chapter provides information on how that understanding can be used as a check on the predictions of such flows.

Firstly, a correlation is used to show that the prediction for the onset location of wake induced transition is reasonably accurate. However, the onset location is shown to always be just after the position of flow separation, where Re_θ is approximately 260 for an exit blade Reynolds number of 130,000. A highly forward loaded pressure distribution is also shown, where wake induced transition still occurs in the separation bubble. Despite the forward loaded nature of the profile, separation still occurs in a roughly the same location as for the other *aft* loaded profiles. It is then shown that there is no real need to predict the onset location for wake induced transition as it always occurs just after the position where boundary layer separation would occur in steady inflow.

Unsteady intermittency variations are compared to that predicted by a code that calculates the time variation of intermittency for wake induced transition, Schulte and Hodson (1999). The intermittency is then used with a numerical code for predicting the unsteady wake boundary layer flows incorporating separation bubbles.

7.2 Boundary layer behaviour on high lift profiles

To understand the loss generation and behaviour of the profiles presented in earlier chapters, it is necessary to understand the development of the boundary layer. To this end

it is necessary to discover how the boundary layer properties change as the pressure distributions are altered.

7.2.1 Onset Location for Wake Induced Transition

For attached flows a Reynolds number based on momentum thickness is a useful parameter in determining the state of the boundary layer. The momentum thickness was calculated using the equation due to Thwaites, shown in equation 7.2.1.

$$q_x = \sqrt{\frac{0.45n}{U_x^{\,6}}}\int_0^x U^5 dx \qquad \text{Equation 7.2.1}$$

This expression is valid up to where the boundary layer separates and only where the radius of streamline curvature is much greater than the boundary layer thickness. This is an approximate method and is based on a one parameter family of velocity profiles. Since there are limits on the validity of this version of the Thwaite's expression, the results obtained using equation 7.2.1 have been compared with those generated by the Cebeci Carr (1978) boundary layer code. Although some differences were observed between them, the errors were small. Interestingly the values of Re_θ converged around the separation regions. The errors in the separation region were less than 2.5% compared to the Cebeci calculations.

Figure 7.2.1 shows the variation in Re_θ for some of the aft loaded profiles shown in previous chapters. There are few differences in the values of Re_θ over the leading part of the blade surface. The primary differences occur after peak suction where the levels of diffusion are different. Profile B has higher values of Re_θ compared to profile A, because the back surface diffusion level for this profile is larger, see figures 5.5.3a and 5.5.7a in Chapter 5.

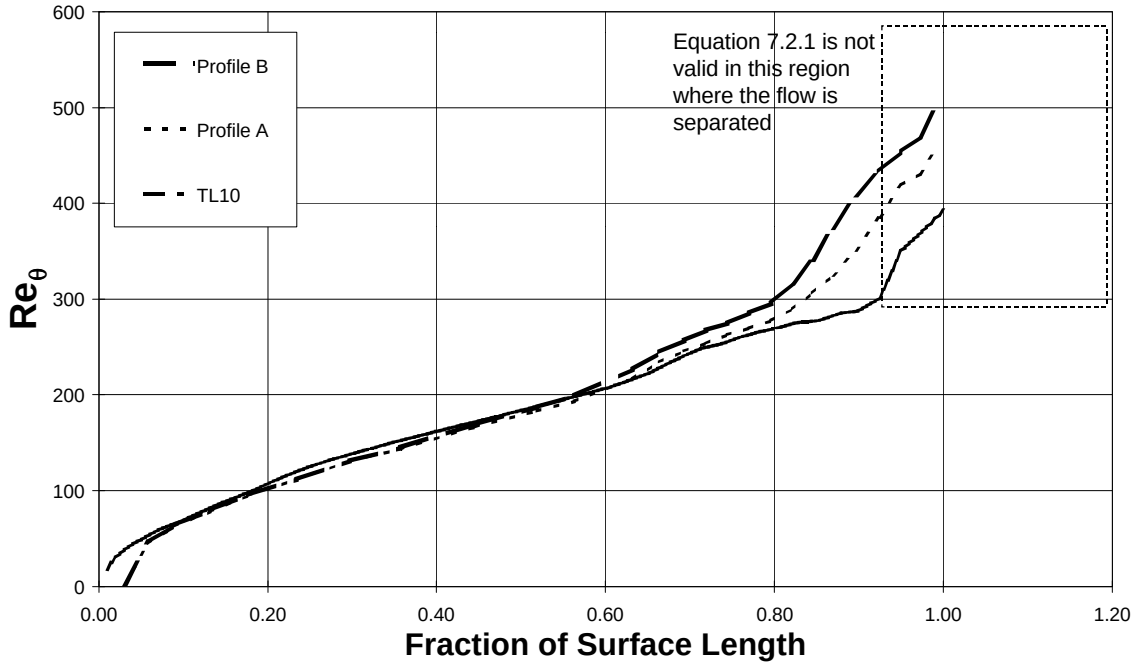

Figure 7.2.1 Variation of the momentum thickness Reynolds number for some of the high lift blades.

The values of momentum thickness Reynolds number where the boundary layers separate but the values tend to be around 260.

It is possible to predict the onset location for wake induced transition by considering the variation of Re_θ for the blade surface boundary layers above and using the correlation due to Mayle (1990) shown in equation 7.2.2.

$$Re_{qt} = 400Tu^{-5/8} \qquad \text{Equation 7.2.2}$$

Equation 7.2.2 requires knowledge of the variation of freestream turbulence level through the blade passage. For the datum profile, TL10, measured values of freestream turbulence are available.

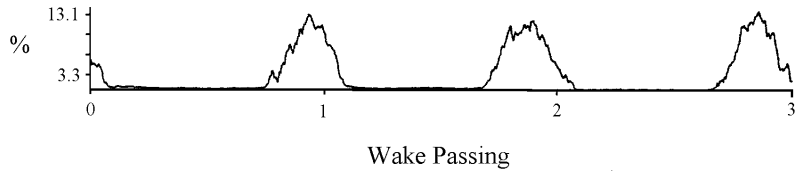

Figure 7.2.2 Variation of inlet turbulence to TL10 measured with a single hot wire 0.1 axial chords upstream of the cascade leading edge. Reynolds number 130,000. $\bar{f} = 0.78$, $\Phi = 0.7$, 2.05mm bars.

However, for the more highly loaded profiles produced by the flap tests it is necessary to calculate the variation of turbulence in the freestream due to the wakes. To calculate the variation of peak turbulence (i.e. the centre line of a wake), the measured turbulence intensity at *inlet* to TL10 is used (see Figure 7.2.2). For a given peak inlet turbulence intensity it is possible to calculate roughly how that turbulence level reduces as it is accelerated in the blade passage. To a very crude approximation, the variation of turbulence level through the blade passage can be calculated by assuming that the turbulence level at a point over the surface scales with the ratio of inlet velocity to the velocity at the point under consideration, see equation 7.2.3.

$$Tu(x) = Tu_{Inlet} . \frac{V_{Inlet}}{V(x)} \qquad \text{Equation 7.2.3}$$

Profiles with different loadings will distort the wake and its turbulence at inlet and inside the blade passage, but effect this is not taken into account. The calculated minimum in turbulence level is around 5%, so according to Mayle (1990) and Abu-Ghannam and Shaw (1980) it is quite reasonable to assume that equation 7.2.2 is valid for all the profiles shown here because they showed that pressure gradients effects were negligible for turbulence levels of about 3%. For TL10 the values of the turbulence level around the separation region (which is where the values should be matched) agreed very well with those measured by Schulte (1995). Schulte's measurements gave a turbulence level in the

freestream above the position of flow separation to be approximately 5.5%. The value of turbulence given by expression 7.2.3 was approximately 6%. This closeness of this measurement and the value given by the expression gives some confidence in the approach for its use with the other profiles.

If one uses the values of $Tu(x)$ with equation 7.2.2 the result is the value of Re_θ required at that turbulence level before transition is likely to occur. Before this position, transition is unlikely as the boundary layer is not receptive enough to amplify the periodic or random disturbances from the wakes. In the case of TL10 the position given is *just* before boundary layer separation which occurs at 74%s. Measured wake induced transition occurs for this profile between 74 and 77%s i.e. at or after separation.

Schulte (1995) showed hot film measurements with an increased wake strength produced by replacing the 2.05mm bars with 4mm bars. These measurements give the wake induced transition onset location to be around 61%s and equation 7.2.2 gives the position to be about 57%s.

For the profiles used here, this approach to predicting the transition onset location indicates that it predicts onset slightly early and usually before separation. However, measurements have shown that if the peak inlet turbulence intensity to the cascade is less than about 13% at inlet, wake induced transition is unlikely to occur before separation for a laminar boundary layer on these profiles at this Reynolds number. The loss generated by the 4mm bars is approximately double that produced by the 2.05mm bars. The smaller diameter bars were sized to give the same profile loss as generated by an upstream rotor blade at design conditions. Under design circumstances therefore LP turbine blades should produce much less loss than that generated by the 4mm bars. It is therefore most likely that wake induced transition will occur around the separation region of a high lift LP turbine

profile. High pressure turbine blades often have trailing edge cooling slots. Such blades are likely to produce larger wakes with a higher peak turbulence intensity. The prediction approach used here is unlikely to work for turbine blades with thick trailing edges.

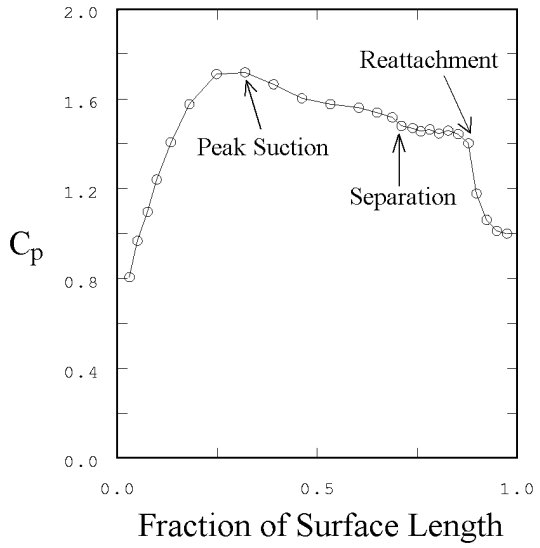

(a)

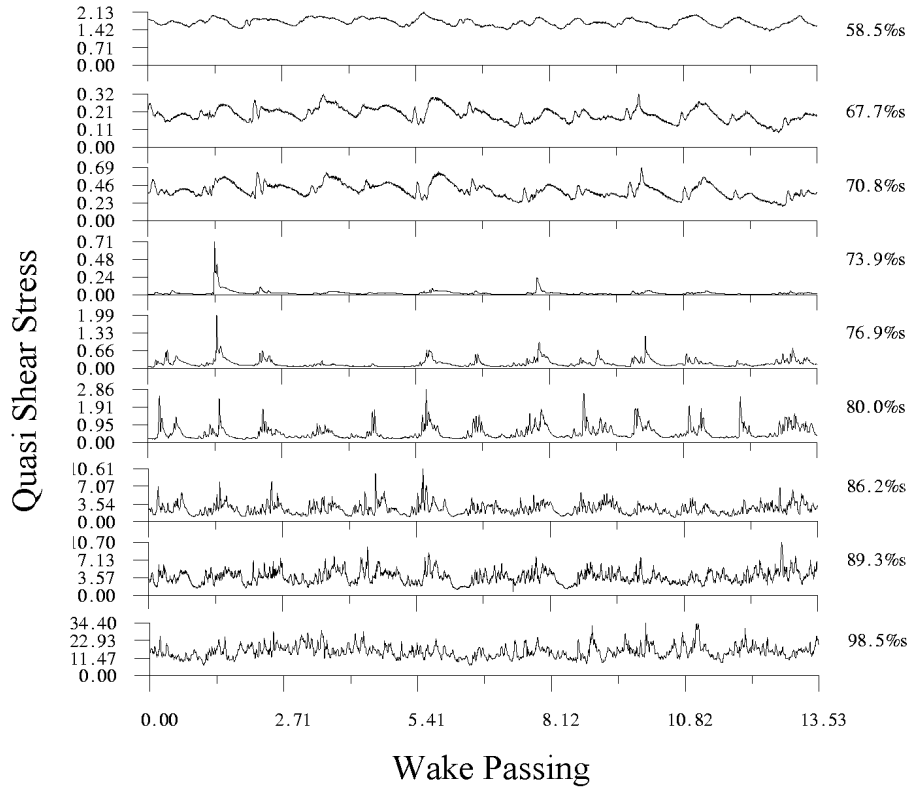

(b)

Figure 7.2.3 The static pressure distribution (with no wakes) and the hot film measurements (with wakes) for a forward loaded pressure distribution.

To further illustrate that wake induced transition usually occurs at or around separation, a forward loaded pressure distribution is presented in Figure 7.2.3a. This pressure distribution was taken using with the addition of the flap and also inserts during the cascade experiments described in Chapter 5. The position of peak suction in this profile occurs at 30%s, but separation still occurs at around 74%s as with all the previous pressure distributions. The high diffusion increases the receptivity of the boundary layer and amplifies disturbances faster than in a zero pressure gradient flow, Walker and Gostelow (1989). Wake induced transition once again does not occur until around the separation region, see Figure 7.2.3b. The correlation gives the transition onset location to be at approximately 65%s. As can be seen from Figure 7.2.3 the actual location is later between 74 and 77%s, i.e. after separation.

The steady state velocity profile of a separated boundary layer is inflexional and it is therefore unstable, Schlichting (1979). Any small disturbances in the freestream are likely to cause the flow to break down in this region. As the velocity ratio (defined from inlet to peak suction) increases on higher lift profiles, the turbulence intensity around peak suction (and therefore separation) will be further reduced for a given value at inlet. The greater acceleration makes the likelihood of wake induced transition occurring before separation even more unlikely on future higher lift profiles.

The work presented here shows that using the correlation above for calculating the onset location for wake induced transition gives reasonable results. However, for all the profiles considered here it may also be said that there is no real need to predict the onset of wake induced transition. Once the position of boundary layer separation is known it can be assumed (for ‘normal’ turbine wakes) that wake transition occurs at around this location.

7.3 Prediction of unsteady boundary layer flows

Schulte (1995) showed that one can predict the growth of a calmed region of a turbulent spot using the unsteady laminar boundary layer equations. He then went on to predict the development of a turbulent spot (and calmed region) in a transitional boundary layer using an adaptation of the Cebeci and Carr (1978) boundary layer solver. The Cebeci and Carr code employed an eddy viscosity turbulence model which was weighted using an intermittency pre-multiplier (g) as shown below

$$u_{eff}(x,z,t) = u_{lam} + g(x,t)u_{turb}(x,z,t) \qquad \text{Equation 7.3.1}$$

where $u_{turb}(x,z,t)$ was determined from the instantaneous velocity profiles. The unsteady intermittency $g(x,t)$ was determined in a separate calculation and therefore prescribed for the boundary layer calculation. The values of $g(x,t)$ were uniformly applied across the entire height of the boundary layer. The approach builds on the work of Addison and Hodson (1992), but included the effects of calming.

The Cebeci Carr code was only able to predict the development of attached flows and is therefore of limited use for the profiles used in this thesis which have large separations. To predict boundary layer flows on high lift LP turbine profiles therefore, an adaptation of the UNSFLO code (Giles, 1990) was used. To prescribe the unsteady intermittency the method due to Schulte and Hodson (1999) was applied.

To compare the predicted intermittency with the hot film measurements, an estimation of the intermittency from the hot film data is required. A simple intermittency measurement algorithm was therefore developed for this purpose. The simple code contains no new developments beyond what is available in the open literature. This is described in Appendix B.

Many intermittency measuring methods have been developed in the past. These have been shown to work in what *seem* to be relatively simple environments, Solomon (1996). If it difficult for the human eye to determine which parts of a signal are turbulent and which are laminar, producing a computer code capable for such a feat is also likely to be difficult. For an example see Figure 7.3.1, particularly the sensor at 98.5%s where the flow changes from laminar to turbulent and calmed (i.e. around the region marked 'B'). Solomon (1996) applied more elaborate processes to the signals to try to produce more accurate and consistent variations in intermittency. These additional process included iterating with the use of probability density function methods (Ramesh *et al*, 1995) to set the threshold levels. However, as Solomon admits this produced only very minor changes in the time averaged intermittency and so were deemed unnecessary for the current application. 7

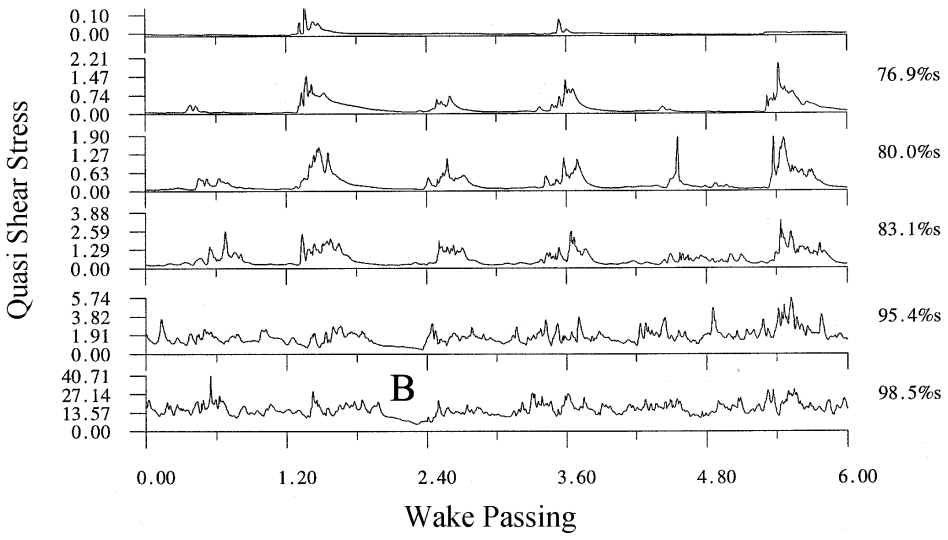

Figure 7.3.1 Quasi shear stress data from the TL10 profile with unsteady. Reynolds number 130,000. $\bar{f}$ =0.78, $\Phi = 0.7$.

Other data presented in Chapters 4 and 5 helps to illustrate the difficulties that face intermittency measurement codes. When data is taken from high speed rigs there is often not enough high frequency information available from the sensors. The frequency response

from the hot film sensors used in Chapter 4 was less than 30kHz. The wake passing frequency was approximately 6kHz. When then maximum frequency in the data is so similar to that of the wake passing frequency, it is likely to be difficult to distinguish which parts of the signal are laminar, turbulent or occur at the wake passing frequency. Indeed, a further complication to the process occurs in the rig environment when there are a number of stages upstream of the blades where data was taken, for example NGV3 of the BR715 LP turbine, see Figure 4.5.2. The data contains disturbances to the laminar boundary layers that are caused by wakes from upstream stages. It is easy to incorrectly identify some of these signals as turbulent. The simple approach presented in appendix B was thought to be adequate in obtaining intermittency data from the hot film measurements from the low speed rigs. At present programming automated intermittency codes seems to be more of an art that a science.

The prescribed unsteady intermittency code (PUIM) is described in more detail in Chapter 3 and Schulte and Hodson (1999).

7.3.1 Comparison of measured and predicted intermittency for TL10.

The measured intermittency from the hot film sensors on the TL10 profile is shown in Figure 7.3.2a. There are some non zero values of intermittency between 58%s and 75%s. These are caused by problems with the intermittency algorithm, where the low levels and RMS levels of the signals at this part of the surface are incorrectly identified at turbulent. It can be seen that by the trailing edge, the flow is not fully turbulent. This is agrees with the interpretation of the RMS and skew data (not shown).

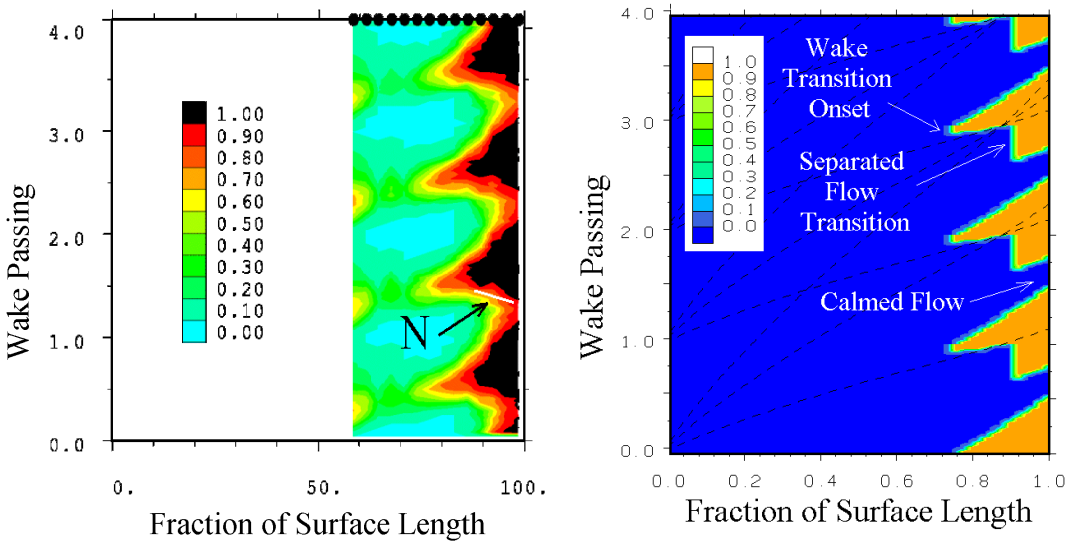

(a) Measured (b) PUIM

Figure 7.3.2 Resulting intermittency distribution from the TL10 profile, (a) measured and (b) predicted. Reynolds number = 130,000. $\bar{f} = 0.78$. $\Phi = 0.7$.

A turbulence distribution measured at inlet to the TL10 cascade was used as an input to the PUIM code. The resulting intermittency ST diagram is shown in Figure 7.3.2b. The onset location was well reproduced and the initial spreading angle of the turbulent wedges was also similar. However, the trajectory labelled ‘N’ from the measured data implies a negative propagation velocity. This is in fact a consequence of two effects. One effect is due to ensemble averaging as described by Addison and Hodson (1990) as averaging a large number of wake passings leads to the roughly triangular region of non zero intermittency. It is also due to separated flow transition starting to occur before the next wake arrives. This is not explicitly modelled by the PUIM code. As a result the predicted intermittency from PUIM shows a clear distinction between the separated flow transition and the arrival of the wake transition region. In the measurements these multi-mode transition regions are somewhat blurred.

This predicted intermittency was then used with the UNSFLO code to predict the boundary layer development as turbulent regions passed through the separation on the TL10 profile.

7.4 Discussion of Initial Flow Predictions

The first set of numerical predictions shown are of the relatively simple flow where individual turbulent spots travels through the separation bubble. The intermittency used for this prediction is shown in Figure 7.4.1 for four spot passings. The pressure distribution used to generate this calculation was the TL10 profile shown in Chapter 5.

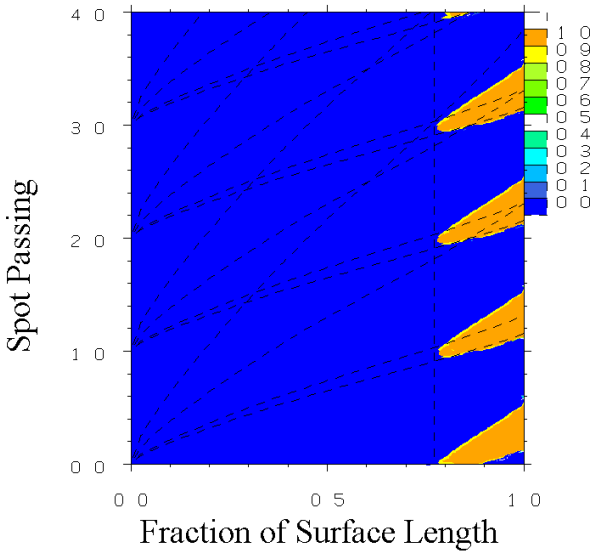

Figure 7.4.1 Predicted intermittency distribution for single mode transition where a turbulent spot travels through a separation bubble. Reynolds number 130,000. $\bar{f} = 0.78, \Phi = 0.7$.

On inspection of the initial solutions, errors with the predictions were noted when the turbulent regions passed into (or formed within) and then travelled through the separation bubble. This problem is best illustrated using Figure 7.4.2 which shows the rear part of the TL10 LP turbine blade and the developing boundary layer above. The colour contours are of turbulent viscosity where red is highest (i.e. in a turbulent spot) and blue is lowest. The error in the prediction occurs where the velocity vectors under the turbulent

spot are reversed. The elliptical region below the spot is blue because it is the laminar sub-layer and is therefore a region of laminar viscosity. It would seem that information regarding the high shear flow above (in the turbulent region) is not transmitted rapidly enough to the sub-layer. The sub-layer therefore continues to flow in the direction it did before the turbulent spot arrived. This results in extremely low wall shear stresses under the turbulent spot. This is physically incorrect as shown in Chapter 6 where the inner part of the separated boundary layer was shown to deform first as the turbulent spot travelled through it. The question raised by this problem would seem to be how to increase the rate at which information travels into the sub-layer?

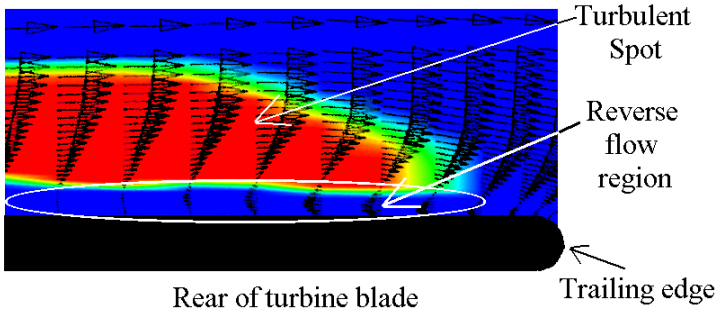

Figure 7.4.2 Contours of turbulent viscosity (red is high and blue is low) as a turbulent spot travels through a separation bubble. Reynolds number 130,000. $\bar{f} = 0.78$.

The turbulent spot certainly does not travel over the separation as indicated by the first predictions. Indeed, if it did, then the hot film sensor measurements would not pick up the passage of the spot as its high shear stress would not be seen by the sensors. To understand this problem a very brief discussion of the turbulence model used by UNSFLO is required.

The inner region of the boundary layer is modelled using Prandtl's mixing length formulation shown in equation 7.4.1

$$(m_t)_{inner} = rl^2\left|\frac{du}{dy}\right| \qquad \text{Equation 7.4.1}$$

The van Driest damping term is used in the inner layer model to give the correct behaviour near the wall and is shown below

$$l = ky(1-e^{-y/A}) \qquad \text{Equation 7.4.2}$$

where k is the von Karman constant, $A = \frac{26m}{ru_t}$ where $u_t = \sqrt{\frac{t_w}{r}}$.

There is very little viscosity at the interface of the sub-layer and mid-layer regions. When the region above the sub-layer changes direction due to the sudden passage of a turbulent spot (i.e. region of high viscosity), there is therefore no mechanism to transfer that information into the sub-layer. Hence, the sub-layer takes a relatively long time to react to the changes in the outer part of the boundary layer. A number of calculations were performed to determine the length of time the sub-layer takes to react to changes in the outer parts of the boundary layer. From the time the high viscosity region arrives at the separation bubble until the sub-layer velocity vectors start to point in a streamwise direction can take the entire duration of the turbulent part of the spot. In the recirculating region of a separation bubble, there are only small velocity gradients and therefore low values of viscosity, as given by equation 7.4.1. To increase the viscosity in the sub layer, the van Driest damping factor could be modified so that the turbulent viscosity does not reduce so rapidly in the near wall region. Information should then be transferred into the sub layer such that it responds more rapidly to the changes in the outer layer.

The UNSFLO code was modified so that the effect of the damping term was reduced until further into the sub-layer. This ‘correction’ was only executed downstream of the separation location. However, this modification alone did not entirely solve the problems. If a turbulent region was initiated upstream of the separation position, then the

reduction in the damping factor (by an order of magnitude) proved sufficient. However, if the predicted start of wake induced transition occurred within the separation bubble (as it usually does) them the problem remained. The correction for this was to increase the outer boundary layer length scale and hence viscosity. The outer region viscosity needed to be doubled for the flow in the sub-layer to follow the flow direction when a turbulent spot was formed within the separation bubble.

7.5 Predictions for a TL10 style profile

The results presented in this section are for the TL10 pressure distribution. The predictions are compared to some of the measurements shown in Chapter 5. The predicted and measured intermittency used for this calculation were shown earlier in Figure 7.3.2.

Figure 7.5.1 shows the predicted and measured results and that most of the basic features of the flow are reproduced. Wake induced transition occurs at approximately the same streamwise locations and the high shear regions due to the reattachment of the separation bubble are also clearly present. It is possible to clearly see the multi-mode transition that is occurring in the predictions. After the region of high shear has passed due to the wake transition causing the formation of turbulent spots, a region of reducing skin friction can be seen. This is due to the calmed region. The next region of high shear is caused by the reattachment process of the separation bubble. The measurements of non dimensional ensemble mean shear stress do not show that the multi-mode transition occurring as clearly. However, it has been shown in Chapter 5 that the reattachment process can be seen in the measured data. At this point it should be explained why it is necessary to compare non-dimensional ensemble mean shear stress with skin friction coefficient. It is not possible to compare changes in values of measured non dimensional shear stress with changes in skin friction. However, the data is presented in this way

because the non dimensional shear stress most clearly shows the trajectories of the wake transitional regions.

The most detailed boundary layer information is available from the set of experiments taken from the flat plate. Comparisons of the velocity profiles and quasi shear stress are therefore made with the PUIM/UNSFLO predictions from the TL10 style pressure distribution data taken from the flat plate.

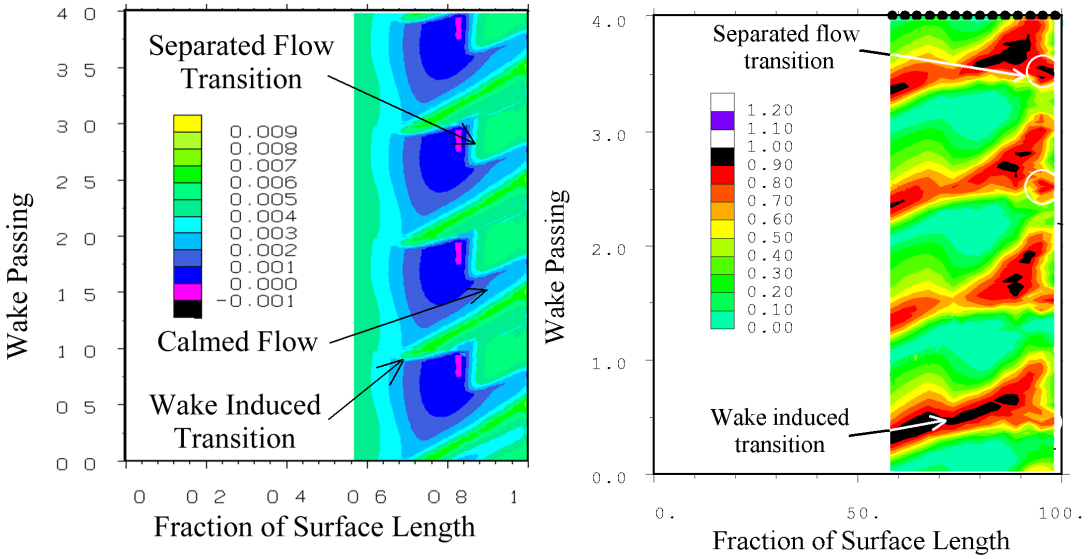

(a) (b)

Figure 7.5.1 Predicted skin friction coefficient (a) and measured non dimensional ensemble mean quasi shear stress (b) from a TL10 style pressure distribution. Reynolds number 130,000, $\bar{f} = 0.78, \Phi = 0.7$.

To the blade designer, the details of the transition mechanisms are ultimately only important in how they effect the losses generated. The variation of the momentum thickness at the at 96%s of the TL10 profile are therefore compared to the predicted variations. Given that the primary weakness of the predictions is likely to be the separation bubble and its reattachment, the absolute values of the momentum thickness are unlikely to be predicted with any great accuracy. The errors are likely to be greater at lower reduced frequencies ($\bar{f} \le 0.4$) where the separation bubble occupies a greater extent of the wake

passing cycle. Conversely, when reduced frequencies are higher (for example $\bar{f} \geq 0.7$), one would expect smaller errors as the separation bubble occupies a smaller fraction of the wake passing cycle.

Figure 7.5.2 show the variation of the predicted momentum thickness at 96%s for the TL10 profile. The measured momentum thickness at this streamwise location is shown in Figure 7.5.3, but for half the reduced frequency used for the predictions. The three main parts of the flow are reproduced, including the separated flow transition region. The effect of the calmed flow can be seen as the minimum in momentum thickness, but this is terminated by the arrival of the separated flow transition. Before the separated flow transition region arrives, the momentum thickness in the calmed region can be seen to increase slightly as trailing edge of the calmed region approaches. Figure 7.5.3 shows the measured momentum thickness from the TL10 cascade at a reduced frequency of 0.39. This lower reduced frequency allows the separated flow transition to be seen before the next wake arrives. The same measurements at a reduced frequency of 0.78 would not show the separated flow transition as the next wake would arrive at the time marked by an 'X' in Figure 7.5.3. The difference between the predicted and measured time histories occurs where the prediction very clearly shows the separated flow regime which the measurements would not. This is due to the intermittency that is used as an input to the prediction as this also shows the presence of the intermittency due to the separated flow transition. The measurements of intermittency blur this multi-mode transition.

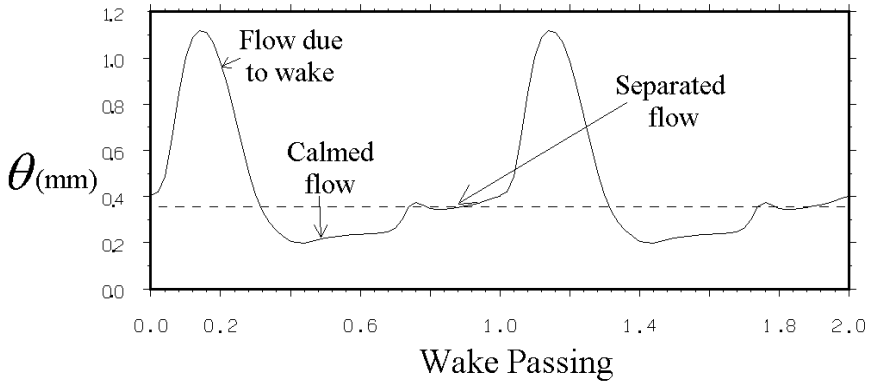

Figure 7.5.2 Predicted variation of momentum thickness at 96%s. Reynolds number 130,000, $\bar{f} = 0.78, \Phi = 0.7$.

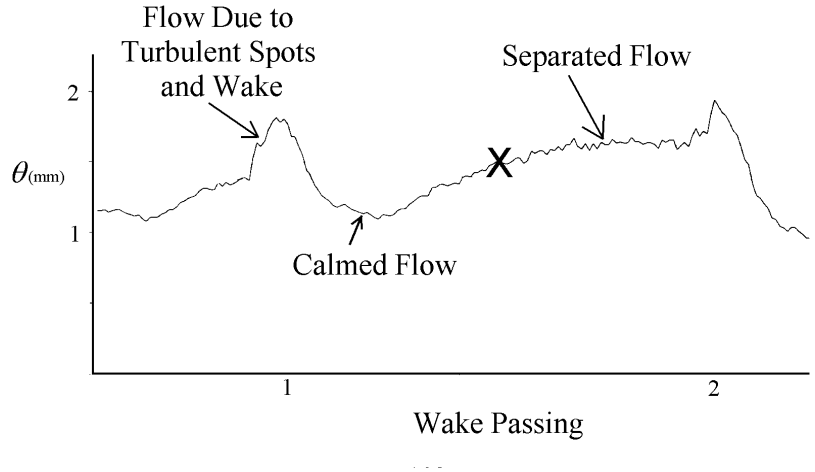

Figure 7.5.3 Measured momentum thickness from the TL10 profile at 96%s. Reynolds number 130,000, $\bar{f} = 0.39, \Phi = 0.7$.

7.5.1 Predicted variation of the velocity profiles in a separation bubble

Using the same intermittency distribution that is shown in Figure 7.4.1 the variation of the velocity profiles was investigated as turbulent spots travel through the separation on a TL10 style pressure distribution. Figure 7.5.4 shows the measured and predicted variations of the velocity profiles that occur as the turbulent part of a turbulent spot travels though the separation bubble. Initially, profile '1' is that of a separated boundary layer and the separation reduces in size until by profile 4, it has nearly assumed the shape of a turbulent boundary layer. Velocity profile 4 occurs at the very rear of the turbulent spot. The same behaviour was noted in the measurements from the flat plate. There the profile

also assumed the shape factor of a turbulent boundary layer only at the very rear of the turbulent spot. For laminar boundary layers on a zero pressure gradient flat plate Seifert (1996) showed that the shape factor reached 1.6 for nearly all the turbulent part of the spot. This obviously is not the case when the spot forms in and then travels through a separation bubble. Figure 7.5.5 shows the variation of the velocity profiles as the calmed region passes through the separation bubble. Initially, the profile has relaxed slightly from the turbulent profile seen in the previous figure.

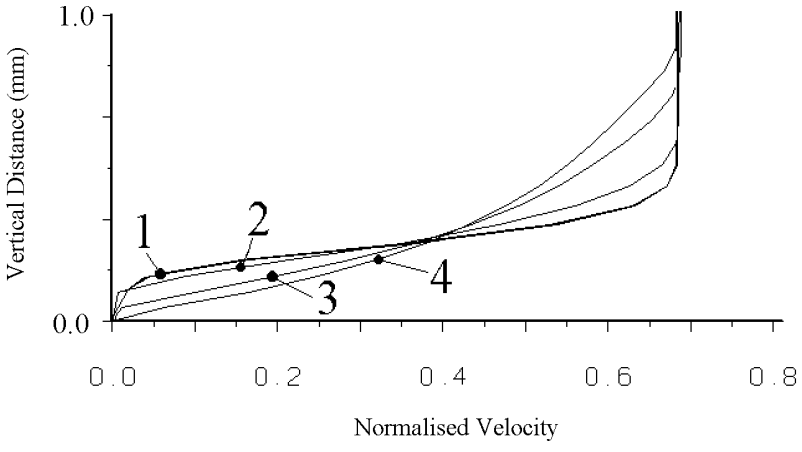

(a)

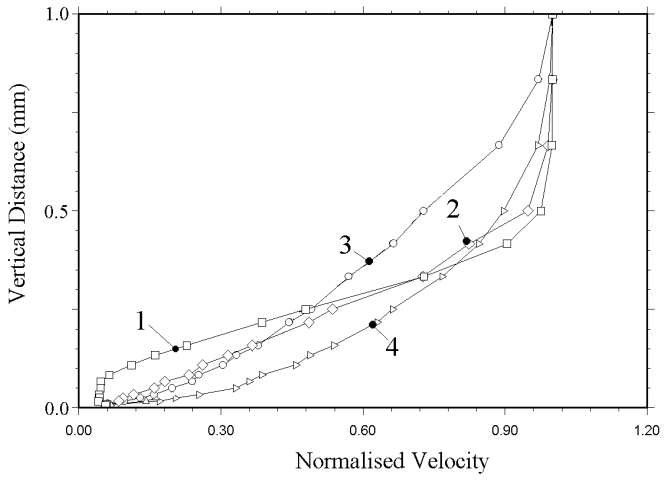

(b)

Figure 7.5.4 The predicted (a) and measured (b) variation of the velocity profiles as the turbulent part of a turbulent spot travels through a separation bubble on the flat plate. Reynolds number 130,000. $\bar{f} = 0.78$. $\Phi = 0.7$. Surface location 78%s.

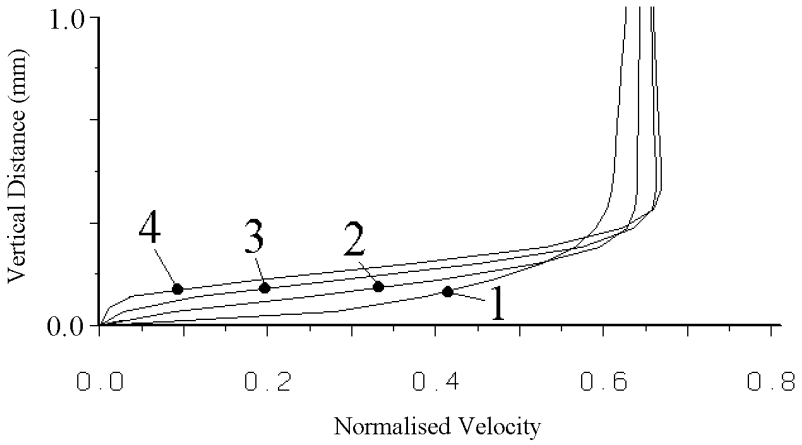

(a)

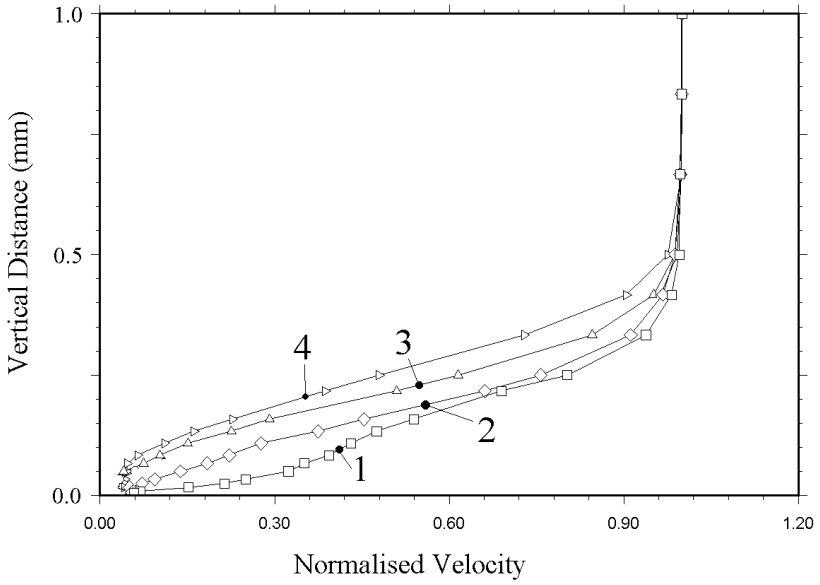

(b)

Figure 7.5.5 The predicted (a) and measured (b) variation of the velocity profiles as the calmed region of a turbulent spot travels through a separation bubble on the flat plate. Reynolds number 130,000, $\bar{f} = 0.78, \Phi = 0.7$. Surface location 78%s.

The simple approach to predicting the development of separation bubbles subjected to the effects of wakes agrees well from a qualitative view point with the measurements for this profile.

7.5.2 Predictions of the suction side boundary layers of NGV3 of the BR715 LP turbine

One of the most difficult flows to predict is that from the NGV3 of the BR715 LP turbine which was described in Chapter 4. This contains the beating effects of rotors 1 and 2 and their interactions with wakes from NGV2. This results in a two streamwise onset locations for wake induced transition that occur at different positions of the upstream rotor.

Unfortunately information regarding the inlet turbulence profile was not available. This means that one must attempt to construct the variation of inlet turbulence that will give rise to the correct intermittency. That in turn should then allow the UNSFLO code to predict the unsteady variation of skin friction coefficient etc. However, the simple intermittency code discussed earlier completely failed to give what were considered to be reasonable results of intermittency for this NGV. This is due to the extreme complexity of the flows on this turbine. In this case the intermittency was inferred from all the available hot film data. The resulting intermittency (shown in Figure 7.5.6) was used for the predictions.

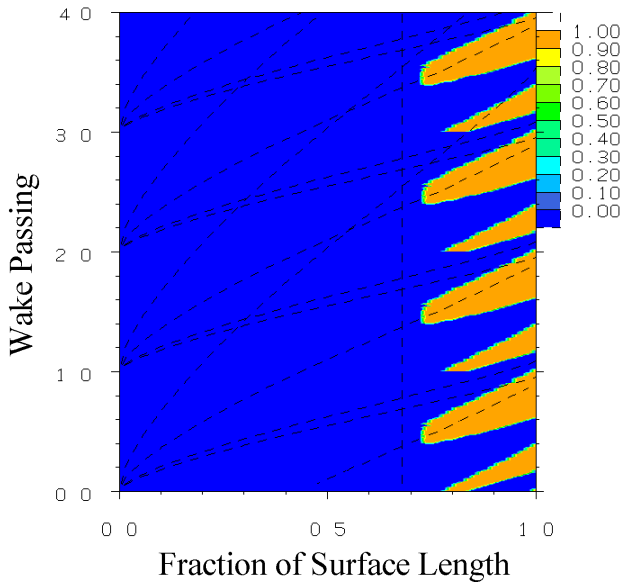

Figure 7.5.6 ‘Assumed’ intermittency for NGV3 of the BR715 LP turbine.

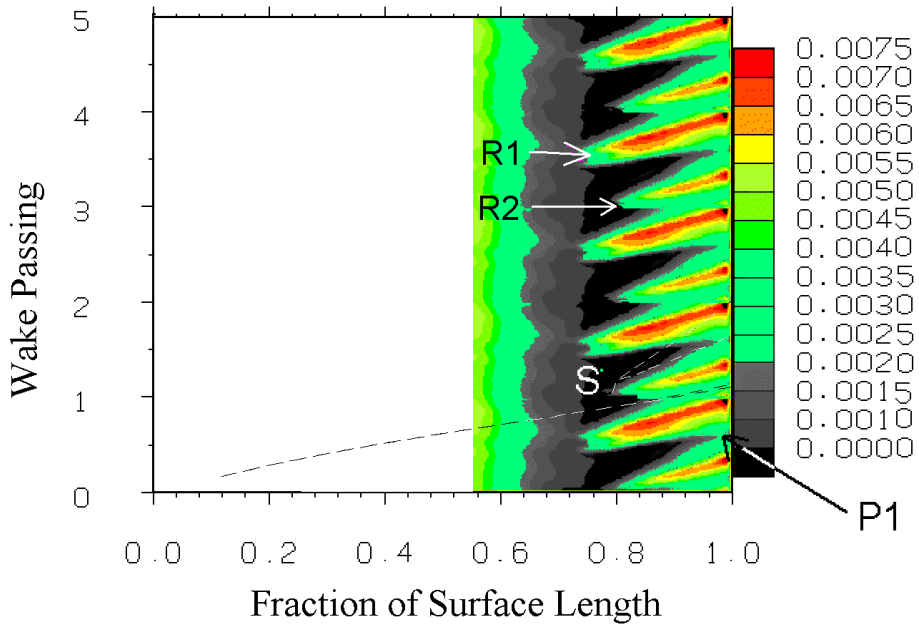

Figure 7.5.7 ST diagram of the predicted variation in skin friction coefficient for NGV3 of the BR715 LP turbine. Reynolds number = 130,000, $\bar{f} = 0.78$, $\Phi = 0.7$.

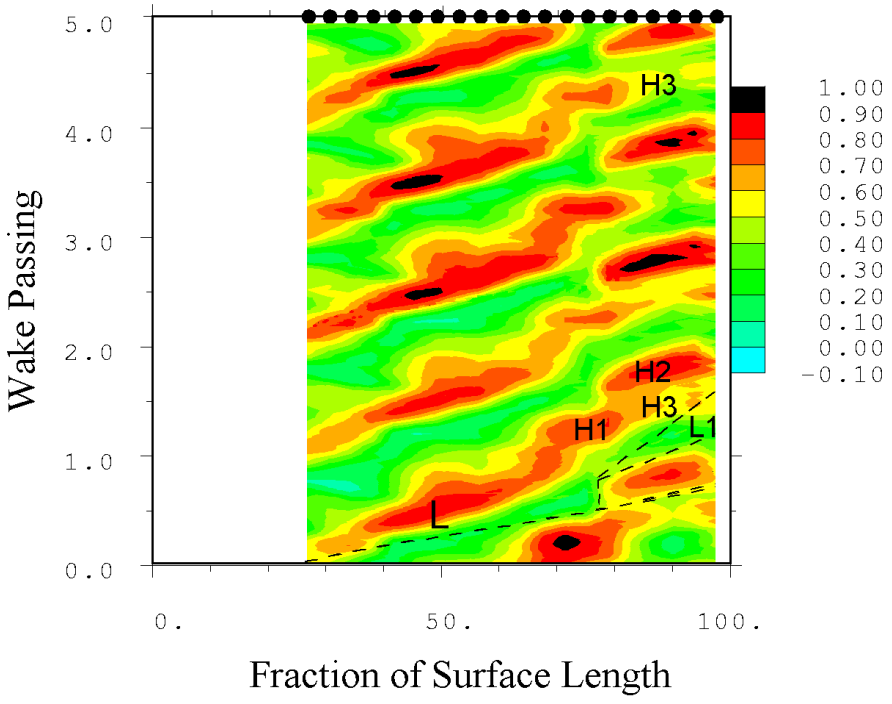

Figure 7.5.8 ST diagram of non dimensional ensemble mean quasi shear stress for NGV3 of the BR715 LP turbine. Reynolds number = 130,000, $\bar{f} = 0.78$, $\Phi = 0.7$.

Figure 7.5.7 shows the predicted variation in skin friction coefficient for NGV3. Figure 7.5.8 is taken from Chapter 4 and shows the variation in measured non dimensional ensemble mean quasi shear stress from hot film sensors. These two figures initially look very different, but on closer inspection all the important features of the measurements are correctly predicted. The primary difference between the two results occurs in the region from the leading edge up to near where the flow separates. The perturbations in the laminar boundary layer are not reproduced because this effect due to wakes convecting in the freestream were not accounted for in the calculation.

The onset location for wake induced transition regions caused by rotor 2 wakes are fairly well reproduced see region ‘R2’. Transition onset for the regions marked ‘R2’ appear later along the surface than the measurements indicated. The region marked ‘L1’ is due to calming. This is also reproduced in the predictions in Figure 7.5.7 and is marked region ‘P1’. As the effect of this calmed region reduces (this is seen as a reduction in skin friction), the turbulent region due to the next wake arrives before the boundary layer can separate. From the measurements it is difficult, if not impossible, to determine if the flow was separated at any positions between the transitional regions on such ST diagrams. The time mean levels of shear reached a minimum at 75%s, indicating that at some positions of the upstream rotor the boundary layer did separate. However, the predicted shear stress tends to indicate that between wake passings up to 90%s (the black contours) the flow can be separated. However, because of the effects of calming and the turbulent boundary layer due to wake transition, the predicted boundary layer at the trailing edge is always attached.

It is interesting to note that the predicted skin friction coefficient remains roughly constant along the path of the of the wedge shaped regions of transitional flow. In a constant pressure gradient flow as a boundary grows, the skin friction reduces. In the

diffusing flow found on the rear of an LP turbine blade profile, this reduction should occur faster. The reduction in shear variation was seen in the hot film measurements as high shear transitional regions ‘H1’ reach the surface location marked ‘H3’.

7.6 Conclusions

This chapter has shown that wake induced transition occurs around the region of flow separation on the high lift LP turbine profiles presented. At the Reynolds number that the all the tests were carried out (130,000) the Reynolds number based on momentum thickness was approximately between 250 and 270. The exact value of the momentum thickness Reynolds number is obviously a function of the pressure distribution and Reynolds number.

For LP turbine applications the use of steady flow correlations for the prediction of the wake induced transition onset location were shown to be adequate. Evidence was presented that showed that one can simply assume that the onset location is the same as the position of flow separation.

Unsteady wake induced transition and separation bubble interactions have been predicted by weighing an eddy viscosity turbulence model with a prescribed unsteady intermittency. The unsteady intermittency was prescribed for the calculation using the code of Schulte and Hodson (1999). The predictions of skin friction coefficient were compared to measurements of quasi shear stress. These showed that the wake induced transition onset location and also the wake spreading angle were correctly predicted. Measured quasi shear stress somewhat blurred the multi-mode transition that was occurring on the blade, but the predictions were clearly showing wake and separated flow transition.

The unsteady variation of the measured velocity profiles in a separation bubble on a flat plate were correctly predicted. As a turbulent spot travelled through the separation, the

flow was forced to reattach to the surface. The effect of the calmed region was to keep the flow attached but gradually allow the separation bubble to reform.

8. Validation - An Ultra High Lift Profile

8.1. Introduction

This chapter aims to show that the understanding and work carried out in the previous chapters can be translated into an LP turbine blade profile with a 15% increase in lift over the previous design. The profile was design by Rolls Royce plc. (Harvey, 1997) following work carried out in Chapters 4 to 6. The experimental measurements were carried out by O.N. Ramesh of the Whittle Laboratory and not by this author. However, the analysis of these measurements is the sole work of author and is presented here for completeness.

8.2. Description of the ultra high lift profile TL11

This profile, designated TL11, has the same inlet and exit angles as the datum profile described in Chapter 5, but was designed to have a 15% increase in pitch chord ratio. Table 8.1 shows the basic parameters for the profile and cascade.

Zweifel coefficient	1.208
Pitch/Chord ratio	1.281
Cascade pitch	179mm
Reduced Frequency (at Re=130,000	0.54
Aspect ratio	2.37
Bars upstream of cascade leading edge	*0.5 axial chord*
Number of blades	6

Table 8.1 Design parameters of the high lift LP turbine profile

The same (2.05mm) bars were used to generate the upstream wakes as the datum cascade. The upstream bar pitch and reduced frequencies were calculated for the new profile, and were therefore not the same as for the TL10 profile. It should be noted that for

a given stage of these ultra high lift LP turbine blades to produce the same loss as a stage containing the datum profiles would allow each ultra high lift blade can produce 15% more loss than the datum profile TL10. This means that the if one were to simulate an upstream blade row of the same high lift blades, then the bar diameter to simulate the same losses, must be increased to give a larger loss.

The design Reynolds number was the same as that for the measurements presented in Chapters 5 and 6, i.e. 130,000. From Chapter 5, the best lift - loss profiles seemed to be those that produced peak suction at 65%s and separation at around 80%s. The position for laminar separation for the new profile was therefore designed to occur at approximately 80%s, where the value of Re_θ (around 250 at a blade Reynolds number of 130,000) would ensure that wake induced transition would be initiated in this region. Wakes and turbulent spots would therefore control the separation bubble growth.

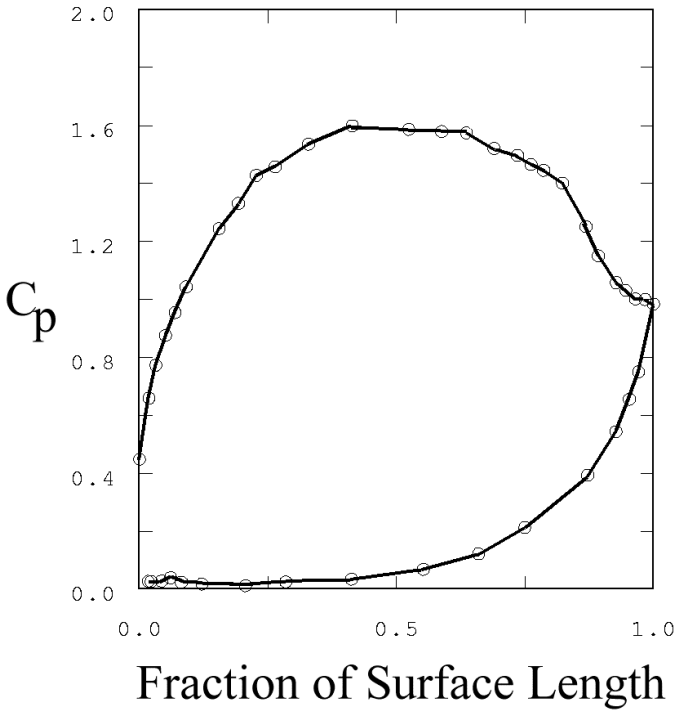

Figure 8.2.1 Pressure distributions for the datum profile and the ultra high lift profile. Unsteady inflow, Reynolds number 130,000, $\bar{f} = 0.54$, $\Phi = 0.73$.

The measured pressure distribution obtained from the cascade of blades resulted in a position of peak suction at around 50%s. As a result, this profile was not properly aft loaded, see Figure 8.2.1 and one of the design objectives for this profile was therefore not achieved.

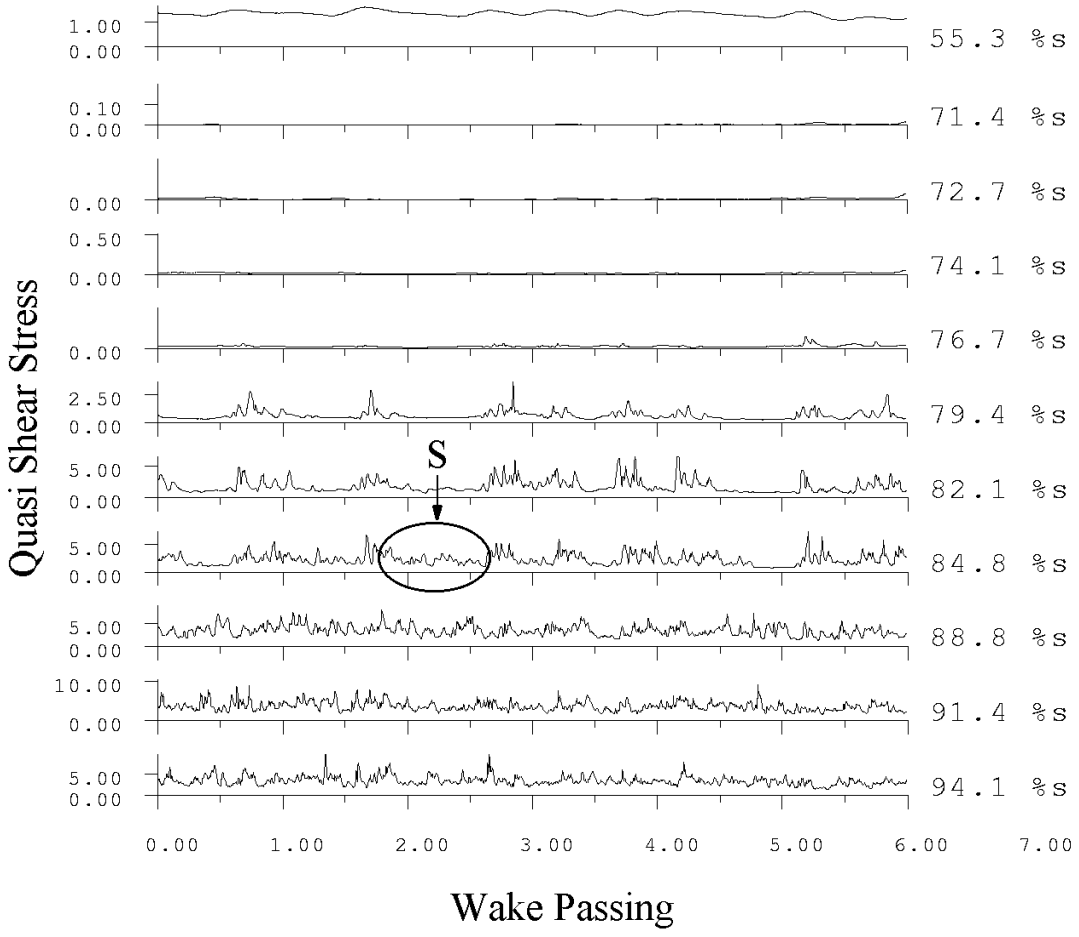

Figure 8.2.2 Raw hot film data from the ultra high lift LP turbine profile. Reynolds number 130,000. $\bar{f} = 0.54$, $\Phi = 0.73$. Peak turbulence intensity = 13.5%.

Figure 8.2.2 shows the raw hot film data as a set of time history plots. Separation occurs at around 72%s. At 77%s some small disturbances are seen in the data, which, by 79%s, are fully formed turbulent spots. These spots convect downstream and through the separation. Fluctuations between wake passings start at 85%s and indicate separated flow

transition is starting to occur, see the region marked ‘S’. The final sensor on the blade surface was located at 94%s and shows a fully attached but not fully turbulent boundary layer. It is interesting that there is very little evidence of calming in the raw hot film data when compared to that of the TL10 profile, see Figure 5.2.3 of Chapter 5.

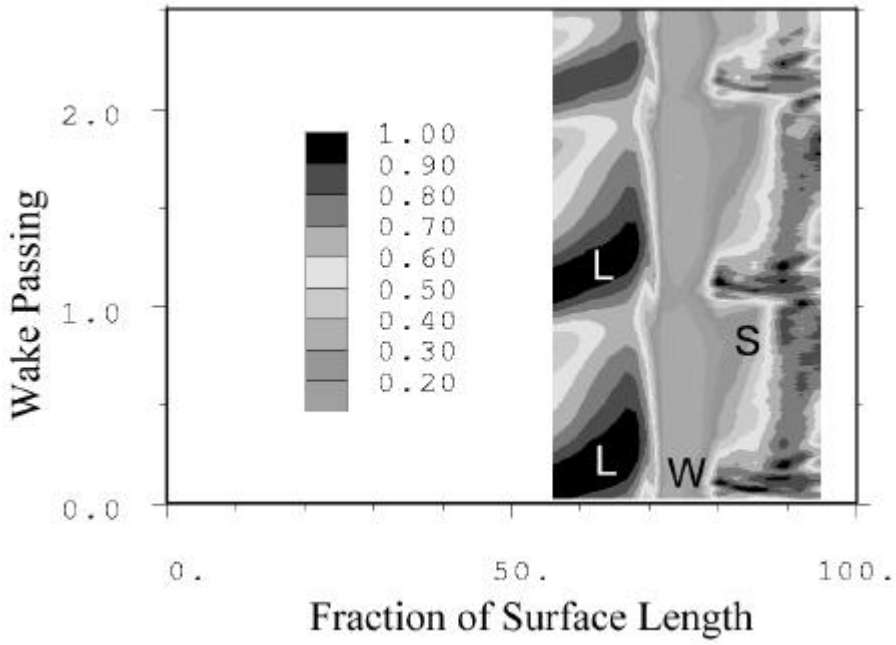

Figure 8.2.3 ST diagram of non-dimensional ensemble averaged shear stress for the same conditions as Figure 8.2.2.

Figure 8.2.3 shows the variation of the non-dimensional ensemble mean wall shear stress ($\bar{t}_w(s,t)/\bar{t}_{w,\max}(s)$) as an ST diagram. This allows one to see the variation of a quantity in time and space more easily than is possible when data is presented as a time history. Low shear stress occurs at around 74%s and wake induced transition occurs at around 80%s, see region marked ‘W’. Separated flow transition occurs at around 85%s, see region marked ‘S’. Interestingly, the flap test experiments produced laminar separation at roughly the same surface location despite a number of increased diffusion levels. The increased diffusion of the TL11 profile seems to cause flow separation earlier.

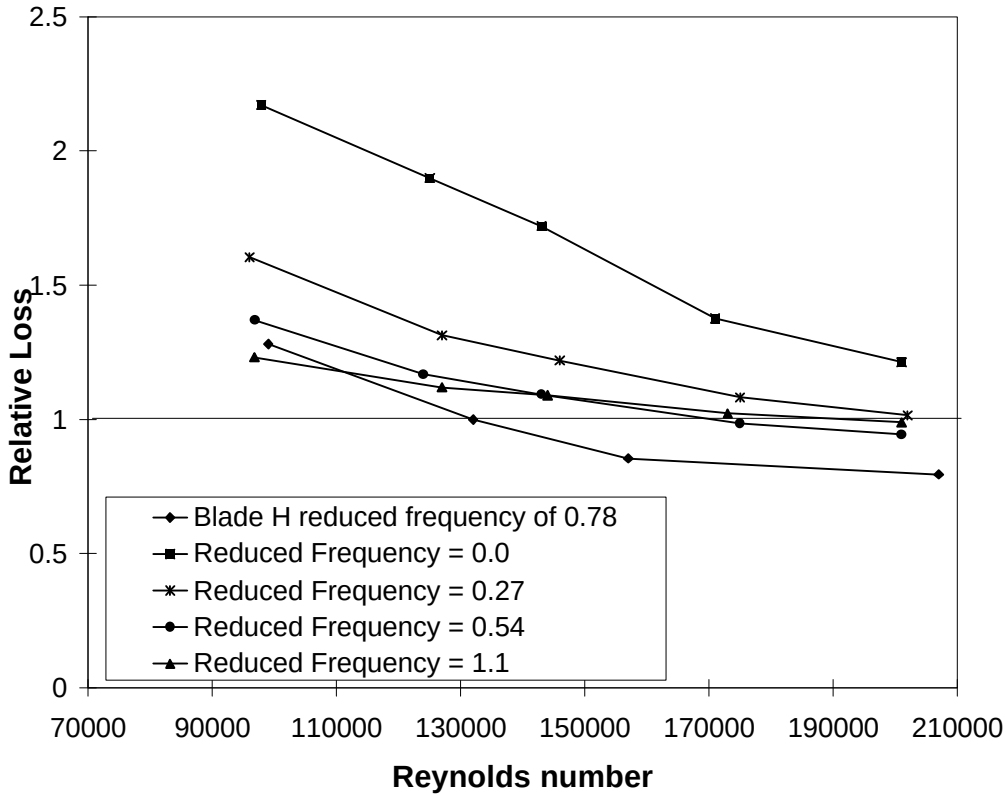

Figure 8.2.4 Non-dimensional loss variation vs. Reynolds number for the ultra high lift profile.

Figure 8.2.4 shows the variation of relative loss from the ultra high lift profile for a number of reduced frequencies. All values are non-dimensioned by the loss for the datum profile at a Reynolds number of 130,000 and a reduced frequency of 0.78. At the lowest Reynolds numbers with steady inflow the design produces extremely high (and unacceptable) losses. However, when wakes are present the losses reduce dramatically and the higher the reduced frequency, the lower the losses. At higher Reynolds numbers, the losses follow similar trends, but the size of the loss reduction is much reduced as the separation bubble (and associated losses) are smaller in steady flow.

At Reynolds numbers above 150,000 and at a reduced frequency of 1.1 the losses rise above those for a reduced frequency of 0.54. This indicates that the wake passing frequency is higher than optimum. Rather than just suppressing the separated flow losses

more of the blade surface is covered by wake generated turbulent flow (and its losses). The new profile produces a greater profile loss than the datum profile at Reynolds numbers above 100,000. This is probably because boundary layer separation occurred earlier than intended. This has lead to more turbulent boundary layer after reattachment, resulting in greater losses.

8.3. Further discussion

The new ultra high lift profile produced slightly greater losses than that for TL10, but resulted in an decrease in the number of blades by 15%. Laminar separation occurred on the new profile at approximately the same surface position as for the datum profile. Hot film measurements indicted the presence of turbulent boundary layer near the trailing edge. If the separation location could be moved further aft, a loss reduction should result.

The measurements have shown that at very low Reynolds numbers, the greater the reduced frequency, the lower the losses produced by TL11 profile. Measurements in Chapter 4 showed that stator 3 of the BR715 LP turbine had wake induced turbulent regions on the suction surface appearing at twice the frequency of the wake passing of rotor 2. This effectively results in a doubling of the reduced frequency that stator 3 sees. This can be considered beneficial for the current ultra high lift profile as this effect should further reduce losses if this type of profile was used in an imbedded stage rather than just subjected to the wakes from a single upstream rotor. Higher Reynolds numbers occur in the first stages of the LP turbine while lower Reynolds numbers occur in later stages. This is fortuitous as high reduced frequencies (caused by multistage interactions) occur in later stages in the LP turbine where the larger separations (due to lower Reynolds numbers) are likely to be better controlled. In the first few stages (at higher Reynolds numbers), there

are less blade row interactions, but as Figure 11 showed one does not desire reduced frequency doubling as this could increase the losses.

The profile loss measurements were conducted with a freestream turbulence level of 0.5%. This level is much lower than that found in the engine environment. The size (and losses) of separation bubbles reduce when subjected to elevated levels of freestream turbulence. With a higher turbulence level, and the addition of wakes this may reduce losses further at low Reynolds numbers.

As can be seen, there are a number of other parameters that can be used in the design of more highly loaded LP turbine profiles, if the designer takes into account unsteady effects. More research is necessary to see just how far the unsteady effects of wakes can be used in the LP turbine for either gains in efficiency or reductions in manufacturing costs and weight.

8.4. Conclusions

A new highly loaded LP turbine profile was designed using the data presented in Chapter 5. As expected with steady inflow the profile, performs poorly. When subjected to unsteady inflow the profile loss reduced dramatically. The profile generates 15% more lift than the datum. The position of separation was in the same position for the datum and new profile. It may be possible to achieve further loss reductions if proper aft loading of the profile could be achieved.

Controlled diffusion blading takes no account of the effects of upstream wakes and should no longer be thought of as good design practice. Instead, wake controlled high diffusion blading should be employed. This removes the limits placed on the diffusion level

and location of peak suction and separation. Higher lift blade profiles that generate acceptable losses will therefore be possible than the current high lift designs.

9. Conclusions and Suggestions for Future Work

9.1. Introduction

The interactions between the surface flows and incident wakes on high lift low pressure turbine blades has been investigated both experimentally and numerically. Experiments were carried out in low and high speed rigs. The measurement from the high speed rigs confirm that the experimental approach used in the low speed measurements captures the physics of the flows. Further experimental measurements were carried out to illustrate some of the details of the flows see elsewhere. All the experiments formed a data base with which to compare and test numerical predictions. This chapter draw the work together into a summary. Suggestions for future work are also presented.

9.1.1. Measurements of Wake Boundary Layer Interaction

High speed measurements from full size LP turbines showed that in no way can the surface flow in an LP turbine be considered steady. The separation and transition mechanisms present are highly unsteady and their behavior is dominated by the passage of wakes. In a three stage machine, more complicated effects are present, where the wakes from all the upstream blade rows interact in a complicated manner. This interaction caused wake transition regions to form at twice the frequency of the rotor immediately upstream of the NGV where measurements were taken. The strength of these regions varied periodically in time. A beating was seen to occur at a frequency equal to the difference in blade numbers between the rotors.

The low speed measurements (in a moving bar rig) were shown to reproduce the transitional effects of a single upstream blade row. Such a rig cannot reproduce the effects

seen in a true multistage machine. However, with an understanding of the additional effects that are present in a multistage machine, one is aware of the limitations of the low speed rig and can interpret measurements accordingly. The low speed measurements showed that a reduction in loss occurred when wakes were present compared to the same profile with steady inflow. The addition of a flap on the blade below the one being tested allowed increased lift profiles to be investigated.

Higher lift profiles were tested with wakes present. These produced loss levels comparable to the datum profile with steady inflow only when their lift coefficients were up to 20% greater than the datum with steady flow. Hot film measurements showed that the laminar region of the separation bubble decreased and more turbulent flow was seen towards up to the trailing edge. To reduce the additional losses generated by this turbulent flow, the profiles were aft loaded with the use of additional inserts placed into the blade passage. These new profiles produced pressure distributions with peak suction moved towards the trailing edge. As a result the position of flow separation and therefore separated flow transition was also moved aft. With steady flow, the separations on these profiles did not always reattach by the trailing edge of the blade. With wakes present the flows were always reattached by the trailing edge. Due to the reduction in turbulent wetted surface these profiles produced lower losses that their equivalent, more forward loaded profiles. Aft loading was shown to be beneficial in terms of loss production.

9.1.2. Flat Plate Measurements

Measurements on a flat plate with the pressure distribution of the datum blade showed some of the details of the flows that occur when a turbulent spots and wakes interact with separation bubbles. These observations were not possible on the other rigs as

the scale were to small to allow such detailed measurements. These measurements showed that turbulent spots traveled through a separation and not over it as was indicated by some of the first numerical predictions of the process. It was also shown that turbulent spots are not entirely alone in producing the loss reductions seen with unsteady inflow. Wake turbulence was also seen to play a role. Measurements showed that turbulent spots alone produced only about 60% of the total loss reduction that was measured when wakes were present. Wake turbulence was therefore shown to be important in gaining the maximum loss reductions.

9.1.3. Numerical Predictions

Numerical predictions were shown that reproduced most of the physics of the interactions of turbulent spots and separation bubbles. The code used a simple mixing length turbulence model where the turbulent viscosity was weighed with an intermittency. The values of intermittency were calculated previously. The changes in the velocity profiles of a separation bubble were well predicted as a turbulent spot traveled through it. The variation of momentum thickness at the trailing edge of the profile was also fairly well predicted as was the variation in skin friction.

9.1.4. The ultra high lift profile

A new profile was designed and tested in cascade. The design and testing was not carried out by the author, but the analysis of the results is entirely the work of the author. The new profile was intended to be aft loaded with a position of peak suction approximately 10%s further along the blade surface than the datum profile. Unfortunately, when this profile was tested in cascade it was found that it was no more forward loaded

that the datum profile. Nevertheless, it was tested to see how if performed with various frequencies of wake passing. Although the resulting profile was not entirely as intended the losses generated by it were reasonable. However, with steady inflow the profile performed extremely poorly and would never be used as a standard for production. The higher the reduced frequency of wake passing the lower the profile losses measured. The profile was designed using steady flow procedures, but with the knowledge from this thesis of how such a profile *should* perform with unsteady inflow. The ability of wakes to suppress losses was undeniably illustrated on this very highly loaded profile.

9.2. Suggestions for Future Research

The most important piece of work to be carried out should be redesign of the ultra high lift profile such that the position of peak suction and separation occur later along that blade surface. If the measurements of profile losses reduce then this would confirm the principal of aft loading low pressure turbine profiles as a method of obtaining loss reductions. It is expected that aft loaded profiles will only function correctly with unsteady inflow.

Anticipating that aft loading of LP turbine profiles proves to be successful, the next logical step would be to attempt a new design (using the design tools described in this thesis) to increase the lift coefficient of the profiles still further. There will always be a trade off between efficiency and cost of manufacture. One might determine the a cost saving was more important and allow a slight drop in efficiency of the LP turbine. Matching the wake passing frequency may also become important if separations are severe enough that they start to re-establish between wake passings. The effects of multistage blade rows are also important. These have implications on wake passing frequencies that

downstream blade rows are subjected to. The effects of the multi-stage environment should be researched. This cannot be carried out in a cascade fitted with a moving bar traverse system.

The exact nature of how a separation bubble re-establishes after the passage of a wake or turbulent spot should be studied under conditions of variable diffusion. Question such as, does the speed of the re-establishment of the separation and it's loss vary with increased diffusion and unsteady inflow.

The development of wake turbulence in a blade passage should be studied. Correlations used in Chapter 6 showed errors that could be due to the poor assumptions regarding the frozen turbulence used. It has become increasingly evident that information regarding the disturbance environment that boundary layers are subjected to should be studied in more detail. Better predictions of the skin friction coefficient for NGV3 of the BR715 LP turbine might have been possible with an inlet turbulence profile.

The effect of the negative jet transports high turbulence fluid in the wake towards the suction side boundary layer on turbine blades. High turbulence fluid is transported away from the suction side in compressor blades. It is therefore not possible to investigate the effects of wake direction on the transition mechanisms by moving the bar wake generators in different directions. An experimental technique should be devised that would allow the question of velocity defect and it effects on transition to be answered.

Details of turbulent spot and wake interaction should be carried out using a two dimensional measurement system i.e. a two dimensional hot film array. This would provide a greater understanding of the interactions and should provide more information on how important exactly wake turbulence is in controlling the separation bubbles.

This research has primarily been of a two dimensional nature. However, it should be remembered that increasing loading (and therefore the pressure difference between the suction and pressure sides of the blade) results in a greater aerodynamic load at the endwalls. This may well increase the spanwise extent and loss generation that occurs in the secondary flow regions. It would be unfortunate to have produced a profile that required perhaps 20% fewer blades that a datum profile, but increased the secondary flow losses and perhaps increase the losses above the datum profile.

The work presented in this thesis was carried out at a blade Reynolds number of 130,000. Similar studies to those presented here should be carried out at least another two Reynolds numbers, one higher and one lower that that used here. This is because a variation in Reynolds number will effect the size of the separation bubble and the losses generated by it. The onset location for wake induced transition will also change with Reynolds number.

The mechanical effects of reducing blade numbers must also be considered. If a total of 40% of blades are removed from the LP turbines designs used in engines such as the Trent 700 then this makes supporting the rotor shrouds more difficult. The shrouds themselves may have to be strengthened because of the reduction of blade numbers and this may tend to offset the decrease in weight achieved by using fewer blades.

Bibliography

Abu-Ghannam, BJ, and Shaw, R., "Natural transition of boundary layers - the effects of turbulence, pressure gradient and flow history," J. Mech. Eng. Sci., Vol. 22, No. 5, 1980, pp 213-228.

Addison, JS, and Hodson, HP, 1992, "Modelling of Unsteady Transitional Boundary Layers", ASME Jnl. of Turbomachinery, Vol. 114, No. 3, pp 580-589, Jul.

Arndt, N, 1991, 'Blade Row Interaction in a Multistage Low Pressure Turbine', ASME paper 91-GT-283.

Bearman, PW, 1971, 'Correction for the effects of ambient temperature drift on hot-wire measurements in incompressible flow', DISA information, No 11, pp 25-30.

Bellhouse, BL, and Schultz, DL, 1966, 'Determination of Mean and Dynamic skin friction Separation and Transition in Low-speed Flow with a Thin-Film Heated Element', Jnl. Fluid Mechanical Vol. 24, No 2.

Banieghbal, MR, Curtis, EM, Denton, JD, Hodson, HP, Huntsman, I, and Schulte, VS, 1995, "Wake Passing in LP Turbines", Paper No. 23, AGARD conf. Loss Mechanisms and Unsteady Flows in Turbomachines, Derby.

TM 78470, March 1978.

Chen, KK. and Thyson, NA., 1971, "Extension of Emmons' Spot Theory to Flows on Blunt Bodies", AIAA Journal, Vol 9, No 5, pp 821-825.

Chin and LaGraff, 1995, 'Measurements of turbulent spot convection rates in a transitional Experimental thermal and fluid science, 1996 11:52-60.

Coupland, JJ, 1998, private communication.

Cumpsty, NA., Dong, Y., and Li, YS., 'Compressor blade boundary layers in the presence of wakes', 1995, ASME paper no. 95-GT-443.

Curtis, E.M, Hodson, HP, Banieghbal, MR, Denton, JD, Howell RJ and Harvey, NW, 1996, 'Development of blade Profiles for Low Pressure Turbine Applications',

Dhawan, S, Narasimha, R, 1957, 'Some properties of boundary layer flow during

Dawes, WN, 1990, 'A comparison of Zero and One equation Turbulence Modelling for Turbomachinery Calculations', ASME paper number 90-GT-303.

Denton, JD., 1992, 'Entropy Generation in Turbomachinery Flows', 7th Cliff Garrett Turbomachinery Award Lecture, SAE paper 902011.

Deregel.,P, and Tan, CS., 1996, 'Impact of rotor wakes on Steady State axial compressor Performance', ASME paper number 96-GT-253.

Dibelius and Ahlers, 1990, 'Influence of periodically unsteady Wake Flow on the Flow separation in Blade Channels', ASME paper 91-GT-253.

Dong, Y and Cumpsty NA., 1989, 'Compressor Blade Boundary Layers: Part 1:test Facility and Measurements with No Incident Wakes, part 2, Measurements with Incident wakes', ASME papers 89-GT-50 and 89-GT-51.

Emmons, HW, 1951, 'The laminar-turbulent transition in a boundary layer- Part 1', Journal of Aerospace Science, Vol. 18, No7, pp490-498.

Evans, B.J., 1971, 'The effects of free stream turbulence on blade performance in a compressor cascade', PhD thesis, Cambridge University.

Funazaki, K, and Koyabu, E, 1998, 'Effects of periodic wake passing upon flat plate boundary layers experiencing Favourable and adverse pressure gradients', ASME paper number 98-GT-114.

Gaster, M, 1967, 'The Structure and Behaviour of Separation Bubbles' reports and Memo No. 3595, March 1967.

Gostelow, JP, and Dey AR., 1991, 'Spot formation Rates in Transitional Boundary Layers under Zero and Adverse Pressure Gradients', R. Ae. Soc. Conf. Boundary Layer Transition and Control, Cambridge, April 8-12.

Gostelow, JP, Walker, GJ, Solomon, WJ, Hong, G, Melwani, N, 1996, "Investigation of the calmed region behind a turbulent spot", ASME-paper 96-GT-489.

Giles, MB, 1991, 'UNSFLO: A numerical method for the calculation of unsteady flow in turbomachinery', MIT GTL report number 205, May 1991.

Moore H. and Gregory-Smith, DG., 1996, 'Transition effects on the secondary flows in a turbine cascade', ASME paper no 96-GT-100.

Hourmouziadis, J, 1989, "Aerodynamic Design of Low Pressure Turbines", AGARD Lecture Series, 167.

Halstead, DE, Wisler DC, Okiishi., TH., Hodson, HP. and Shin, H., 1995, 'Boundary Layer Development in Axial Compressors and Turbines', Part 1: Composite Picture, part 2: Compressors, Part 3: Turbines, Part 4: Computations and Analysis, presented at the IGTI comference in Houston, Texas.

proceedings, AGARD conf. PEP 74a on Unsteady Flows in Turbomachinery, AGARD CP 468. Also ASME journal of Turbomachinery, Vol. 112, No Oct. 1990, pp 691-701.

Hodson, HP, 1985, 'A blade to Blade Prediction of a wake Generated Unsteady Flow', ASME journal of Engineering for Gas Turbines and Power, vol. 107, April.

Hodson, HP, 1996, 'Turbomachinery Aerodynamics', University of Cambridge Advanced Program for Industry', University of Cambridge Whittle Laboratory.

Hodson, HP, Addison, JS, and Shepherdson, CA, 1992, 'Models for Unsteady Wake-Induced Transition in Axial Turbomachines', Journal de Physique, Vol. 2, No. 4, April, pp 545-574.

Hodson, HP, 1983, 'Unsteady Boundary Layers and Losses on Axial Flow Turbine Rotor Blades', PhD thesis, Cambridge University.

Hodson, HP, Huntsman, I. And Steele, AB, 1993, 'An Investigation of Boundary Layer Development in a Multistage LP Turbine', ASME paper no. 93-GT-310.

Hodson, HP and Schulte. V, 1998, 'PUIM users manual', Whittle Laboratory, Cambridge University.

Horton, HP, 1969, 'A semi-Emperical Theory for the growth and Bursting of Laminar Separation Bubbles', ARC CP 1073.

Ladwig, M, and Fottner, L, 1993, 'Experimental investigations of the influence of incoming wakes on the losses of a linear turbine cascade', ASME paper number 93-GT-394.

Malkiel, E, and Mayle, RE, 1995, ' Transition in a separation bubble', ASME 95-GT-32.

Mayle, RE, and Dullenkopf, K, 1989, 'A Theory for Wake Induced Transition', ASME paper number 91-GT-57.

Mayle, RE, 1991, 'The role of laminar-turbulent transition in gas turbines engines', ASME Journal of turbomachinery, Vol. 113 October , 13/509.

Meyer RX , 1958, 'The effect of Wakes on the transient Pressure and Velocity distribution in Turbomachines.', ASME 57-A-83.

Moore, H, and Gregory-Smith, DG, 1996, 'Transition Effects on secondary Flows in a Turbine Cascade', ASME paper number 96-GT-100.

Doktor-Ingenieurs dissertation, Technischen Universität Darmstadt, 1998.

Wisler, DC., ‘The Technical and Economic Relevance of Understanding Boundary Layer Transition in Gas Turbine Engines’, Minnobroke I, 1995 Workshop on Boundary Layer Transition in Turbomachines’, NASA/CP-1995-206958.

Wisler, DC, ‘The Technical and Economic Relevance of Understanding Blade Row Interactions Effects in Turbomachinery’, von Karman Institute for Fluid Dynamics Lecture series 1998-02, February 9-12, 1998.

Walker, GJ, 1974, ‘The Unsteady Nature of Boundary Layer transition on an Axial-Flow Compressor Blade’, ASME Paper 74-GT-135.

Walker, GJ, and Gostelow, JP, 1989, ‘The effect of adverse Pressure Gradients on the Nature and Length of Boundary Layer transition’, ASME Paper number 89-GT-274.

Walker, GJ, Solomon, WJ, and Gostelow, JP, 1993, ‘Observations of Wake-Induced Turbulent Spots on an Axial Compressor Blade’, 1993, ASME Paper 93-GT-378.

Walraevens RE, and Cumpsty, NA, 1993, ‘Leading Edge Separation bubbles on turbomachine Blades’, ASME 93-GT-91.

semi-empirical theory for Surface mounted aerodynamic Wall shear stress gauges.’ ASME paper number 95-GT-193.

Zhong, S, Kittichaikarn, C, Ireland, PT, and Hodson, HP, 1998, ‘A Study of Unsteady wake-Induced Boundary Layer Transition with thermochromic Liquid Chrystals’, IMechE Conference Transactions of International Conference on Optical Methods and Data Processing in Heat and Fluid Flow, London, UK.

Appendix A

This appendix gives the surface locations for the hot film sensors used on the BMW Rolls-Royce LP turbines.

Sensor number (trailing edge sensor is number 7)	Position (as a percentage of suction surface length)
1	71
2	75
3	79
4	84
5	88
6	92
7	96

Table A1 Position of hot film sensors on the blade suction surface of NGV2 of the BR710 LP turbine.

Sensor number (trailing edge sensor is number 9)	Position (%s)
1	Not connected
2	Not connected
3	70.8
4	74.6
5	78.4
6	82.2
7	86.0
8	89.8
9	93.7
10	97.5

Table A2 Position of hot film sensors on the suction surface of NGV2 of the BR715 LP turbine.

Sensor number (trailing edge sensor is number 20)	Position (% s)
1	26.8
2	30.5
3	34.2
4	38.0
5	41.7
6	45.4
7	49.1
8	52.9
9	56.6
10	60.3
11	64.0
12	67.7
13	71.5
14	75.2
15	78.9
16	82.6
17	86.4
18	90.1
19	93.8
20	97.5

Table A3 Position of hot film sensors on the suction surface of NGV3 of the BR715 LP turbine.

Appendix B

A Description of a Method of Measurement of Intermittency from Hot Film Sensors

To compare the predicted intermittency with the hot film measurements, an estimation of the intermittency from the hot film data is required. A simple intermittency measurement algorithm was therefore developed for this purpose. There are three basic parts to such a code which are briefly discussed below.

The first part of a intermittency measurement code is a detector function which sensitises the signals by exaggerating the differences between the high and low frequency components. Ideally, a method of correlating the signals with the Reynolds stress uv is therefore required. Unfortunately, boundary layer measurements in this thesis use either a single hot wire or hot film sensors. Blair (1991) obtained good results using the detector function $(du/dt)^2$, for hot wire measurements where only one component of velocity was available. The only quantity available from hot film measurements is quasi shear stress, so the detector function $|dt/dt|$ was used here. This has often been used by other workers with good results, see Solomon (1997) and Ramesh et al (1995).

The next step in the process is to smooth the signal which reduces the number of drop outs and spikes caused by the sensitizing. A spike is a region identified as turbulent in an otherwise laminar region and smoothing reduces the chance that it will be identified as turbulent. A dropout is a region identified as laminar in an otherwise turbulent region. The current algorithm smoothes the samples over a short window time. This effectively acts as a crude low pass filter on the signals. The window times can be chosen by considering

appropriate time and length scales of the flows under consideration. Large window times have the disadvantage of increasing the coarseness of the final intermittency distribution in time, whereas too short a window time does not smooth the signals enough, resulting in dropouts. Since different data from various rigs was sampled at different rates, the windowing time and threshold levels have to be changed accordingly. A number of window times were tested and the final value was chosen on the bases of the subjective quality of the final intermittency distribution.

The final part to an intermittency code is the level of the smoothed signal above which it is decides that the flow is turbulent. Below that level the flow is deemed laminar (or calmed). Solomon (1996) set the threshold level where the smoothed signal became greater than $T|dt/dt|_{rms}$, where T = 0.7. The intermittency algorithm developed for this work required the threshold constant, T, to be set to around 1.7 to produce realistic intermittency distributions.

For a given sensor, each ensemble of data was sensitized, smoothed and a threshold limit set. Then the time variation of intermittency is calculated for that ensemble. The intermittency for that sensor was then averaged over up to 200 ensembles.